NYLON 12/GRAPHENE NANOCOMPOSITES

by

Rehman Rafiq

A doctoral thesis submitted in partial fulfilment of the requirements

for the award of Doctor of Philosophy of

Loughborough University

Supervisor: Professor Mo Song

Department of Materials, Loughborough University

ACKNOWLEDGEMENTS

I would like to express profound gratitude to my advisor, Professor Mo Song for his invaluable support, encouragement, supervision and useful suggestions throughout this research work. His moral support and continuous guidance enabled me to complete my work successfully. I am also highly thankful to Dr. Jie Jin for helping me with many different aspects of the research, testing and analysing the results and her valuable suggestions throughout this study.

My heartfelt appreciation also goes to Dr. Dongyu Cai for his co-operation during my research. Moreover, my sincere thanks to the whole technician team of the Department of Materials, Loughborough University, for their training and advises.

My deepest gratitude goes to my wife for her moral support and whose prayers were in incessant and enabled me to reach this stage. I would also like to thank my parents who have been supporting me so patiently throughout my research.

Rehman Rafiq

October, 2011

ABSTRACT

A unique combination of excellent mechanical, thermal and barrier properties has made graphene a multifunctional reinforcement for polymers. The goals of this research were to prepare exfoliated functionalized graphene sheets (FG) from expanded graphite, the uniform dispersion of these graphene sheets in the nylon 12 matrix, and understanding the effect of graphene on mechanical, thermal and barrier properties of nylon 12. FG were successfully prepared from various methods and was confirmed by XPS and TEM analysis. FG were melt blended with nylon 12 and their dispersion in the matrix was characterized by SEM. Crystallization behaviour of Nylon 12/ FG was investigated by means of differential scanning calorimetery (DSC). Non isothermal crystallization analysis revealed that the addition of only 1wt% FG in nylon 12 improved its crystallinity to about 67%. Application of Avrami analysis; to study isothermal crystallization kinetics; disclosed an unchanged nucleation mechanism and growth geometry. Polarized optical microscopy (POM) results indicated that FG did act as nucleating agent but hindered the formation of larger size crystals. Study of mechanical performance revealed that the incorporation of very small amount (about 0.6wt %) of the FG caused a significant improvement in ultimate tensile strength, elongation, impact strength and toughness of the nylon 12. With 0.6wt% FG ultimate tensile strength and elongation at break of the nylon 12 is improved by ～ 35% and ～200%, respectively. FTIR confirmed the hydrogen bonding between nylon 12 and FG, which contributed towards strengthening of the interface. The K_{Ic} of the nylon 12 is ～1.28 MPa.m$^{0.5}$ and the incorporation of 0.6wt% FG causes a significant increase of 72 % (～2.2 MPa.m$^{0.5}$). 0.6wt% FG causes also a significant improvement of 175 % in impact failure energy of the nylon 12. The incorporation of FG caused the increase in amount of γ phase of nylon12 and decreased its crystal size which could be the direct reason for the enhancement of the toughness. Nano-graphite, MWCNTs and carbon black were surface functionalized and their effect on the toughness was investigated. The results proved graphene to be the best nanofiller among three for the toughening of nylon 12. Oxygen and water permeability of nylon 12 was decreased to ~40%, implying the high aspect ratio of graphene which forced the permeant to pass through longer path.

TABLE OF CONTENTS

LIST OF FIGURES

LIST OF TABLES

List of abbreviations

Ω	ohm
nm	nanometre
GONPs	graphene oxide nanoplatelets
EG	expanded graphite
FG	functionalised graphene sheets
GO	graphene oxide
CNTs	carbon nanotubes
Tg	glass transition temperature
2D	two dimensional
MPa	mega Pascal
K_{IC}	mode I fracture toughness parameter
K_{IIC}	mode II fracture toughness parameter
K_{IIIC}	mode III fracture toughness parameter
ΔT	super cooling temperature
Tm	melting temperature
Tc	crystallization temperature
Xc	degree of crystallization
ΔH_m	enthalpy at a given temperature
ΔH^o_m	enthalpy of 100% crystalline polymer
X_t (t)	relative degree of crystallinity
t	crystallization time
n	Avrami exponent
K	Avrami constant

P	permeability coefficient
P_o	penetrant permeability coefficient
D	diffusivity
D_o	diffusivity coefficient of pure polymer
S	solubility
S_o	penetrant solubility coefficient
Ψ	volume fraction of the filler
f	tortuosity factor
α	aspect ratio of the filler
L	length of the filler
W	width of the filler
M_w	weight average molecular weight
M_n	number average molecular weight
µ	micron
UF4	nanographite
E'	elastic modulus
E″	loss modulus
Tanδ	damping factor
ΔHt	Heat generated at a certain time
$\Delta H\infty$	total heat by the end of crystallization
W/g	heat flow measured in watts per gram
P	load at fracture
Y”	compliance calibration factor
ɣ	crystallization phase
H_z	frequency

Chapter 1

INTRODUCTION AND AIMS OF THE PROJECT

1.1 Introduction

In recent times, polymers had been the first choice to be used in many structural applications because of their novel characteristics e.g. light weight, good elongation, easier processing and much lower cost than other structural applications [1]. However compared to metals and ceramics; reduced stiffness and toughness, lower strength and higher permeability to different solvents can be their weaknesses in the end use engineering applications [1]. To overcome these drawbacks; polymer-based composites were heralded in the 1960s as a new concept for materials. Dispersing strong and highly stiff fibres in different polymer matrices, high-performance lightweight composites were developed and tailored to the individual applications [2].

At present, to improve the functional performance of the polymers dramatically, nanotechnology provides the most versatile potential. Polymer nanocomposites are commonly defined as the combination of a polymer matrix and additives that have at least one dimension in the nanometre range [3]. These additives can be one-dimensional (examples include nanotubes and fibres), two-dimensional (which include layered minerals like clay), or three-dimensional (including spherical particles). The mixing of phases occurs over a much smaller-length scale in comparison to the micrometer-length scale of conventional composites gives rise to much more interfacial area which results in better dispersion of the nano-particles and hence better properties.

Nanocomposites have been shown to exhibit a significant increase in the properties of polymers and even generate certain new properties that cannot be derived from their individual constituents [3, 4]. Nanofillers have been nominated as better reinforcements for polymer matrix than conventional micro fillers because smaller amount of nano-materials causes a great deal of positive change in properties (mechanical, thermal, electrical etc) and these nanofiller-filled composites can be processed very easy as well. Moreover stress transfer in polymer nanocomposites is more efficient than conventional composites due to its increased surface area and good adhesion at the interface. Other superior properties of polymer nanocomposites include barrier resistance, flame retardancy, scratch/wear resistance, improved optical, magnetic and electrical properties [3, 4]. Following are the governing factors for the successful preparation of polymer nanocomposites:

i. Properties of the polymer used as a host matrix (crystallinity, molecular weight distribution etc.)
ii. Type of reinforcement used and type of surface treatment used to improve its surface properties for better adhesion
iii. Fabrication techniques (melt blending, solvent blending, in-situ polymerization and emulsion polymerization)
iv. Morphology of the nanocomposites

Many researchers have debated on increase in the stiffness and strength of polymers by incorporating various nanofillers [5, 6]. The degree of improvement mainly relies on the dispersion of nanofillers in polymeric matrices and the strength of nanofiller-polymer interactions. However, the effect of nanofillers on the toughness of polymers is still not completely understood. Although most of research reported the deteriorated ductility of polymers when combined with nanofillers, however some researchers found the toughening effects of nanofillers in polymers under some

specific circumstances. They have attributed this enhancement in toughness to different practical aspects like (a) improved mechanical interlocking and adhesion between nanofiller and polymeric matrices; (b) increased the mobility of nanofillers in polymeric matrices provided that the testing temperature is above glass transition temperature; and (c) change in the crystalline phase resulting from the addition of nanofillers [7].

The most famous nanofillers which had been extensively utilized in polymer nanocomposites to improve their performance are organo-clays and carbon nanotubes (CNTs). Carbon nanotubes are hollow sheets of graphite available as single wall (SWNTs) and multi wall nanotubes (MWNTs) as shown in figure 1.1. Incorporation of very low contents of carbon nanotubes has caused extraordinary improvements in thermal, mechanical and electrical properties of the polymer nanocomposites [8, 9].

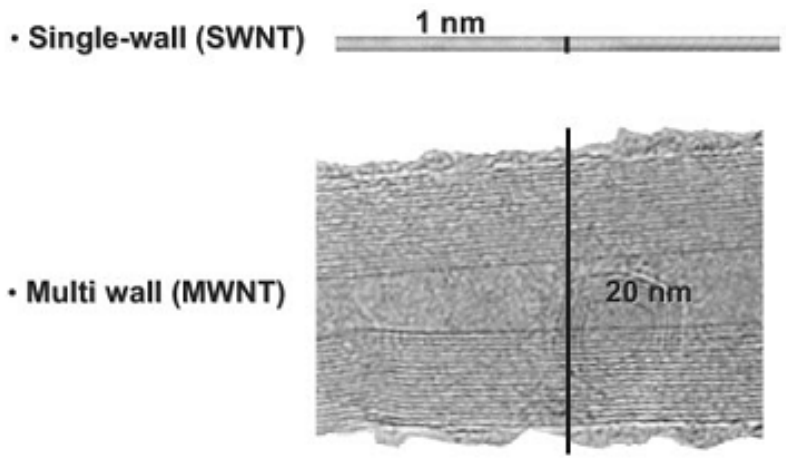

Fig.1.1 Types of carbon nanotubes (CNTs) [8]

Graphene (one atom thin sheet of carbon) has proved to be an excellent replacement for CNTs due to following properties;

i. Reduced cost than carbon nanotubes

ii. Ease of availability

iii. The resistivity of the graphene sheet is 10^{-6} Ω·cm, less than the resistivity of silver, the lowest resistivity substance known at room temperature.

iv. Natural ability to stop penetration of gas and moisture.

To exploit the practicality of this unique nanofiller, there is a need to prepare graphene (and its derivatives) and to employ them in polymer nanocomposites to improve specific properties [10]. Very recently, the development of graphene based polymer nanocomposites has been significantly driven by some research groups [11-13]. Even at a very low fraction of graphene, a great improvement in the strength and stiffness at the cost of toughness has been observed [7, 10]. We believe that still there is a lack of research in the area of exfoliation of graphite into graphene oxides and using them to improve the mechanical properties as well as the toughness, barrier and thermal properties of polymers. Given these recent results and exceptional properties of graphene, we believe that the successful exfoliation of graphene into highly exfoliated graphene oxide nanoplatelets (GONPs) and their proper dispersion in a polymer would result in a cost effective nanocomposites with outstanding mechanical, thermal and barrier properties. Considering these aspects and potential of graphene, in this project, we aimed to prepare highly exfoliated graphene oxide nanoplatelets (GONPs), named as functionalized graphene sheets in this particular research, from the expanded graphite (EG) , to prepare GONPs based nylon12 composites and to investigate their effect on crystallization behaviour, thermal, mechanical and barrier properties of nylon12.

1.2 Aims of the project

The overall objective of the project is to develop high performance FG based nylon12 nanocomposites. In order to achieve this target following aspects of the research were explored;

i. Preparation of functionalized graphene sheets (FG) from the expanded graphite. The chemical modification is believed to enhance the interfacial interaction between nanofiller and the polymer matrix.
ii. Fabrication of a series of nylon12- FG nanocomposites.
iii. Characterization of morphology of the nanocomposites.
iv. Investigation of interaction between FG and nylon12.
v. Investigation of effect of FG on the mechanical properties of nylon12.
vi. Investigation of the thermal behaviour of nylon12 and its nanocomposites.
vii. Investigation of the oxygen and water barrier properties of nylon12 and its nanocomposites.

From the technical point of view, the ambition is to develop nylon12 nanocomposites with improved mechanical, thermal and barrier properties for practical uses. The scientific goal of this research is to gain fundamental understanding of how and why functionalized graphene sheets affect the mechanical, thermal and barrier properties of nylon12.

1.3 Thesis outline

This thesis is divided into eight chapters including this introductory chapter.

Chapter 2 gives a brief introduction to general polymer nanocomposites properties, establishes background knowledge to understand the mechanism of nanofillers effecting toughness, strength, thermal and barrier properties of different polymers.

Chapter 3 describes the materials utilised in this study, as well as the preparation of FG and their nanocomposites with nylon12 powder. This chapter also gives a brief introduction of equipments used for characterization of the polymer systems under investigation.

Chapter 4 explores the effect of FG on thermal behaviour, crystalline structure, degree of crystallization and the shape of crystals of nylon12.

Chapter 5 presents the results of mechanical behaviour of nylon12 as a function of FG percentage. Isothermal frequency response of nylon12 and its nanocomposites at various temperatures has been discussed. Results for mode I fracture toughness (K_{1c}) tests have been critically highlighted in this chapter.

Chapter 6 gives a comparison of effect of various nanofillers on the toughness of nylon12.

Chapter 7 discusses the results obtained from the analysis of water and oxygen barrier properties of nylon12 and its nanocomposites.

Finally, chapter 8 presents the main conclusions of this particular project and suggests possible directions for the further research.

1.4 References

1. Gerald L. Steele. Exploring the world of plastics; 1977, chapter 1, page 6.
2. Leonard Hollaway. Handbook of polymer composites for engineers; 1994, chapter 1, page 4.
3. Joseph H. K. Polymer nanocomposites processing, characterization and applications; McGraw-Hill Nanoscience and Technology Series; 2006, chapter 1, page 9
4. Yiu-Wing Mai, Zhong-Zhen Yu, Polymer nanocomposites; CRC Press, 2006, chapter 1, page 3
5. A. K. Kaushik, , A. Ramamoorthy , A. M. Waas, B. S. Shim, B. G. Pumplin, H. Nandivada, J. Lahann, J. Xu, N. A. Kotov, P. Podsiadlo. Ultra-strong and stiff layered polymer nanocomposites. Science 2007; 318: 80-83
6. J. N. Coleman, K. Gun'ko, U. Khan. Mechanical reinforcement of polymers using carbon nanotubes. Adv Mater 2006; 18: 689-706
7. R. Rafiq, D. Cai, J. Jin, M. Song. Increasing the toughness of nylon12 by the incorporation of functionalized graphene. Carbon 2010; 15: 4309-4314
8. J.N. Coleman, U. Khan, W.J. Blau, Y. K. Gun'ko. Small but strong: a review of the mechanical properties of carbon nanotubes –polymer composites. Carbon 2006;44: 1624-1652
9. Xiong J., Zheng Z. QIN X. , LI M. , LI H. , WANG X. The thermal and mechanical properties of a polyurethane/multi-walled carbon nanotube composite. Carbon 2006; 44: 2701-2707
10. A.K. Geim , K.S. Novoselov, the rise of graphene. Nat Mater. 2007; 6: 183-191

11. S. Stankovich, R. D. Piner, R. S. Ruoff, T. S. Nguyen. Synthesis and exfoliation of isocyanate-treated graphene oxide nanoplatelets. Carbon 2006; 44: 3342-47
12. D. Cai, K. Yusoh, M. Song. The mechanical properties and morphology of a graphite oxide nanoplatelet/polyurethane composite. J of Inst. Phys. Nanotechnology 2009; 20: 85712.
13. J. Liang, L. Zhang, T. Guo, Y. Huang, Y. Wang, Y. Ma, Y. Chen. Molecular-level dispersion of graphene into poly (vinyl alcohol) and effective reinforcement of their nanocomposites. Adv. Func. Mater. 2009; 19: 2297-2302

Chapter 2

LITERATURE REVIEW

Over the past five decades, industrial scale `composite materials` have been produced by adding numerous minerals and metals to thermosetting, thermoplastic and elastomeric polymers [1]. As compared to the bulk polymers, these composites have shown moderate mechanical performance improvements in properties [1, 2] such as young's modulus, tensile strength, abrasion resistance and storage modulus. However, recent advances in nanoscale particle synthesis have dramatically accelerated the growth of the composite industry [3]. The capacity to synthesize and characterize atomic-level particles has produced a new generation of high-performance fillers. A remarkable improvement in thermal, mechanical, optical and barrier properties at the cost of very low loading of nanofillers have changed the world of composites to a great extent [3, 4]. Among the variety of polymers, polyamides exhibit high strength, toughness, and stability, and therefore have received numerous applications in fiber products and engineering plastics, and recently has found great potentials for many functional applications [5, 6]. In this chapter, an overview of various types of nylons and their nanocomposites with various nanofillers has been given.

2.1 Background of polyamides

The aim of this review is to discuss the basics of different types of nylons and to explore their commercial importance. Polyamides, also known as nylons, are melt

processable thermoplastics characterized by an amide linkage (CONH). These engineering thermoplastics offer a distinctive combination of high mechanical strength, low wear and abrasion with better chemical resistance. Nylons cover a range of material types, e.g. nylon 6, 6; nylon 6, 12; nylon 4, 6; nylon 6; nylon12 etc., providing an extremely broad range of available properties. Nylons are condensation products of equal parts of a diamine and a dicarboxylic acid, so that amides are formed at both ends of each monomer. The nomenclature of nylons is based upon the numbers of carbons; for example in nylon 6 there are six carbon atoms in its monomer unit, therefore it is named as nylon 6 [6]. The history of nylons dates back to 1905-10 when for the first time, production of polyamide 6 was reported at Gottingen university by J. Von Brown. At that time, there were efforts in progress to produce polyamide 6, 6. Pilot plant production of polyamide 6 was reported in 1940s [6]. One year later full scale production of polyamide 6 was started. The production of polyamide 6 and polyamide 6, 6 brought about an innovative change in the field of polyamides [7]. Since then, researchers have produced a variety of polyamides by using various combinations of dicarboxylic acids and diamines. Polyamides have a linear structure and their production from different methods can be represented in the following general equations [8];

1: A condensation reaction between diamines and dibasic acids produces a nylon salt [8].

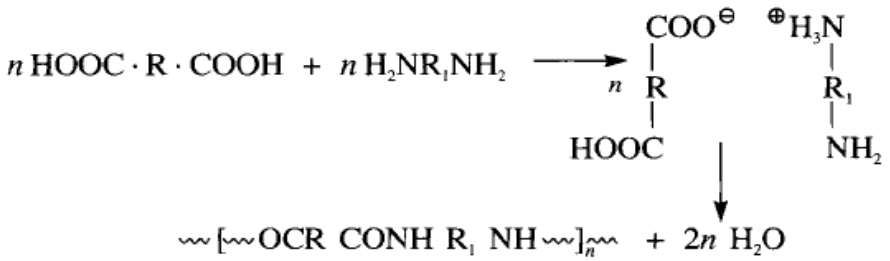

2: Self-condensation of α-amino acid.

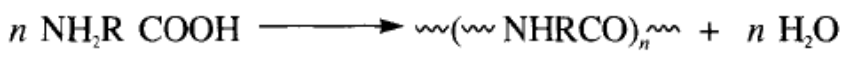

3: Opening of a lactam ring.

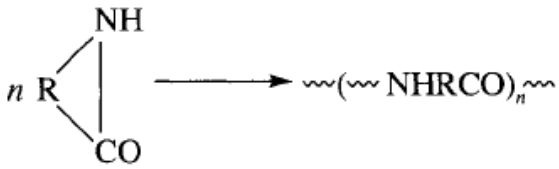

4: The reaction of diamines with di-acid chlorides.

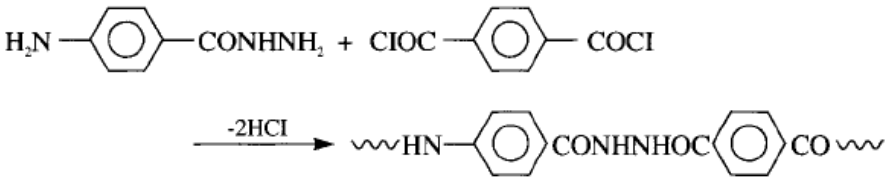

5: The reaction of di-isocyanates with dicarboxylic acids.

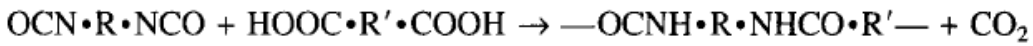

2.2 Nylon 12

Polyamide 12 (nylon 12) is a semi-crystalline engineering plastic with very high toughness and good chemical resistance for varied applications. This is named as nylon 12 because it has a straight-chain structure with acid amide groups and 12 carbon atoms in its monomer unit.

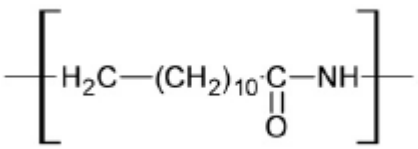

Fig.2.1 Chemical structure of nylon 12 [9]

Nylon 12 is at the 5th number in terms of overall polyamide usage. The most popular type is nylon 6, 6, followed by nylon 6, then nylon 6, 12, nylon 11 and nylon12 [6].

The properties of nylons are mainly dependent upon their ability to crystallize and absorb moisture. Hydrogen bonding between carbonamid groups (-CO—NH-), present along the polymer chain, gives rise to the crystallinity. This hydrogen bonding is depicted in figure 2.2. Nylons made of diamines and dibasic acids (like nylon 6.6) tend more to crystallize than those prepared of amino acids or lactams (like nylon12) because of their higher ratio of CH_2 /CONH-groups which actually is the quotient of the molecular weight of the CONH- groups and molecular weight of the molecule chain. This quotient tells us at how many points chains are reversibly linked by hydrogen bonding. The quotient values for nylon 6, 6, nylon 6 and nylon12 are 0.38, 0.35 and 0.21 respectively. Since water is bonded to CONH groups therefore higher ratio of CH_2 /CONH-groups means enhanced water absorption. Also water absorption has a plasticizing effect on nylons which results in deteriorated properties [10].

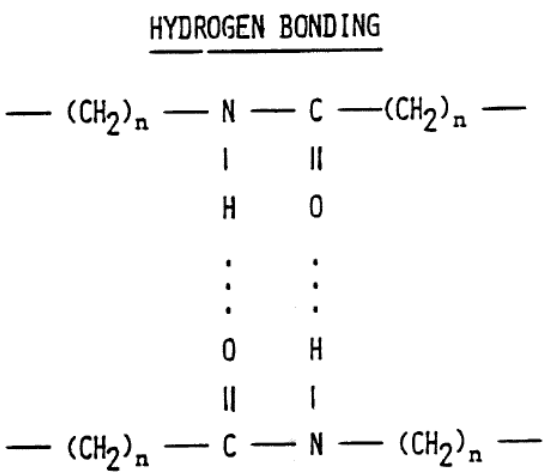

Fig.2.2 Hydrogen bonding in nylon [10]

A comparison of moisture absorbance between nylon 6, 6, nylon 6 and nylon12 is shown in figure 2.3. Hence nylons with higher CH_2 /CONH ratio (like nylon 6, 6 and nylon 6) will tend to be more moisture adsorbent as compared to nylon 12 with lower CH_2 /CONH ratio which is also prominent in figure 2.3. As mentioned above although nylon12 is less hygroscopic but at the same time it is less crystalline as well which results in decreased mechanical properties as compared to other important types of nylon. Hence efforts must be made to improve the mechanical performance of nylon12.

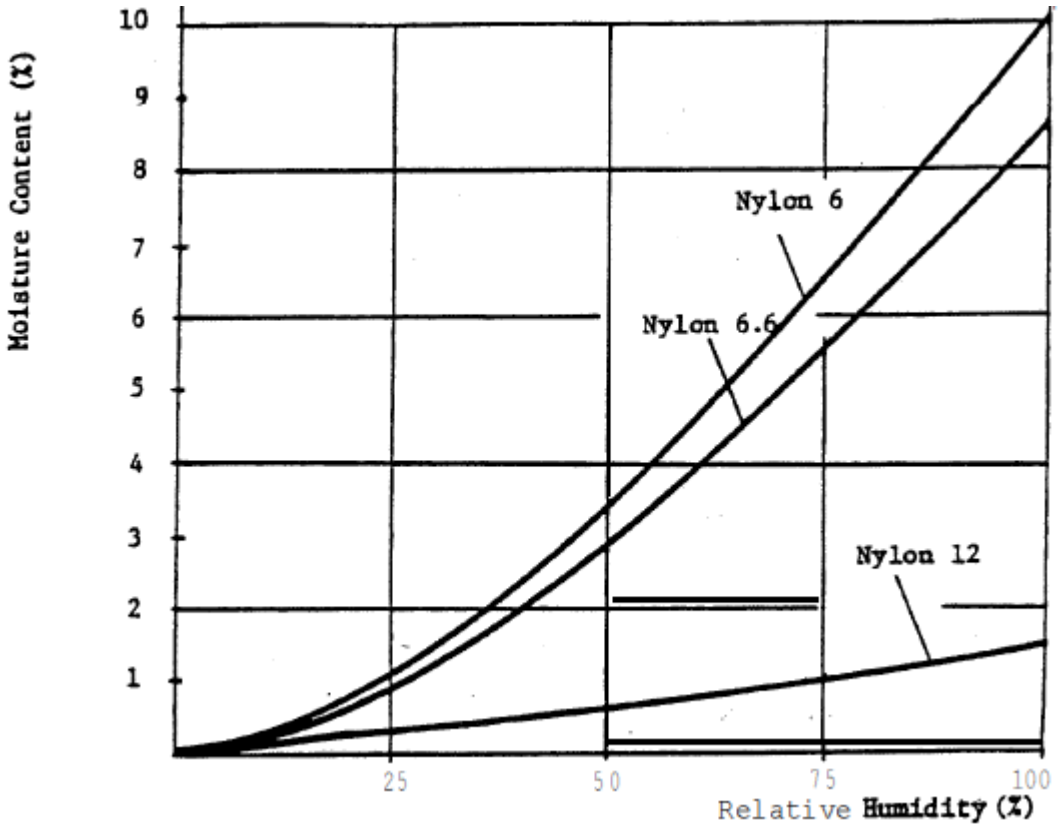

Fig. 2.3 Moisture absorbance versus relative humidity for different nylons [10]

In this study, we chose nylon12 as polymeric matrix because it does not only give the better mechanical properties, such as hardness, tensile strength, and resistance

to abrasion, of the well-known polyamides i.e., of nylon 6 and 6, 6, but also have comparable water-sensitivity and density to polyolefins. Although nylon12 has the lowest melting point among all the important polyamides but still it is good enough for the practical applications [12]. There is no appreciable change in glass transition temperature (T_g) with increase in carbon chain length. Furthermore, nylon12 has the lowest density among the popular types of nylon [11, 12].

Nylon 12 is commonly used in transport and conveyor technology, food technology, textile, packing and paper processing machinery, printing and drinks dispensing machinery, electrical engineering and the automotive industry. Some miscellaneous applications of nylon12 are;

- Conveyor screw sleeves
- Friction strips
- Gear wheels
- Fan impellors
- Castors
- Impact plates
- Cutting pads
- Friction bearings
- Housing parts
- Switch parts
- plug parts
- Damping plates
- Swimwear
- Food packaging (blown nylon12 films)
- Clothing (socks etc)

In this particular research, nylon12 was chosen as polymeric matrix because of its outstanding multidimensional and comparable properties to other types of nylon. In the last few years, several researchers have used nylon 12 as a matrix in their particular composites studies [9, 13-16]. Their work was focused on improving electrical, barrier, mechanical and thermal properties by using variety of fillers/ nanofillers individually. There is a very few literature available on multiproperty enhancement of nylon 12 by combining it with multifunctional fillers (nanofillers). This is what tempted us to prepare and characterize nylon12 composites which not only had improved strength, better thermal characteristics and good water/ oxygen barrier properties but also had better toughness characteristics.

2.3 Reinforcements for nanocomposites

Use of carbon nanotubes (CNTs) as reinforcement brought a revolution in the world of polymers. These nano-sized, nearly perfect whiskers (known as nanotubes) were first noticed and fully characterized in 1991 by Sumio Iijima of NEC Corporation in Japan [17]. CNTs are unique nano-structured materials with remarkable physical and mechanical properties. These properties have encouraged interest in using CNTs as filler in polymer composite systems to obtain ultra-light structural materials with improved electrical, thermal and optical characteristics. A carbon nanotube is a hexagonal network of carbon atoms rolled up into a seamless, hollow cylinder, with each end capped with half of a fullerene molecule. Although similar in chemical composition to graphite, CNTs are highly isotropic, and it is this topology that distinguishes nanotubes from other carbon structures and gives them their unique properties. There are two main kinds of nanotubes: single-walled nanotubes (SWNTs), individual cylinders of 1-2 nm in diameter, which are actually a single molecule; and multi-walled nanotubes (MWNTs), which are a collection of several

concentric graphene cylinders, a “Russian doll” structure, where weak Wander Waals forces bind the tubes together [18,19]. A schematic of these species is shown in figure 2.4.

The first CNTs based polymer nanocomposite was developed in 1994 [20]. Since then an extensive research and development has been devoted for using CNTs to improve various properties of the polymers [21-23]. At the present many researchers are interested in modifying the properties of polymer nanocomposites and reducing the cost of production. Although CNTs based polymer composites have been a hot topic in this context but it is being obsolete because of its economical drawbacks.

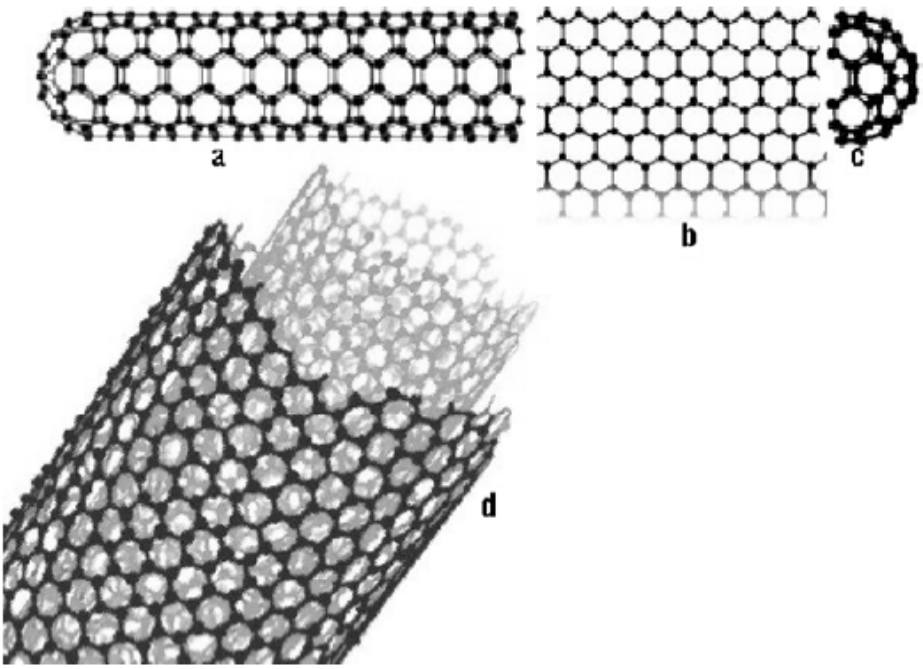

Fig.2.4 Schematics of a (a) single-walled carbon nanotube, (b) a graphite sheet , (c) a hemispherical end cap and(d) a multiwalled carbon nanotube The solid circles in each figure represent the carbon atoms [18]

The role of CNTs in polymer nanocomposites has been limited by the use of graphene sheets which are cheaper and have comparable mechanical, thermal,

barrier properties to CNTs. Graphene is the name given to a flat monolayer of carbon atoms tightly packed into a two-dimensional (2D) honeycomb lattice, and is a basic building block for graphitic materials of all other dimensionalities [24]. The basics of graphene are shown below in figure 2.5.

Although a comparable mechanical and electrical property improvement has been reported for CNTs and graphene but graphene based nanocomposites are believed to provide greater thermal conductivity and better barrier properties. The multifunctional property enhancement with graphene coupled with the potential of cheap and abundant production makes graphene a better choice than CNTs. A comparison of selected physical and mechanical properties of graphene and CNTs are presented in Table 2.1 [25].

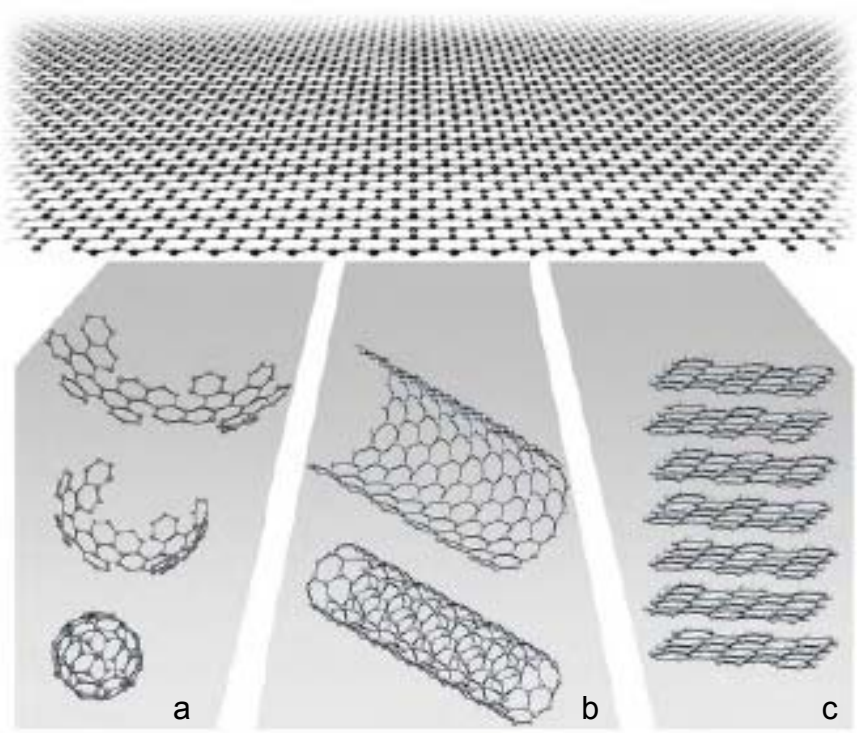

Fig.2.5 Mother of all graphitic forms. Graphene is a 2D building material for carbon materials of all other dimensionalities. It can be wrapped up into (a) 0D buckyballs, (b) rolled into 1D nanotubes or (c) stacked into 3D graphite [24]

Graphene sheets in graphite are strongly bonded with each other and have a little spacing between each other. Therefore, it is very difficult to strip graphene sheets from graphite. Expandable graphite (EG), also known as a graphite intercalation compound, is produced by intercalating sulphuric acid into natural flaked graphite via chemical or electrochemical processes [26]. Due to intercalation of these atoms and molecules, d- spacing of EG increases [27]. Therefore oxidants can penetrate easily into d-spacing which favours exfoliation of EG to expandable graphite oxide (EGO) [28]. For the first time in 1958, W. S. Hummers and R. E. Offema reported the production of graphitic oxide which was the first practical step towards production of graphene. They treated graphite with water free mixture of sulphuric acid (H_2SO_4), nitric acid (HNO_3) and potassium permanganate ($KMnO_4$) [29]. Recently Titelman et al. [30] developed highly oxidized graphite oxide (GO) from natural graphite powder by oxidation with KM_nO_4 in concentrated H_2SO_4 followed by hydrolysis, washing and centrifugation.

Property	CNTs	Graphene
Specific gravity	0.8 g/cm^3	1.8–2.2 g/cm^3
Elastic modulus	~1 TPa (axial direction)	~1 TPa (in-plane)
Strength	50–500 GPa	~100–400 GPa
Resistivity	5–50 μΩ cm	50 μΩ cm (in-plane)
Thermal conductivity	Up to 2,900 Wm^{-1} K^{-1} (estimated)	5,300 Wm^{-1} K^{-1} (in-plane) 6–30 Wm^{-1} K^{-1} (c-axis)
Magnetic susceptibility	22 × 10^6 emu/g (radial) 0.5 × 10^6 emu/g (axial)	22 × 10^6 emu/g (⊥ to plane); 0.5 × 10^6 emu/g (∥ to plane)
Thermal expansion	Negligible in the axial direction	−1 × 10^{-6} K^{-1} (in-plane) 29 × 10^{-6} K^{-1} (c-axis)
Thermal stability	>700 °C (in air); 2800 °C (in vacuum)	450–650 °C (in air)
Specific surface area	Typically 10–200 m^2/g Up to 1,300 m^2/g	Typically 100–1,000 m^2/g, up to >2,600) m^2/g

Table 2.1 Comparison of physical properties of CNTs and graphene [25]

Concentrated gel like dispersions were prepared, filtered, washed and analyzed using various characterization techniques like small angle X-ray scattering, X-ray diffraction, light scattering (LS), Scanning Electron Microscopy and Fourier Transform Infrared Spectroscopy (FTIR).

O.Y. Kwon et al. [31] prepared exfoliated graphite from the microwave treatment of graphite - sulphur trioxide (SO_3) intercalated compounds. The compounds, prepared by the direct reaction of graphite and SO_3, were named as graphene intercalated compounds (GIC). B. Tryba et al. [32] also used microwave irradiation to prepare exfoliated graphite and reported the effect of varying microwave power, type of intercalation and graphite precursors. Two residual compounds were prepared from electrochemical intercalation and chemical intercalation respectively and their degree

of exfoliation was studied. For comparison, both graphite precursors were also exfoliated by a rapid heating to 1000°C. It was concluded that graphite exfoliated using microwave irradiation can give comparable properties to the one exfoliated with rapid heating to1000°C. Novoselov and his co-workers [24, 33] prepared single sheet graphene by using scotch tape method to peel graphene from graphite one sheet at a time. Although this method is not acceptable for the large-scale production of graphene, yet their work was good enough to be adopted for laboratory scale production of individual graphene sheets and to use them for improving electric conductivity of polymers. For the commercial scale production of graphene and its derivatives, techniques which involve chemical or thermal exfoliation of graphite or graphite oxides, have been more likely to be used. Stankovich and his co-workers [28] treated graphite oxide (GO) with organic isocyanates. They called treated GO as isocyanate treated GO (iGOs). They prepared stable suspensions of these iGOs in polar aprotic organic solvents. FTIR and elemental analysis study of iGOs proved that isocyanate treatment imparted some carboxyl and hydroxyl groups in GO via formation of amides and carbamate esters, respectively as shown in figure 2.6. These iGOs were exfoliated in N,N-dimethylformamide (DMF) to form graphene oxide nanoparticles.

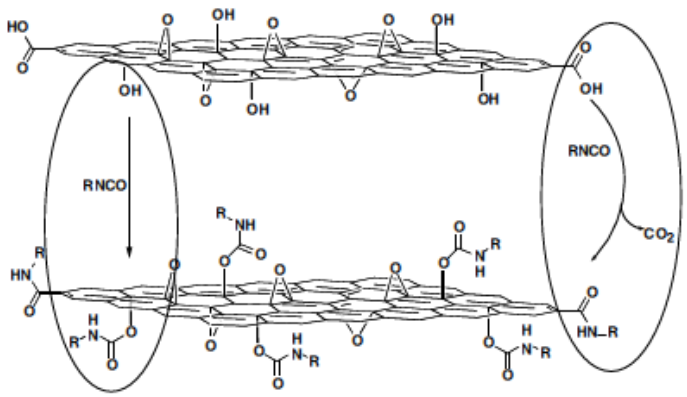

Fig.2.6 Chemical modification of graphite oxide (GO) to isocyanate treated GO [34]

Chen et al. [34] expanded natural flake graphite into exfoliated graphite via an acid intercalation procedure. The resulting exfoliated graphite was a worm-like particle composed of graphite sheets with thickness in the nanometre scale. Ultrasonic irradiation was further used for complete exfoliation of these graphite particles into isolated graphene nanosheets. H.C. Schniepp, J.L. Lie et al. [35] used thermal exfoliation to obtain conductive functionalized graphene sheets from naturally flaked graphite. Graphite was treated with oxidizing solution of sulphuric acid, nitric acid, and potassium chlorate for more than 92 hours which produced highly oxidized graphite (GO). Degree of oxidation was confirmed using X-ray diffraction. Rapid heating of GO at 1030°C caused evolution of CO_2 which resulted in individual separation of graphene sheets. Wander wall forces, as discussed above, in graphite hold graphene sheets together. When dried GO is heated to such a high temperature; decomposition of epoxy and hydroxyl sites takes place which results in increase in CO_2 emission. When the pressure of this evolving gas is more than the wander wall forces holding graphene sheets together in graphite then exfoliation takes place [36]. This degree of exfoliation was quantified by measuring surface area and using atomic force microscopy (AFM).

Song et al. [37] proved that chemical treatment is not an essential step for the conversion of GO into GONPs using polar organic solvent. They prepared GO by Hummer's method [29] and confirmed the exfoliation of expanded graphite (EG) into GO by using X-Ray photoelectron spectroscopy (XPS). Elemental analysis results revealed that atomic ratio of C/O in GO decreased about 76% as compared to untreated expanded graphite. This decrease in ratio confirmed the oxidation of EG into GO using Hummer's method. Then they used strong ultrasonic treatment to exfoliate GO in an organic solvent called DMF. A suspension of EG and DMF was

also prepared under the same conditions as that of GO. After two months of ultrasonic treatment; they found out that EG particles were settled down while GONPs were still there as such. The settling down of EG particles shown in digital picture has been depicted in the figure 2.7. The ability of GONPs to form a stable suspension with organic liquid proved that GONPs can also be fully exfoliated in the organic solvents. TEM analysis was performed to figure out the existence of GONPs in DMF, which is shown in figure 2.8.

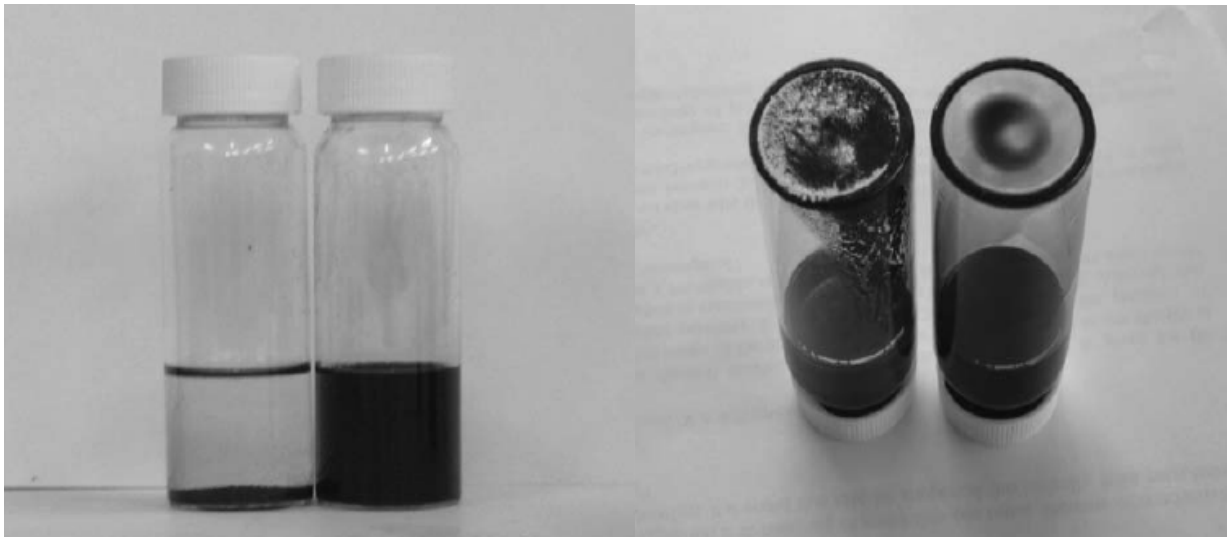

Fig.2.7. Digital pictures of EG/DMF (on the left) and GONPs/ DMF (on the right hand side) taken after two months of ultrasonic treatment [37]

Horiuchi and co-workers [38] have a significant contribution in the preparation of graphite oxide nanoplatelets which they named as" carbon nanofilms ". Their method of production of these nanofilms was also based upon two common steps (a) preparing graphite oxide using Hummer's method and (b) purification of GO to obtain graphite oxide nanoparticles. They claimed that in the first step acidic groups were introduced between layers of graphite and later purification forced the sheets to

separate from each other due to interlayer electrostatic repulsion. The resultant GO sheets were then exfoliated in water.

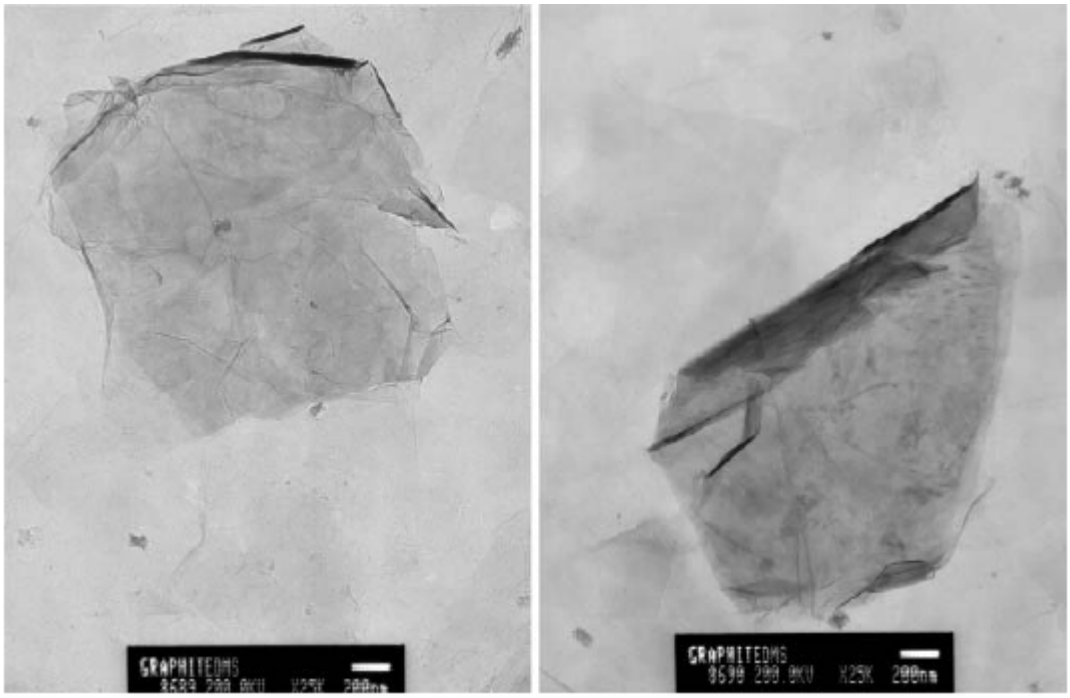

Fig.2.8. GONPs suspended in DMF [37]

The production of graphene from graphite directly and from its derivative (GO) has been summarised in the following block diagram (figure 2.9);

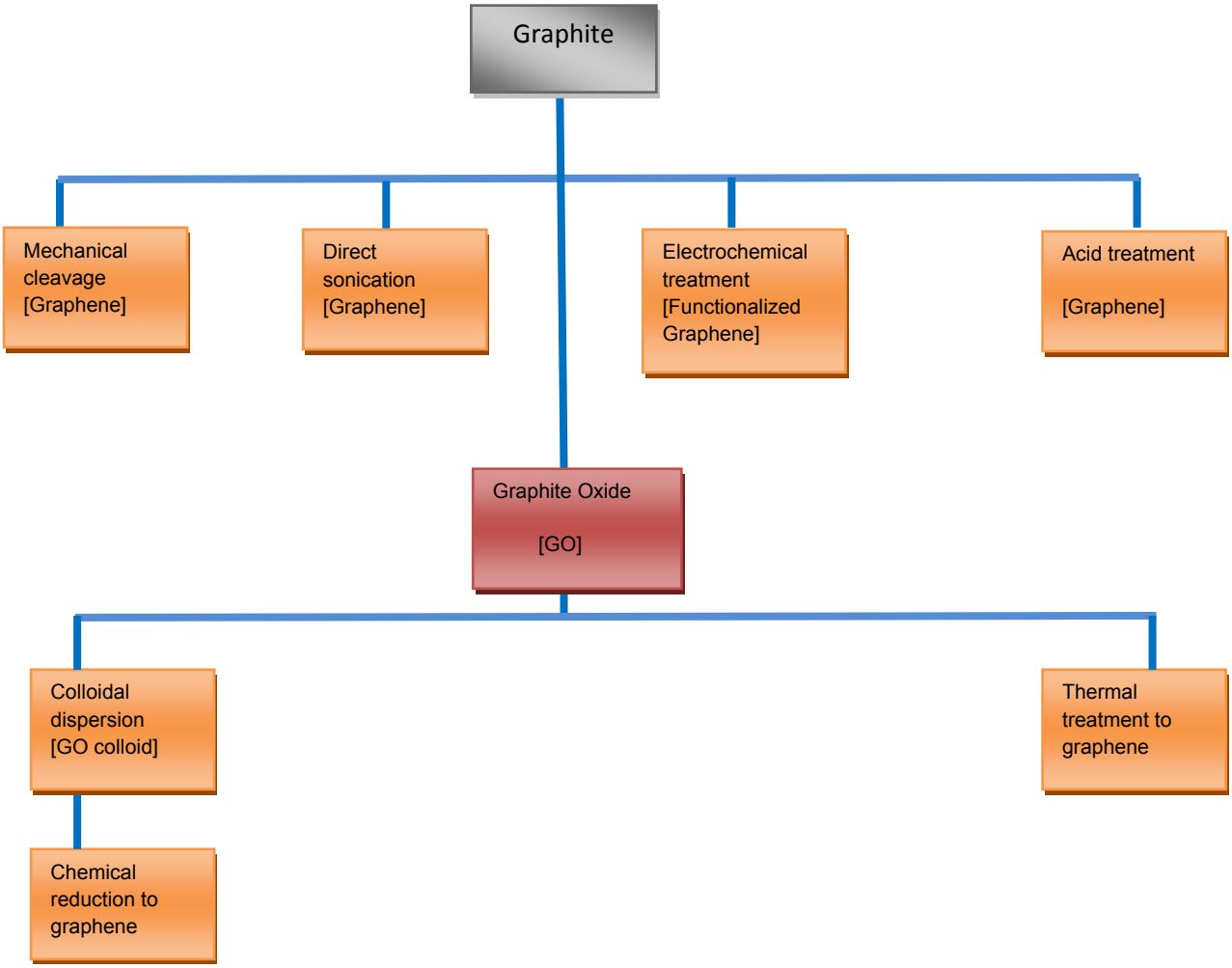

Fig.2.9. Methods for production of graphene [36]

The graphene sheets produced from thermal reduction of graphite has an advantage to produce chemically modified graphene sheets without the need of dispersion in a solvent. But at the same time cost of heating, smaller sheet size and higher carbon to oxygen ratio of graphene sheets are the disadvantages of this technique. The chemical reduction of GO to graphene is also a compatible method which leaves significant oxygen as compared to thermally treated graphite. Although these suspensions of GO can be used to prepare polymer/ GO nanocomposites but poor thermal stability of GO, hazardous nature and cost of chemicals used are the major

drawbacks of this process [36]. A brief discussion of various techniques used for the preparation of graphene sheets concluded that all those routes which start from preparation of GOs and then their exfoliation in different solvents are the most promising ones.

The above discussion about various methods for production of graphene exposed that the complete exfoliation of GO to graphene has not been achieved yet by any of the known methods e.g. thermal treatments, dispersion of GO in polar solvents followed by the sonication, etc. To achieve this goal, we attempted to prepare highly exfoliated GONPs using recently patented Song's method. GO was produced from expanded graphite using Hummer's method and was, then, exfoliated in the water to achieve graphene sheets.

2.4 Preparation methods of polymer/ graphite nanocomposites

The production of graphene and its composites has been a frontier area of interest for a significant number of researchers. This is shown in the figure 2.10.

In an attempt to prepare graphene based composites several techniques had been applied which can be broadly classified into three basic approaches [25]. The first approach includes intercalation of monomers into inter layer spacing of GO followed by in-situ polymerization. The second approach involves dissolution of polymer in a GO dispersed solution called as solution blending. In the third method exfoliated graphene oxide platelets or graphene is mixed with polymer using melt blending.

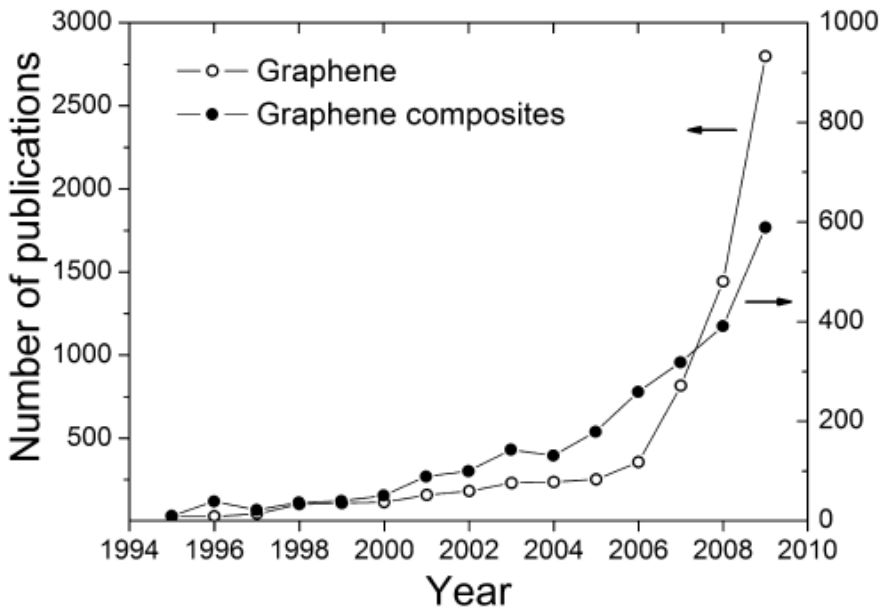

Fig.2.10 Research on graphene and its composites in recent years [36]

In in-situ intercalative and/or exfoliation polymerization, the layered expanded graphite or exfoliated graphite nanosheets are swollen within the liquid monomer or a monomer solution, so that the polymer formation can then occur in between the intercalated graphite sheets or graphene layers. Once this intercalation process of monomers into graphite is completed then polymerization can be started. The polymerization can be initiated either by heating or radiation, by the diffusion of a suitable initiator or by an organic initiator inside the interlayer of graphite after the swelling step by the monomer. During polymerization the monomers in the gallery spaces of graphite are gradually converted into polymer. This conversion of monomers into polymer creates space for more monomer to enter to these galleries hence resulting in more delamination and exfoliation of graphite sheets. The advantage of this technique is that a well-dispersed intercalated or exfoliated polymer/graphite nanocomposite is generally obtained. Under this process the nanocomposites can also be prepared through emulsion polymerization where expanded graphite is well dispersed in the aqueous phase [39, 40]. Figure 2.11 is a

schematic illustration of the exfoliation process of expanded graphite during in-situ polymerization.

The solution blending approach to prepare graphite based polymer composites involves exfoliation of expanded graphite using a solvent in which the polymer is soluble. This exfoliation of graphite produces graphene sheets (bundles) and single graphene layers. In this method the polymer and expanded graphite are dispersed in a solvent. The expanded graphite, because of its very weak forces that bond the graphene layers together, can be easily dispersed in an adequate solvent. Intensive stirring such as sonication is employed to enhance the degree of dispersion of graphite into the polymer solution. When the solvent is evaporated polymer is intercalated into the gallery spaces of graphite. Resultant is an ordered multilayer polymer composite where polymer chains are sandwiched between graphene sheets [40, 41].

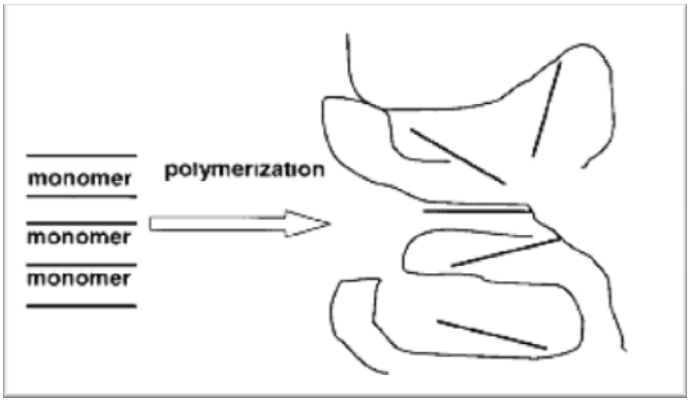

Fig.2.11 Exfoliation of graphite during in-situ polymerization [39]

In the melt blending (melt intercalation) technique expanded graphite (or its derivatives) are blended with the molten polymer. At an optimum melting temperature, appropriate mixing time and speed of blades and if the layered

surfaces of expanded graphite are sufficiently compatible with the selected polymer, the polymer can be inserted into the interlayer space and form either an intercalated or an exfoliated nanocomposite [41]. In our work, nanocomposites were also fabricated by melt blending due to its simplicity and compatibility with the existing polymer processing techniques which resulted in well dispersed composites of nylon 12.

2.5 Morphology of polymer/ graphite nanocomposites

Possible structures of graphite / polymer nanocomposites, depending upon the type of graphite (graphite oxide, expanded graphite, graphene nanoplatelets or graphene sheets) and the polymeric matrix used, are shown below in figure 2.12.

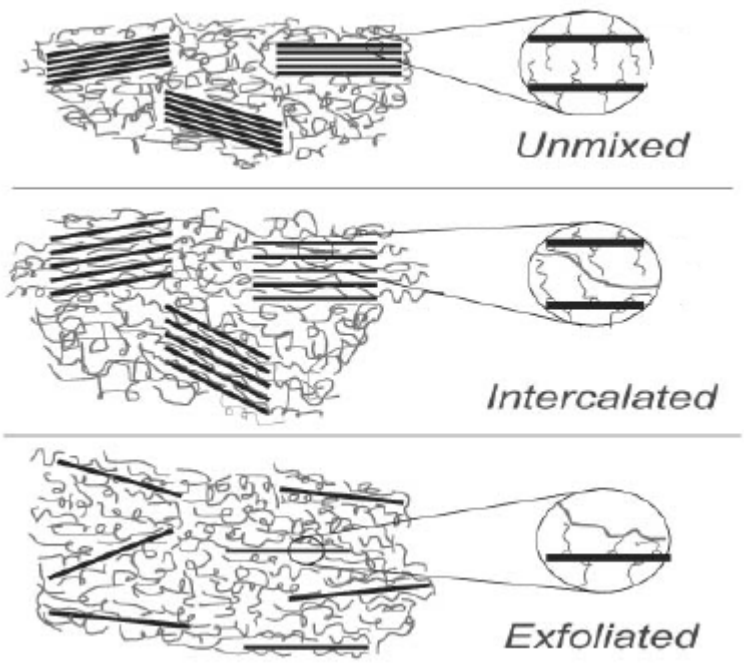

Fig.2.12 Illustration of possible structures of polymer /graphite composites [43]

Possible structures of these nanocomposites can be studied by various microscopy techniques like SEM and TEM. The layered structure of functionalized graphene sheets remains unchanged even when it has been dispersed in the polymeric matrix as confirmed by the SEM images. Figure 2.13 gives a comparison between expanded graphite (EG) and functionalized graphene sheets (FGS) based PMMA nanocomposites. Although the layered structure of both the fillers has not been affected in the dispersed phase but it is clear that FGS has a stronger interfacial adhesion with PMMA because of its surface chemistry [44].

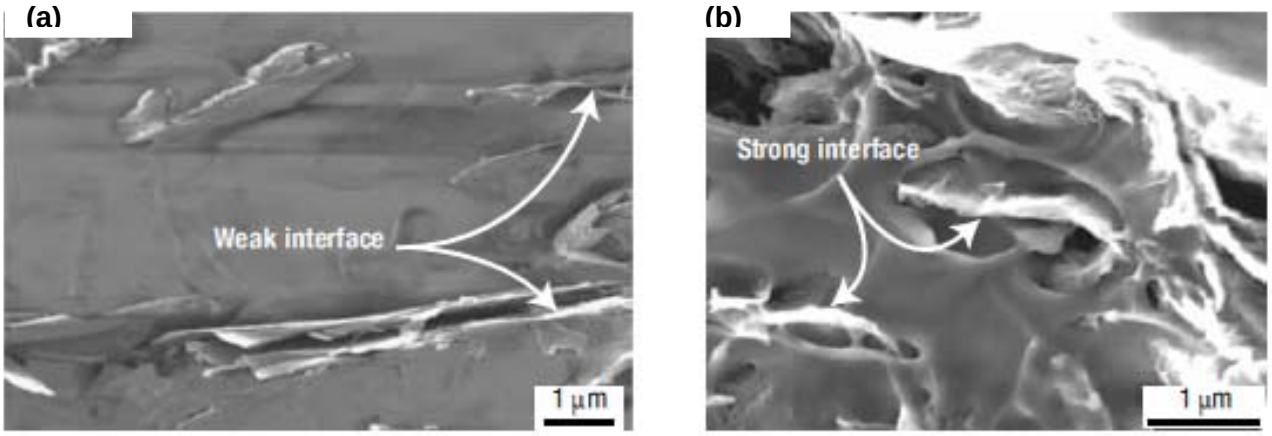

Fig.2.13 SEM images of (a) EG –PMMA and (b) FGS- PMMA nanocomposites representing how surface chemistry results in better interfacial adhesion [44]

Transmission electron microscopy (TEM) studies confirmed the random dispersion of graphite based fillers in various polymeric matrices. Fawn M. et al. [27] used melt blending to prepare expandable graphite (EG) / polyamide 6 (PA-6) nanocomposites. TEM confirmed the well dispersed graphite layers in PA-6 as shown below in figure 2.14.

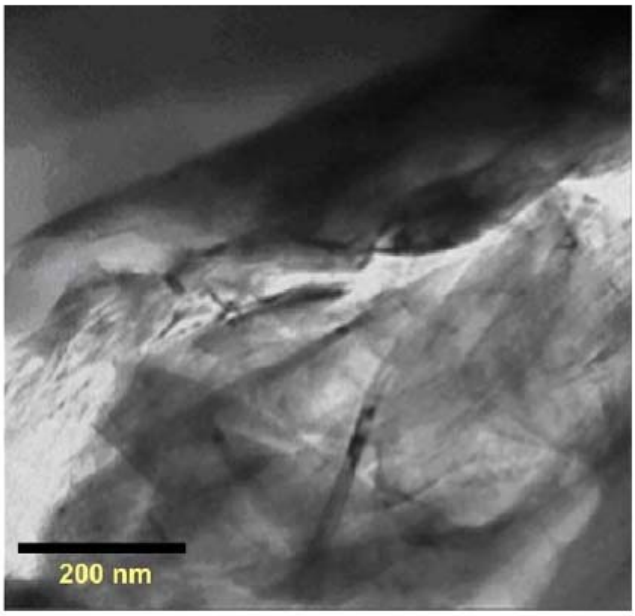

Fig.2.14 TEM image representing dispersion of EG in PA-6 [27]

Morphology of polystyrene – graphite nanosheets composites prepared via in-situ polymerization was also studied with the aid of TEM [45]. Results indicated that graphite nanosheets were successfully dispersed in the polystyrene matrix as shown in figure 2.15;

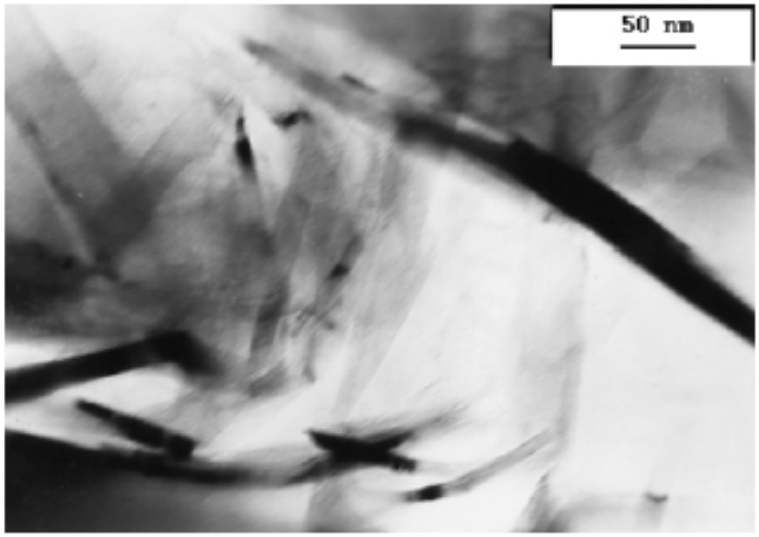

Fig.2.15 TEM image confirming dispersion of graphite nanosheets in polystyrene [45]

In conclusion TEM and SEM had been extensively used to investigate the morphological features of graphite based nanocomposites and hence were used in our work too.

2.6 Toughness of polymer nanocomposites

Energy absorption capability (toughness) during fracture is a crucial property of structural materials for several reasons. It is defined as the amount of energy per unit volume which a material absorbs before fracture. For example, in the design of automobiles, rail cars, aircraft and rotorcraft structural crashworthiness is now an essential requirement. The ability of a structure to absorb shock is designed such that in the event of a crash, it absorbs the impact energy in a controlled manner before the energy gets transmitted into the passenger compartment [46]. Traditionally, metals had been used for this purpose because of their higher toughness and hence their ability to absorb the shock in a controlled way. Polymers or traditional polymer composites do not have such an energy absorption capability that they can compete with metals during such structural applications. Polymer nanocomposites can provide an alternative for these special sudden shock absorbing applications under some special circumstances. Recent studies on improving energy absorption capability of polymer nanocomposites are based on the experimental results. The results have been quoted by varying several design parameters like type, size and shape of the filler, change in the filler concentration and different matrices etc [47, 48]. There is a lack of analytical and numerical analysis on how nanofillers affect the toughening behaviour of the polymers. Although a lot of polymer nanocomposites with a variety of fillers and matrices have been developed but the research on toughened nanocomposites is still in its early years. There are several reasons for this: (1) lack of acceptable evaluation

parameters and methods for energy absorption capability of nanocomposites, such as evaluating indicators, test methods and test conditions; (2) lack of theoretical models that can predict the energy absorption capability; (3) lack of a systematic comparison of limitations and advantages among the existing research methods; (4) lack of a fundamental understanding of energy absorption mechanisms in nanocomposites; (5) need to search potential applications of energy-absorbing nanocomposites [46].

To evaluate the energy absorption capability of the materials various parameters have been studied. They include impact strength, notched Charpy or Izod impact toughness, fracture toughness, strain energy release rate, fracture energy, essential work of fracture, non-recoverable area under the stress–strain curve and loss modulus or loss factor during vibration [46,49,50,51].

There are actually three different types of fracture toughness parameters, K_{IC}, K_{IIC}, and K_{IIIC}. All three are used to measure a material's fracture toughness of a sample that has a thickness that is greater than some critical value, B. When the material's thickness is less than B, and stress is applied, the material is said to be in a state of plane stress. The differences between K_{IC}, K_{IIC}, and K_{IIIC}, however, do not depend on the thickness of the material. Instead, K_{IC}, K_{IIC}, and K_{IIIC} are the fracture toughness of a material under the three different modes of fracture, mode I, mode II, and mode III, respectively. The different modes of fracture I, II, and III are all illustrated in figure 2.16. Among three of the above, mode I fracture toughness (K_{IC}) is the one of most reported parameters in the context of toughness characterization. K_{IC} is a quantitative way of expressing a pre-cracked material's resistance to fracture [52, 53]. A higher value of K_{IC} corresponds to the better ductility of the material.

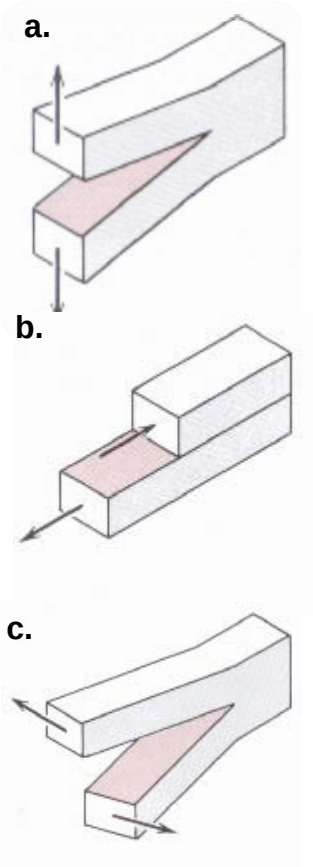

Fig.2.16 (a) Mode I fracture (**b)** Mode II fracture **(c)** Mode III fracture[52]

In our work, we focused on characterizing the toughness of our systems using three different ways; (i) calculating area under stress strain curve which is an indication of toughness, (ii) failure energy taken from falling weight impact tester (IFWIT) under sudden impact of a known weight from a constant height and (iii) analysis of Mode I fracture toughness (K_{IC}).

Indeed most of the research reveals that nanofillers cause a significant improvement in strength and stiffness. However, enhancing the toughness of polymers, by adding

nanofillers, is still in debate [54-56]. Strength and toughness are both desirable properties of a material, however, toughness is considered to be more important than strength in many structural applications.

Although most of research reported the deteriorated ductility of polymers combined with nanofillers, some researchers found the toughening effects of nanofillers in polymers under some specific circumstances. They have attributed this enhancement in toughness to different practical aspects like (a) improved mechanical interlocking and adhesion between nanofiller and polymeric matrices; (b) increased mobility of nanofillers in polymeric matrices providing the testing temperature is above glass transition temperature; and (c) change in the crystalline phase resulting from the addition of nanofillers. Intensive reviews have also been prepared relating to polymer/nanofiller interaction, in an attempt to understand the toughening mechanism in polymer composites [57-59]. Unfortunately, fracture toughness and ductility of nanocomposites usually are known to deteriorate because of the presence of the rigid, inorganic nanofillers. It is not yet known the exact fundamental causes for such significant drops in fracture toughness and ductility. It is possible that either polymer nanocomposites inherently contain incomplete dispersion of nanoparticles, which form aggregates, that cause premature crack formation, or the presence of nanoparticles restricts molecular mobility of the surrounding matrix material which might lead to embrittlement [57-59].

In semicrystalline polymer nanocomposites hard and nearly spherical particles can, in the right size volume combination, increase the toughness. Liu et al. [60] prepared HDPE nanocomposites by the incorporation of rigid nanofiller ($CaCO_3$) by using a coupling agent. Based on results of Izod impact testing of pre-notched samples, an increase in toughness of HDPE was claimed. Moreover the optimum weight ratio of

coupling agent to $CaCO_3$ particles for achieving the highest toughening efficiency was found to be about 0.05, which was claimed to be independent of the particle diameter (d), volume fraction (V_c) and size distribution of $CaCO_3$ particles. They believed that the shear yielding of the polymer matrix induced by debonding at the interface between $CaCO_3$ and HDPE was the major toughening mechanism.

The effect of different shaped nanofillers, particles, tubes and platelets, has been studied by several researchers. Generally it was found that the layer- shaped nanofiller especially clays on their own did not have the ability to toughen the polymeric matrices. Gam et al. [61] studied the morphology and fracture mechanisms of nanoclay-filled epoxy systems with the aid of microscopic and spectroscopy tools. Although addition of clay improved strength and stiffness but it failed to improve toughness of the matrix. They concluded that upon addition of core-shell rubber (CSR), one of the most effective rubber tougheners, a significant improvement in impact energy (toughness) can be achieved. Shear yielding of the matrix, cavitation of CSR were concluded to be the operative toughening mechanisms. The same deterioted toughness effect was observed when clay (2, 4 and 6% montmorillonite) based high density polyethylene (HDPE) nanocomposites were prepared by melt blending. Fracture toughness of 6% clay filled HDPE was the minimum. Addition of an elastomer (maleated styrene–ethylene–butylene–styrene) to clay based HDPE composites enhanced their toughness. Again shear yielding of HDPE was believed to be the toughening mechanism [61].

Very recently it has been claimed by Ramsaroop et al. [62] that it is not the geometry of clay which is hindrance towards its toughening ability. They claimed that it is the type of nanocomposite produced i.e. exfoliated or intercalated. They prepared polypropylene (PP) composites filled with nanoclay at various concentrations (1, 2, 3,

4 and 5 wt %) by using melt blending extrusion method. It was observed that up to 3 wt% nanoclay in the PP matrix, an exfoliated structure was formed and further addition of nanoclay formed an intercalated structure. Even though the fracture toughness parameter (K_{IC}) continuously increased as clay content increased in the nanocomposites, the rate of increase was reduced at higher clay content due to intercalated structures that affected the net aspect ratio of the clay platelets. It was found that at 5% clay loading the nanocomposites goes through brittle deformation while at 3% nanocomposites show rather extended and elongated deformations before failure. The structural change in composites upon the addition of clay is manifested in SEM results (figure 2.17).

Similar findings of improved toughness as a function of nanocomposite morphology were reported by Kim et al. [63]. They prepared intercalated and exfoliated nanocomposites of nylon 6 by using organoclay (3.2 wt %) as reinforcement. TEM results revealed that for the same loading of the clay, the degree of exfoliation increases with the molecular weight of the polymer matrix. Hence with a higher molecular weight matrix a well-defined exfoliated morphology can be observed in the nanocomposite. Whereas the nanocomposite with a low-molecular-weight matrix resulted in a partially exfoliated morphology. Impact strength of exfoliated nanocomposite (based on high molecular weight nylon 6) was reported to be improved while that of the low molecular weight composite (intercalated) was found to be decreased by 10% as compared with untreated nylon 6.

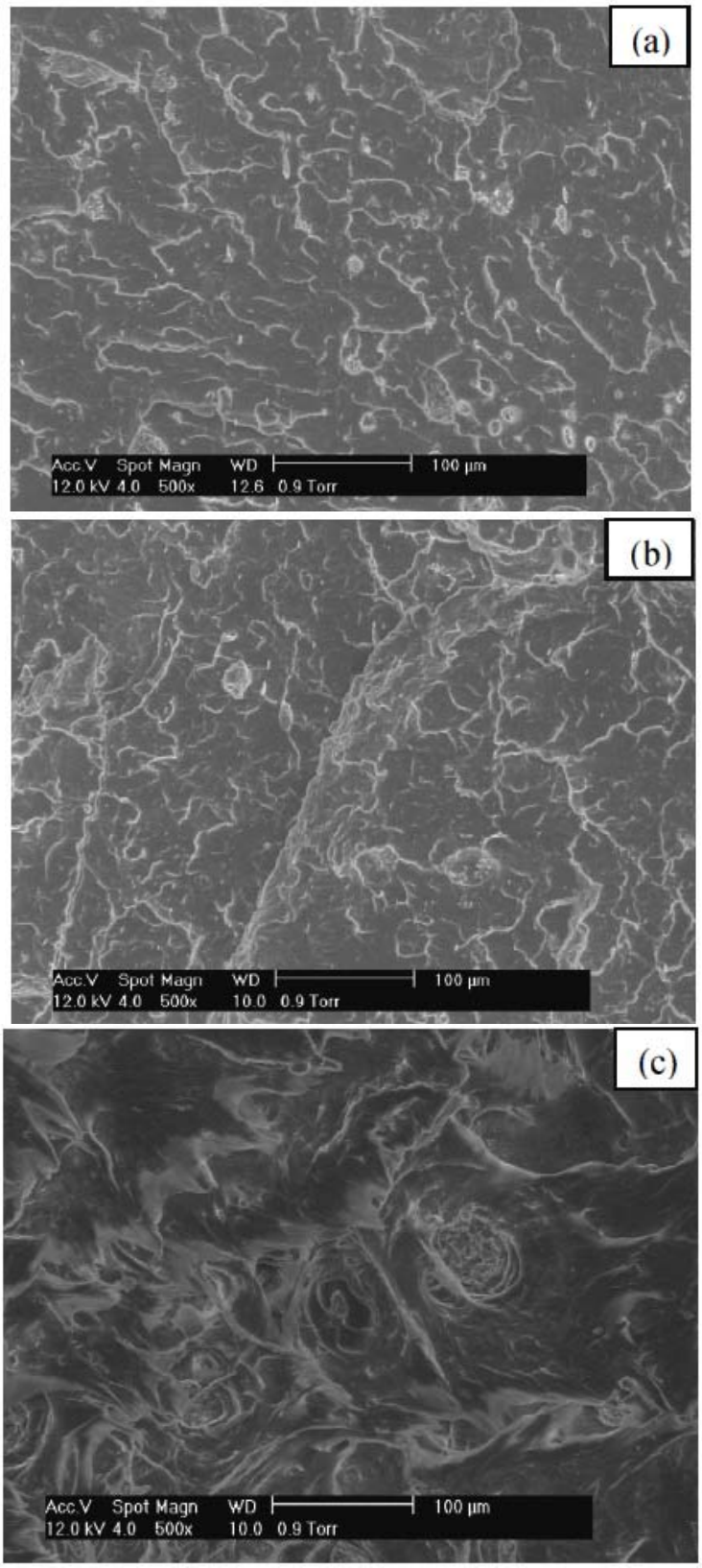

Fig.2.17 SEM of fractured surface of (a) PP, (b) PP with 5 wt.% nanoclay and (c) PP with 3 wt. % nanoclay [62]

T. D. Fornes and D. R. Paul [64] studied the effect of degree of exfoliation on the toughness of polyamide nanocomposites. They compared organoclay based nanocomposites of PA6, PA11 and PA 12. They found out that the polarity of the repeat structure is an important factor that determines the level of interaction of the polymer with the organoclay. Increase in the aliphatic content relative to nylon-6 results in a lower thermodynamic affinity between the polymer and organoclay, thus reducing the driving force for the exfoliation of clay by the polymer. This decrease in degree of exfoliation resulted in reduced impact strength of PA11 and PA 12 based nanocomposites as shown below in figure 2.18;

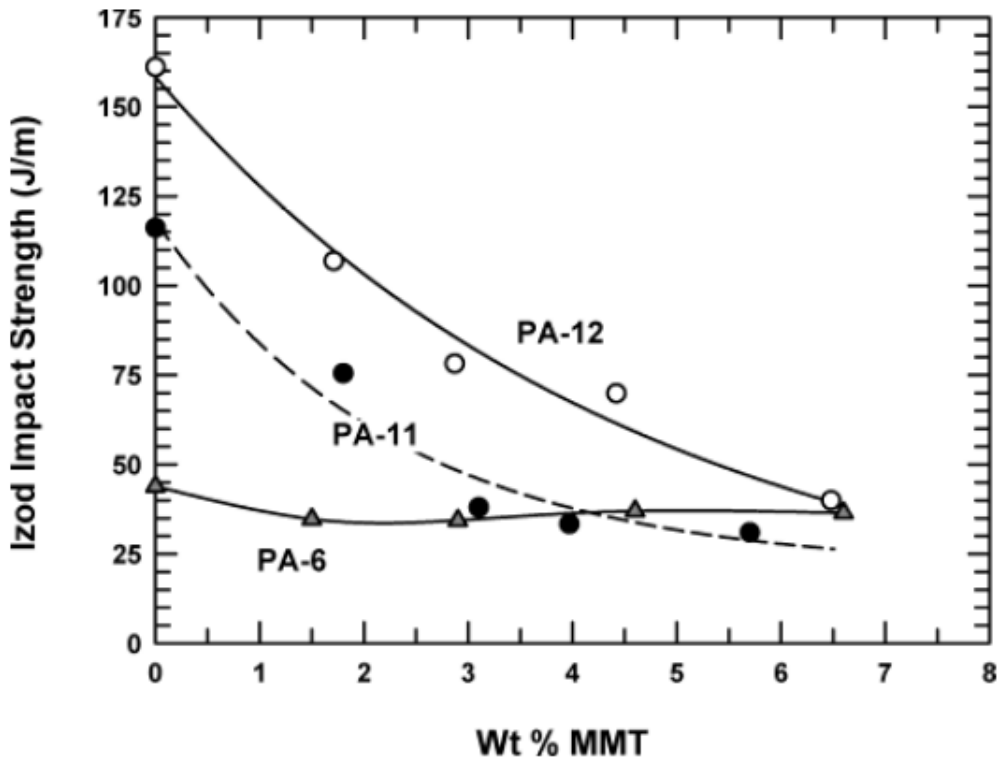

Fig.2.18 Effect of organoclay concentration and polyamide structure on the impact strength [64]

The effect of nanofillers with high surface area, like CNTs, carbon black, on the energy absorption capability of the virgin polymers has been studied by many researchers. Zhang et al. [65] studied the effect of multi walled carbon nanotubes (MWNTs) on the toughness and other mechanical properties of nylon 6. The nanocomposites were prepared using simple melt blending. Tensile testing was carried out to calculate stress, percentage strain, stiffness and elongation at break. Area under the stress strain curve was used to calculate the ductility of the nanocomposites. Uniform dispersion of MWNTs was confirmed by SEM. Close inspection of fractured surface of nanocomposites, using SEM, indicated that upon failure most of the MWNTs were broken rather than just pulled out of the matrix. This interesting and typical breakage phenomenon of the CNTs upon tensile stretching indicates a strong interfacial adhesion between MWNTs and PA6 matrix. This breaking of a typical single MWNT and MWNT keeping two lumps of matrix together ,indicating by arrows 1and 2 respectively, is shown in figure below;

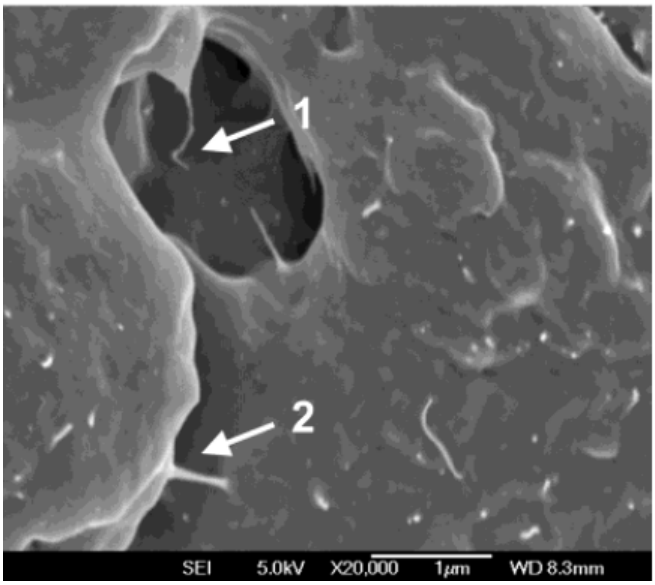

Fig.2.19 SEM image representing the overall morphology of 1 wt% MWNTs/ PA6 nanocomposite [65]

Upon incorporation of only 1 wt % MWNTs, the elastic modulus of PA6 was improved by about 115% from 396.0 to 852.4 MPa, and the tensile strength at yield was improved by about 124% from 18.0 to 40.3 MPa. The elongation at break (about 125%) slightly decreased, indicating that the composite became somewhat brittle as compared to neat PA6 (which breaks at above 150% of elongation). This means only uniform dispersion of the nanofillers in polymeric matrices is not the only reason for their toughening.

In contrast, Cooper et al. [66] reported a significant improvement in the fracture toughness of PMMA incorporated CNTs systems with unclear toughness mechanism. They studied the effect of both SWNTs and MWNTs on the impact properties of PMMA. The impact resistance of PMMA was increased from 40 to 160 kJ/m^2 by addition of only 0.1 wt% SWNTs. While on the other hand, 4 wt% MWNTs inclusion increased the toughness of neat PMMA from 40 to only 110 kJ/m^2. Interestingly the interfacial adhesion between CNTs and PMMA was not that strong as was evidenced by an unchanged Young's modulus. Extensive buckling and bending of nanotubes was assumed to be the toughness mechanism.

Shah et al. [56] suggested that it might be the mobility of the nanofiller, added in polymer, which controls its ability to dissipate energy and hence can result in toughening of polymer nanocomposites. They used poly vinylidene fluoride (PVDF) as their matrix and an organoclay as nanofiller. Nanocomposites with intercalated morphology were prepared by using melt extrusion. A uniform dispersion of the nanofiller was assured by TEM and X-ray analysis. The toughness of clay filled nanocomposites was reported by calculating area under the stress strain curve and elongation at break. A significant increase in toughness of PVDF was observed when the tensile testing was carried out above glass transition temperature (Tg) and

vice versa. T_g of PVDF has been reported to be -40°C. Figure 2.20 depicts the stress strain behaviour of PVDF and its nanocomposite with clay (5 wt %) at different temperatures. They believed that when testing was done at a temperature which was well above the T_g of the neat polymer, the nanoparticles were allowed to move and align. This resulted in additional energy dissipation mechanism which was absent in the neat polymer.

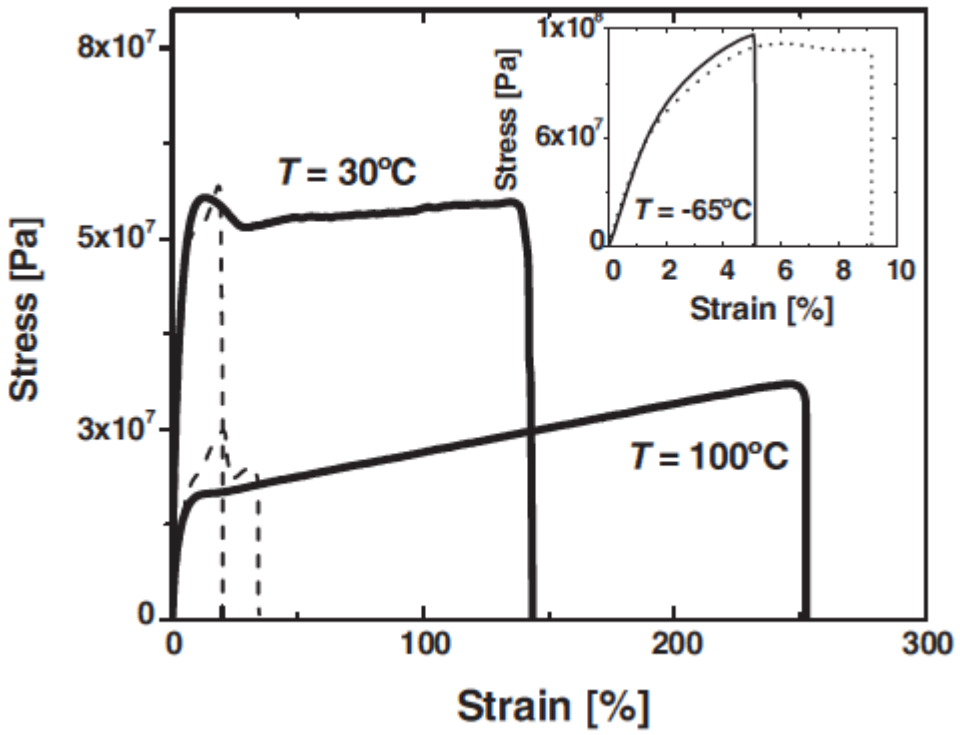

Fig.2.20 Stress strain curves for PVDF (dashed) and its nanocomposites (solid lines) at various temperatures [56]

Zhang et al. [67] used the same concept of mobility of nanoparticles to investigate the toughening ability of non-layered nanofiller silica. They claimed that, in case of non layered nanofillers, their mobility is not enough to increase the energy dissipation capability of the nanocomposites as a whole but their uniform dispersion, i.e. low particle / particle interaction and higher compatibility of matrix with the filler, is

also very crucial. They used PP as their matrix and silica as nano inclusion. The examination of area under the curve and elongation at break revealed that the incorporation of silica brought about deterioration in the toughness no matter whether the temperature was above T_g or not. TEM observations revealed the agglomerations of silica which means the nanofiller was not adhered to polymeric matrix and hence could not dissipate energy. Later on, they dispersed treated silica in PP, which had lesser chances of agglomerations, and this time they found improved toughness. This finding approved their hypothesis that for non layered nanofillers, better dispersion as well as their mobility are the governing factors for them to be used for the toughening of polymers.

Very recently functionalization of expanded graphite, as discussed in the earlier pages of this chapter, has been carried out for the production of highly exfoliated graphene sheets in organic solvents which has opened new horizons of using the nanosheets for developing new kind of polymer nanocomposites. Functionalized graphene (FG) has been reported to be excellent nanofiller for the improvement of stiffness of polymers due to its intrinsic strength and active surface functionalities [51, 52]. Presence of very active edge functional groups is the advantage for the FG to form a good dispersion and strong interactions with polymeric matrices. However, can the FG toughen polymers? The answer is ambiguous. Not a long ago, Rafiee et al. [52] first reported considerably enhanced fracture toughness of graphene filled epoxy composites. Toughness was calculated in terms of fracture toughness parameter (K_{IC}). The toughness of graphene filled epoxy exhibited a maximum at 0.125 wt % and then decreased continuously up to 0.55 wt% of graphene fillers because of agglomerations. They believed that it was the planar morphology of the graphene layers which enabled the system to deflect the cracks more effectively.

Moreover these graphene based nanocomposites of epoxy had 45 and 50% improved ultimate tensile strength and Young's modulus respectively. This increase in fracture toughness and other mechanical properties are shown in figure 2.21.

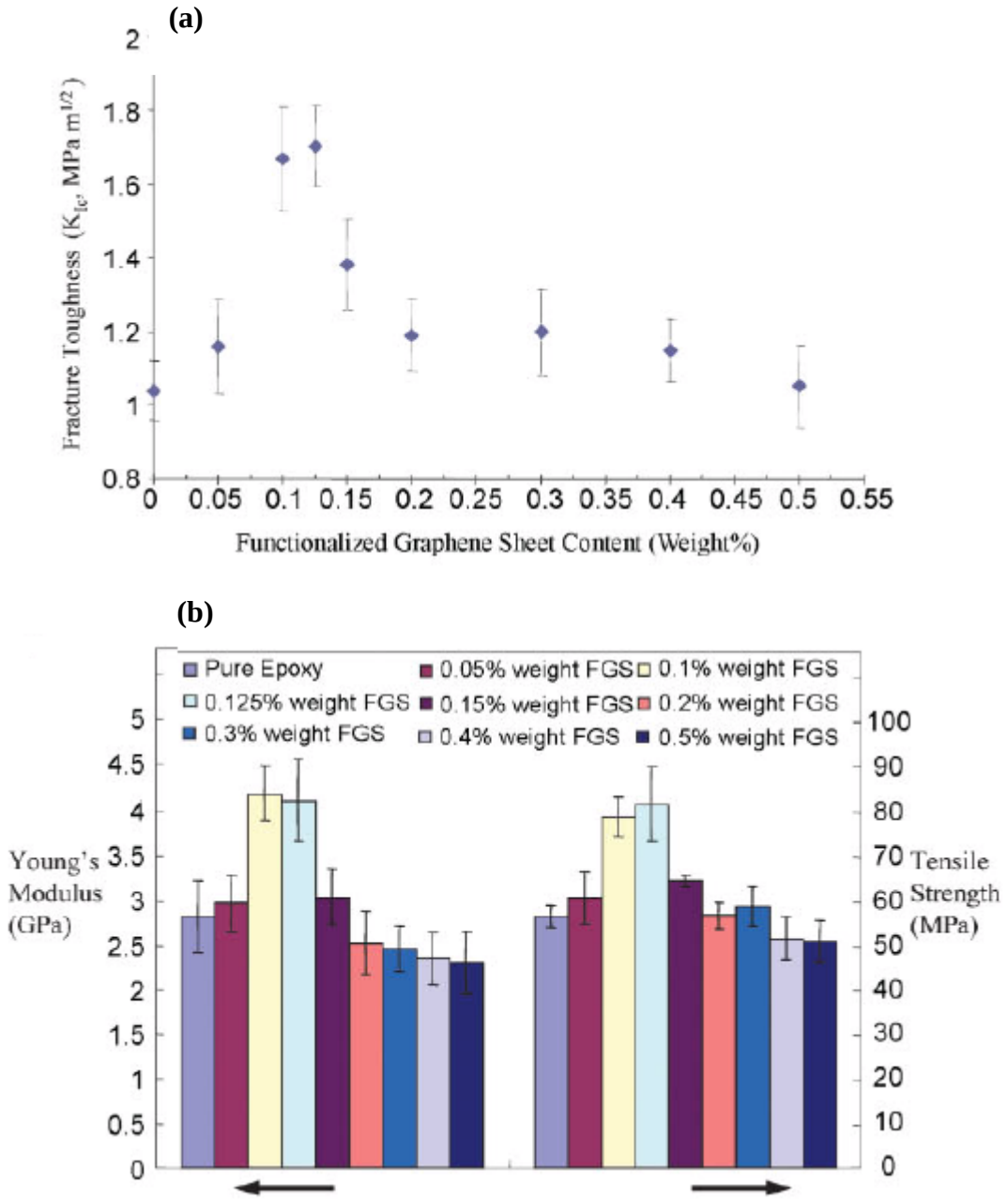

Fig.2.21 Mechanical properties of graphene/ epoxy nanocomposites [52]

In this context Wang et al. [68] compared the effect of functionalized graphene on the mechanical performance of low density polyethylene (LDPE). Graphene was

functionalized using vinyl triethoxysilane (VTES) and later were blended with LDPE. VTES–graphene not only remarkably improved the tensile strength of LDPE, but also enhanced its toughness by 17.7%.

In the case of the LDPE/VTES–graphene composites, the vinyl groups of the VTES-functionalized graphene sheets can react with the active redials on the LDPE chains under the initiator and molten blending, resulting in chemical interaction between graphene and LDPE matrix. This improved adhesion was believed to be the toughening mechanism. Reinforcement of graphene resulted in the increases of up to 27.0 and 92.8% in the tensile strength and Young's modulus of the nanocomposites, respectively, compared to neat LDPE. This improvement in the mechanical properties of LDPE as a function of functionalized graphene is shown in figure 2.22.

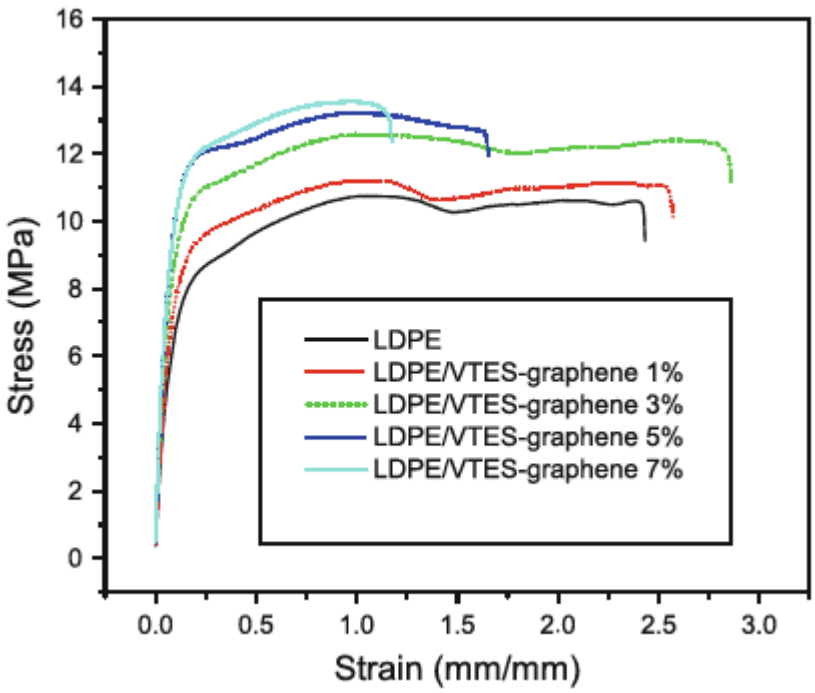

Fig.2.22 Mechanical properties of LDPE/ graphene composites [68]

Some researchers believed that graphene or its derivatives, like many other nanofillers, cannot toughen the polymers [36, 42, and 69]. Kim et al. [69] prepared thermoplastic polyurethane (TPU) nanocomposites using exfoliated graphite (EG) as reinforcement. They observed a significant improvement in stiffness of the TPU upon addition of EG but a decrease in toughness of the nanocomposite was observed.

A mechanical reinforcing effect of poly (vinyl alcohol) using graphene has also been reported by Rouff et al [70]. Although tensile strength and stiffness increase but there is a significant decrease of 40% in the toughness as calculated by area under the curve. This decrease of toughness is shown in figure 2.23.

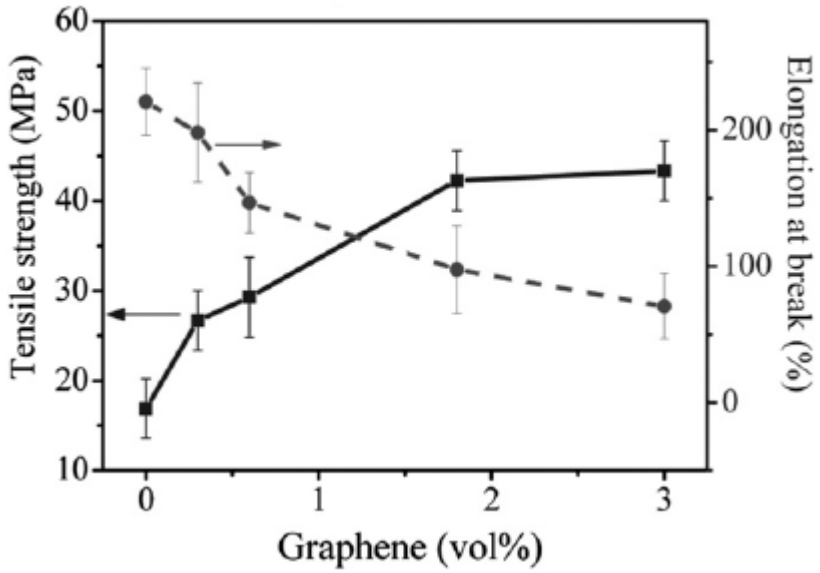

Fig.2.23 Mechanical properties of PVA as a function of graphene loading [70]

[46] Hence we can conclude that in theory if the nanofillers are fully exfoliated, the energy absorption capability of the nanocomposites will increase. Increase in the nanofillers inclusion in polymeric matrices enhances the contact area between nanoparticles and matrix which directly affects the debonding energy between particles and matrix. In reality the situation is different. Certain limitations of

manufacturing technology, the increasing filler volume fraction or concentration will lead to agglomeration which brings about local stress concentrations and hence decreases the energy absorption capability of the nanocomposites. Especially in the case of graphene it is not only difficult to prepare its isolated sheet but it is also ver difficult to assure its uniform dispersion. This situation becomes more challenging when anyone tries to use graphene to improve toughness. These tremendous features and great challenges of graphene inspired us to be adapted as our nanofiller for nylon 12 matrix.

2.7 Crystallization behaviour of polymer nanocomposites

A crucial dispute in the fabrication of polymer nanocomposites is to investigate how does nanoreinforcements contribute towards the crystallinity of the matrix. Since the thermal, mechanical, chemical and physical properties of semicrystalline polymers are predominately affected by their; (i) crystallization morphology (ii) rate and degree of crystallization (iii) the amount of amorphous/ crystalline phase, it is of supreme importance to enquire how nanofillers affect the above parameters. In conventional melt processing of polymers or its nanocomposites, crystallization behaviour and its kinetics are controlled by their thermal and shear history. Nanofillers added into polymer matrices either decrease or increase the crystallization of polymers depending upon dispersion of nanofillers in matrix and loading contents of nanofiller [71, 72].

The crystallization of polymers can be divided in three parts on the basis of its origin

i) Crystallization during polymerization (a process in which the monomers forming a crystal can be joined up into chains by solid state polymerization, while the original “monomer” crystals are preserved)

ii) Crystallization induced by orientation (Here stretching of long chains to form fibrous crystals takes place)

iii) Crystallization under quiescent condition

Since crystallization under quiescent conditions (from polymer melt) is the related topic to this study so its brief detail will be discussed. The quiescent polymer crystallization can be divided into two general types, (i) crystallization from the dilute solutions and (ii) crystallization from the melts. [73] Crystallization from dilute solutions often gives you a clear picture of polymer crystals as these entities can be isolated and precisely studied. Crystallizing the polymers from their melts under quiescent conditions gives rise to crystalline regions (spherulites) which can be easily seen through polarized optical microscopy. The nucleation, growth and kinetics of development of these crystalline regions are the fundamentals questions to be answered. The basic understanding of these concepts is directly linked with the morphological studies of these crystalline regions. A lot of models have been developed to explain the morphological questions [74]. Two very basic models are (1) the fringed micelle model and (2) lamellar type of morphology. The fringed micelle model is based on the concept that the segments of polymer melt align themselves together to form bundles of crystalline regions as shown in fig.2.24.

Fig.2.24 The fringed micelle model [74]

It is believed that most of the semi-crystalline polymers crystallized either from the polymer solution or melt give rise to lamellar crystals (folded chains). According to the lamellar type of models, the spherulites are composed of lamellae or blades radiating from centre. Using electron microscopy, a structure of lamellae is obtained that looks like pyramids, wherein, the longitudinal axes of the chain appear perpendicular to the surface of the lamella. Even with this model, 100% crystallinity cannot be reached, as the surfaces of folds, ends of chains, and other structural dislocations contribute towards the existence of an amorphous phase [80]. Hence we can say that crystallizing polymers from the melt leads to a combined morphology consisting of amorphous domains (tie lines) connecting zones of single crystals as shown in figure 2.25.

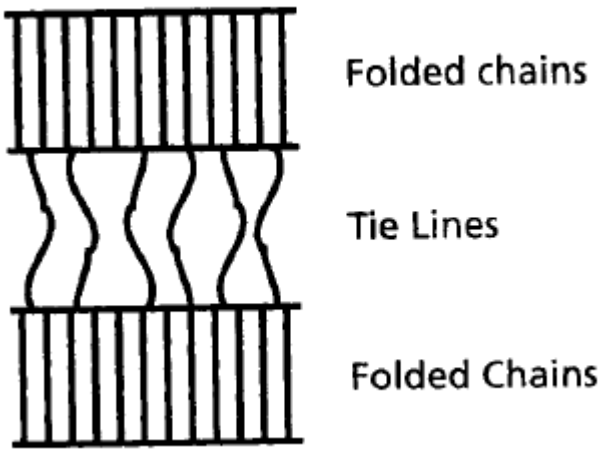

Fig.2.25 Morphology of crystallites from polymer melts [75]

Let us now discuss the kinetics of this crystallization process. As in any crystallization, the first step consists of nucleation, where nuclei are formed by cooling the melt (or solution) below the melting (solidification) temperature. The nucleation can also be defined as formation of a small amount of crystalline material due to fluctuations in density or order in the super cooled melt. This is a reversible

process when nuclei are formed and destroyed. When a critical size is obtained, these nuclei remain as the centres for the growth of crystallites. Nucleation is the most rapid, therefore, as the temperature drops; the determining factor being the degree of super cooling $\Delta T = T_m - T_c$, where Tm is the melting temperature and T_c is the crystallization temperature. This formation of nuclei is called as primary nucleation (first step of crystallization process). Second important step of crystallization is the growth of these crystallites (formed in first stage). Under ideal conditions, macroscopic spherical structures (spherulites) are apparent which can be easily detected with a polarizing optical microscope. It is believed that the spherical shape arises usually due to small angle branching and splaying microstructure. The initial stages of such a structure may not be spherical but rather may resemble a sheaf kind of morphology. An illustration of spherulites in nylon 11 is given in figure 2.26. The rate of crystallization of one polymer is always different to another, mainly depending on temperature and chain length [71].

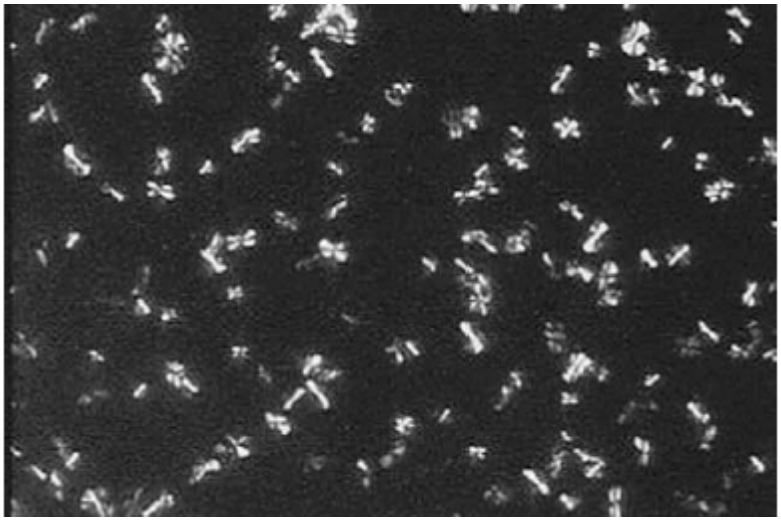

Fig.2.26 Polarized optical microscopy images of spherulites of Nylon 11 [71]

Under the most suitable conditions existing for any individual polymer, the degree of crystallization is dependent on the chain structure and the time for which the sample is annealed. Differential scanning calorimeter (DSC) is one of the most convenient techniques for studying crystallization and melting kinetics of the semi crystalline polymers and their nanocomposites. The degree of crystallization (X_c), using DSC, is often calculated by the following equation;

$$X_c\,(\%) = \frac{\Delta H_m}{(1-\psi)\,\Delta H^o_m} \times 100 \qquad (2.1)$$

Where ΔH_m is the measured melting enthalpy, ψ is the fraction of nanofiller and ΔH^o_m is the extrapolated value of the enthalpy corresponding to the melting of 100 % polymer under investigation.

The degree of crystallinity, rate of crystallization and shape of the spherulites can be studied by using Avrami equation [76, 81];

$$X_t\,(t) = 1 - \exp\,(-Kt^n) \qquad (2.2)$$

Where 'X_t (t)' is the relative degree of crystallinity, t the crystallization time, 'n' is a constant which depends on the type of nucleation and growth of the crystals and 'K' is the crystallization rate constant involving both nucleation and growth rate parameters under isothermal conditions. Table 2.2 presents various values of Avrami exponent (n) for various types of crystal growth geometries.

Avrami Exponent (n)	Crystal Geometry	Nucleation type	Rate determination
0.5	Rod	Athermal	Diffusion
1	Rod	Athermal	Nucleation
1.5	Rod	Thermal	Diffusion
2	Rod	Thermal	Nucleation
1	Disc	Athermal	Diffusion
2	Disc	Athermal	Nucleation
2	Disc	Thermal	Diffusion
3	Disc	Thermal	Nucleation
1.5	Sphere	Athermal	Diffusion
2.5	Sphere	Thermal	Diffusion
3	Sphere	Athermal	Nucleation
4	Sphere	Thermal	Nucleation

Table 2.2 Avrami exponent for different crystal geometries [77]

A lot of work has been done on studying crystallization behaviours of various polymers like PE, PP, PEO and their nanocomposites [78]. Since this report, in particular, highlights the work done related to the polyamides, therefore in next few pages a brief review of crystallization behaviour of polyamides (nylon12 more significantly) has been given. A number of research articles have addressed the issue of crystallization and melting behaviours of different polyamides. Clay and CNTs have been popular nanofiller for polyamides. In almost all the systems, nanofillers did act as nucleating agent and facilitated the crystallization process [78, 79, and 80].

Li et al. [81] studied the effect of MWNTs on isothermal and non-isothermal crystallization of nylon 66 using DSC. A decrease in crystallization temperature of nylon 66 was observed upon addition of MWNTs. They believed that the MWNT network imposed a confinement effect on polymer chain diffusion and crystal growth. This confinement might had slowed down the crystallization process, which had led to lower crystallization temperatures for nanocomposites. This decrease in T_c, upon addition of MWNTs, has been shown in the following figure 2.27.

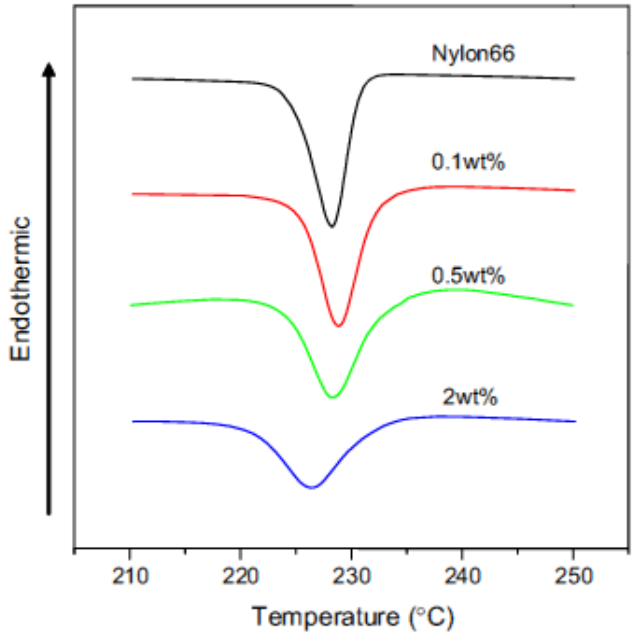

Fig.2.27 DSC scans of nylon 66 and its nanocomposites showing decrease in crystallization temperature of nylon 66 upon addition of MWCNTs [81]

Avrami analysis revealed that incorporation of MWNTs decreased the size of spherulites as indicated by decrease in the value of 'n' and also observed by optical microscope. They thought that because of the dense nucleation on the MWNT surfaces, the growth of the polymer crystals was confined between the adjacent crystals and the dimensions were thus decreased. Moreover the rate of crystallization increased up to 0.1 wt% concentration of MWNTs and decreased for

its higher loading. In contrast an increase in the spherical crystal geometry of poly (ethylene oxide) (PEO) was observed upon addition of MWNTs [82]. Mo et al. [82] studied the crystallization of PEO as a function of three different types of MWNTs i.e. pure MWCNT, chemically modified MWCNTs with carboxylic functional groups (MWCNT–COOH) and chemically modified MWCNTs with hydroxyl functional groups (MWCNT–OH). The incorporation of any type of MWNTs resulted in the decrease in melting and crystallisation temperatures, and also reduced the crystallinity of PEO. With increase in amount of CNTs this effect was more prominent. These results are summarized below in table 2.3.

Sample	T_c (°C)	T_m (°C)	χ_c (%)
PEO	40.1	67.6	86.7
PEO/CNT (0.1)	31.6	60.6	61.4
PEO/CNT (0.5)	28.1	54.2	47.8
PEO/CNT (1)	11.7	43.7	14.1
PEO/CNT–OH (0.1)	28.9	55.3	58.7
PEO/CNT–OH (0.5)	20.2	47.6	43.5
PEO/CNT–OH (1)	7.0	44.7	24.3
PEO/CNT–COOH (0.1)	30.8	57.1	60.1
PEO/CNT–COOH (0.5)	28.6	51.3	53.4
PEO/CNT–COOH (1)	11.7	50.1	35.4

Table 2.3 Effect of CNT on crystallization temperature, melting temperature and degree of crystallinity of PEO [82]

Morphological observations of PEO/CNTs nanocomposite using a polarized optical microscope (POM) suggested an increase in spherulite size and decrease in number of nucleation sites upon increase in nanofiller concentration. Avrami analysis was applied to calculate the effect of MWCNTs on the rate and degree of crystallization. It shows that incorporation of MWNTs caused a slow growth in crystals. When CNT concentration was higher the results were more effective as shown in figure 2.28.

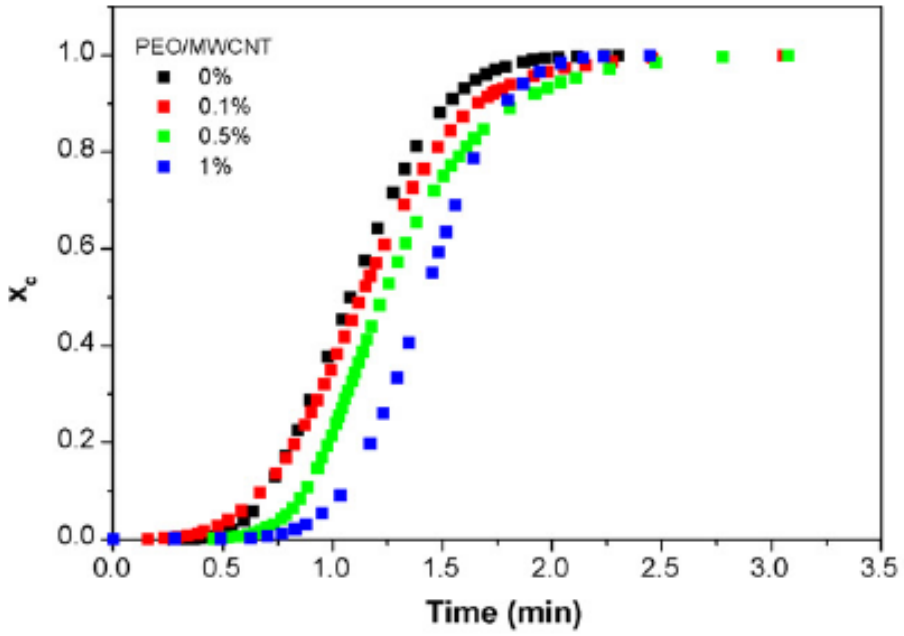

Fig.2.28 Plots of relative crystallinity (X_c) vs. crystallisation time for PEO and its nanocomposites at isothermal conditions. [82]

McFerran et al. [72] studied the non-isothermal and isothermal crystallization behaviour of neat nylon 12. The value of the Avrami exponent 'n' (calculated by applying Avrami analysis) was found to be in the range of 2.05 to 2.55. Since the Avrami exponent was essentially greater than 2, depending on the crystallization temperature, the primary stage of crystallization was concluded to be a three-dimensional growth phenomenon. The decrease in value of 'n' in the later stages of crystallization was thought to be due to the spherulites impinging on each other.

Paul et al. [83] reported that how organically modified montmorillonite (MMT) effects the crystallization behaviour of nylon 6. Nanocomposites were produced using a twin screw extruder. Isothermal and non-isothermal studies, using DSC, revealed that very low concentration of clay result in dramatic increase in crystallization kinetics. The degree of crystallization was calculated by the ratio of heat of fusion at particular

temperature (ΔH_f) to the heat of fusion of the purely crystalline forms of nylon 6 (ΔH^o_f). Addition of clay up to 1.6% decreased the crystallization time but further addition of clay reverses this trend. At levels of 1.6 wt% MMT and beyond, the peak location of each exotherm occurs at times comparable to, and in some cases longer, than the pure extruded nylon 6 as shown in figure 2.29.

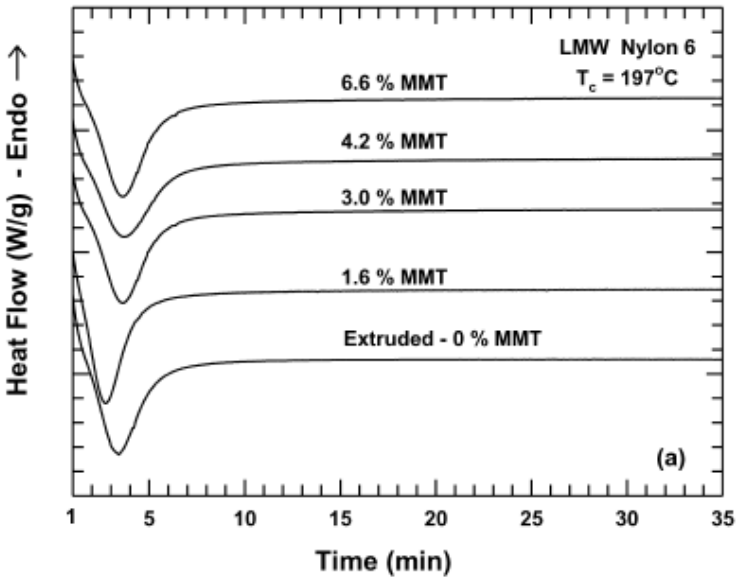

Fig.2.29 Isothermal crystallization of nylon 6 and its nanocomposites [83]

The clay particles might had served as additional nucleation sites; however, addition of more clay retarded the growth process. At low concentration of clay, the distance between dispersed platelets is large so it is relatively easy for the additional nucleation sites to incorporate surrounding polymer hence increasing the rate of crystallization. However, at high concentrations of clay, diffusion of polymer chains to the growing crystallite was hindered which caused decrease in rate of crystallization. The combination of a larger number of nucleation sites and limited crystal growth is expected to produce crystals of fine grain size. Avrami analysis also confirmed a decrease in spherulites size with decreased value of ‘n’ for higher loading of clay.

Moreover crystallization rate constant K; shows a maximum at the lowest clay concentrations and decreases for the nanocomposites having more clay.

The similar effect of clay on crystallization of nylon 6 was reported by Liu et al. [84] They concluded that the clay increases the crystallization rate and has a strong heterophase nucleation effect on nylon 6. However they found no change in crystallinity even at 6.7 wt% loading. Yan et al. [85] studied the effect of organically modified montmorillonite (OMMT) on the crystallization and thermal properties of nylon 12 powder used for laser sintering processes. The degree of crystallization (X_c), which they called as crystallinity Index (CI), was calculated by incorporating the fraction of the nanofiller added. The formula for calculation of CI is given in equation 2.1. The melting enthalpy for a theoretically 100 percent crystalline nylon-12 was 209.2 J/g. An increase of 6% in crystallinity was observed upon addition of clay. An increase in crystallization temperature was observed for OMMT/ Nylon 12 nanocomposite (figure 2.30 b) which indicates that the OMMT had a heterogeneous nucleation effect on nylon 12 resin. However there was no significant change in melting temperature of nylon 12/ OMMT nanocomposite as compared to neat nylon as shown in figure 2.30 (a).

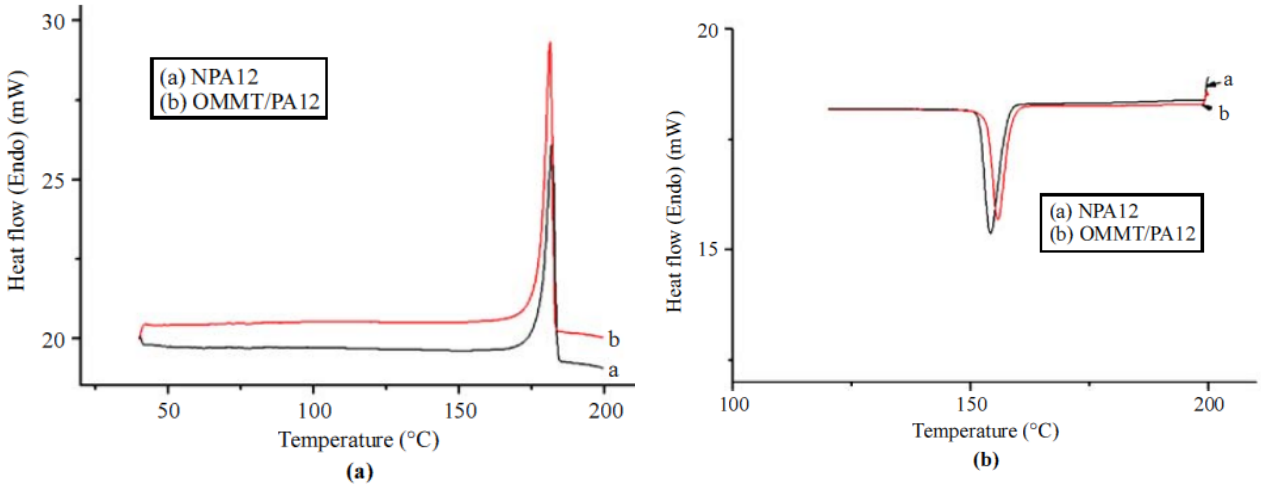

Fig.2.30 (a) The heating curves, (b) cooling curves of nylon 12 and its nanocomposite [85]

Concluding all the above discussion about crystallinity, the existence of crystallinity has a crucial effect on many chemical and physical properties of polymers. In general, increasing in percent crystallinity improves resistance to the attack of chemicals and solvents. In practice, it is difficult to dissolve a crystalline polymer in appropriate solvents unless temperatures approaching the melting point are used. From the mechanical point of view, highly crystalline polymers are more rigid and strong (mostly determined by the increase of modulus and yield strength) but at the same time decreases elongation and impact strength. The optical properties are also affected by the presence of crystallites, as the transparency decreases [82]. Presence of smaller spherulites is desirable for improving optical and mechanical properties [83]. A significant effect of crystallization on the various properties of composites encouraged us to investigate the effect of graphene on crystallization of nylon 12.

2.8 Barrier properties of polymer nanocomposites

Apart from the exceptional mechanical and thermal properties of nano-filled polymers, these nano-sized materials are often exploited in the field of membrane applications, such as to reduce gas and water permeability of the polymeric membranes. Although the barrier performance of materials have perhaps never attracted so much industrial attention as over recent decades. Since some modern food and drinks packaging technologies has started making use of plastic materials, permeability has become an important issue associated with food commercialization, food shelf life extension, its quality and safety [86]. Among a variety of nanofillers, layered nanofillers (like clay and graphene) are considered to be most promising candidates for improving barrier properties because of their layered shape. These plate shaped nanofillers can prolong the path of the permeant passing through

polymer, hence decreasing the permeability [87]. The mass transport mechanism of gas/liquid permeating through a nanoplatelet reinforced polymer is similar to that in a semicrystalline polymer. In most theoretical treatises nanocomposite is considered to consist of a phase (polymer matrix) in which non-permeable nanoplatelets are dispersed. There are three main factors influencing the permeability of a nanocomposite: the volume fraction of the nanoplatelets; their orientation relative to diffusion direction; and their aspect ratio.

For a homogenous polymeric system, penetration of the penetrant can be demonstrated by simple solution–diffusion theory, which means that the permeability coefficient, P, is the product of solubility (S) and diffusivity (D) coefficients, i.e.

$$P = D \times S \qquad (2.3)$$

A similar form has been assumed to apply for composites consisting of fillers, which do not absorb or conduct the penetrant, dispersed in a polymeric matrix [88]. Simple composite theory for the type of systems mentioned above, in the absence of adsorption by the filler or effects of the filler on the surrounding polymer matrix, would predict the penetrant solubility in the composite to be;

$$S = S_o (1 - \Psi) \qquad (2.4)$$

Where, S_o is the penetrant solubility coefficient in the pure polymer matrix and Ψ is the volume fraction of particles dispersed in the matrix. The above equation (2.4) assumes that the solubility is not affected by the morphological features of any of the phases. But on the other hand, the diffusion process is more complex. The particles

act as impenetrable barriers so that the penetrant must follow an elongated, or tortuous, path in order to diffuse through the composite. This tortuous path can be considered by a tortuosity factor (f);

$$D = D_o \times f \qquad (2.5)$$

Where D_o is diffusivity coefficient of pure polymeric matrix. According to simple composite theory, this tortuosity factor depends on the content of particles, the particle shape, and the location and orientation of the particles. However, it should not depend on absolute particle size or on the nature of the penetrant. Combining the above equations (2.4) and (2.5);

$$P = D \times S$$

$$= (1 - \Psi)\, S_o \times D_o \times f$$

or

$$f = P / P_o\,(1 - \Psi) \qquad (2.6)$$

Where, P_o is the penetrant permeability coefficient in the pure polymer matrix.

Generally the transport mechanism of a penetrant within the polymer matrix follows Fick's law [87]. It is generally accepted that the transport mechanism and that the matrix maintains the same properties and characteristics as that of neat polymer. Since addition of nanofillers will reduce the volume of polymeric matrix, hence a decrease in solubility is expected in the nanocomposites. Moreover addition of nanofillers (specially layered), because of its ability to force the diffusing molecules through prolonged path, causes decrease in diffusion as well. The reduction of diffusion coefficient (D) is much higher than solubility parameter (S) because of very small reduction in matrix volume which is due to very small amount of added

nanofillers [88]. It means that the major factor for permeability of nanocomposites is 'tortuosity' which indeed is directly linked with shape and dispersion of the nanofillers. A simple permeability model for a regular arrangement of platelets has been proposed by Nielsen. According to his model, the rectangular platelets with finite width, L, and thickness, W are uniformly dispersed throughout the matrix. Their orientation is perpendicular to the diffusion direction. According to his theory, the nanoplatelets act as impermeable barriers to the diffusing molecules and force them to follow long and more tortuous path while diffusing through nanocomposites. Figure 2.31 gives an illustration of how layered shape nanofillers increase tortuosity (diffusion path) according to Nielson's model [89];

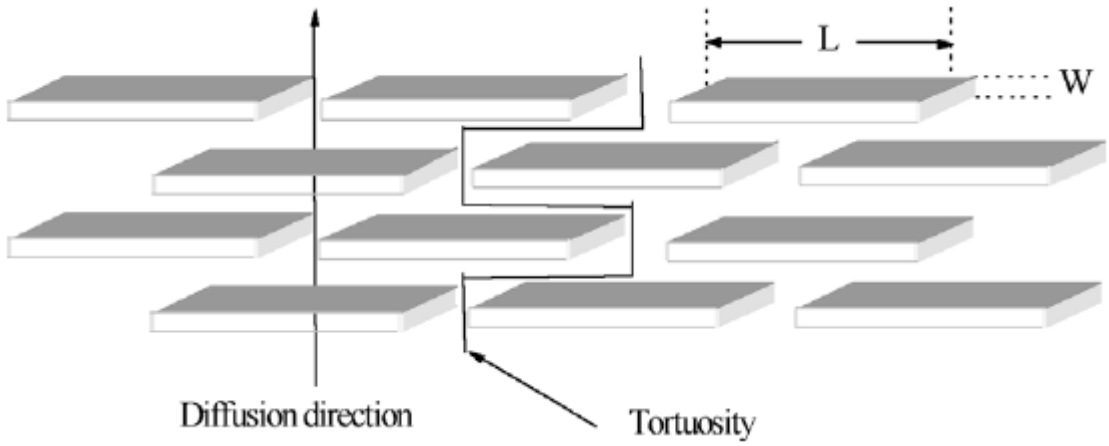

Fig.2.31 Tortuosity affected by incorporation of nanofiller [89]

Mathematical form of Nielson's model is given in equation (7);

$$\frac{K_{composite}}{K_{matrix}} = \frac{1-\Psi}{1+0.5\alpha \times \Psi} \qquad (7)$$

Where Ψ is the volume fraction of nanofiller, $K_{composite}$ and K_{matrix} are the permeability of the nanocomposite and the neat polymeric matrix respectively and α is the aspect

ratio of nanofiller given by $\frac{L}{W}$ of the nanofiller. The equation (2.7) shows that the permeability of the nanocomposite decreases with the increase of Ψ and α. In practise however, the limit for its validity is Ψ ≤10%, because the particles have a tendency to aggregate, which increases with Ψ. The predictions of this model for different values of the aspect ratio, α, are shown in figure 2.32.

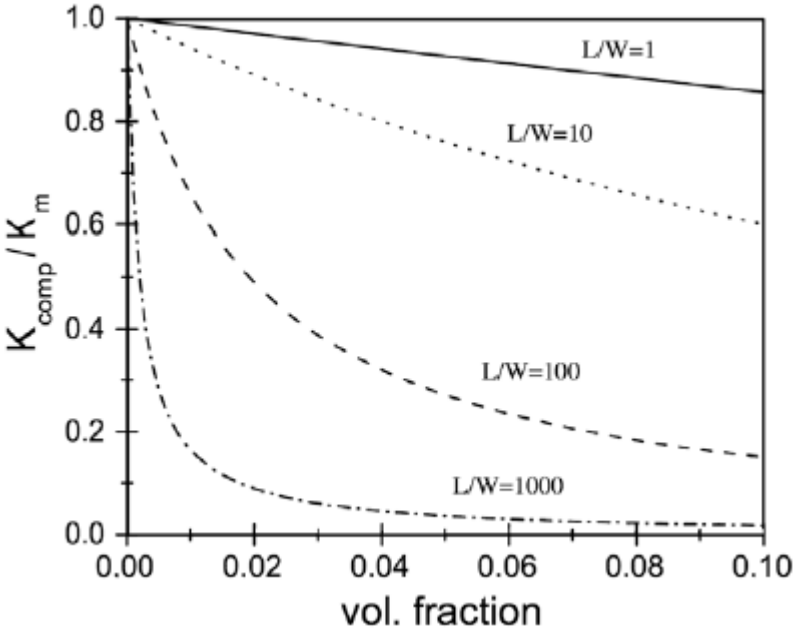

Fig.2.32 Prediction of relative permeability of nanocomposite as a function of filler aspect ratio [89]

Among food packaging materials, nylon 6 (polyamide 6) and nylon 12 (polyamide 12) are the most frequently used polyamides. Typical applications of nylon 12 films are sausage and cooked meat casings. During the process of cooking meat or sausages, the nylon film will be exposed to hot water or steam on the outside and fatty food on the inside. Hence it is crucial to study the barrier properties of nylons and how the added fillers will affect their barrier performance. Espuche et al. [90] prepared nanocomposites of nylon 6 with wide range of montmorillonite contents (0

to 13 wt%) by melt blending. A significant decrease in water permeability of nylon 6 was observed upon addition of clay. This decrease in permeability was attributed to tortuosity effect, as clay particles might had forced the diffusing molecules to pass through a prolonged path. At higher loading than 13%, because of aggregation, no decrease in permeability was observed. The matrix crystalline morphology was not significantly affected by the presence of clays. The crystallinity was equal to 30% for any filler content and only a slight increase of the γ-phase proportion was observed when the clay content increased. It was considered that whatever the system under investigation was, the organic impermeable clay layers behaved in a same way in regard to water transport.

Alexandre et al. [78] studied the effect of addition of organo-modified montmorillonite (C30B) on the water barrier properties of polyamide 12. They used Nielson's model (eq.7) to calculate the decrease in water permeability. It was found that, upon increasing the concentration of C30B, the water permeability of polyamide 12 decreases as suggested by Nielson. This decrease in permeability was attributed to the increase in tortuous path provided by the nanofillers. The decrease in diffusivity was an evidence for the increase in tortuous path. This tortuosity is a complex parameter, because it depends on several factors, like the aspect ratio, the stiffness and the crystallinity which are functions of the C30B volume fraction. Upon addition of more than 2.5% (by volume) of C30B, no decrease in permeability was observed. Change in morphology of the matrix and the water induced plasticization were thought to be the possible reasons for this behaviour [91].

These polymer–clay nanocomposites (PCNs), containing exfoliated clay nanosheets and stacks, have been studied for well over a decade due to promising improvements in their barrier properties as compared to the neat polymers.

However, the hydrophilic nature of clay and the difficulties in exfoliating clay aggregates during melt-state processing, has limited the range of possible PCNs to be used as impermeable membranes [92]. Recently discovered polymer–graphene nanocomposites (PGNs), where the graphene sheets can be chemically tailored to maximize their interaction with the polymer matrix to the point of complete dispersion, can address these limitations of PCNs [44, 45, and 52]. Oxygen barrier properties of polystyrene have been significantly improved by incorporation of graphene sheets. These graphene sheets have much more ability to decrease permeability as compared to clay. A comparison Relative permeability plots for films of polystyrene-graphene (represented as PGN) and polystyrene-montmorillonite (represented as PCN) compared to a pristine polystyrene film of graphene and clay based nanocomposites along with predicted values from Nielsen and Cussler's theories (calculated assuming aspect ratio α = 500) has been given below in figure 2.33 [92];

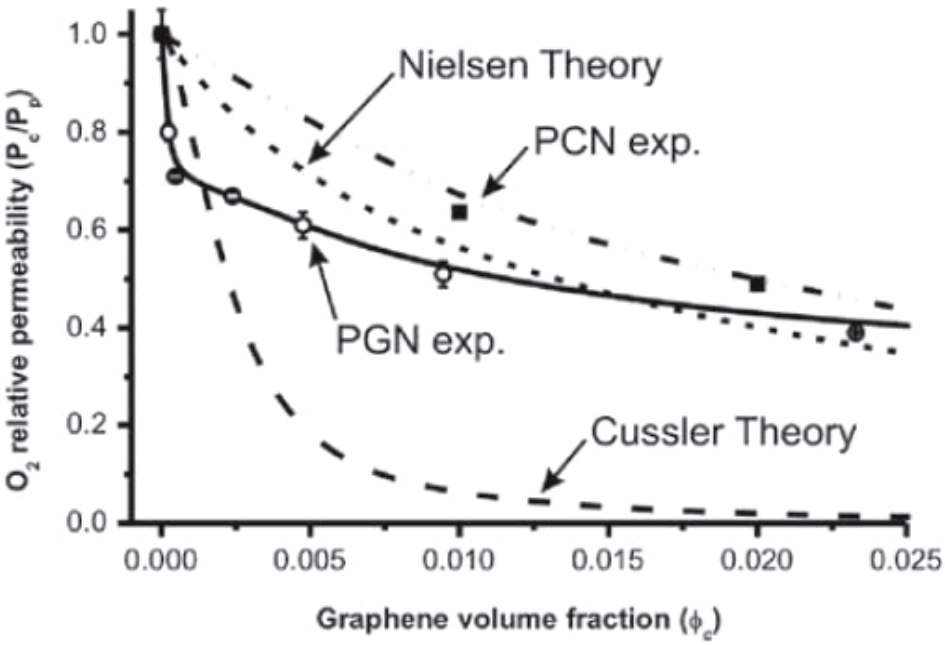

Fig.2.33 Comparison of oxygen permeability of graphene and clay based polystyrene nanocomposites [92]

By keeping in mind that nylon 12 has excellent water barrier properties and relatively poorer oxygen barrier properties, addition of layered nanofiller like graphene which has more length than its thickness would be of great interest. This is what which provoked us to study the effect of graphene on oxygen and water barrier properties of nylon 12.

2.9 Summary

Nylon 12 is one of very important member of polyamides family and its properties needs to be improved. Graphite and derivatives have proven their potential to improve the overall performance of various polymers. Inclusion of a unique derivative of graphite, functionalized graphene, in nylon 12 matrix can have significant effect on its various properties!

2.10 References

[1] S. T. Peters. Handbook of composites 2nd edition; Chapman & Hall: 1998

[2] M. Biron. Thermosets and composites; Elsevier Science & Technology Books: 2003

[3] Joseph H. K. Polymer nanocomposites processing, characterization and applications; McGraw-Hill Nanoscience and Technology Series; 2006: chapter 1

[4] Yiu-Wing Mai and Zhong-Zhen Yu, Polymer nanocomposites; CRC Press, 2006: chapter 1

[5] http://en.wikipedia.org/wiki/Nylon

[6] I.B. Page. Polyamides as engineering thermoplastic materials; 2000, chapter 1, page 6

[7] US Patent 2,130,523, Linear polyamides suitable for spinning into strong pliable fibers

[8] J.A. Brydson. Polymeric materials 7th edition; 1999, chapter 1

[9] N. Dencheva, T.G. Nunes, M. J. Oliveira, Z. Denchev. Crystalline structure of polyamide 12 as revealed by solid-state NMR and synchrotron WAXS and SAXS. Journal of Polymer Science: Part B: Polymer Physics, 2005; 43: 3720–3733

[10] G. Hopf. A Publication of Nylon 12-Huels in comparison to Other Nylons, Chemische werke huels AG, West Germany. Data sheet 2001: 1–22.

[11] G. Wolfgang, D. Ruestem. Nylon 12 preparation, properties and applications, Ind. Eng. Chem. 1970; 62: 16-22

[12] http://www.ptsllc.com/nylon_intro.htm

[13] J. L. White, S. Rhee. Crystal structure and morphology of biaxially oriented polyamide 12 films, J. Polym. Sci. 2002; 40: 1189-1200.

[14] I. Y. Phang, T. Liu , M. Ashiq, K.P. Pramoda, L. Chen, L. Shen, S. Y. Chow, C. He, X. Lu, X. Hu. Morphology, thermal and mechanical properties of nylon 12/organoclay nanocomposites prepared by melt compounding 2005; 54: 456-464

[15] N. Ait Hocine, P. Mederic, T. Aubry. Mechanical properties of polyamide-12 layered silicate nanocomposites and their relations with structure 2008; 27: 330-339

[16] S.R. Athreya , K. Kalaitzidou, S. Das. Processing and characterization of a carbon black-filled electrically conductive nylon-12 nanocomposite produced by selective laser sintering, Material Science and Engg. A 2010; 527: 2637-2642

[17] I. Sumio. Helical microtubules of graphitic carbon, Nature 1991; 354: 56-58

[18] O. Breuer, U. Sundararaj. Big returns from small fibers: a review of polymer/carbon nanotube composites, Polymer Composites 2004; 25: 630-645

[19] D.S. Bethune, C.H. Kiang et al., The discovery of single-wall carbon nanotubes at IBM, Nature 1993 ;363: 605-607

[20] P.M. Ajayna., O. Stephan , Aligned carbon nanotube arrays formed by cutting a polymer resin-nanotube composite, Science, New Series, 265; 1994,1212-1214.

[21] M. Moniruzzaman , K.I. Winey. Polymer nanocomposites containing carbon nanotubes. Macromolecules 2006; 39: 5194 - 5205

[22] Y. Lin , M.J. Meziani, Y.P. Sun. Functionalized carbon nanotubes for polymeric nanocomposites, J Mater. Chem. 2007; 17:1143.

[23] J.H. Du, J. Bai, H.M. Cheng. The present status and key problems of carbon nanotubes based polymer composites. Express Polym. Lett. 2007; 1: 253-273

[24] A.K. Geim, K.S. Novoselov. The rise of graphene, Nat. Mater.; 2007 :183-191

[25] B. Z. Jang , A. Zhamu. Processing of nanographene platelets (NGPs) and NGP nanocomposites: a review. J. Mater. Sci. 2008; 43:5092–5101

[26] S. Duquesne , L.M. Bras et al., expandable graphite: a fire retardant additive for polyurethane coatings, Fire Mater. 2003; 27:103–117

[27] F.M. Uhl et al. Expandable graphite/ polyamide-6 nanocomposites. Polymer degradation and stability 2005; 89: 70-84

[28] S. Stankovich. R.D. Piner et al. Synthesis and exfoliation of isocyanate-treated graphene oxide nanoplatelets, Carbon 2006; 44 : 3342–3347

[29] US Patent 2,798,878, William S. Hummers et al. Preparation of Graphitic acid. 1957

[30] G.I. Titelman, V. Gelman, S. Bron et al. Characteristics and microstructure of aqueous colloidal dispersions of graphite oxide. Carbon 2005; 43: 641–649

[31] O.Y. Kwon, S.W. Choi, K.W. Park, Y.B. Kwon. The preparation of exfoliated graphite by using microwave. J. Ind. Eng. Chem. 2003; 6: 743-747

[32] B. Tryba, A. W. Morawski, M. Inagaki. Preparation of exfoliated graphite by microwave irradiation. Carbon 2005; 43: 2397- 2429

[33] K.S. Novoselov, A.K. Geim, S.V. Morozov et al. Electric field effect in atomically thin carbon films. Science 2004; 306: 666-669

[34] G. Chen, W. Weng et al. Preparation and characterization of graphite nanosheets from ultrasonic powdering technique. Carbon 42 ;2004: 753–759

[35] H. C. Schniepp, J.L. Li, M. J. McAllister et al. Functionalized single graphene sheets derived from splitting graphite oxide. The J. of Phys. Chem. B. 2006; 110: 8535-8539

[36] H. Kim, A.A. Abdala, C.W. Macosko. Graphene/Polymer Nanocomposites. Macromolecules 2010; 43: 6515–6530

[37] D. Cai, M. Song. Preparation of fully exfoliated graphite oxide nanoplatelets in organic solvents. Journal of Materials Chemistry 2007; 17: 3678-3680

[38] S. Horiuchi, T. Gotou , M. Fujiwara. Single graphene sheet detected in a carbon nano-film. Appl. Phys Lett. 2004; 84:2403-2405

[39] Y.X. Pan, Z.Z. Yu, Y.C. Ou, G.H. Hu. A new process of fabricating electrically conducting nylon 6/graphite nanocomposites via Intercalation polymerization. J Polym. Sci. Part B Polym. Phys. 2000; 38: 1626-1633

[40] Yiu-Wing Mai and Zhong-Zhen Yu. Polymer nanocomposites; CRC Press, 2006, chapter 19, page 524-530

[41] X.M. Chen, J.W. Shen ,W.Y. Huang. Novel electrically conductive polypropylene/ graphite nanocomposites. J. Mater. Sci. Lett. 2002; 21: 213–221

[42] M. A. Osman, J. E.P. Rupp, U. W. Suter. Tensile properties of polyethylene-layered silicate nanocomposites. Polymer 2005;46 : 1653–1660

[43] Joseph H. Koo. Polymer nanocomposites: Processing, characterization and applications; McGraw Hill Nanoscience and technology series, 2006, chapter 2, page 14

[44] T. Ramanathan, A. Abdala et al. Functionalized graphene sheets for polymer nanocomposites. Nature Nanotechnology 2008;3: 327- 331

[45] C. Chen, C. Wu, W. Weng, D. Wu, W. Yan. Preparation of polystyrene/graphite nanosheet composite. Polymer 2003; 44: 1781–1784

[46] L. Sun, R.F. Gibson, F. Gordaninejad, J. Suhr. Energy absorption capability of nanocomposites: A review. Composites Science and Technology 2009; 69: 2392–2409

[47] W. Tang, M.H. Santare, S.G. Advani. Melt processing and mechanical property characterization of multi-walled carbon nanotube/ high density polyethylene (MWNT/HDPE) composite films. Carbon 2003; 41:2779–85.

[48] Z. Bartczak, A.S. Argon, R.E. Cohen, M. Weinberg. Toughness mechanism in semi crystalline polymer blends: II high-density polyethylene toughened with calcium carbonate filler particles. Polymer 1999; 40:2347–65.

[49] J.L. Yang , Z. Zhang ,H. Zhang. The essential work of fracture of polyamide 66 filled with TiO_2 nanoparticles. Compos. Sci. Technol. 2005; 65:2374–79

[50] J. Suhr , N. Koratkar, P. Keblinski ,P. Ajayan. Viscoelasticity in carbon nanotube composites. Nature Mater 2005; 4:134–137.

[51] B. Cotterell , J.Y.H. Chia, K. Hbaieb. Fracture mechanisms and fracture toughness in semicrystalline polymer nanocomposites. Engineering Fracture Mechanics 2007; 74 :1054–1078

[52] H. Song, I. Srivastava, J. Rafiee, M.A. Rafiee, N. Koratkar, Z. Wang and Z. Yu. Fracture and fatigue in graphene nanocomposites, Small 2009; 6:179–183.

[53] R. Rafiq, D. Cai, J. Jin, M. Song. Increasing the toughness of nylon 12 by the incorporation of functionalized graphene. Carbon 2010; 48 :4309-4314

[54] B. X. Yang, G. Q. Xu, K. P. Pramoda, S. H. Goh. Mechanical reinforcement of polyethylene using polyethylene-grafted multiwalled carbon nanotubes Adv. Func. Mater. 2007; 17: 2062-69

[55] B. Chen, J. R. G. Evans. Impact strength of polymer-clay nanocomposites. Soft Mater 2009; 5: 3572-84

[56] C. A. Batt, D. Shah, D. D. Jiang, E. P. Giannelis, P. Maiti. Effect of nanoparticle mobility on toughness of polymer nanocomposites Adv Mater 2005;17: 525-28

[57] S.C. Tjong, S.P. Bao. Fracture toughness of high density polyethylene/SEBS-g-MA/montmorillonite nanocomposites. Composites Science and Technology 2007; 67: 314-323

[58] B. Lauke, S.Y. Fu, X.Q. Feng, Y.W. Mai. Effects of particle size, particle-matrix interface adhesion and particle loading on mechanical properties of particulate polymer composites Compos 2008; 39: 933-41

[59] A. Galeski. Strength and toughness of crystalline polymer systems. Prog. Polym. Sci. 2003; 28: 1643-99

[60] Z.H. Liu , K.W. Kwok, R.K.Y. Li, C.L. Choy. Effect of coupling agent and morphology on the impact strength of high density polyethylene/$CaCO_3$ composites. Polymer 2002;43(8):2501–6.

[61] K. T. Gam, M. Miyamoto, R. Nishimura, H.J. Sue. Fracture behaviour of core-shell rubber-modified clay -epoxy nanocomposites. Polym. Engg. and Sci. 2003; 43: 1635-1645.

[62] A. Ramsaroop, K. Kanny, T. P. Mohan.Fracture toughness studies of polypropylene - clay nanocomposites and glass fibre reinfoerced

polypropylene composites. Materials Sciences and Applications, 2010; 1: 301-309

[63] G.M. Kim, S. Goerlitz, G. H. Michler. Deformation mechanism of nylon 6/layered silicate nanocomposites: role of the layered silicate. Journal of Applied Polymer Science 2007; 105: 38–48.

[64] T. D. Fornes, D. R. Paul. Structure and properties of nanocomposites based on nylon-11 and -12 compared with those based on nylon-6. Macromolecules 2004; 37: 7698-7709.

[65] W.D. Zhang, L. Shen, I.Y. Phang, T. Liu. Carbon nanotubes reinforced nylon-6 composite prepared by simple melt-compounding. Macromolecules 2004; 37:256-259.

[66] C.A. Cooper, D. Ravich, D. Lips, J. Mayer, H.D. Wagner. Distribution and alignment of carbon nanotubes and nanofibrils in a polymer matrix. Composites Science and Technology 2002; 62:1105–1112.

[67] T.H. Zhou, W. H. Ruan, M.Z. Rong, M.Q. Zhang,Y.L.Mai. Keys to toughening of non-layered nanoparticles/polymer composites. Adv. Mater. 2007; 19: 2667–2671.

[68] J. Wang, C. Xu, H. Hu et al. Synthesis, mechanical, and barrier properties of LDPE/ graphene nanocomposites using vinyl triethoxysilane as a coupling agent. J Nanopart. Res. 2010; DOI 10.1007/s11051-010-0088-y

[69] H.Kim, Y. Miura, C.W. Mocosko. Graphene/polyurethane nanocomposites for improved gas barrier and electrical conductivity. Chem. Mater. 2010; 22: 3441–3450

[70] J.R. Potts, R.S. Rouff, D.R. Dreyer, C.W. Bielawski. Graphene-based polymer nanocomposites. Polymer 2011; 52: 5-25.

[71] X. Zhang, T. Xie, G. Yang, Isothermal crystallization and melting behaviours of nylon 11/ nylon 66 alloys by in situ polymerization, Polymer 2006; 46: 2116-2126.

[72] N. McFerran, C.G. Armstrong, T. McNally, nonisothermal and isothermal crystallization kinetics of nylon 12, J. Appl. Polym. Sci.110 (2008) 1043–1058.

[73] A. Keller. Organization of the Macromolecules in the condensed Phase; page145

[74] IUPAC Compendium of Chemical Terminology 2nd Edition; 1997

[75] A.N. Hocine et al., Mechanical properties of polyamide-12 layered silicate nanocomposites and their relations with structure, Polymer Testing 2008;27: 330-339.

[76] M. Avrami. J Chem Phys 1939; 7:1103

[77] Hiemenz, P.C. Polymer Chemistry: The Basic Concepts ; 1984, page 219.

[78] A. Saiter, B. Alexandre, D. Langevin, H. Couderc, Q.T. Nguyen, P. Médéric, S. Marais, T. Aubry, Water barrier properties of polyamide 12/ montmorillonite nanocomposite membranes: Structure and volume fraction effects. J. Membrane Sci.2009; 328:186–204.

[79] J. L. White, S. Rhee, Crystal structure and morphology of biaxially oriented polyamide 12 films. J. Polym. Sci. Part B 2002; 40:1189-1200.

[80] G. Zhang, D. Yan, Crystallization kinetics and melting behavior of nylon 10, 10 in nylon 10, 10 – montmorillonite nanocomposites. J. of appl. Polym. Sci. 2003; 88 : 2181-2183.

[81] L. Li et al. Structure and crystallization behaviour of Nylon 66/multi-walled carbon nanotube nanocomposites at low carbon nanotube contents. Polymer 2007; 48: 3452-3460.

[82] J. Jin, M. Song , F. Pan. A DSC study of effect of carbon nanotubes on crystallisation behaviour of poly(ethylene oxide). Thermochimica Acta 2007; 456 : 25–31.

[83] T.D. Fornes, D.R. Paul. Crystallization behaviour of nylon 6 nanocomposites. Polymer 2003; 44:3945–3961.

[84] L. Liu, Z. Qi, X. Zhu. Studies on nylon 6/clay nanocomposites by melt-intercalation process. Journal of Applied Polymer Science 1999; 71:1133–1138

[85] C.Z. Yan, Y.S. Shi, J.S. Yang , J.H. Liu. An organically modified montmorillonite/ nylon-12 composite powder for selective laser sintering. Rapid Prototyping Journal 2011; 17: 28-36.

[86] G.D. Moggridge , N. K. Lape , C. Yang, E.L. Cussler. Barrier films using flakes and reactive additives. Progress in Organic Coatings 2003; 46: 231-240.

[87] B. Xu, Q. Zheng , Y. Song, Y. Shangguan. Calculating barrier properties of polymer/clay nanocomposites: Effects of clay layers. Polymer 2006; 47 : 2904–2910

[88] S. Takahashi , H.A. Goldberg, C.A. Feeney, D.P. Karim, M. Farrell, K. O'Leary , D.R. Paul. Gas barrier properties of butyl rubber/vermiculite nanocomposite coatings. Polymer 2006;47: 3083–3093.

[89] G. Choudalakis , A.D. Gotsis. Permeability of polymer/clay nanocomposites: A review. European Polymer Journal 2009;45:967–984.

[90] E. Picard, J.F. Gerard, E. Espuche. Water transport properties of polyamide 6 based nanocomposites prepared by melt blending: On the importance of the clay dispersion state on the water transport properties at high water activity. Journal of Membrane Science 2008; 313:284–295.

[91] B. Alexandre , S. Marais , D. Langevin, P. Médéric , T. Aubry, Nanocomposite-based polyamide 12/montmorillonite: relationships between structures and transport properties. Desalination 2006; 199: 164–166.

[92] S.T. Nguyen, O.C. Compton, S. Kim, C.Pierre, J.M. Torkelson. Crumpled graphene nanosheets as highly effective barrier property enhancers. Adv. Mater. 2010:1-5.

Chapter 3

EXPERIMENTAL

3.1 Introduction

This chapter is mainly divided into three parts. The first part is about the materials used in this particular study. Second part is about preparation of nanofillers and fabrication of nanocomposites. The characterization techniques used to characterize the systems is the final part of this chapter. The employed materials, instrumentation, sample fabrication, experimental procedures, and characterization techniques are discussed as follow;

3.2 Materials

3.2.1 Nylon 12

Nylon 12 (Polyamide PA 2200) ,with M_w = 76950 g/mol and M_n = 38800 g/mol, used in this study was provided by 3T RPD Ltd, UK as a white powder and was dried in a vacuum oven for 24 hrs at 40°C to remove any residual moisture. This grade of nylon is the most common material used in selective laser sintering (SLS) prototyping.

3.2.2 Graphite

EG (expanded graphite) used for the production of EGO (expanded graphite oxide) and was purchased from Qingdao Company, China. The specifications of expandable graphite are given in table 3.1.

3.2.3 Nitric acid (HNO_3)

Concentrated nitric acid, which had density of 1.42g/cm^3, was purchased from Fisher Scientific Company, UK. HNO_3 was used as supplied for the treatment of the fillers used.

3.2.4 Sulphuric acid (H_2SO_4)

Concentrated sulphuric acid was purchased from Fisons Scientific Company (UK) and was used as supplied for the treatment of the fillers used.

Expandable graphite	
Ash	1.45%
Moisture	0.84%
Expansion volume	200 cc/g
pH value	6.40
Volatiles	11.60%
Size	0.30mm (300μm)
Sieving residual	82%

Table 3.1 Characteristics of expanded graphite

3.2.5 Potassium permanganate ($KMnO_4$)

$KMnO_4$ (98% pure), used for exfoliation of EG, was purchased from Fisher Co. Ltd, UK. It had density of 2.70 g/ml. The composition of potassium (K), Manganese (M) and oxygen (O_2) was 24.74%, 34.76% and 40.50% respectively.

3.2.6 Barium chloride ($BaCl_2$)

$BaCl_2$, having density equals to 3.86 g/ml, was supplied by Fisher Co. Ltd, UK and was used to exfoliate EG. The composition of Ba and Cl_2 was 65.95% and 34.05% respectively.

3.2.7 Hydrochloric acid (HCl)

HCl 40% was bought from Fisher Co. Ltd, UK and was used as supplied for the treatment of expanded graphite.

3.2.8 Hydrogen peroxide solution (H_2O_2)

Hydrogen peroxide solution 100 volumes 30% w/v was kindly supplied by Fisher Co. Ltd, UK. It was used as supplied for the treatment of expanded graphite.

3.2.9 Carbon black (CB)

Carbon black (N-330) was purchased from Columbian Chemicals Company, Georgia. The particle size of CB was about 26nm. It was used for the comparative study of nanofillers contributing towards toughness of polymer nanocomposites.

3.2.10 Carbon nanotubes

The carbon nanotubes used were multi-walled carbon nanotubes (MWCNTs) , which were obtained from Chengdu Institute of Organic Chemistry, Chinese Academy of Science, China. The diameter of the nanotubes was about 8–15 nm. MWCNTs were used for the comparative study nanofillers contributing towards toughness of polymer nanocomposites.

3.2.11 Nylon 12 pellets

The nylon 12 pellets, used as supplied for the preparation of master batches, were supplied by Plastim Ltd, UK.

3.2.12 Nano-graphite (UF4 graphite)

Nano-graphite, sold as UF4 graphite, was purchased from Graphite Kropfmühl AG, Germany. Carbon content of UF4 were 94~ 99.9%. The particle size was about 4~7μm. Exfoliation behaviour of UF4 graphite was compared with the larger sized graphite supplied by Qingdao Company, China.

3.3 Preparation of Functionalized graphene

As discussed in chapter 2, better routes for the production of graphene are those which involve exfoliation of expanded graphite and then its suspension in water or organic solvent. Considering this fact, in this particular attempt for the preparation of functionalized graphene, exfoliated graphite oxide (EGO) was prepared from EG by using Hummer's method because of following three important reasons;

i. This method gives good quality product with low C/O ratio (2.1-2.9) compared to other available methods.

ii. It is a less processing time method with comparatively less danger of hazards

iii. Materials are easily available

Following steps were followed to prepare EGO;

1: 2.5 g of expanded graphite was mixed with 57.5 ml of concentrated H_2SO_4 in an ice-bath for half hour.

2: $KMnO_4$ was added slowly into the mixture in order to keep the temperature of mixture not exceeding than 20°C.

3: The mixture was then heated to 35±3°C and kept stirring for 30 minutes.

4: Drop wise addition of 115 ml distilled water increased the temperature of mixture to 98°C.

5: The reaction mixture was kept at this temperature for 15 minutes.

6: The oxidation reaction was terminated by addition of 350 ml distilled water and 25 ml of H_2O_2 solution.

7: Collection of EGO by filtering and successive washing with 5% HCl aqueous solution was repeated three times until there was no sulphide detected by $BaCl_2$ solution.

8: Finally EGO was dried at 50°C under vacuum for one week.

The exfoliation of 100mg EGO in 10g water was conducted using ultrasonication with a power of 300W for 1 hour at room temperature to obtain the functionalized graphene (FG) in water.

Transmission electron microscopy (TEM, JEOL 2100FX) was used to investigate the existence of FG in water and it was found that EGO was fully exfoliated to FG, as shown in figure 3.1.

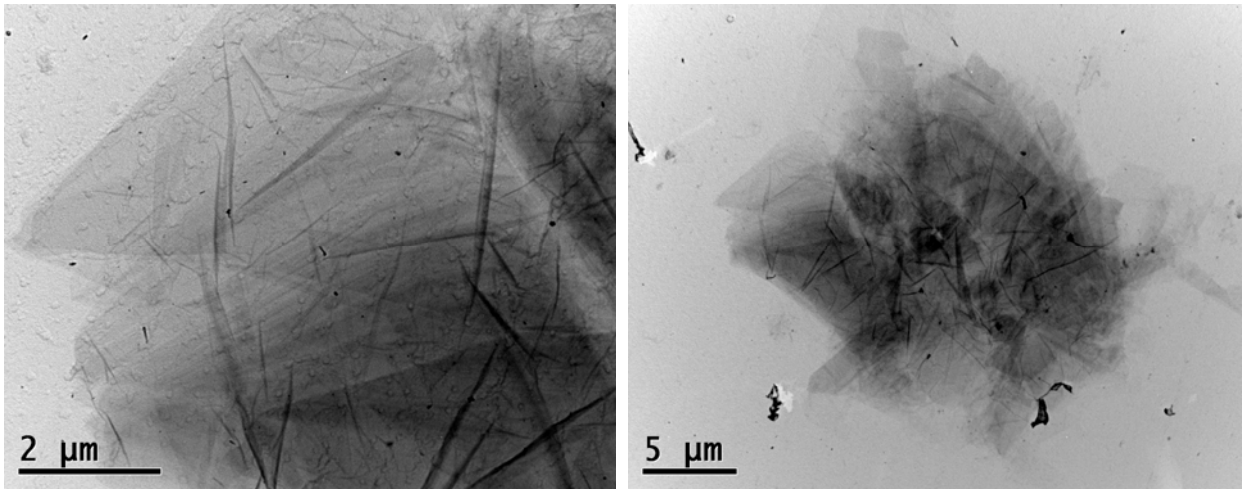

Fig.3.1 TEM proved successful exfoliation of functionalized graphene sheets in water

Hummer's method, because of the corrosive nature of used $KMnO_4$ and difficulties in scaling up the production of graphene oxide, needs to be updated. A new, safer and massively scalable route for the exfoliation of expanded graphite was discovered. The experimental details of this method cannot be provided in this report because the method is at its confidential stages. The complete exfoliation of EG to graphene sheets, using the recently discovered 'new method', is shown in figure 3.2.

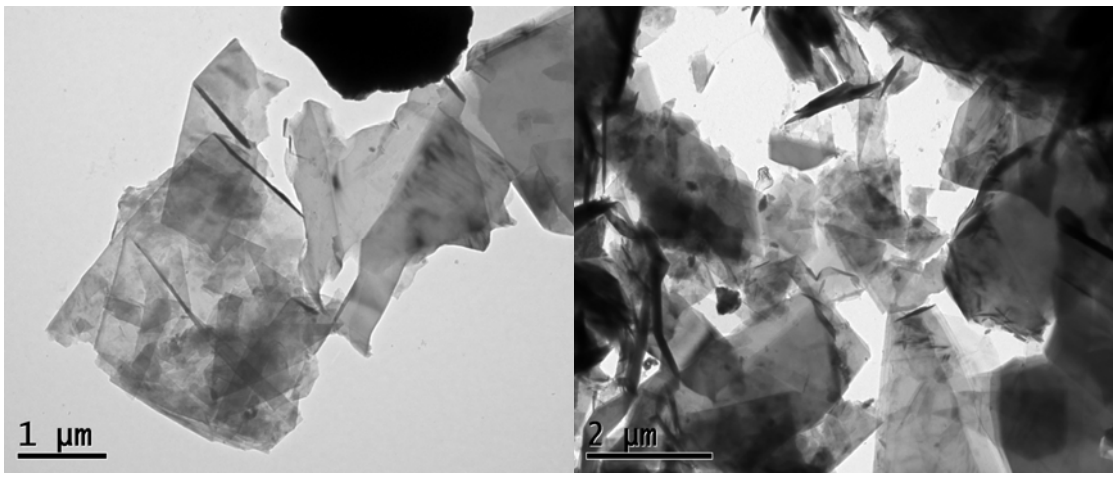

Fig.3.2 TEM images for FG produced by 'new method'

The stability of EGO produced by Hummer's method and by our 'new method' was characterized by dispersing it in water and both dispersions were subjected to ultrasonic treatment for 20 minutes. Even after three months, similar to the application of Hummer's method, a stable aqueous dispersion was obtained using our 'new method' as shown in figure 3.3.

In order to find out the effect of size of graphite on several properties of nylon 12 matrix UF4 graphite which is of much smaller size as compared to the one bought

from Qingdao Company, was also exfoliated to prepare exfoliated UF4 by using both methods i.e. Hummer's method and the 'new method'.

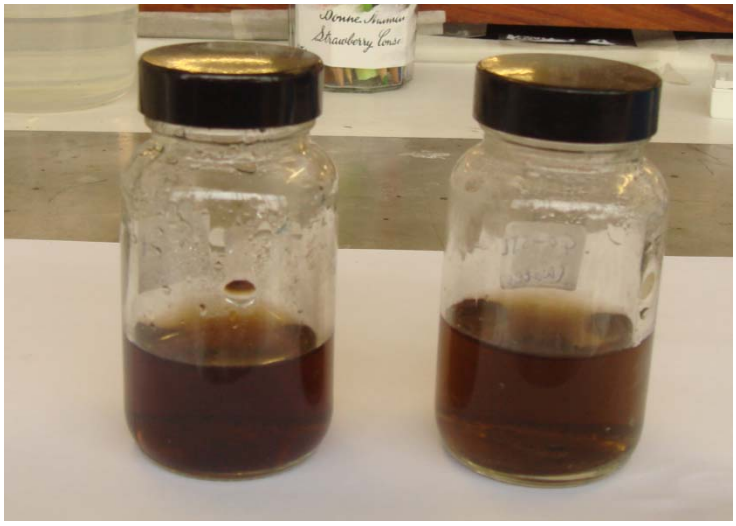

Fig.3.3 Digital picture of the EGO/water dispersions, the left one produced by Hummer's method and the right one produced by the 'new method'.

3.4 Exfoliation of UF4 graphite by physical method using an ultrasonic technique

To evaluate whether any chemical treatment was necessary for the successful exfoliation of UF4 graphite, a physical method was applied. The graphite was exfoliated in water using ultrasonication (Fisher Scientific Dismembrator Model 500, 300W) which was applied for different times (0, 10, 20, 30 and 60mins) at room temperature. TEM was employed for the observation of exfoliation of graphite. The TEM samples were prepared by dropping 1~2 droplets of the suspension onto 400 mesh holey carbon mesh grids. The images of exfoliated graphite for different sonication time are shown in Figure 3.4. The results indicate that the successful exfoliation of graphite by ultrasonic technique was achieved.

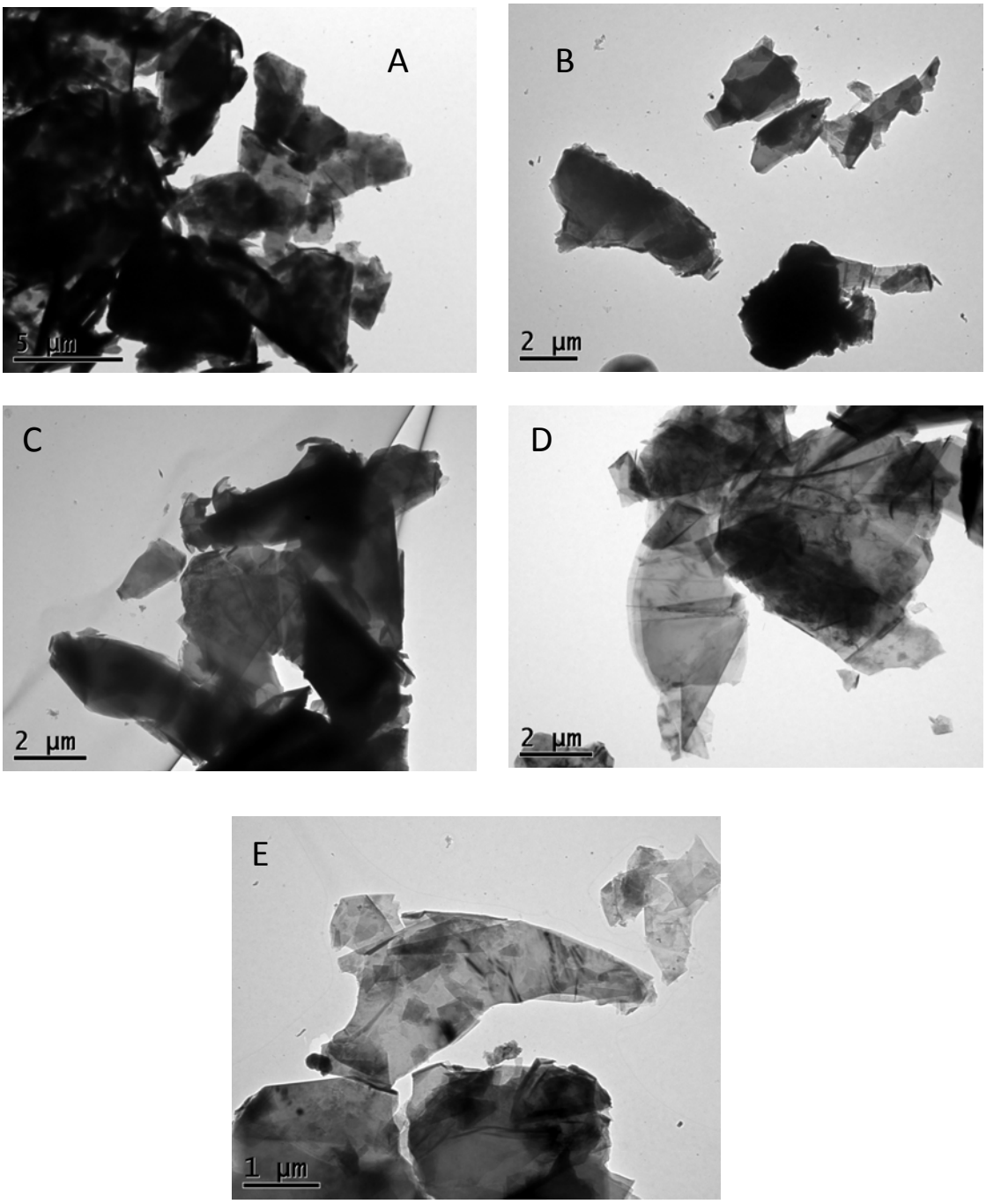

Fig.3.4 TEM images of the graphite flakes/water dispersions; (A) pure graphite; (B), (C), (D), and (E) images of the graphite flakes/water dispersion with different ultrasonication times 0, 10, 20, 30 and 60 minutes respectively.

The stability of the exfoliated graphite dispersion was also studied. Figure 3.5 shows the digital pictures of the UF4 graphite/water dispersions taken after 1 hour of sonication treatments at various times.

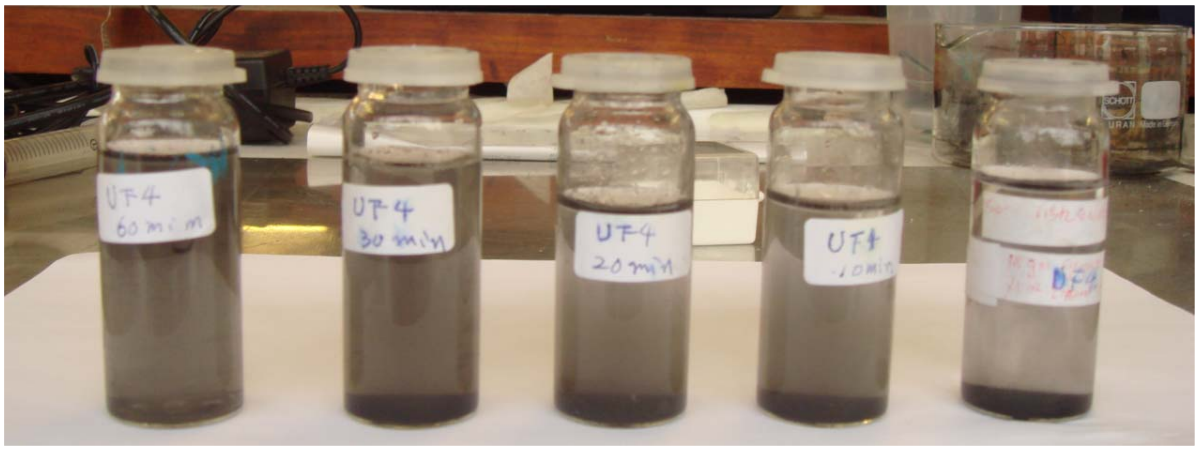

Fig.3.5 The digital picture of graphite flakes/water dispersions with different sonication time; from right to left, 0min, 10mins, 20mins, 30mins, and 60mins, respectively.

Figure 3.5 shows that the stability of the dispersion depends on the duration of ultrasonication. However, all of the dispersions were not able to keep their dispersed state for more than 3 hours, and then the graphite flakes started to fall down at the bottom of the containers. Although the graphite flakes were successfully exfoliated (as shown in figure 3.4), but because of the non-polar surface and the too high surface energy solvent (water) the stability was very weak. Hence the exfoliated graphite flakes re-aggregated to large flakes and dropped down.

3.5 Preparation of acid treated nanofillers

Nano-graphite (UF4) was treated by using a mixture of acids and a certain treatment times as given below [1];

i. Expanded graphite (1g) was suspended in 40ml mixture of concentrated

sulphuric and nitric acids. The volumetric ratio of HNO_3 to H_2SO_4 in the mixture was 1:3.

ii. The whole mixture was heated to 60^oC using a stirrer hot plate and was maintained at that temperature for 20 minutes.

iii. The mixture was filtered and washed with deionised water until pH=7 was achieved.

iv. Finally the mixture was dried in a vacuum oven at 100^oC for 2 days.

In order to study the effect of fillers with different geometries (tubes, particles or layered) on certain properties of polymers, multiwalled carbon nanotubes (MWCNTs) and carbon black were also treated by following the above described procedure.

3.6 Fabrication of nanocomposites

3.6.1 Nylon 12/ FG nanocomposites

0.1, 0.3 and 0.6, 1 and 3wt % FG/Nylon 12 nanocomposites were fabricated by melt blending due to its simplicity and compatibility with the existing polymer processing techniques. Pre-mixing of Nylon12 and FG were applied by Song's method. Finally, the prepared nylon 12/FG powders at different weight percentage ratios (Nylon/FG: 99.9/0.1, 99.7/0.3, 99.4/0.6, 99/1, 97/3) were mixed again using a Haake mixer (Rheomix 600, Germany). The total weight of the raw materials added into the mixer was 45g every time. The processing conditions were as follows:

Rotor speed	60 rpm
Mixing time	10 min
Mixing temperature	200^oC

Table 3.2 Melt blending parameters

3.6.2 Nylon 12/ UF4 based FG nanocomposites

0.1, 0.3 0.6 and 1 % UF4 based graphene/Nylon 12 nanocomposites were also fabricated by melt blending under similar conditions after the nylon 12 powders were pre-mixed with UF4 using Song's method.

3.6.3 Treated CB, MWCNTs and UF4 nanocomposites with nylon 12

Acid treated carbon black (CB), multiwalled carbon nanotubes (MWCNTs) and UF4 graphite were premixed with nylon 12 via Song's method and were melt blended with the aid of Haake mixer under same processing conditions as for FG/ nylon 12 systems.

3.6.4 Nanocomposites of Nylon 12 and UF4 (exfoliated with different techniques)

Expanded graphite was exfoliated to EGO and hence was converted to functionalized graphene sheets (FG) by using Hummer's method and the 'new method'. These graphene sheets were premixed with nylon12 and were melt blended in the later stages. In order to compare the effect of these graphene sheets (rich in functional groups) on barrier properties of nylon 12, untreated UF4 based nylon 12 nanocomposites were prepared. To achieve this goal, the untreated UF4 was suspended in water using ultrasonic treatment as described above under the heading of 3.4.

3.6.5 Master-batch based nanocomposites

A promising improvement in mechanical, thermal and barrier properties of nylon 12 powder was achieved by dispersing graphene sheets in it. Since use of the nylon 12 powder is restricted to mainly selective laser sintering processes and for laboratory

scale production of nanocomposites and industrial scale production of nanocomposites majorly involves pellets, therefore it was considered that production of premixed masterbatches of FG/nylon 12 powder, to be mixed with nylon 12 pellets will be of great practical importance. A 2wt% FG based nylon 12 powder was prepared using Song's method and was diluted, later on, with nylon pellets using Haake mixer to produce 0.1, 0.3 and 0.6 wt% FG masterbatches.

3.7 Characterization of nanocomposites

The detail of techniques and equipments used to characterize various properties of graphene based nylon 12 nanocomposites is discussed as below;

3.7.1 Differential scanning calorimetery (DSC)

Thermal analysis refers to a variety of techniques in which a property of a sample is continuously measured as the sample is programmed to go through a predetermined temperature profile. One of the most common thermal analysis techniques is thermal differential scanning calorimetry (DSC). In a DSC, the difference in energy input into a sample and a reference material is measured while the sample and material are subjected to a controlled temperature programme. In other words, DSC measures the power [heat energy / time] difference between small weighed samples of polymer (10-15 mg) in a sealed aluminium pan with reference to an empty aluminium pan. DSC requires two cells equipped with thermocouples in addition to a programmable furnace, recorder, and gas controller as shown in block diagram of DSC (figure 3.6) [2]. A DSC curve (enthalpy vs. Temperature) is interpreted by relating the changes in curve to chemical and physical changes occurring in the sample. DSC is often used as a qualitative or comparative technique. This technique is commonly used for characterizing the melting temperature (T_m), crystallization temperature (T_c), glass

transition temperature (T_g) and heat of fusion of the polymers as shown in figure 3.7 [3].

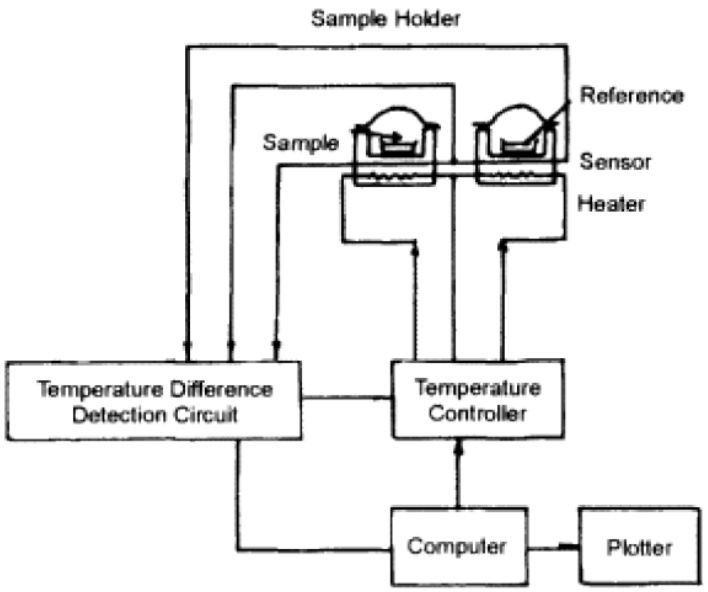

Fig.3.6 Block diagram of Differential scanning calorimeter [2]

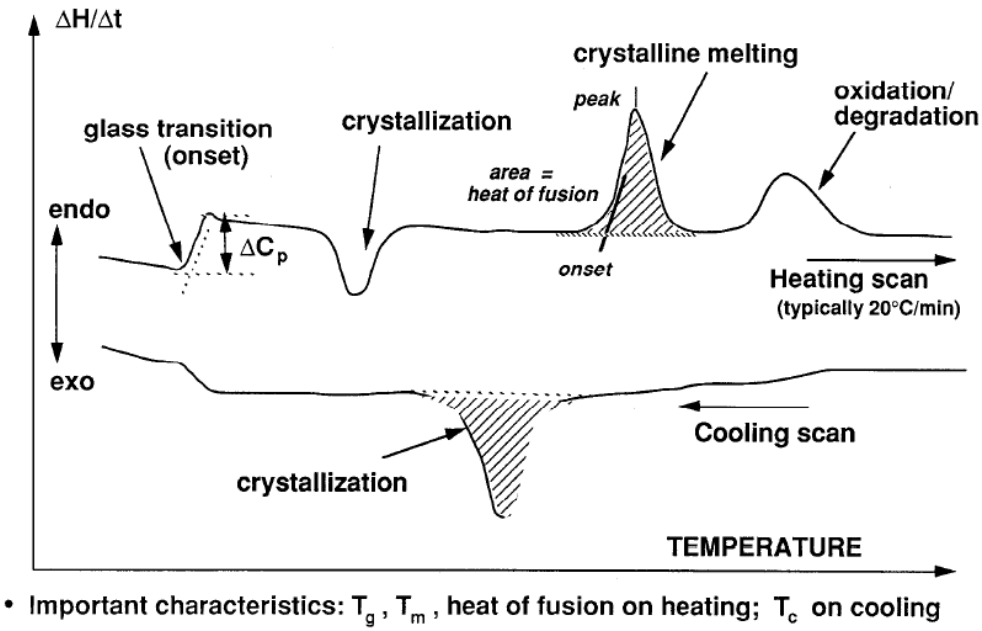

Fig.3.7 A typical DSC curve [3]

In this study, a TA Instrument DSC 2920 differential scanning calorimetry (DSC) was used to understand the effect of FG on T_m, T_c and T_g of nylon 12. The crystallization analysis of nylon 12 and its nanocomposites was also performed by using DSC under both non-isothermal and isothermal conditions. Typical sample weights ranged from 10 to 15 mg for the individual sample. Heating rate was 10°C/min for the non-isothermal experiments, in which each sample was melted at 210°C for 10 minutes and then cooled down to room temperature. Isothermal crystallization studies were carried out by melting the samples at 210°C for 5 minutes, cooling to the predetermined crystallization temperature (T_c) and then isothermally crystallizing it for 30 minutes. Aluminium pans were used and nitrogen was used as purge gas at the flow rate of 50 ml/min.

3.7.2 Tensile testing

The mechanical properties of polymeric materials are of great importance in several engineering applications. When a mechanical force is applied to a specimen, deformation of the specimen is described in terms of its stress-strain behaviour. The stress has dimensions of force per unit area e.g. N/m^2, MPa, GPa. The strain is a dimensionless quantity. For a tensile deformation, it is defined simply as the fractional change in length of the specimen as a result of the deformation. Tensile strength is indicated by the maximum of a stress-strain curve. As tensile strength is an intensive property, its value does not depend on the size of the test specimen. It is, however, dependent on the preparation of the specimen and the temperature of the test environment and material.

Specimens for tensile testing were prepared using compression moulding operating at a temperature of 210°C and a load of 20 tons. Mechanical testing was performed

on a LR50K Plus, Lloyd Instruments tensile testing machine at crosshead speed of 5 mm/min by following ASTM D638 standard test method. A load cell of 1kN was used for all the tests and an average of five test results was reported as final value of tensile strength at break, percent elongation and Young's modulus etc. All the tensile tests were carried out at room temperature.

3.7.3 Instrumented falling weight impact tester (IFWIT)

Impact resistance tests were performed using Rosand Instrumented Falling Weight Impact Tester (IFWIT). ASTM D5420 standard test method was followed to assess the impact behaviour of nylon 12 and its nanocomposites. One of the biggest advantages of using IFWIT is that it can provide a series of results. It also has the flexibility to use specimens of any shape and size (which can fit mass/ striker assembly). The samples (2mm thick sheets) were prepared using compression moulding at 210°C and at a load of 20 tons. A standard dropping mass of 10 Kg, at a speed of 3.12 m/s, was employed on the entire specimens from a drop height of 0.5m. All the reported results were the average of at least five tests.

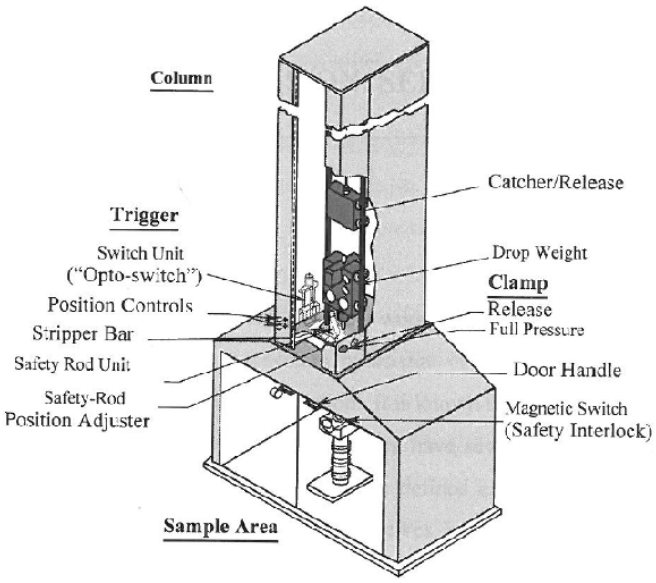

Fig.3.8 Rosand instrumented falling weight impact tester (IFWIT) [3]

3.7.4 Toughness parameter (K_{1c}) calculation

Mode I fracture toughness (K_{1c}) tests for pre-notched samples of nylon 12 and its nanocomposites were conducted on LR50K Plus, Lloyd Instruments tensile testing machine by following ASTM standard D5045-99. The fracture toughness tests were conducted at a crosshead speed of 60 mm/min and a span width of 50mm. A load cell of 1kN was used for all the tests and an average of five test results was reported as final value of K_{1c}.

3.7.5 Dynamic mechanical analyzer (DMA)

A DMA applies an oscillating force to a sample and measures its response to the applied force.DMA is considered to be a useful tool for characterizing the damping properties, phase lag and other certain mechanical properties of polymers. Measuring response of material under applied oscillating force gives properties like the tendency to flow (called viscosity) from the phase lag and the stiffness (modulus) from the sample recovery. In DMA we are actually focusing on the relaxation behaviour of the polymer chains and the changes occurring in the free volume of the polymer during deformation. The modulus measured in DMA is, however, not exactly the same as the Young's modulus of the classic stress–strain curve. Young's modulus is the slope of the initial linear region of a stress–strain curve, while in DMA; modulus is calculated from the material response to the applied sinusoidal force at each point. In other words, these different moduli calculated at various points allow better characterization of the material. In DMA we can examine the ability of the material to return energy i.e. elastic modulus (E'), to lose modulus (E″), and the ratio of E' and E″ (tanδ), which is called damping [4]. This mechanical damping or internal friction gives the amount of energy dissipated as heat during the deformation.

The TA instruments Q800 Dynamic Mechanical Analyzer (DMA) was used in this work to test the thermo-mechanical properties of nylon12 and its nanocomposites. Small rectangular bar specimens of approximately 35mm x 10mm x 2mm, made by compression moulding, were tested. The three point bending mode was used in all the tests and the specimens were held by dual cantilever clamps. This clamping arrangement is shown in figure 3.9.

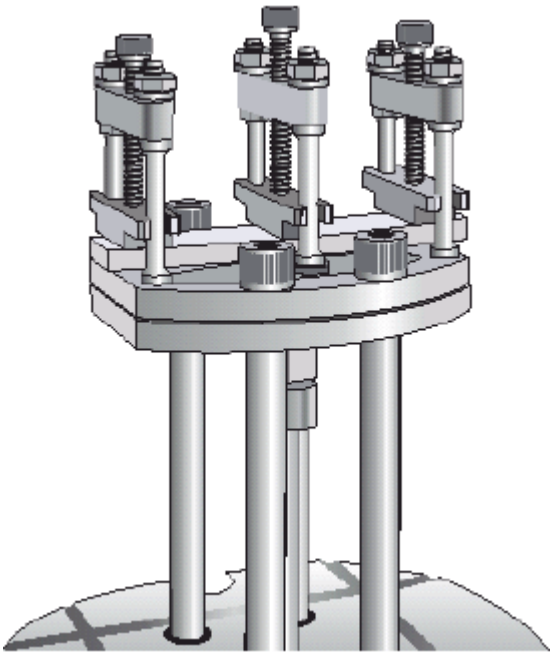

Fig.3.9 Dual cantilever of DMA [4]

The specimens were tested from -50°C to 150°C at frequenies of 1 and 10Hz at the heating rate of 3°C/min. Liquid nitrogen was used to achieve the lower temperatures such as -50°C. DMA was also used to evaluate the effect of variable frequency at constant temperatures. All the specimens were characterized by using Isothermal frequency sweep at 28, 32 and 36°C and by varying the frequency from 0.1 to 100Hz.

3.7.6 X-ray diffraction (XRD)

XRD is a useful technique to derive information about the structure of semi crystalline polymers. It is primarily used for phase identification of a crystalline material and can provide information on unit cell dimensions.

In this work, X-ray diffraction (XRD) patterns were recorded at a Philip-X' Pert X-ray diffractometer (anode 40 kV, filament current 35 mA) with nickel-filtered CuKa (ƛ = 0.1542 nm) radiation at a scan speed of 1°/min. Scans were taken from 0 to 30° on the thin sheet samples which were made by compression moulding.

3.7.7 Fourier Transform Infrared Spectroscopy (FTIR)

In infrared spectroscopy, IR beam is passed through a sample. Part of the infrared radiation is absorbed by the sample and the rest of it is transmitted (passed through the sample). The resulting spectrum represents the molecular absorption and transmission, creating a molecular fingerprint of the sample. An infrared spectrum is a fingerprint of a sample with absorption peaks which correspond to the frequencies of vibrations between the bonds of the atoms making up the material. FTIR has a wide application in the field of polymer analysis, not only because of its ability to look at intractable, thick and intensely absorbing materials but also because of the ability to observe chemical and physical change in the polymeric structure. Moreover FTIR can also be used to identify the unknown compounds by matching different peaks of spectrum of unknown compound to the reference spectrum. A brief reference table of IR is summarized in table 3.3. FTIR is a preferred method of qualitative analysis over other spectral analysis techniques because of the following reasons:

- It provides a precise measurement method which requires no external calibration as it is self calibrated.
- It can increase speed, collecting a scan every second.
- It is a non-destructive technique.
- Sensitivity is dramatically improved with FTIR for many reasons. The detectors employed are much more sensitive, the optical throughput is much higher
- The moving mirror in the interferometer is the only continuously moving part in the instrument. Thus, there is very little possibility of mechanical breakdown.

The IR beam emitting from the light source passes through an aperture which controls the amount of energy is incident on the sample [5]. This IR beam enters the interferometer from which interferogram signal is projected upon the sample. This is where specific frequencies of energy, which are unique characteristics of the sample, are absorbed. The beam finally passes to the detector for final measurement. The detectors used are specially designed to measure the special interferogram signal. The measured signal is digitized and is sent to the computer where the Fourier transformation takes place. The final infrared spectrum is then presented to the user for interpretation and any further manipulation. This working of FTIR is shown in figure 3.10.

Since infrared spectroscopy exploits the fact that molecules absorb specific frequencies that are characteristic of their structure, therefore these resonant frequencies can be associated with the type of bond present in a particular sample. Bonds in a molecule can vibrate in six different ways; symmetric and antisymmetric stretching, scissoring, rocking, wagging and twisting. These vibrations are shown in figure 3.11.

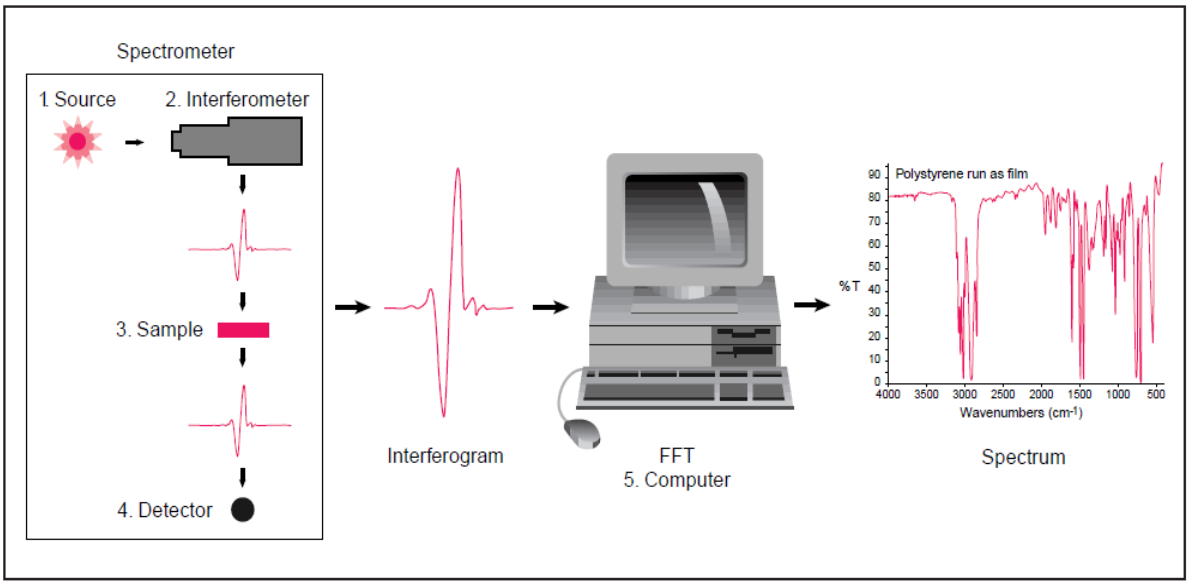

Fig.3.10 Basics of FTIR [5]

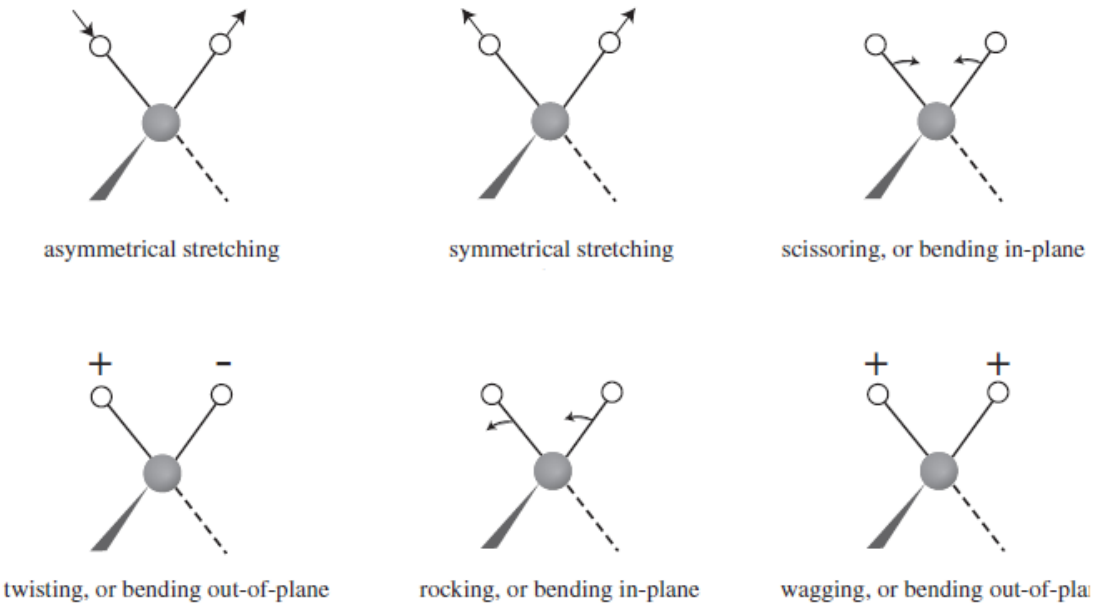

Fig.3.11 A variety of vibrations of a CH_2molecule. '+' indicates motion from the page towards the reader and '–'indicates motion away from the reader [6]

Functional Group	Characteristic Absorption(s) (cm^{-1})	Notes
Alkyl C-H Stretch	2950 - 2850 (m or s)	Alkane C-H bonds are fairly ubiquitous and therefore usually less useful in determining structure.
Alkenyl C-H Stretch Alkenyl C=C Stretch	3100 - 3010 (m) 1680 - 1620 (v)	Absorption peaks above 3000 cm^{-1} are frequently diagnostic of unsaturation
Alkynyl C-H Stretch Alkynyl C≡C Stretch	~3300 (s) 2260 - 2100 (v)	
Aromatic C-H Stretch Aromatic C-H Bending Aromatic C=C Bending	~3030 (v) 860 - 680 (s) 1700 - 1500 (m,m)	
Alcohol/Phenol O-H Stretch	3550 - 3200 (broad, s)	
Carboxylic Acid O-H Stretch	3000 - 2500 (broad, v)	
Amine N-H Stretch	3500 - 3300 (m)	Primary amines produce two N-H stretch absorptions, secondary amides only one, and tertiary none.
Nitrile C≡N Stretch	2260 - 2220 (m)	Nitrile C≡N Stretch
Amide N-H Stretch	3700 - 3500 (m)	As with amines, an amide produces zero to two N-H absorptions depending on its type.
Aldehyde C=O Stretch Ketone C=O Stretch Ester C=O Stretch Carboxylic Acid C=O Stretch Amide C=O Stretch	1740 - 1690 (s) 1750 - 1680 (s) 1750 - 1735 (s) 1780 - 1710 (s) 1690 - 1630 (s)	The carbonyl stretching absorption is one of the strongest IR absorptions, and is very useful in structure determination as one can determine both the number of carbonyl groups (assuming peaks do not overlap) but also an estimation of which types.

Table 3.3 Characteristic infrared absorption frequencies [6]

In this particular study, FTIR has been used to observe the functional groups attached with treated nanofillers. The transmission spectra were recorded using a Mattson 3000 FTIR spectrometer for 64 scans at a resolution of 4cm^{-1} over the frequency range of 400-4000 cm^{-1}.

3.7.8 X-ray photoelectron spectroscopy (XPS)

XPS, also known as Electron Spectroscopy for Chemical Analysis (ESCA), is a quantitative spectroscopic technique which is widely used to measure the elemental composition of the elements present in any sample. It is a surface chemical analysis technique that can be used to analyze the surface chemistry of a material in its "as received" state, or after some treatment. A typical XPS spectrum is a plot of the number of electrons detected versus the binding energy of the electrons detected. Each element of a material under investigation produces a characteristic set of peaks at their characteristic binding energies. These characteristic peaks are related with configuration of electrons within the atoms i.e. 1s, 2s, 2p etc. The number of detected electrons in a certain peak is directly linked with the amount of element present [7, 8].

In this study, the degree of oxidation of expanded graphite into expanded graphite oxide (GO) was analyzed by using XPS. X-rays were generated by AlKα radiation which was operated at a voltage of 8kV and a current of 20 mA. The oxidation of graphite using Hummer's method as well as using 'new method' was confirmed by XPS results. The degree of oxidation was based on atomic ratio of carbon (C) and oxygen (O) i.e. lower is the C/O ratio; higher is the degree of oxidation. The broad scan XPS spectra of the pure graphite and the chemical functionalized graphite using Hummer's method are shown in Figure 3.12. The elemental analysis

demonstrates that the C/O atom ratio (2.707) of the chemical functionalized graphite is lower than that of the pure graphite (22.25). This confirms the successful oxidation of the graphite.

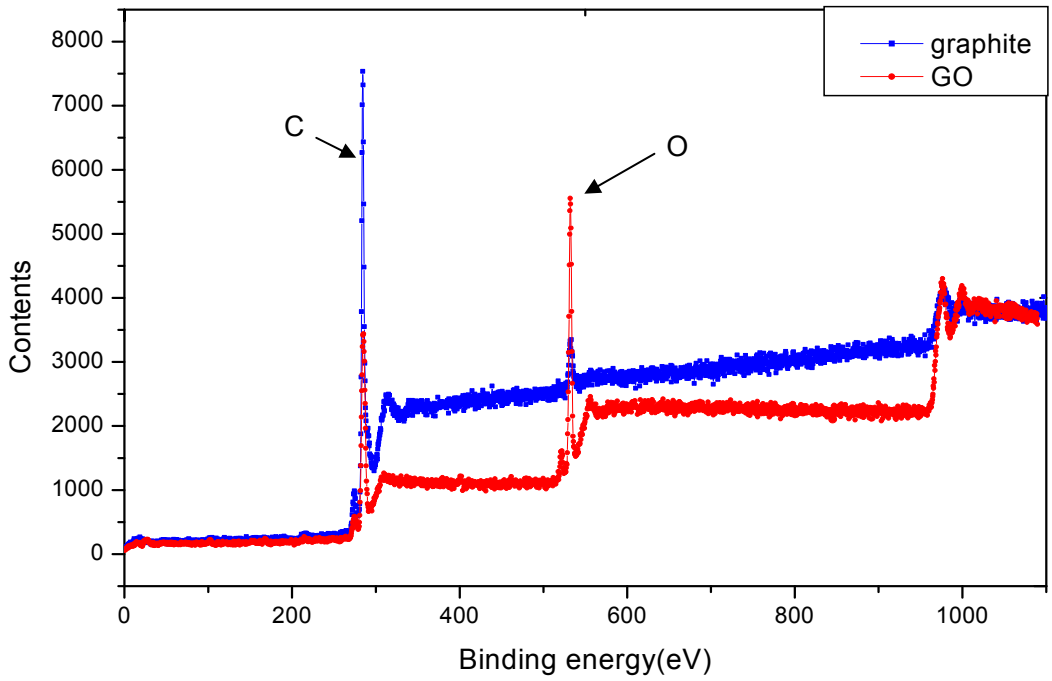

Fig.3.12 XPS spectra of pure graphite and graphite oxide

Similarly, the oxidation of UF4 graphite by following our 'new method' was also confirmed using XPS. The elemental analysis demonstrates that the C/O atom ratio (3.9) of the chemical functionalized UF4 graphite is lower than that of the pure UF4 graphite (25.2), hence confirming the oxidation. XPS spectra of pure UF4 graphite and expanded UF4 graphite oxide are shown in figure 3.13.

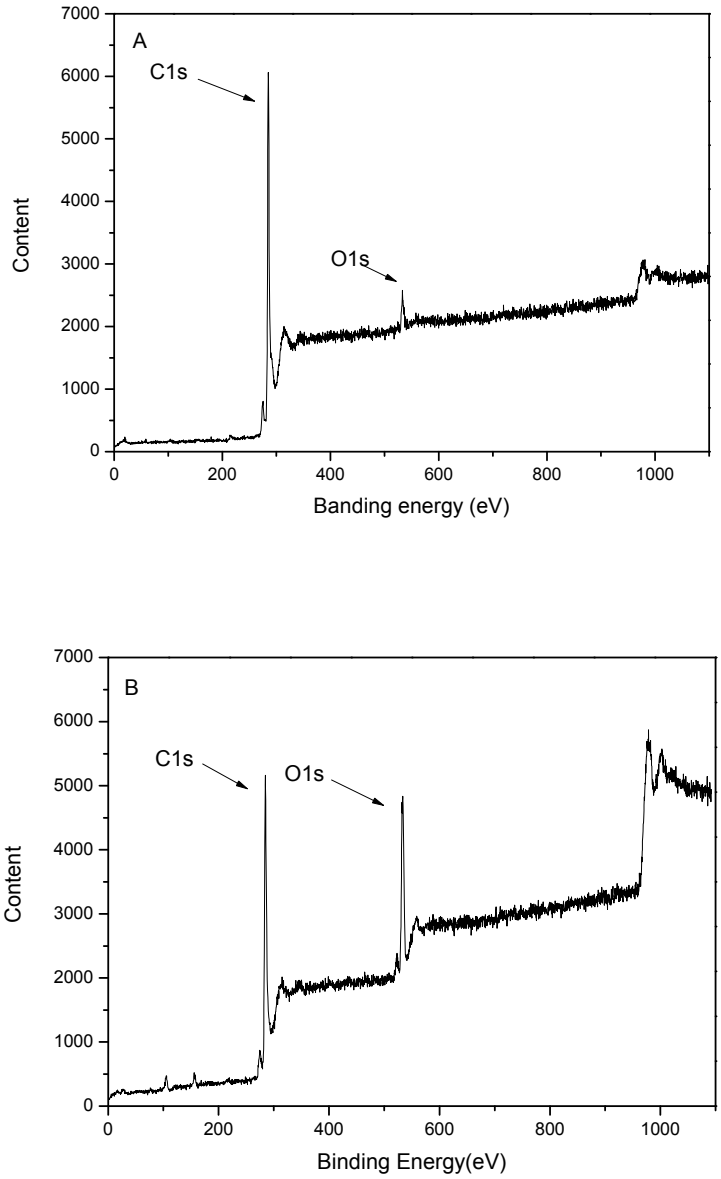

Fig.3.13 XPS spectra for UF4 graphite (A) and the chemical functionalized UF4 graphite (B)

3.7.9 Scanning electron microscopy (SEM)

In a typical SEM, a finely focused electron beam scanned across the surface of the sample generates secondary electrons (electrons from the sample itself), backscattered electrons (beam of electrons that bounce off nuclei of atoms in sample), X-rays, heat, light and even transmitted electrons. The reflected electrons

bounce back into a cathode ray tube detector, which analyzes the shape of an object based on how the electrons are reflected. Unlike a light microscope (where an instant real image of the sample is formed), SEM does not give a real image. Electron beam in SEM scans back and forth across a sample raster scanning). Because of this raster scanning SEM creates a three dimensional image of the sample. Microscopic study of the fractured surface can generate valuable information on failure of filled polymers around crack tips [9].

In this study, the scanning electron microscopy (SEM) images were taken on field emission gun scanning electron microscopy (FEGSEM) LEO 1530VP instrument. The samples were prepared from the tensile fractured specimens. The samples were gold coated to provide an electrically conductive layer, to suppress surface charge and to increase electron emission. The coating thickness was minimized for fine surface texture and higher resolution.

3.7.10 Transmission electron microscopy (TEM)

The basic working mechanism of TEM resembles with a light microscope with a very prominent difference of use of electron beams. Since electron beams have a shorter wavelength, therefore TEM is capable of producing a higher resolution. The beam of electrons shot by the electron gun is condensed by the electromagnetic lenses (condensers). When the electron beam goes through the sample being viewed, only a few electrons (which can pass through the specimen) are recorded by the detector screen present below the specimen. TEM can be used to analyse the morphology, i.e. shape and size, of the samples and then relate it with their properties [10].

In this study, JEOL 2000FX TEM was used to study the exfoliation of graphite to exfoliated graphene sheets (called as functionalized graphene sheets (FG) in this

study). The TEM samples were prepared by dropping 1 ~2 droplets of FG and water dispersions onto 400 mesh carbon mesh grids.

3.7.11 Polarized Optical Microscopy (POM)

Optical microscopes are usually used to obtain a magnified image of relatively smaller objects by utilising visible light. There are two light filters in an polarized optical microscope known as polarizer and analyzer. The polarizer is positioned beneath the specimen stage while analyzer is located above the objectives of a microscope. When both the analyzer and polarizer are inserted into the light path, their transmitted light vibrations are positioned at right angles to each other. In this configuration, the polarizer and analyzer are said to be crossed and the microscope is said to be cross polarized microscope [9].

A cross polarized Leica DMRX optical microscope was used to observe spherulites in nylon 12 and its nanocomposites. Samples were melted at 210°C for 10 minutes and were squeezed between microscope cover glass slides to prepare thinnest possible film and were cooled down to the room temperature.

3.7.12 Thermal gravimetric analysis (TGA)

TGA is a thermal analysis technique which quantifies thermal stability and decomposition of material by analyzing its mass loss as a function of temperature [11]. Percentage weight loss of nylon 12 and its nanocomposites was measured using thermo gravimetric analysis (TGA) upon heating from room temperature to 800°C at a heating rate of 10°C/min under air atmosphere.

3.8 References

[1] K Esumi, M Ishigami and A Nakajima et al. Chemical treatment of carbon nanotubes. Carbon 1996; 34: 279–281

[2] T. Hatakeyama, F.X. Quinn. Thermal Analysis fundamentals and applications to polymer science 2nd edition; 1999: chapter 2

[3] N.F. Cheremisinoff. Polymer characterization laboratory techniques and analysis; 1996: chapter 2

[4] H.P. Menard. Dynamic mechanical analysis: A practical introduction 2nd edition; 2008: chapter 1

[5] http://mmrc.caltech.edu/FTIR/FTIRintro.pdf

[6] D. A. Skoog, F. J. Holler, T. A. Nieman. Principles of instrumental analysis 5th edition; 1998: chapter 17

[7] J.F. Watts and J. Wolstenholme. An introduction to surface analysis by XPS and AES ;2nd edition: 2003

[8] J. C. Vickerman, I. Gilmore. Surface analysis: the principal techniques;2nd edition: 2009

[9] L.C. Sawyer, D.T. Grubb, G.F. Meyers. Polymer microscopy 3rd edition ; 2008: chapter 2

[10] http://www.ehow.com/facts_7423896_principle-tem.html

[11] M.E. Brown. Introduction to thermal analysis- techniques and applications 2nd edition; 2001: chapter 3

Chapter 4

Effect of graphene on the crystallization of nylon 12

4.1Introduction

Similar to many other semicrystalline polymers, the crystallization behaviour of nylon 12 depends upon activation energy and the mobility of chain segments. The addition of nanofiller (nucleating agent) is considered to be the best way to decrease this activation energy, hence favouring the crystallization process [1]. In our research, in order to favour the crystallization process, the same concept of decreasing the activation energy by the addition of nanofiller was applied.

Differential scanning calorimetry (DSC) was employed to understand how incorporation of graphene sheets disturbs melting and crystallization process of nylon 12. Two different sized nanofillers, graphene sheets derived from nano and micron size graphite and were named as UF4 and FG respectively, prepared by the same method (Hummer's), were used as nucleating agents for nylon 12. The effect of both nanofillers on thermal behaviour of nylon 12 was investigated under non-isothermal and isothermal conditions. The detailed results and discussion of this study are summarized below;

4.2 Non-isothermal DSC measurements

4.2.1 Effect of FG on thermal characteristics of nylon 12

Pure Nylon 12 and its nanocomposites with varying percentage loading of FG (0.1, 0.3, 0.6, 1 and 3 wt %) were subjected to DSC analysis under non-isothermal

conditions. In an attempt to reduce the effect of oxidative degradation, all DSC runs were carried out under nitrogen atmosphere. The degree of crystallinity was calculated by using the following equation.

$$X_c\,(\%) = \frac{\Delta H_m}{(1-\psi)\,\Delta H^o_m} \times 100 \qquad (4.1)$$

Where ΔH_m is the apparent melting enthalpy, ψ is the weight fraction of functionalized graphene (FG) and ΔH^o_m is the extrapolated value of the enthalpy corresponding to the melting of 100 % crystalline nylon 12 which is 209.2 J/g [2]. Figure 4.1 shows the non isothermal DSC curves of FG/ nylon 12 nanocomposites. It can be seen that the crystallization temperature (T_c) of nylon 12 increases upon incorporation of FG which is a direct evidence of FG acting as nucleating agent [1, 3]. A significant effect of FG on the crystallinity of nylon 12 was also observed. According to equation 4.1, an increase of 67% in the crystallinity of nylon 12 was observed with the addition of only 0.6 wt% of FG. Furthermore, it is interesting to observe that when the contents of FG were increased up to 1 and 3wt%, T_c started to decrease which implies that the higher contents of FG retarded the crystallization growth of nylon 12. This might be because of the formation of FG network structure at higher loadings and these FG networks had restricted the mobility and diffusion of nylon 12 chain segments to crystal growth fronts. It was observed that addition of a small percentage of FG promoted an increase in enthalpy and hence in crystallization. Although FG acted as nucleating agent but there was no significant change in melting temperature (T_m), except for 1 and 3wt% FG/ nylon 12 nanocomposites where a slight decrease in T_m was observed. Moreover the shape of heat flow vs time curve also remained unchanged upon incorporation of FG as

shown in figure 4.2. Melting temperature (T_m), Crystallization temperature (T_c), and degree of crystallinity (X_c) as a function of FG are given in table 4.1.

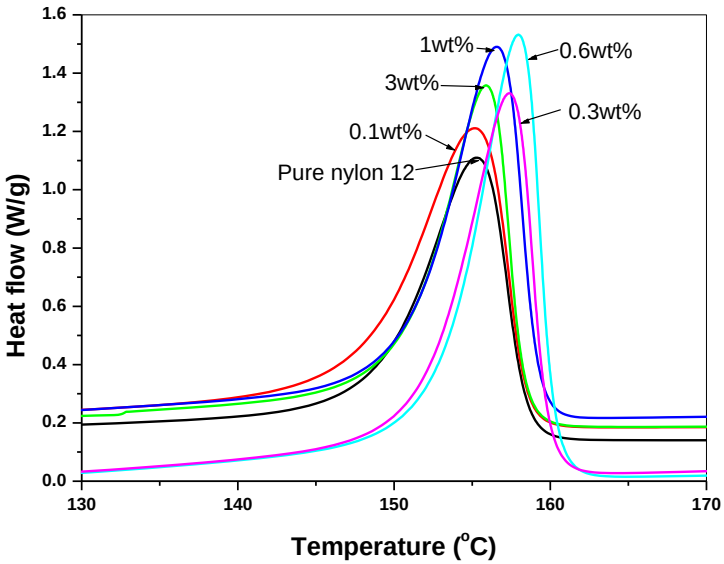

Fig.4.1 Crystallization temperatures of nylon 12 and its nanocomposites with FG

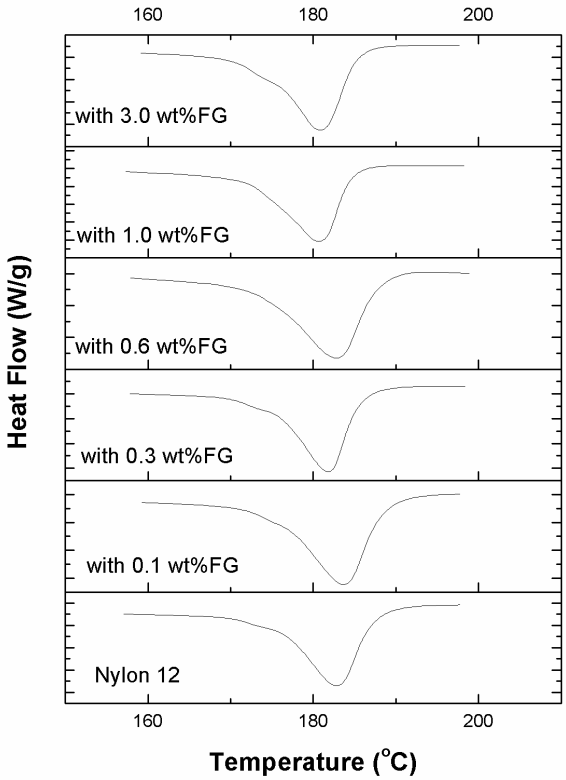

Fig.4.2 Melting temperatures of nylon 12 and its FG based nanocomposites

Sample	T_c (^oC)	T_m (^oC)	X_c (%)
Nylon 12	155.17	183.93	15.23
0.1 FG/ Nylon 12	155.28	183.68	17.80
0.3 FG/ Nylon 12	155.89	183.79	19.03
0.6 FG/ Nylon 12	156.28	183.85	25.50
1.0 FG/ Nylon 12	155.35	181.66	20.80
3.0 FG/ Nylon 12	155.20	180.83	19.43

Table 4.1 The crystallization temperature (T_c), melting temperature (T_m) and degree of crystallinity (X_c) for nylon 12 and its nanocomposites with FG.

4.2.2 Effect of graphene sheets based on nanographite

DSC was also used to understand the effect of graphene sheets (derived from nanographite, named as UF4) on the thermal properties of nylon 12 to compare whether graphene derived from a nanographite have a different thermal characteristics as compared to the one derived from micron size graphite (FG). It was observed that there was no major difference between the effect of different sized graphene on the thermal properties of nylon 12. The effect of nanographite based graphene sheets was only slightly different from that of FG; the T_c and crystallinity of UF4/ nylon 12 nanocomposites increased up to only 0.3 wt% UF4 and then started to decrease at higher loadings which might be because of agglomeration/ network formation. It was more likely as with the relatively smaller size nanofillers, there are more chances of agglomeration. Moreover, a slight increase in T_m was observed upon incorporation of UF4 based FG (up to 0.3wt %). Melting temperature (T_m), Crystallization temperature (T_c), and degree of crystallinity (X_c) as a function of UF4 based FG are given in table 4.2.

Sample	T_c (^oC)	T_m (^oC)	X_c (%)
Nylon 12	155.17	183.93	15.23
0.1 UF4/ Nylon 12	156.91	184.16	17.22
0.3 UF4/ Nylon 12	157.46	184.64	20.40
0.6 UF4/ Nylon 12	156.94	182.67	19.04
1.0 UF4/ Nylon 12	155.93	182.57	18.40

Table 4.2 The crystallization temperature (T_c), melting temperature (T_m) and degree of crystallinity (X_c) for nylon 12 and its nanocomposites with FG.

An increase in T_c and crystallinity (as shown in table 4.2) upon incorporation of UF4 based FG was observed, which witnesses the role of UF4 as nucleating agent. This increase in T_c is shown in figure 4.3. A slight increase in T_m upon incorporation of UF4 (up to 0.3 wt %) has been depicted in figure 4.4.

The glass transition temperature (T_g) of nylon 12 slightly increased (~3°C) upon incorporation of graphene sheets (prepared from both types of graphite) which is an indication of interaction between nylon 12 and the functionalized graphene sheets. This effect of graphene on T_g of nylon 12 is further explained in chapter 5.

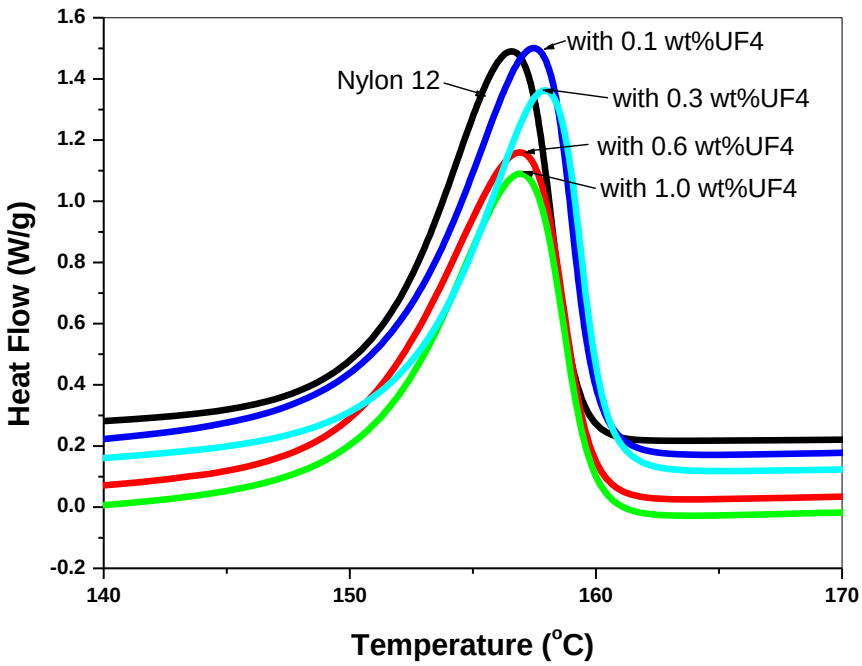

Fig.4.3 Crystallization temperatures of nylon 12 and its UF4 based nanocomposites

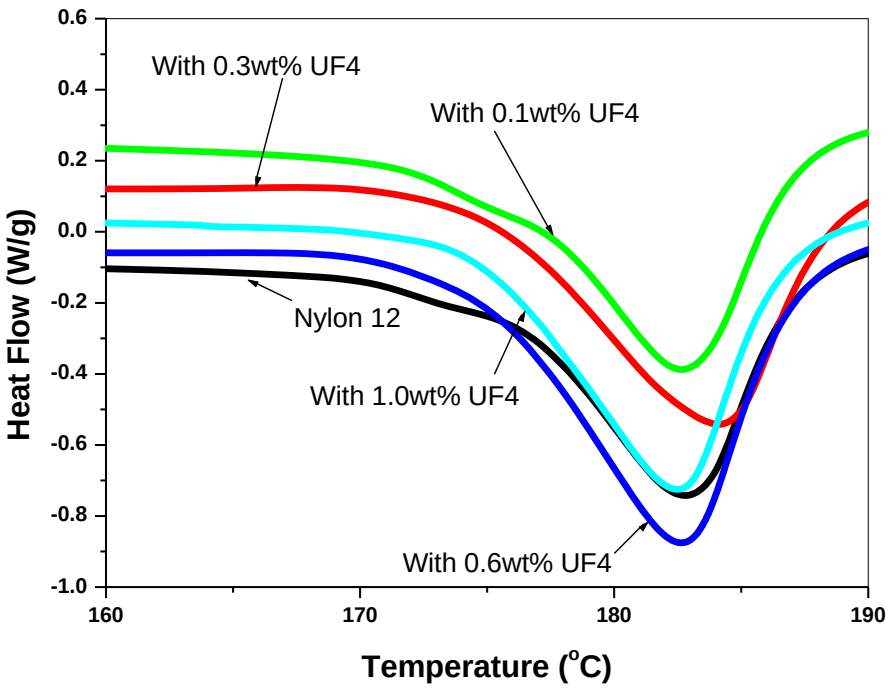

Fig.4.4 Melting temperatures of nylon 12 and its UF4 based nanocomposites

4.3 Isothermal DSC measurements

To further prove the results obtained from non-isothermal crystallization, the isothermal crystallization of nylon 12 and its nanocomposites was studied using DSC and the crystallization kinetics were studied using Avrami analysis. It was believed that isothermal crystallization with slow crystallization rates could be a simple and effective thermal treatment for optimizing small polymer crystallites which were spontaneously nucleated by functionalized graphene sheets [4].

Figure 4.5 shows isothermal crystallization curves for pure Nylon 12 and its nanocomposites. All the samples were heated to 210°C at the rate of 10°C/ minute, held there for 5 minutes and then were cooled down to various pre-determined crystallization temperatures. Because of difference in melting points, the isothermal crystallization temperature ranges are different for each sample. These crystallization temperatures were selected after a series of experiments conducted at various crystallization temperatures. For pure nylon 12 these three crystallization temperatures were found to be T_{c1}= 163°C, T_{c2}= 165°C and T_{c3}= 169°C. The value of crystallization temperature (T_c= 156°C) of nylon 12 was subtracted from selected crystallization temperatures (T_{c1}, T_{c2} and T_{c3}) to get the values of ΔT1, ΔT2 and ΔT3.

$$\Delta T_1 = T_{c1} - T_c = 163^{o}C - 156^{o}C = 7^{o}C$$

Similarly,

$$\Delta T_2 = 9^{o}C \text{ and } \Delta T_3 = 13^{o}C$$

These values of ΔTs of nylon12 were used to calculate T_{c1}, T_{c2} and T_{c3} values for 0.1, 0.3, 0.6, 1 and 3 wt% FG/ nylon12 nanocomposites.

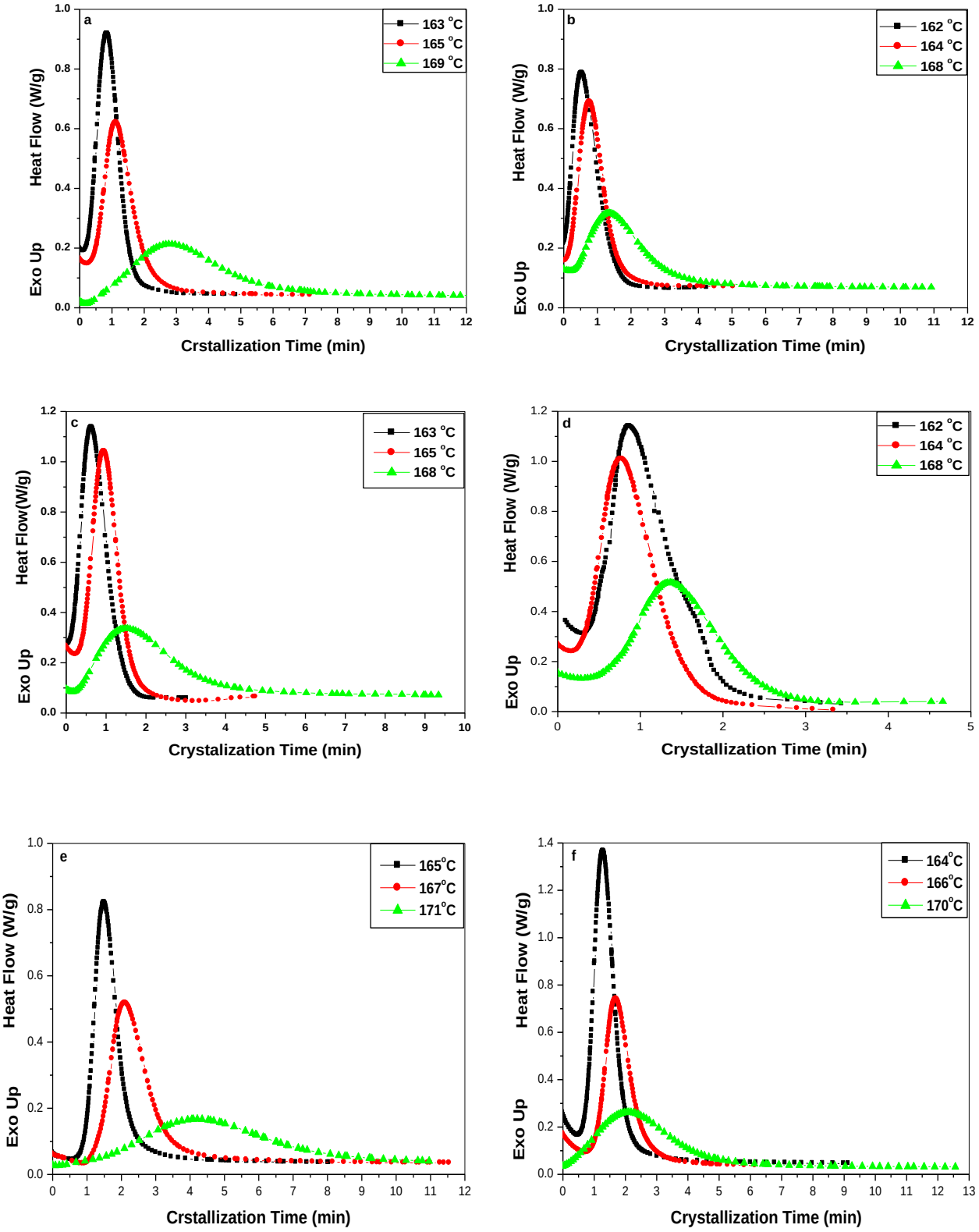

Fig.4.5 DSC traces of samples isothermally crystallized at the specified temperatures (a) Pure nylon 12 (b) 0.1wt% FG / nylon 12 (c) 0.3wt% FG / nylon 12 (d) 0.6 wt% FG / nylon 12 (e) 1.0 wt% FG / nylon 12 (f) 3.0 wt% FG / nylon 12

From figure 4.5, it can be observed that with an increase in crystallization temperature, the crystallization peaks for pure nylon and its nanocomposites shifts to higher crystallization times and flattens out. It implies that with an increase in temperature, the rate of crystallization decreases and all the samples required a longer time to completely crystallize. This increase in crystallization time or decrease in crystallization rate can be attributed to decrease in super-cooling temperature ($\Delta T = T_m - T_c$). Since the temperature gradient was decreased at higher crystallization temperature, the effective quenching of the melt took more time hence slowed down the crystallization process. To further disclose the process of isothermal crystallization, degree of crystallinity was calculated. The relative degree of crystallinity at time t, X(t), is defined as following;

$$X(t) = {\Delta Ht}/{\Delta H\infty} \qquad (4.2)$$

Where ΔHt is the heat generated at time t and $\Delta H\infty$ is the total heat by the end of crystallization process. Figure 4.6 shows the relative crystallinity at different crystallization times in the process of isothermal crystallization. It can be seen that the characteristic sigmoid isotherm shift to the right with increase in crystallization temperature and the rate of crystallization decreases accordingly. Each curve shows an initial linear portion, and then subsequently tends to level off. This is due to the secondary crystallization, which is caused by the impingement of spherulites and the perfection of internal spherulites at the latter stages of the crystallization process.

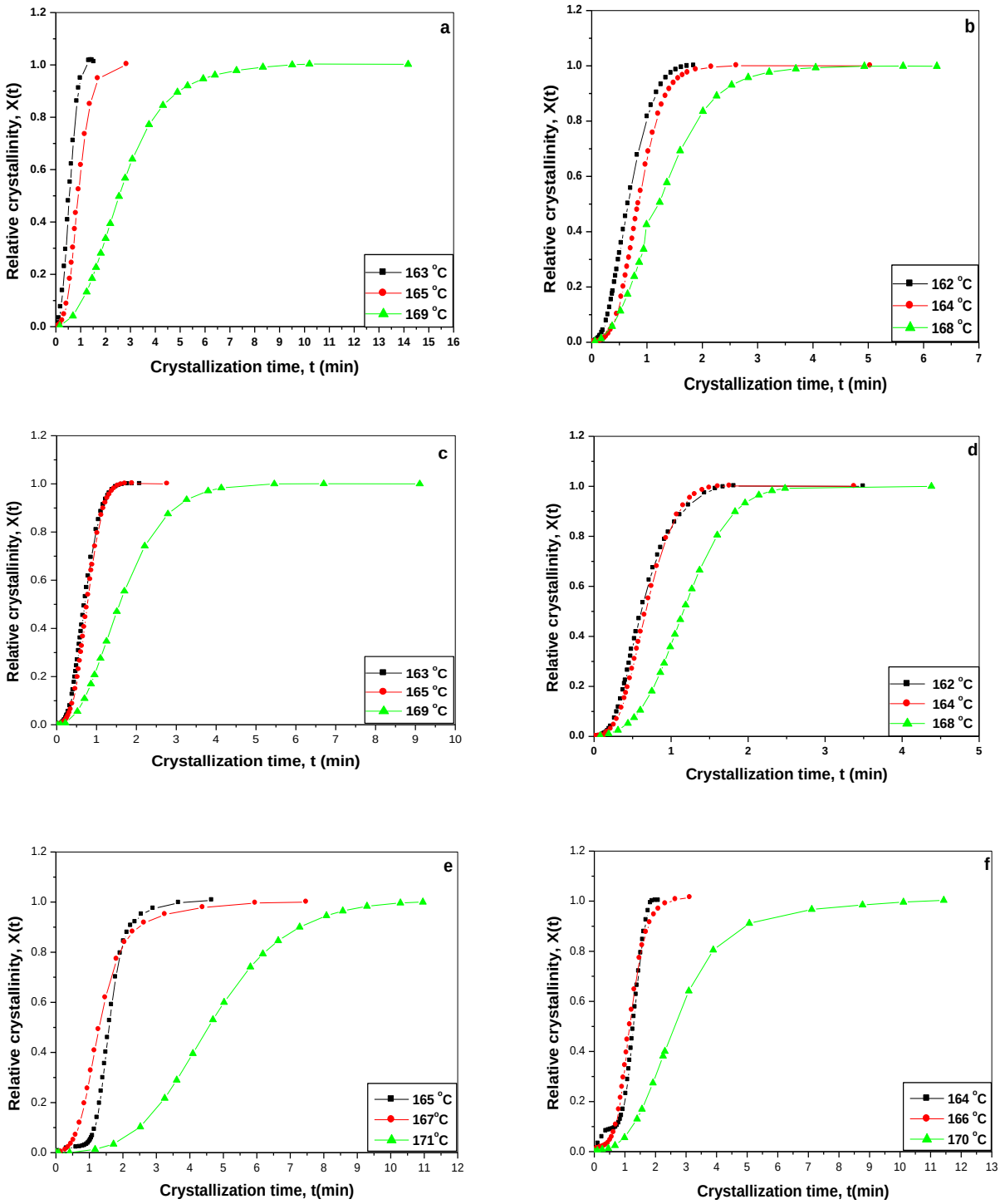

Fig.4.6 Relative crystallinity versus different crystallization time in the process of isothermal crystallization for samples (a) Pure nylon 12 (b) 0.1wt% FG / nylon 12 (c) 0.3wt% FG / nylon 12 (d) 0.6 wt% FG / nylon 12 (e) 1 wt% FG/ nylon 12 (f) 3 wt% FG/ nylon 12

The isothermal crystallization of polymers can usually be well described by the Avrami equation [4]. It was used, in this research as well, in order to investigate the isothermal crystallization behaviour of pure nylon12 and its nanocomposites. The Avrami equation is given below;

$$X(t) = 1 - \exp(-Kt^n) \qquad (4.3)$$

Where

X(t) = The relative degree of crystallinity,

t = Crystallization time,

n = Avrami constant which depends on the type of nucleation and growth of the crystals

K = Crystallization rate constant involving both nucleation and growth rate parameters under isothermal conditions.

It should be noticed that the validity of equation 4.2 is based on the assumption that the type of crystallization (crystal modification, dimension of growth, nucleation and growth conditions) does not change during the whole crystallization process.

It can be clearly seen that each isothermal curve in figure 4.6 presents the similar S-shape, which is in good agreement with the Avrami theory. The values of n and K were determined by non-linear curve fitting. The Avrami exponent (n) is not usually found to be an exact digit because of a diffusion controlled growth mechanism and irregular boundary of spherulites involved in the crystallization process. The values of n (the Avrami exponent), determined from the plots in figure 4.6 by using non-linear curve fitting function in Origin® software (version 6 provided by Microcal Software, Inc.), are listed in table 4.3.

Sample	T_c (^oC)	n	K (min^{-1})
Nylon 12	163 165 169	2.19 2.12 2.15	2.80 0.87 0.11
Nylon 12/ FG (0.1)	162 164 168	2.10 2.15 2.13	1.70 1.05 0.48
Nylon 12/ FG (0.3)	163 165 169	2.18 2.14 2.04	1.68 1.45 0.26
Nylon 12/ FG (0.6)	162 164 168	2.09 2.10 2.03	1.90 1.88 0.46
Nylon 12/ FG (1.0)	165 167 171	2.38 2.79 2.88	1.98 1.87 0.43
Nylon 12/ FG (3.0)	164 166 170	2.90 3.05 3.20	2.12 1.93 0.56

Table 4.3 Avrami exponents from the Avrami equation for the isothermal crystallization of FG based nylon 12 nanocomposites.

For pure nylon 12 the Avrami exponent, n, was found to be in the range of 2.12-2.19, which indicates the mode of nucleation and growth at the primary stage of the isothermal crystallization for nylon 12 must be complex [6]. When functionalized graphene sheets (FG) were added in nylon 12, the value of n was still greater than 2 which illustrates that the spherical crystal morphology was not affected by addition of

FG. As the Avrami exponent was in the range of 2-3 for all the systems, depending on crystallization temperature, the spherulites growth phenomenon was concluded to be three dimensional and spherulites development arising from an athermal heterogeneous nucleation. Various researchers have reported three dimensional crystals of nylon 12 [5]. Moreover, value of K increased with decreasing the crystallization temperature of the same sample which means that addition of FG apparently did not change the crystallization mechanism and the rate of crystallization was decreased upon inclusion of functionalized graphene sheets [7]. It can be noticed from table 4.3 that when 0.6% FG were introduced in the nylon 12, Avrami exponent decreased from 2.15 to 2.03 at a particular temperature (169°C). This decreasing trend in Avrami exponent for 0.6wt% FG inclusion can be witnessed at other two temperatures as well which suggests addition of 0.6wt% FG caused a decrease in crystal growth dimension of nylon 12 [8]. Upon the addition of 1 and 3 wt% FG, Avrami exponent started to increase suggesting a bigger size crystal for these systems.

In order to expand our understanding of change in spherulite size of nylon 12 upon addition of FG, a polarized optical microscope was used to observe the crystal morphology and the results are given in figure 4.7. It clearly shows that the number of nucleation sites increased and spherulites size of nylon 12 was reduced upon addition of 0.6 wt% FG. A great number of nuclei might have produced from FG and simultaneously spherulites grew in limited space, which might had lead to the formation of smaller spherulites. The crystal size started increasing again upon the incorporations of 1 and 3wt% FG, revealing the fact that the higher percentages of FG did not act as strong nucleating agents.

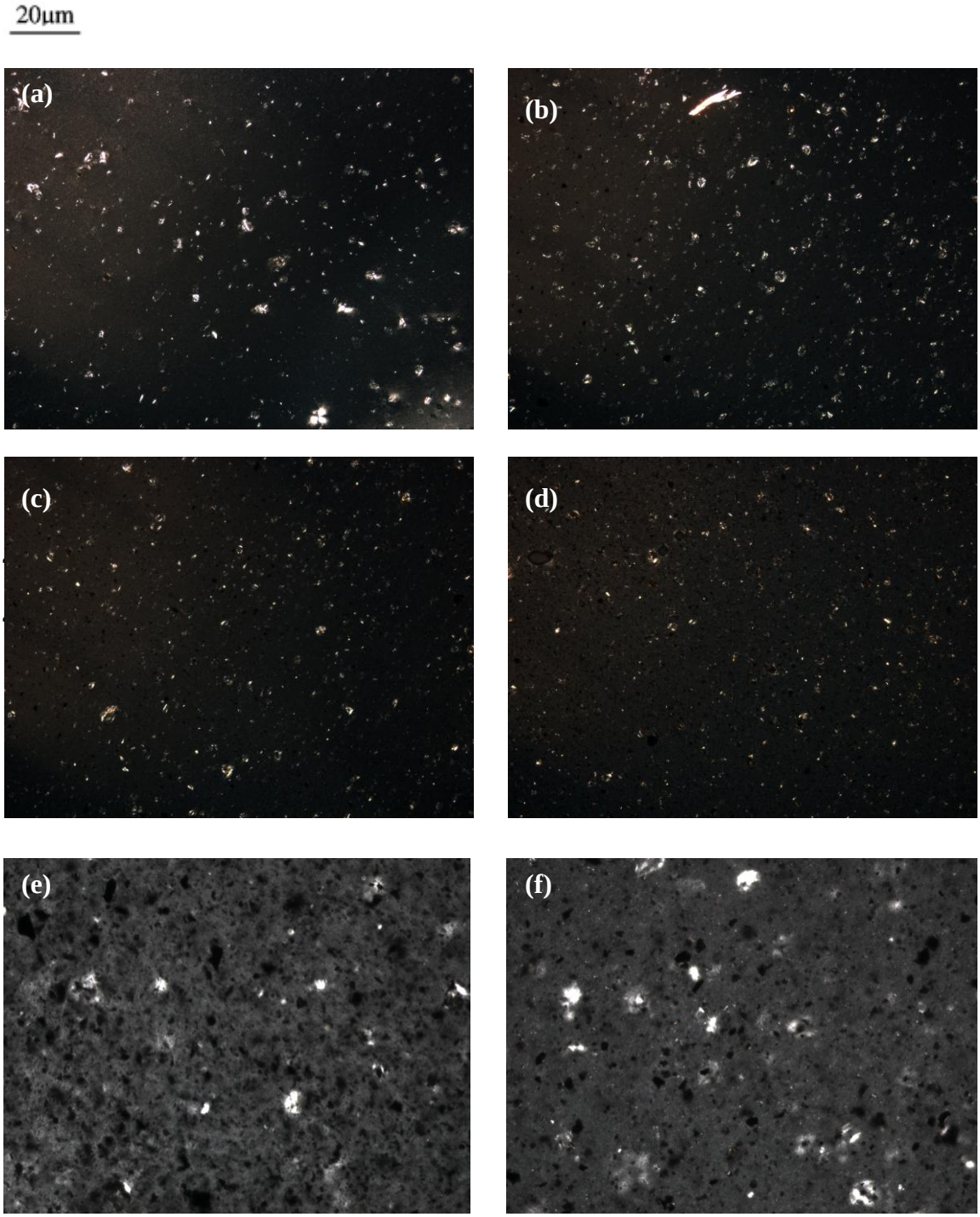

Fig.4.7 Polarized optical microscopy images of (a) Pure Nylon 12 (b) 0.1 wt% FG/ nylon 12 (c) 0.3 wt% FG/ nylon 12 (d) 0.6 wt% FG/ nylon 12 (e) 1.0 wt% FG/ nylon 12 (f) 3.0 wt% FG/ nylon 12

A similar effect of nanographite based graphene sheets (symbolized as UF4 onwards in this chapter) was observed on isothermal crystallization behaviour of nylon 12. Figure 4.8 shows the isothermal crystallization DSC curves for UF4 based nylon 12 nanocomposites. Each of the nanocomposite (nylon 12 with 0.1, 0.3, 0.6 and 1.0 wt% UF4 respectively) was heated to 210°C at the rate of 10°C/ minute, held there for 5 minutes and then was cooled down to its pre-determined crystallization temperature. With the increase in crystallization temperature, the crystallization exothermic peaks shifted to longer times and became flatter which indicates that the total crystallization time was lengthened and that the crystallization rate decreased with increase in T_c. This was again attributed to decrease in super-cooling temperature as was the case for FG based nylon 12 nanocomposites.

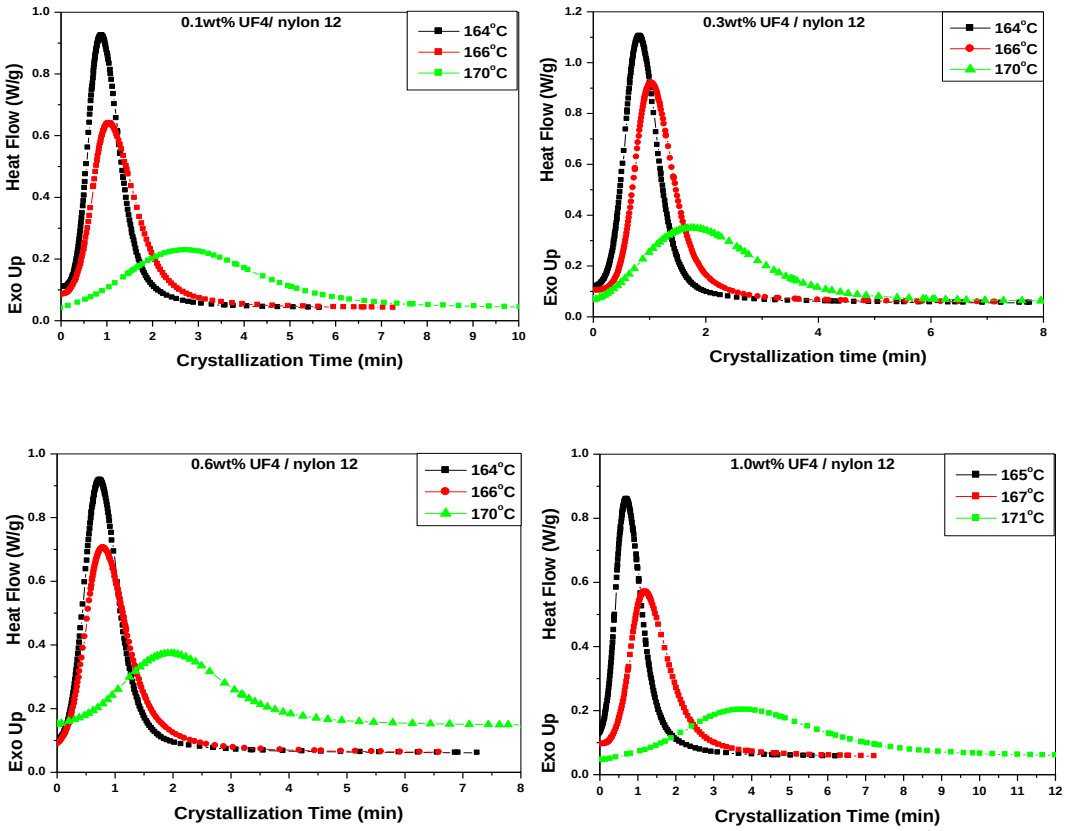

Fig.4.8 Heat flow versus time for UF4 based nylon 12 nanocomposites

Figure 4.9 shows the relative crystallinity (X_t) of neat nylon 12 and its nanocomposites with UF4 varying against time at different crystallization temperatures. It could be readily seen that in the case of UF4 based systems, similar to the FG based nanocomposites, the crystallization kinetics are strongly temperature dependent, and time to complete crystallization obviously increases with increase in crystallization temperature (T_c).

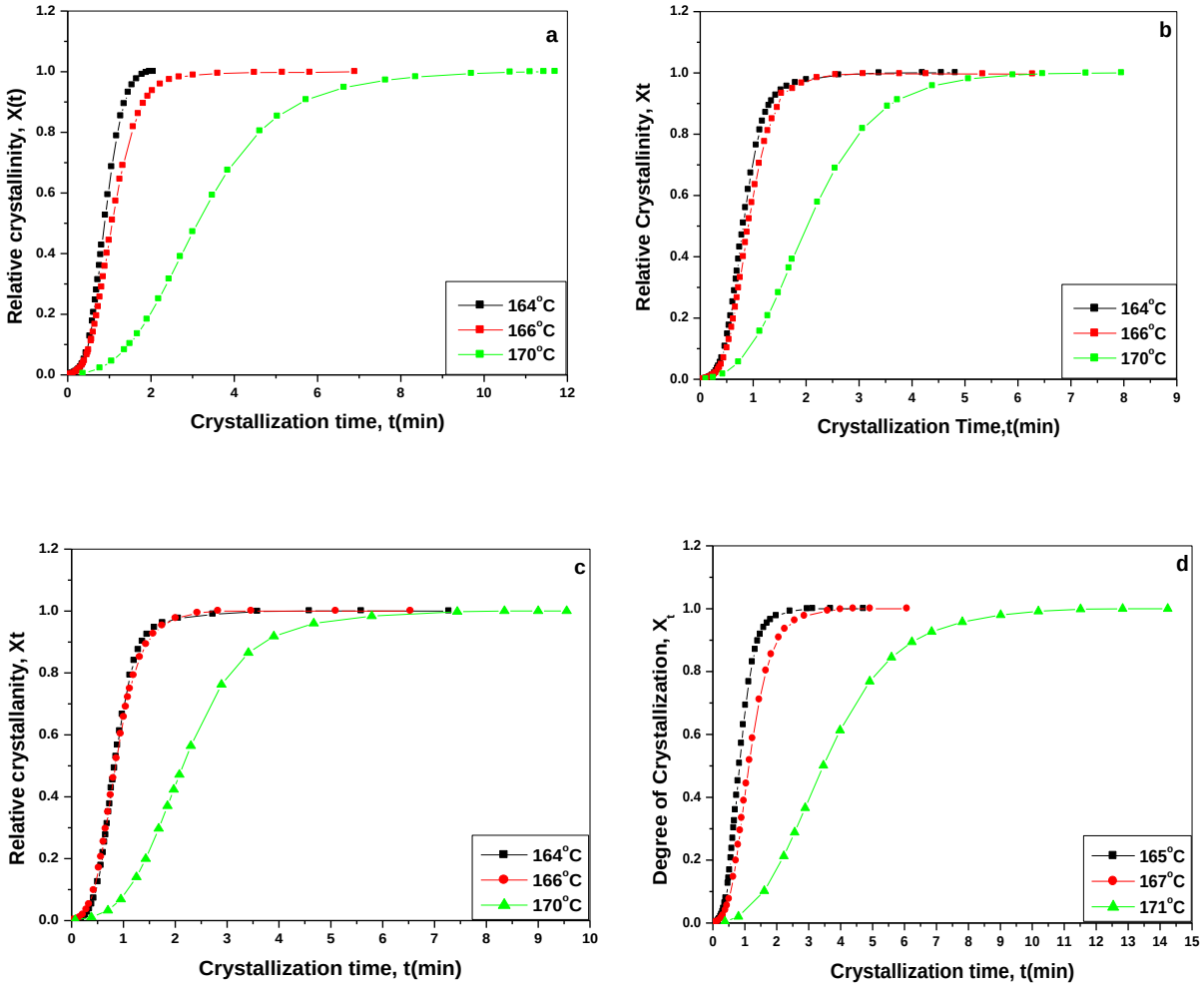

Fig.4.9 Relative crystallinity versus different crystallization time in the process of isothermal crystallization for samples (a) 0.1wt% UF4 / nylon 12 (b) 0.3wt% UF4 / nylon 12 (c) 0.6 wt% UF4 / nylon 12 (d) 1 wt% UF4/ nylon 12

Each isothermal curve in figure 4.9 presents the similar S-shape, which is in good agreement with the Avrami theory. Avrami analysis was applied to investigate the details of isothermal crystallization process. The values of Avrami parameter (n) and rate constant (K) were determined using non-linear curve fitting using Origin® software (version 6). The Avrami exponent (n) was not found to be an exact digit because of a diffusion controlled growth and irregular boundary of spherulites involved in the crystallization process. The values of n (the Avrami exponent), determined from the plots in figure 4.9 using Origin software, are listed in table 4.4.

Sample	T_c (^oC)	K (min^{-1})	n
Nylon 12	163 165 169	2.80 0.87 0.11	2.19 2.12 2.15
Nylon 12/ UF4 (0.1)	164 166 170	1.75 1.08 0.58	2.18 2.15 2.17
Nylon 12/ UF4 (0.3)	164 166 170	1.70 1.03 0.46	2.06 2.10 2.11
Nylon 12/ UF4 (0.6)	164 166 170	1.92 1.84 0.58	2.53 2.49 2.49
Nylon 12/ UF4 (1.0)	165 167 171	1.98 1.87 0.43	2.60 2.58 2.63

Table 4.4 Avrami exponents calculated from the Avrami equation for the isothermal crystallization of UF4 based nylon 12 nanocomposites.

Since the value of n was essentially between 2 and 3, therefore it may be reasonable to consider that the addition of UF4 did not affect the shape of nylon 12 crystals. An overview of table 4.4 also reveals the fact that the Avrami exponent (n) slightly decreases from 2.19 to 2.06 at 169°C upon addition of UF4 (up to 0.3 wt %) and for higher loadings of UF4 (0.6 and 1 wt %) the spherulite size starts to increase. Since Avrami exponent decreases for 0.3wt% UF4 nanocomposite at all crystallization temperatures therefore it is reasonable to say that spherulite size of nylon 12 was decreased at 0.3wt% UF4 addition. Polarized optical microscope (OM) was used to further investigate how addition of UF4 affects the spherulites size of nylon 12 and the results are shown in figure 4.10. These OM results attested the decreasing trend of spherulites size upon incorporation of UF4 (up to 0.3wt %), as given in figure 4.10.

The crystallization rate constant (K) was found to decrease with increase in crystallization temperature which suggests a decrease in the rate of crystallization with increase in crystallization temperature.

Since DSC analysis were not able to give us the detailed picture of the crystallization mechanism therefore XRD was employed to further understand the crystallization mechanism of nylon 12 and its nanocomposites. These XRD results are explained in chapter 5.

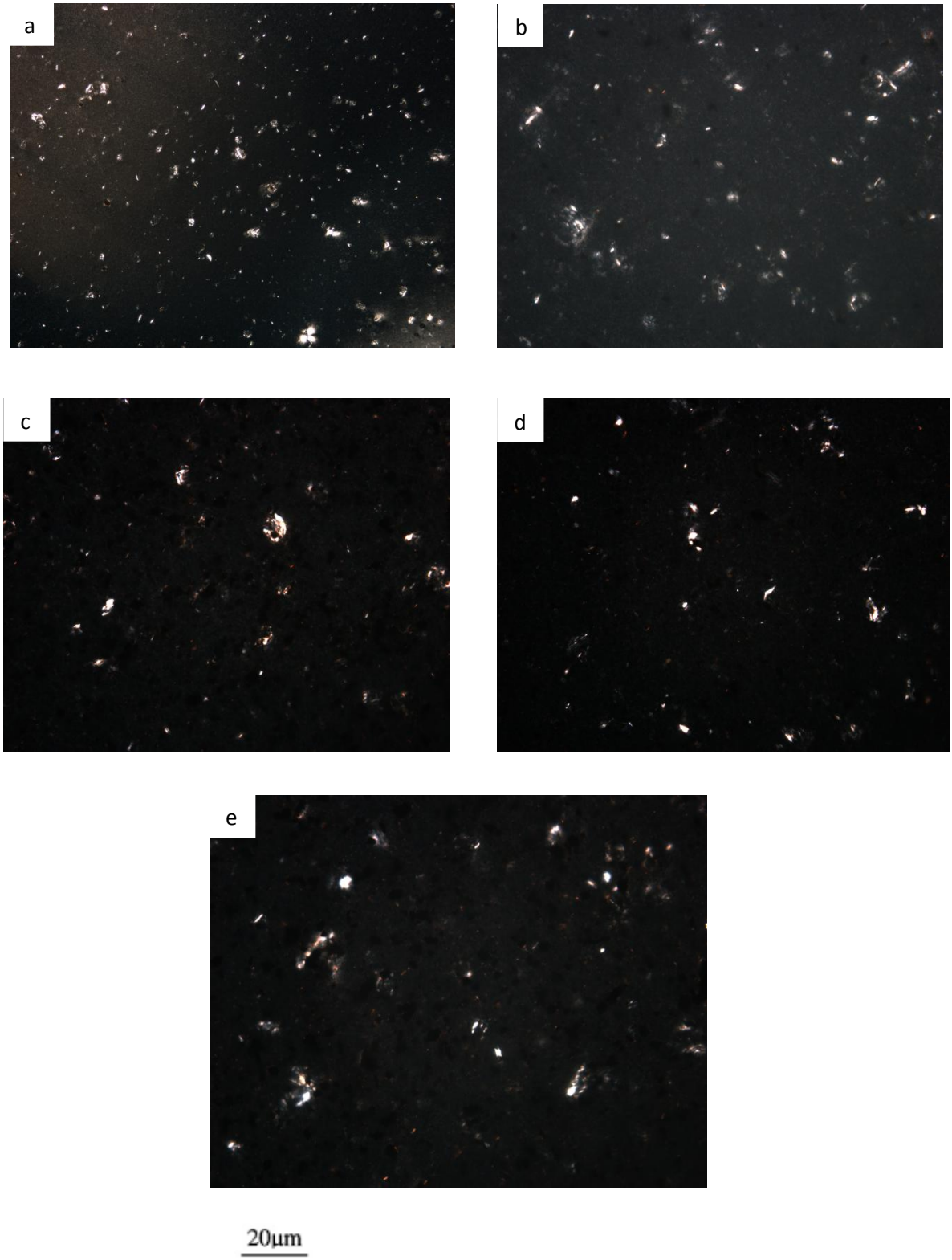

Fig.4.10 Polarized optical microscopy images of (a) Pure Nylon 12 (b) 0.1 wt% UF4/ nylon 12 (c) 0.3 wt% UF4/ nylon 12 (d) 0.6 wt% UF4/ nylon 12 (e) 1.0 wt% FG/ nylon 12

4.4 Conclusions

Overall crystallization behaviour of nylon 12 was not strongly affected by the incorporation of functionalized graphene sheets. There was no significant difference observed on thermal characteristics of nylon 12 under the lights of graphene derived from different size graphite. Our results clarified the fact that the crystallization behaviour of nylon 12 depends upon the contents of the nanofiller used. Lower contents of graphene sheets acted as nucleating agent for nylon 12 and greatly improved the crystallization of nylon 12. Whereas at higher percentages of graphene, the crystallization of nylon 12 was not improved rather was retarded to a certain degree. Upon addition of graphene sheets (either FG or UF4), the nucleation sites were increased whereas the spherulites size of nylon 12 was reduced. The growth geometry of nylon 12 crystals was found to be unaffected with addition of graphene, as was supported by the Avrami analysis results.

4.5 References

[1] Y. Li, X. Li, F. Xiang, T. Huang, Y. Wang, J. Wu, Z. Zhu. Crystallization, rheological and mechanical properties of PLLA/PEG blend with multiwalled carbon nanotubes. Polym. Adv. Technol. 2010; DOI: 10.1002/pat.1702

[2] M. Ferna´ndez de Velasco-Ruiz, I. Quijada-Garrido, R. Benavente, J.M. Barrales-Rienda. Miscibility studies of erucamide (13-cis-docosenamide)/ poly(laurolactam) (nylon 12) (PA-12) blends. Polymer 2000;41:5819-5828

[3] D. Cai, M. Song. A simple route to enhance the interface between graphite oxide nanoplatelets and a semi-crystalline polymer for stress transfer Nanotechnology 2009; 20: 315708.

[4] M. Avrami. Granulation, phase change, and microstructure kinetics of phase change. III, J. Chem. Phys.1941; 9:177-184

[5] Hiemenz, P.C. Polymer Chemistry: The Basic Concepts Marcel Dekker, New York, 1984, p. 219

[6] A. Fichera, C.Garbuglio, V. Malta, R. Zannetti D.M. Chemie, C. Cojazzi. J. Polym. Sci. Part A: Polym. Chem. 1972;10:289-301

[7] G. Zhang, D. Yan. Crystallization kinetics and melting behavior of nylon 10,10 in nylon 10,10-montmorillonite nanocomposite. J.Appl.Polym.Sci.2003;88:2181-2188

[8] L.Li, C.Y.Li,C.Ni, L.Rong,B.Hsiao. Structure and crsyatllization behaviour of nylon 66 /multiwalled carbon nanotubes nanocomposites at low carbon nanotube contents. Polymer 2007;48:3452-3460

Chapter 5

Effect of graphene on the mechanical performance of nylon 12

5.1 Introduction

Polymer nanocomposites, being multiphase materials, are expected to display unusual properties which emerge from each of its constituent [1]. The widespread use of common organic polymers such as polyolefins, nylons, polyesters and polyurethanes boosts up because of their key features such as their lightweight, easy fabrication, exceptional processability, durability and relatively lower cost [1,2]. The challenge of using these materials in structural applications is not only to retain their above listed key features but to improve their strength, modulus, toughness and barrier performance as well [2]. A very familiar approach to enhance the application window of these polymers, especially nylons, is the inclusion of nanoreinforcements in them. Usually it is considered that smaller reinforcement is, stronger it becomes and ultimately transfers its strength to the matrix in which it is being added [3]. Because of the improved surface area, upon incorporation of nanofillers, there are more chances of interfacial adhesion between nanofiller and the polymeric matrix if no agglomeration takes place. As a result of this better interfacial adhesion, the crack propagation path along the interface becomes longer, hence improving the strength and toughness [2, 3].

In this chapter, effect of a new nanoreinforcement, exfoliated graphene sheets (FG), on the mechanical performance of nylon 12 is discussed. The major aim of this

chapter is to investigate the mechanical properties (tensile strength, elongation at break, Young's modulus of elasticity, impact strength and toughness) of nylon 12 and its nanocomposites with functionalized graphene sheets (prepared from Hummer's method).

5.2 Tensile properties of FG/nylon 12 nanocomposites

The nanocomposites were simply prepared via melt compounding of nylon 12 powders pre-mixed with the FG. The premixing process is a key for homogenous dispersion of the FG in the nylon matrix as explained earlier in chapter 3. SEM images of a fracture surface shown in Figure 5.1, which indicates that the FG were well dispersed in the nylon 12 with a thickness of less than 50nm, which was based upon the method described in reference [4].

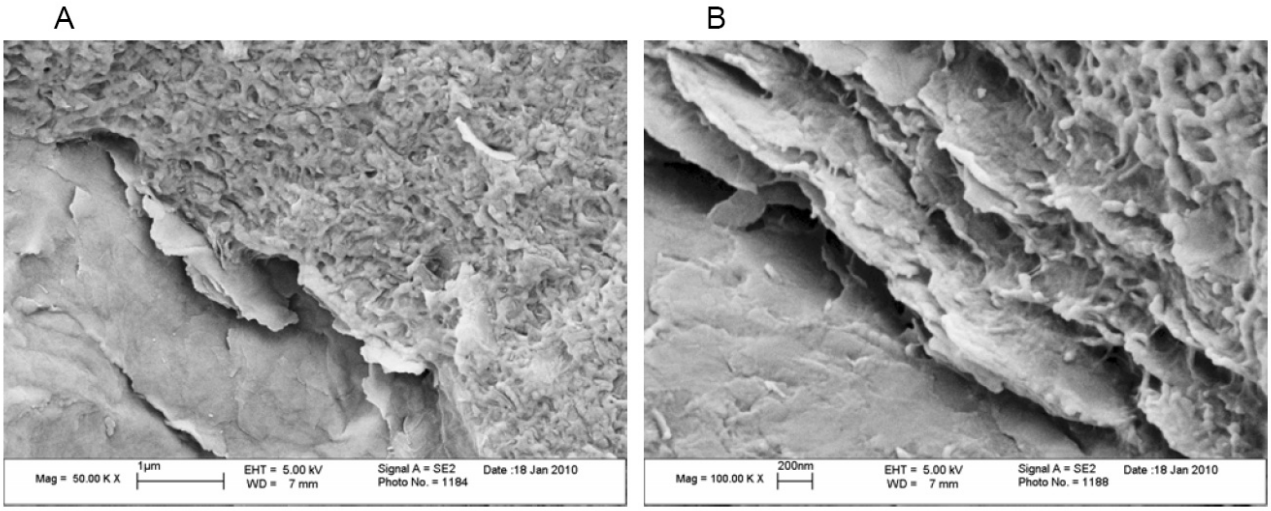

Fig.5.1 SEM images (A and B) of the facture surface of the 0.6wt% FG/nylon 12 nanocomposites, indicating the thin planar graphene sheets embedded in the nylon 12 matrix. Image B reflects the highlighted area in image A with higher magnification.

Figure 5.2 depicts typical stress-strain curves for the FG/nylon 12 nanocomposites with the different FG contents. Figure 5.2 reflects the enhanced strength and ductility of nylon 12 upon inclusion of FG in a straight way which suggests the possibility of interaction between nylon 12 and FG, which probably had resulted in an improvement of tensile properties. Figure 5.3 summarizes the average variation of the ultimate tensile strength and elongation at break of the nylon 12 as a function of the FG. It can be seen that both ultimate tensile strength (UTS) and elongation at break increase with increasing the FG up to 0.6wt%. For 1 wt% FG although there is an increment in UTS but elongation at break starts decreasing which means the system becomes brittle for 1 and 3 wt% FG. With 0.6wt% FG ultimate tensile strength and elongation at break of the nylon 12 is improved by ～ 35% and ～200%, respectively. However, the Young's modulus of the nylon 12 seems nearly unchanged with increasing the FG according to the slopes of stress-strain curves, as shown in Figure 5.4. In figure 5.3 and 5.4, average values calculated over five samples each with error bars for standard deviation are shown.

.

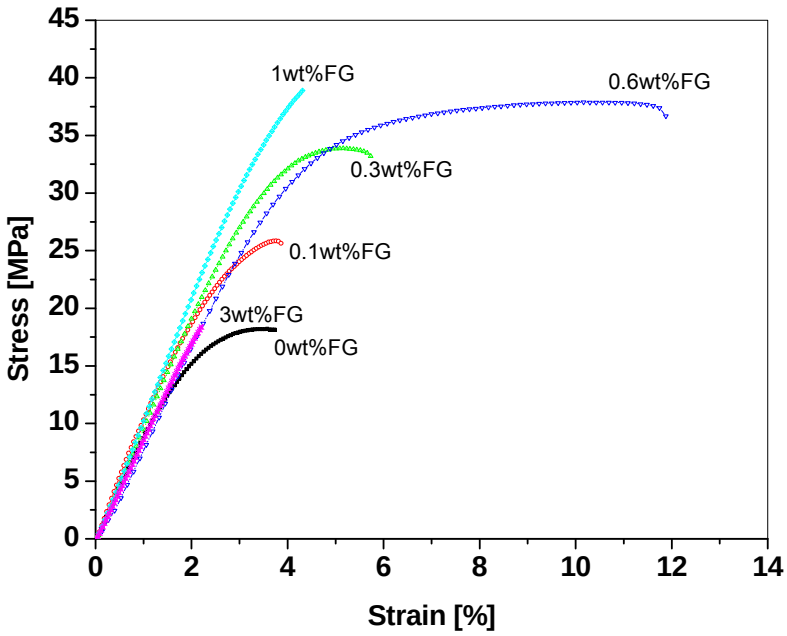

Fig.5.2 Typical stress-strain curves of nylon and its nanocomposite with FG.

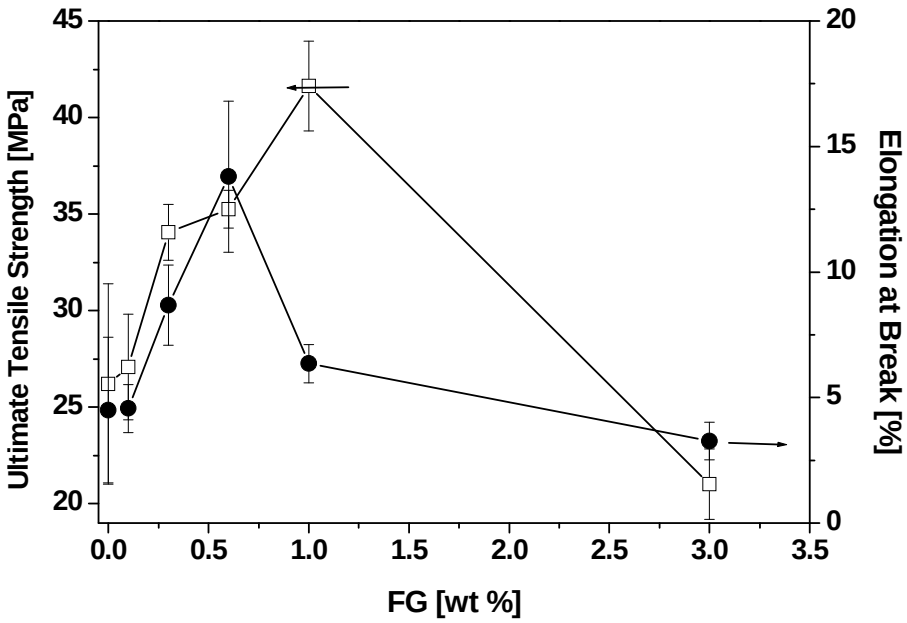

Fig.5.3 The average values of ultimate tensile strength and elongation at break for nylon 12 and its nanocomposites with FG

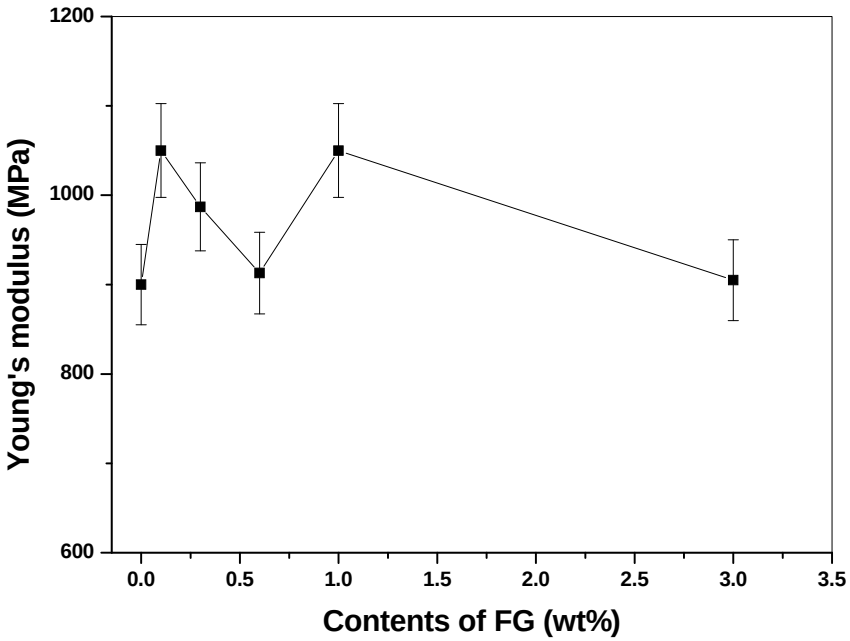

Fig.5.4 Young's modulus of nylon 12 and its nanocomposites as a function of FG loadings

This increase in UTS is an indicative of the improved mechanical interlocking and adhesion between the FG and the nylon 12 matrix, which originates from the rough and wrinkled texture of FG sheets. This nano-scale surface roughness of graphene sheets and the active functional groups on the surface of functionalised graphene most probably results in mechanical interlocking with the polymer chains and consequently bringing about better adhesion. Hydrogen bonding between hydroxyl groups, present on the surface of FG, and the amide groups of nylon 12 was confirmed using FTIR and the results are given in figure 5.9. The glass transition temperature of nylon 12 was also elevated upon incorporation of FG, which itself can arise because of the improved interface [4]. When a homogeneous dispersion of FG sheets (that were in close proximity to each other) is achieved, a large scale hindrance of molecular mobility can be expected, and a larger amount of energy will be required to relax the polymer molecules, hence resulting in an increase of T_g. Although this deviation in Tg is still somewhat small, the effect on material strength can be significant [5]. Such a correlation may exist on the grounds that T_g represents the temperature above which relative sliding between molecules involves large energy dissipation. Therefore, any increase in this temperature must represent increased difficulty for sliding of molecules. This increase in T_g upon incorporation of FG is shown in figure 5.5.

5.3 Toughness of nylon 12 and its nanocomposites

An increase in percentage elongation at break, as given in figure 5.3, gave an initial clue of increase in toughness of nylon 12 upon including functionalized graphene sheets. In order to explore this toughening effect of functionalized graphene sheets, several approaches were used to evaluate the toughness of the FG/nylon 12 nanocomposites.

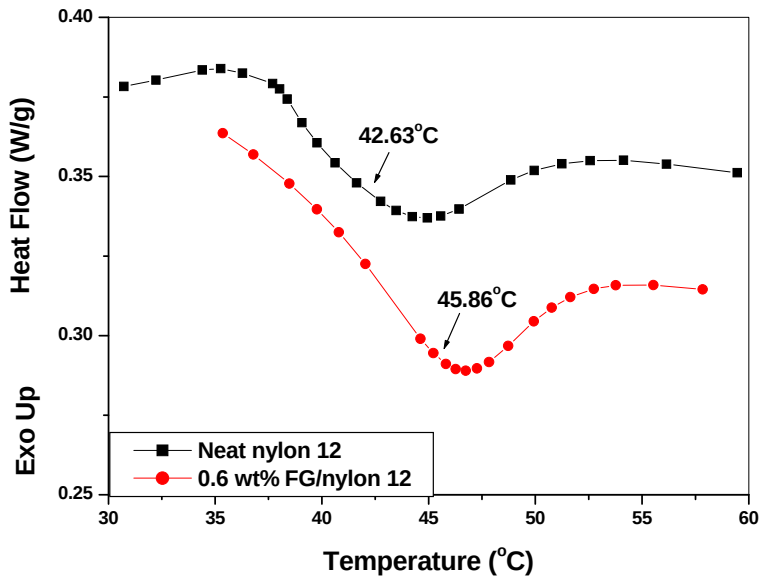

Fig.5.5 DSC curves in the Glass transition region of nylon 12 and its nanocomposite.

Firstly, the necking behaviour of the nanocomposites can be observed in the stress-strain curves. The substantial increase of the elongation at break was a direct evidence to confirm the better ductile performance of the nanocomposites. Since the fracture toughness test is the quantitative way of expressing material's resistance to brittle fracture when a crack is present [6], therefore Mode I fracture toughness (K_{Ic}) tests were further applied to assess the toughness of the FG/ nylon 12 nanocomposites. K_{Ic} value is believed to represent a lower limiting value of fracture toughness which can be used to estimate the relation between failure stress and defect size of a material in service. This particular investigation was focused on determination of fracture toughness through loading of test specimens on a 3-point bending jig, and hence the effects on the value of K_{Ic} were analysed. The following equation was used to calculate K_{Ic} values;

$$K_{1c} = \frac{Y'' \times P}{D \times \sqrt{W}} \qquad (5.1)$$

Where, 'P' is load at fracture, 'D' is specimen thickness, W is the width of specimen, and Y'' is the compliance calibration factor.

The role of the calibration factor in the measurement of fracture toughness is to relate the jig span/specimen width ratio with the specimen's crack length/width ratio, creating a single measurable parameter which contributes to the calculation of K_{1c}. This compliance calibration factor for any sample is a function of its crack length to width ratio (L/W) and it was interpreted from the following graph provided [3].

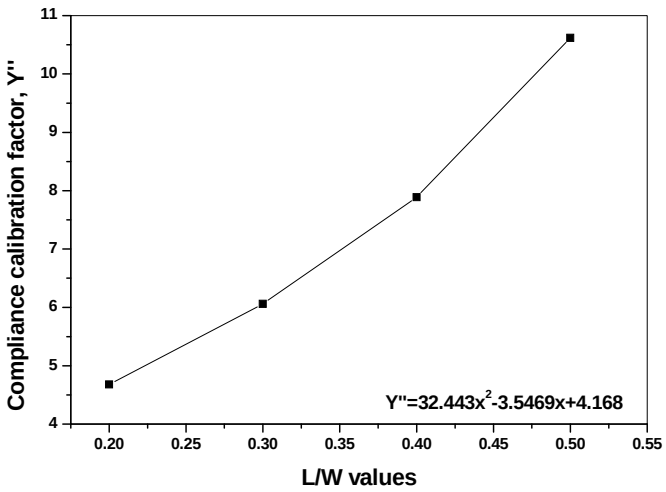

Fig.5.6 Graph of L/W vs. Y''. The equation of the line (interpreted from the best fit of the line) is shown in the inset of the graph, where x is the ratio of length to width of the sample.

By using the equation of line given in figure 5.6, Y'' for all the samples was obtained and finally the values of K_{1c} were calculated by applying equation 5.1. K_{Ic} values has been calculated for five samples each with 2mm,4mm and 6mm slit notches and an average K_{1c} value for all the notches has been presented. As shown in figure 5.7, the K_{1c} of the nylon 12 is ～1.28 MPa.m$^{0.5}$ and the incorporation of 0.6wt% FG causes a significant increase of 72 % (～2.2 MPa.m$^{0.5}$). A decrease in K_{1c} value was found

with the higher amount of the FG. Finally to strengthen our results, the effect of the FG on impact strength of the nylon 12 was investigated using instrumented falling weight impact tester (IFWI). Figure 5.8 shows that the incorporation 0.6wt% FG causes a significant improvement of 175 % in impact failure energy of the nylon 12. The impact energy at ultimate failure has been frequently utilized to evaluate the toughness of the polymer system. This improvement in impact failure energy is also an evidence of increase in energy dissipation capability of nylon 12 upon the addition of the FG. As a rule of thumb, greater is the energy dissipation capability of a system, the tougher it is! It was thought that 0.6 wt% is an optimum concentration of the FG to improve the toughness of nylon 12. It was suggested that increase in FG percentage caused agglomeration which brought about local stress concentration and decreased the energy dissipation capability resulting in a less tougher nanocomposite.

.

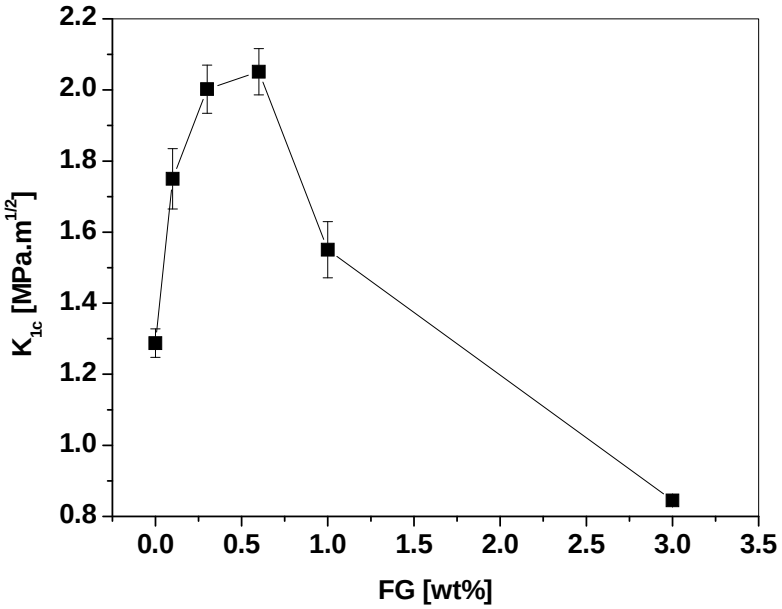

Fig.5.7 Mode I fracture toughness (K_{1c}) of nylon 12 and its various nanocomposites with FG representing 0.6wt% FG as an optimum loading for improvement in the toughness of nylon 12.

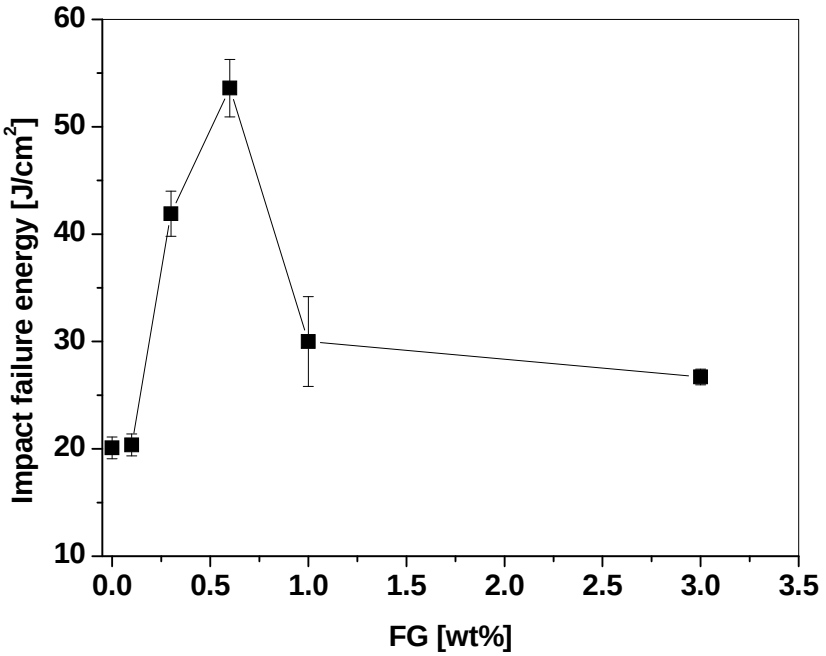

Fig.5.8 Impact failure energy obtained from IFWIT of nylon 12 and its various nanocomposites with FG.

There are not many cases where nanofillers can enhance the toughness of the polymers as well as their strength; therefore it was very important to find out what mechanism could possibly lead to improve the toughness of nylon 12 along with the increase in strength, upon incorporation of FG.

Since nylon 12 is a polar matrix and FG has active functional groups, therefore it was predicted that there must be some sort of interactions between FG and nylon 12. FTIR was used to investigate these molecular interactions between FG and nylon 12. FTIR spectra of nylon 12 and its nanocomposites with 0.6, 1 and 3 % FG are shown in figure 5.9. The characteristic peaks belong to the –NH group of nylon 12, which are located at 3284cm^{-1} (stretching vibration) and 1554cm^{-1} (bending vibration), respectively. The peak at 2800-3000 cm^{-1} and 1637 cm^{-1} is attributed to –OH group and –C=O group, respectively. As shown in Figure 5.9 (b and c), the peak

of –NH group shifts down to 3280 cm^{-1} and 1550 cm^{-1}, respectively, with 0.6wt% FG added into the nylon 12. The FTIR results indicate that the FG could form hydrogen bonding with the nylon 12 with –CONH- groups. But the small shift indicates that the reduced amount of oxygen functionalities on the FG after the high temperature processing provided limited functional sites on the sheets for the formation of the hydrogen bonding. The peaks belonging –OH and –C=O do not present any shift. It further confirmed that the hydrogen bonding was formed between –NH group in nylon 12 and oxygen groups in the FG. It was considered that the hydrogen bonding could play the key role contributing to the transfer the stress from the nylon matrix to the FG, leading to the improvement in the strength of the nanocomposites.

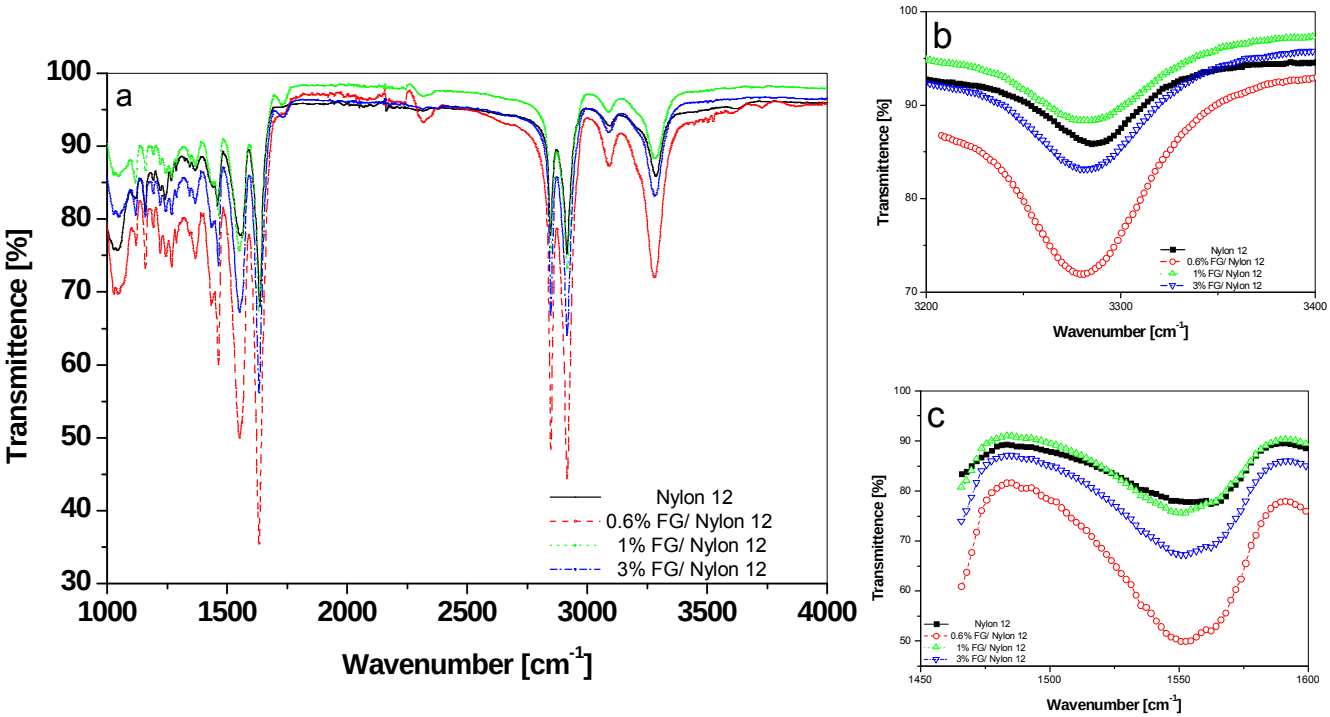

Fig.5.9 (a) FTIR spectra of the nylon 12 and the FG (0.6, 1 and 3 wt %) /nylon 12 nanocomposites. (b) and (c) are magnified images for the peak belonging to stretching and bending vibration of –NH group, respectively.

The crystalline morphology of the nanocomposites was studied by optical microscopy (OM) and x-ray diffraction (XRD). Optical microscopy images shown in chapter 4 (figure 4.7) reveals the fact that the average size of crystal of the nylon 12 obviously decreases with the addition of 0.6% FG and it started to increase with the addition of 1 and 3 % FG. It has been generally recognized that decreased crystal size could benefit the toughness of the polymer [5 and 6].

Two reflections, at $2\theta = 5.5^{o}$ and 21.5^{o}, can be observed in the XRD patterns shown in Figure 5.10, which are attributed to the (200) and (001) planes of γ-phase in semi-crystalline nylon 12 [9, 10]. The increasing reflections of the γ-phase, as a result of 0.6% FG inclusion, indicate the increase in amount of the γ-phase in the nylon 12 nanocomposites. Moreover the γ-phase decreased with 1 and 3% FG which indicates their brittle behaviour as the γ-phase is ductile crystals in nylon materials [11]. Hence it was concluded that the toughness of nylon 12 could be enhanced with increase in γ-phase and decreased crystal size. Figure 5.11 depicts characteristic α and γ bands of nylon 12 at 663 cm^{-1} (–C=O out of plane bend) and 621 cm^{-1} (N-H out of plane bend) respectively. These γ bands were strengthened upon the inclusion of FG as shown in figure 5.11. These FTIR results strengthen our argument that an increase in γ-phase could be one of the reasons for nylon 12 being toughened with functionalized graphene sheets.

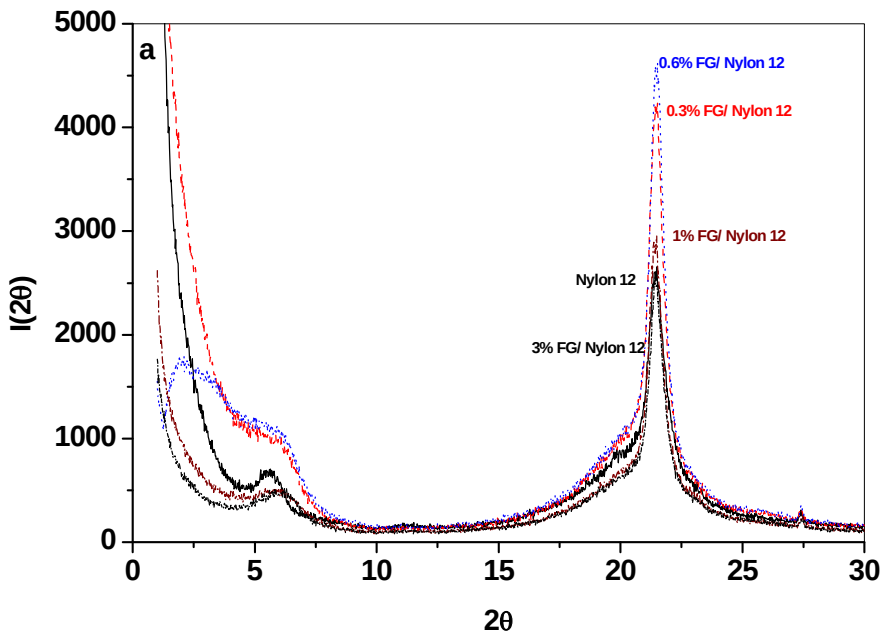

Fig.5.10 XRD pattern of the nylon 12 and its nanocomposites as a function of concentration of FG.

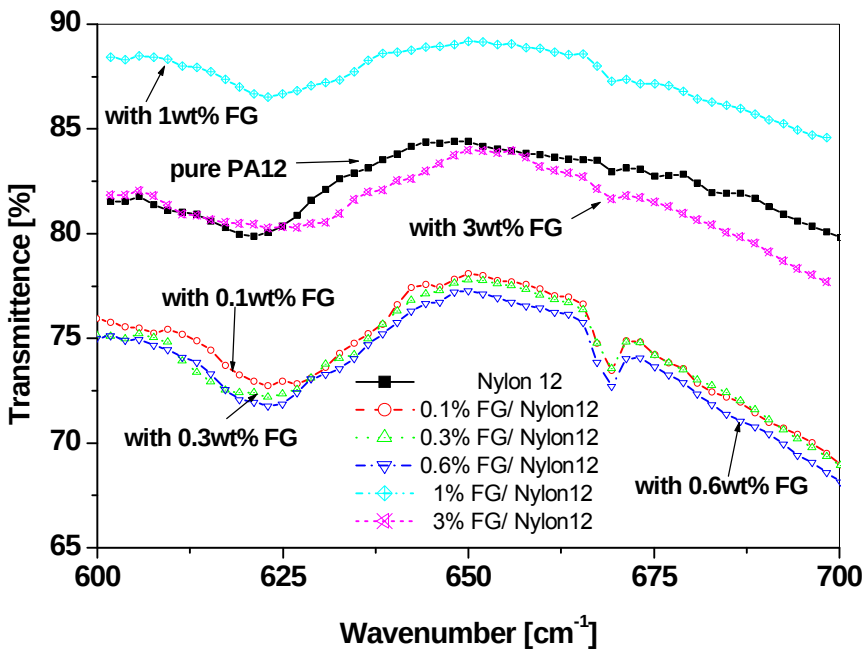

Fig.5.11 FTIR spectra of α and γ forms of the nylon 12 and its nanocomposites.

In order to validate the results from mechanical and thermal analysis, the dynamic mechanical properties of nylon 12 with different contents of FG were investigated at two different frequencies (1 and 10 Hz). Figure 5.12 represents the plot of storage modulus as a function of temperature (at a frequency of 1Hz) for the nylon 12/ FG nanocomposites with various weight percentages of FG. Storage modulus curve of the pure nylon 12 has been overlaid for the comparison purposes as shown in figure 5.12.

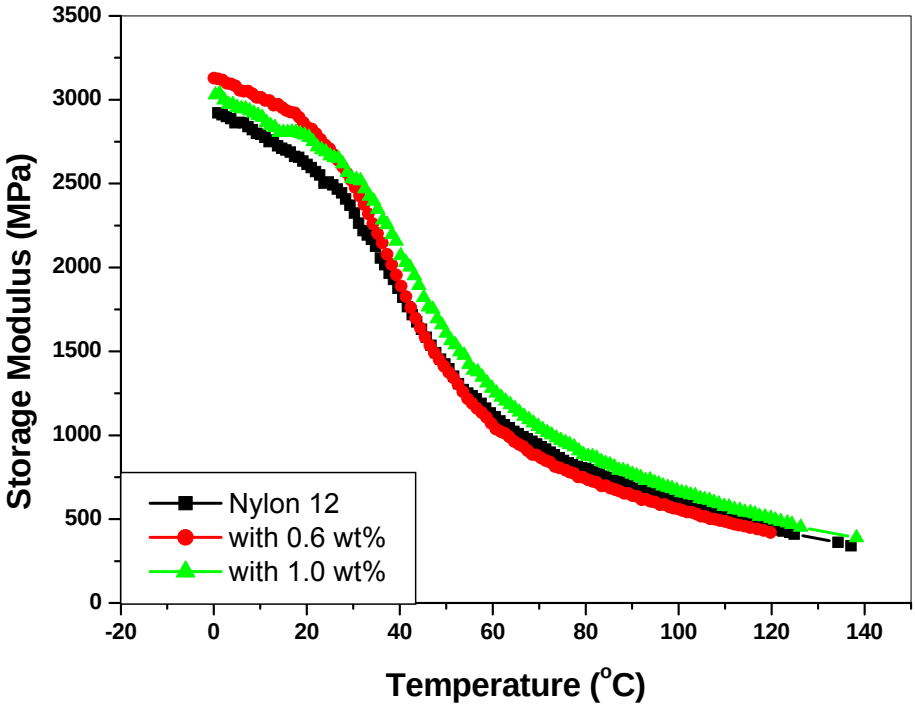

Fig.5.12 Variation of storage modulus of FG/nylon12 nanocomposites as a function of temperature, at a frequency of 1 Hz.

As can be seen from above figure, there is no significant improvement in the storage modulus of nylon 12 upon incorporation of graphene sheets, which confirmed our unchanged modulus results (obtained from tensile testing). A similar trend of storage modulus was observed at a frequency of 10Hz as well, as shown in figure 5.13.

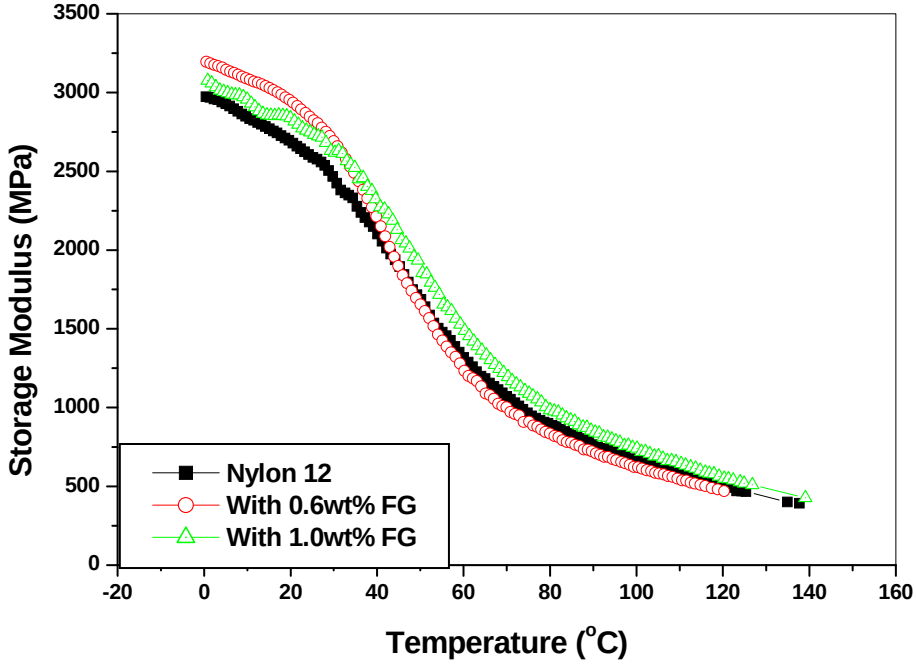

Fig.5.13 Variation of storage modulus of FG/nylon12 nanocomposites as a function of temperature, at a frequency of 10 Hz.

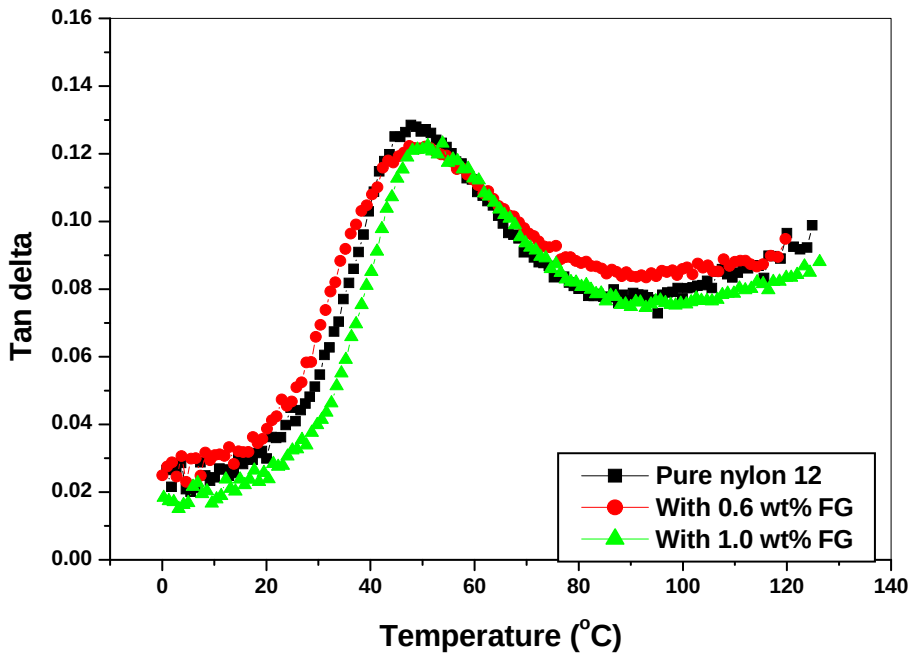

Fig.5.14 Variation of tan δ of FG/nylon 12 composites as a function of temperature, at a frequency of 1 Hz.

From the damping factor (tan δ) curves shown in figure 5.14, T_g of the composites can be determined by the tan δ peak temperature [12]. Glass transition temperature (T_g) of the nylon 12 was slightly increased by the inclusion of FG. This phenomenon is due to the fact that addition of graphene sheets might had restricted the thermally induced segmental motions of the polymer chains in the composites, resulting in a slight increase in T_g. A similar increase in T_g of nylon 12 upon incorporation of FG was also observed by DSC. Tan δ curves for the nylon 12 nanocomposites at a frequency of 10Hz, as shown in figure 5.15, were not different from that at 1Hz. This implies that change in frequency does not affect the thermo-mechanical performance of these particular systems.

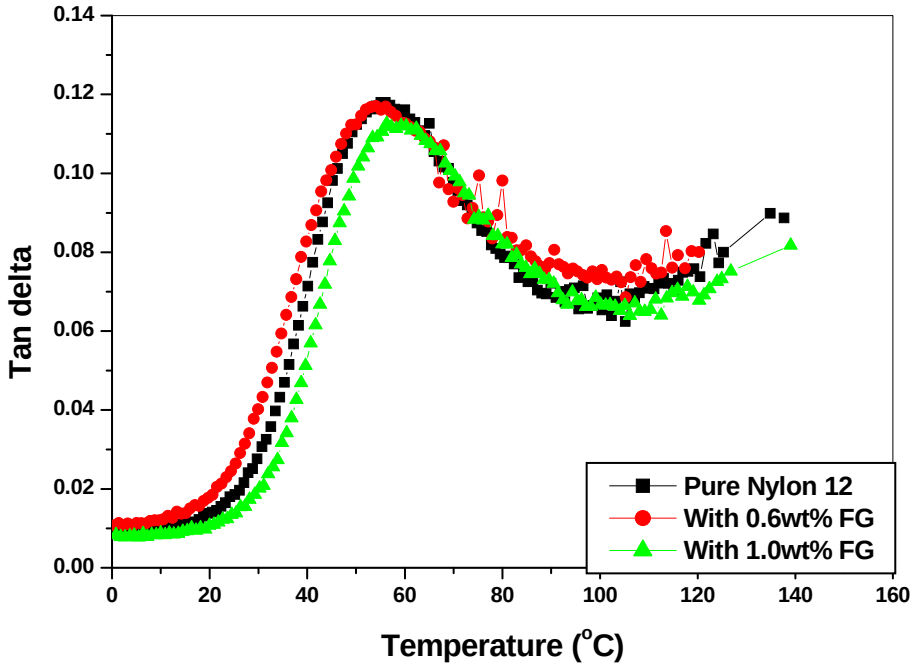

Fig.5.15 Variation of tan δ of FG/nylon 12 composites as a function of temperature, at a frequency of 10 Hz.

5.4 Mechanical response of nylon 12 and its nanocomposites to the frequency sweep using DMA

In dynamic mechanical analysis, DMA, the viscoelastic properties of a polymer are characterized by applying a sinusoidal deformation to the material at a single or at multiple frequencies, and by monitoring the response of that material. Since polymers are viscoelastic materials, i.e. they simultaneously exhibit solid-like and liquid-like properties, they are by definition time-dependent [13, 14]. This means that the response of a viscoelastic material to an imposed deformation will depend on how fast or slow the deformation was applied to the sample. When characterizing a material by using DMA, the time of the deformation is measured in terms of frequency as frequency is the inverse of time (frequency = 1/time). Hence, to find out how a material will behave for prolonged period of time under the given constraints, it will be a great idea to study its response to frequency using DMA [15, 16].

As polymers are viscoelastic materials, therefore the low-frequency range is where viscous or liquid-like behaviour will be dominant. If a material is stressed over long enough times, some flow occurs. As time is the inverse of frequency, this means we predict polymers to have more flow at low frequency [17]. With increase in the frequency, the material will act in a more and more elastic fashion. Silly Putty, the children's toy, shows this clearly. At low frequency, Silly Putty flows like a liquid, while at high frequency; it bounces like a rubber ball. This behaviour is also similar to what happens with temperature changes. Remember how a polymer becomes softer and more fluid as it is heated and it goes through transitions that increase the available space for molecular motions. Over long enough time periods, or low enough frequencies, similar changes occur. So one can move a polymer across a transition by changing the frequency [17]. For the characterization of a material as a

function of frequency, the simplest and most common approach is to hold the temperature constant and scan across the frequency range of interest. This usually referred as isothermal frequency sweep [17, 18].

In this study, isothermal frequency response of nylon 12 and its functionalized graphene sheets based nanocomposites was studied at three different temperatures (28, 32 and 36°C). The samples were mounted on dual cantilever bending clamps and were isothermally run at frequencies in the range of 0.1-100 Hz. In the current chapter, the viscoelastic response of nylon 12 and its nanocomposites at a range of frequency (at various constant temperatures) has been discussed.

Although there are few reports availible on how CNTs can interfere the viscoelastic response of polymers [19, 20 and 21] but to date a limited amount of experimental research has evaluated the viscoelastic response of graphene based polymeric systems. For an attempt to fill this research gap, the isothermal frequency response of nylon 12 and its nanocomposites was studied using DMA. This viscoelastic response was studied at three different temperatures i.e. 28, 32 and 36°C (essentially below Tg). The storage modulus, a measure of the ability of a material to store energy and tan δ, a measure of material's damping characteristics, as a function of frequency are given in figure 5.16 and 5.17 respectively.

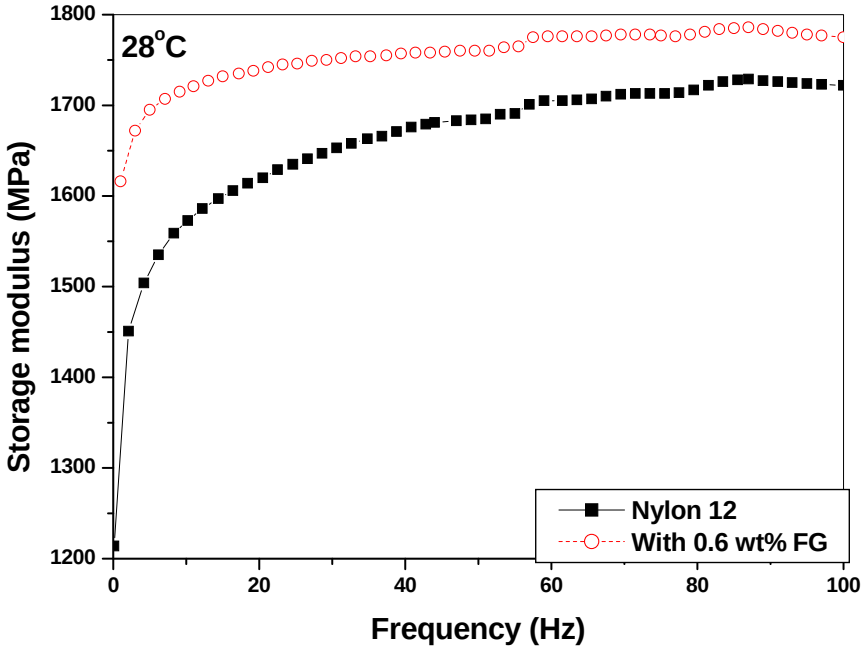

Fig. 5.16 Relation between Storage modulus and frequencies for nylon 12 and 0.6wt% FG-nylon12 nanocomposite at 28°C.

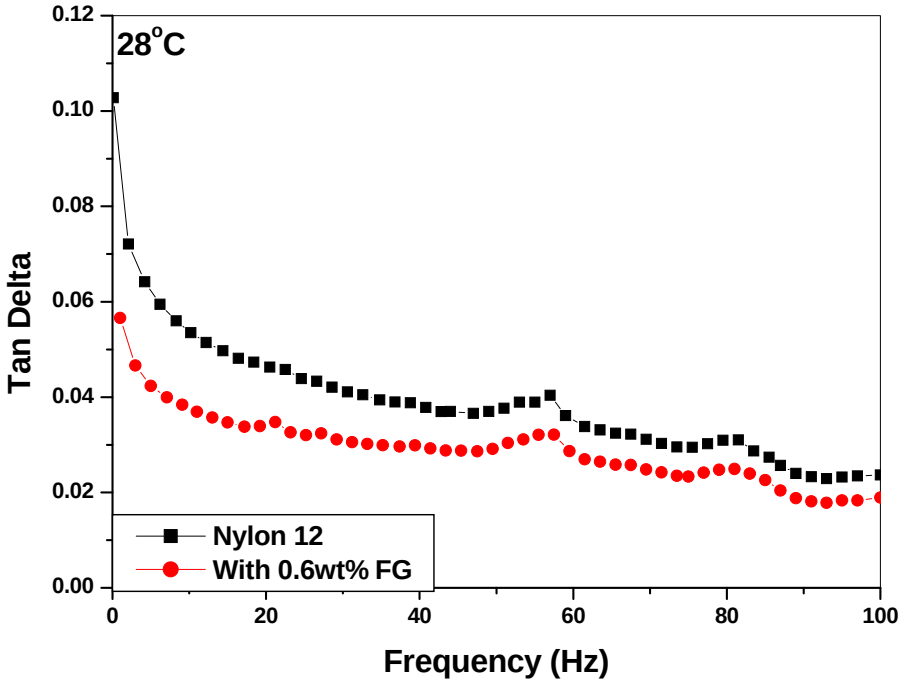

Fig. 5.17 Relation between tan δ and frequencies for nylon 12 and 0.6wt% FG-nylon12 nanocomposite at 28°C.

Referring to figure 5.16, an increase in the storage modulus of nylon 12 upon incorporation of FG was observed at all frequencies. This implies that upon introduction of graphene, elastic response of nylon 12 becomes relatively dominant on its viscous response, hence causing an increase in the storage modulus [16]. It is well known that the end group of nylon 12 is amide, which is capable of reacting with the free hydroxyl groups of functionalized graphene sheets at the interface of the nanocomposite. This interaction might had retarded the mobility of chains in viscous domain, resulting in an increase of storage modulus (lesser compliance) [15].

These results are also confirmed by the tan δ results given in figure 5.17. According to figure 5.17, upon incorporation of 0.6wt% FG, a decrease in the tan δ peak is observed. This lowering of tan δ peak, with inclusion of FG, corresponds to the lesser energy dissipated by the viscous flow in nylon 12. Therefore, by the addition of FG, the reduction of tan δ can also be associated with the decreased mobility of the polymer chains. These results are in agreement with the previous literature [22].

A similar increase in the storage modulus and decrease in compliance of nylon 12 was observed when 0.6wt% FG/nylon 12 nanocomposites were isothermally tested at 32 and 36°C. This means that planar sheets of graphene, disregard to the testing temperature, retarded the mobility of either side chains or in the small groups of adjacent backbone atoms resulting in a decreased compliance and enhanced storage modulus [23]. Isothermal frequency response of nylon 12 and 0.6wt% FG/nylon 12 nanocomposites at a temperature of 32°C are given in figure 5.18 (storage modulus) and 5.19 (tan δ). It is noticeable that although at higher temperatures molecular motion of nylon 12 was enhanced because of increase in free volume, but still FG had tendency to restrict this chain mobility of nylon 12. This also proves the good interfacial adhesion between FG and nylon 12.

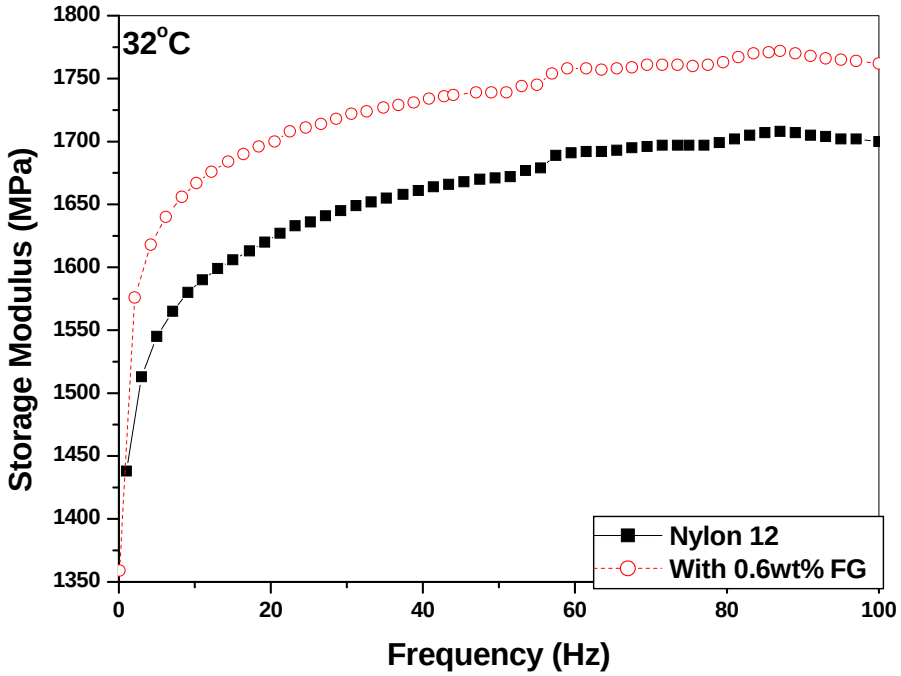

Fig. 5.18 Relation between Storage modulus and frequencies for nylon 12 and 0.6wt% FG-nylon12 nanocomposite at 32°C.

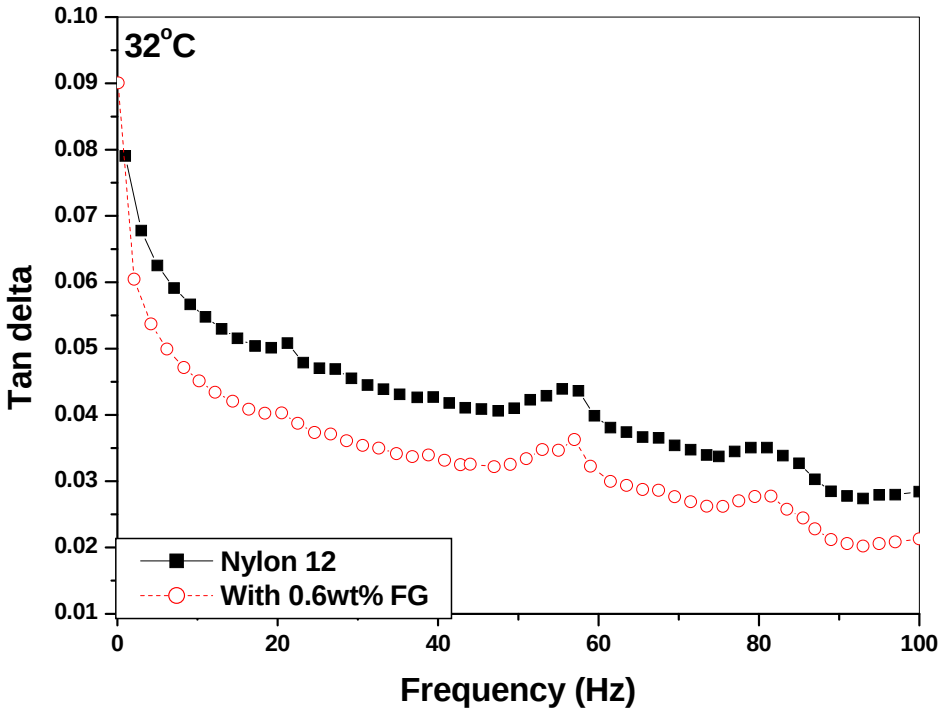

Fig. 5.19 Relation between tan δ and frequencies for nylon 12 and 0.6wt% FG-nylon12 nanocomposite at 32°C.

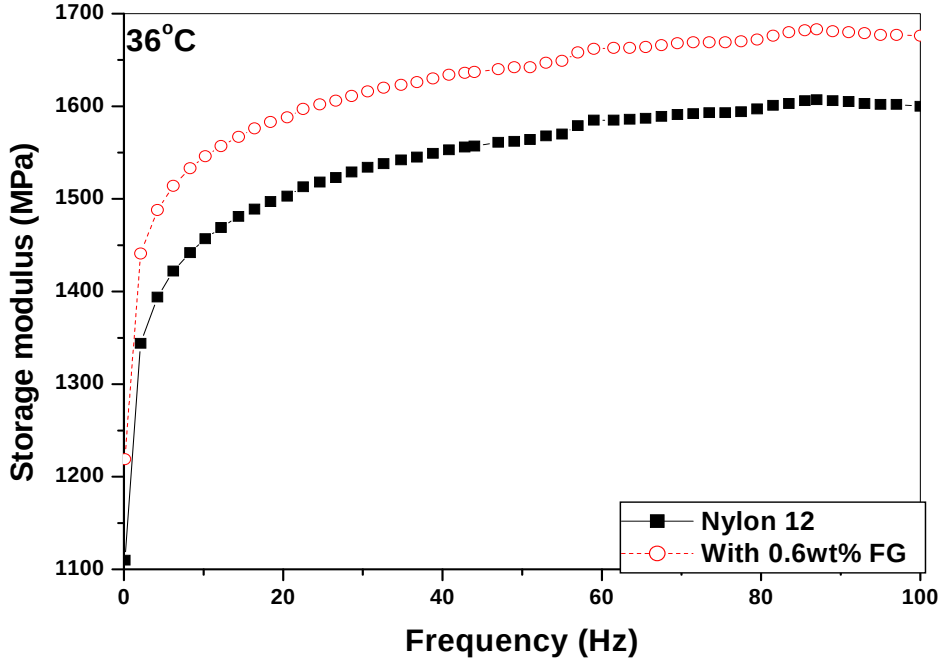

Fig. 5.20 Relation between Storage modulus and frequencies for nylon 12 and 0.6wt% FG-nylon12 nanocomposite at 36°C.

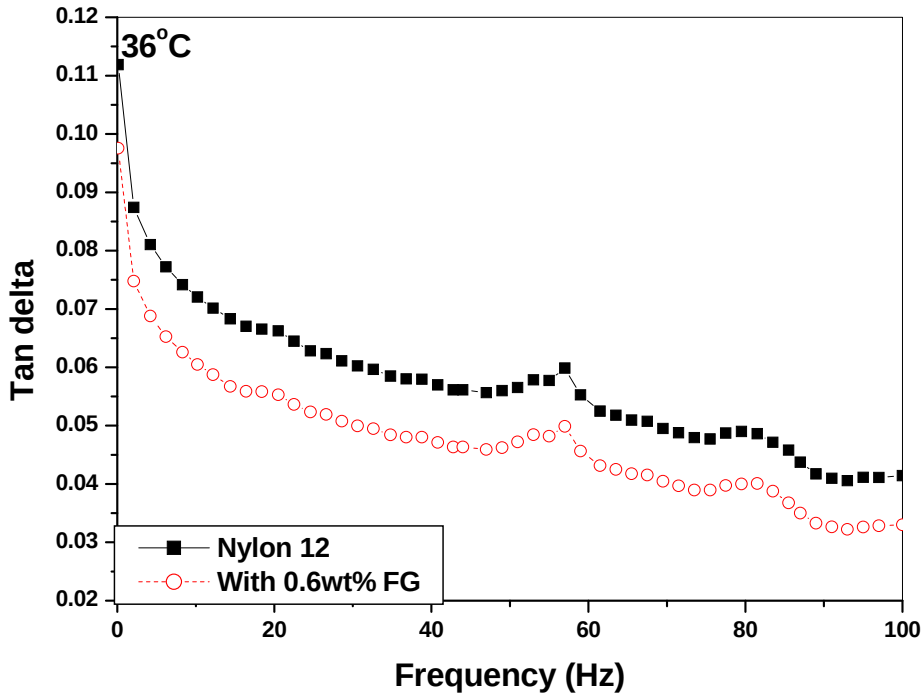

Fig. 5.21 Relation between tan δ and frequencies for nylon 12 and 0.6wt% FG-nylon12 nanocomposite at 36°C.

Isothermal frequency response of nylon 12 and 0.6wt% FG/nylon 12 nanocomposites at a temperature of 36°C are given in figure 5.20 (storage modulus) and 5.21 (tan δ). For all the samples, the storage modulus values increased as the loading frequency increased and tan δ was decreased.

Also, it has been suggested [15] that the rheological characterization is an indirect method to find out the dispersion state of the nanofillers in a given polymer matrix. An increase of the elastic modulus at low frequencies may be associated to the better dispersion of the filler in the polymer matrix [15]. Increase in storage modulus of nylon 12, upon addition of functionalized graphene sheets, indicates the good dispersion of the added nanofiller along with the improved nylon 12-FG interactions.

In conclusion, the viscoelastic properties of a polymer nanocomposite were correlated with the dispersion and the interaction of nanofiller with the matrix using DMA. Dynamic mechanical properties of nylon 12 and its nanocomposite with graphene were successfully analyzed as a function of frequency, at various constant temperatures. It was exhibited that the addition of FG causes an increase in the storage modulus and a decrease in tan δ values of the virgin nylon 12. Furthermore, addition of graphene sheets affected the viscoelastic behaviour of nylon 12 irrespective of the testing temperature. This change in viscoelastic behaviour at all temperatures was considered to be a resultant of better polymer-nanofiller interaction and because of the fine dispersion of FG in nylon 12.

The methodology developed in this work provides a useful tool to study the frequency dependent behaviour of the inter-phases in the polymer nanocomposites.

5.5 Effect of UF4 on the mechanical properties of nylon 12

In order to investigate whether a smaller sized graphene sheets might affect the mechanical performance of nylon 12 in a different way, relatively smaller sized graphene sheets derivated from UF4 (symbolized as UF4 in the rest of this chapter) were used as reinforcement for nylon 12. The method of production of UF4 and UF4/ nylon 12 nanocomposites was the same as that for FG and its nanocomposites with nylon 12. Figure 5.22 depicts typical stress-strain curves for the nylon 12 and its various nanocomposites with UF4. Referring to figure 5.22, an increase in strength and ductility was observed upon addition of UF4. But this effect was only up to 0.3 wt% UF4 and then a decreasing trend in above said properties was observed. The effect of UF4 was different from that of FG in only one way which was that optimum concentration of FG to increase mechanical properties was 0.6wt% while it was 0.3 wt% for UF4.

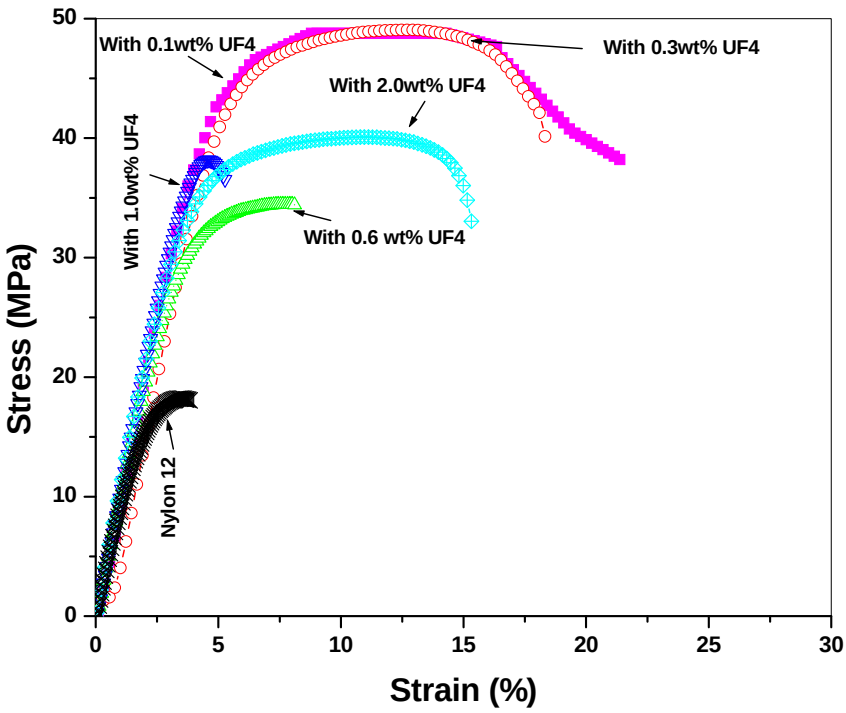

Fig.5.22 Typical stress-strain curves of nylon and its nanocomposite with UF4.

Figure 5.23 (a and b), summarizes the average variation of the ultimate tensile strength (UTS) and elongation at break respectively as a function of UF4 loading. It can be clearly seen in figure 5.23 that upon increment in UF4 loading up to 0.3 wt%, both UTS and elongation at break increases.

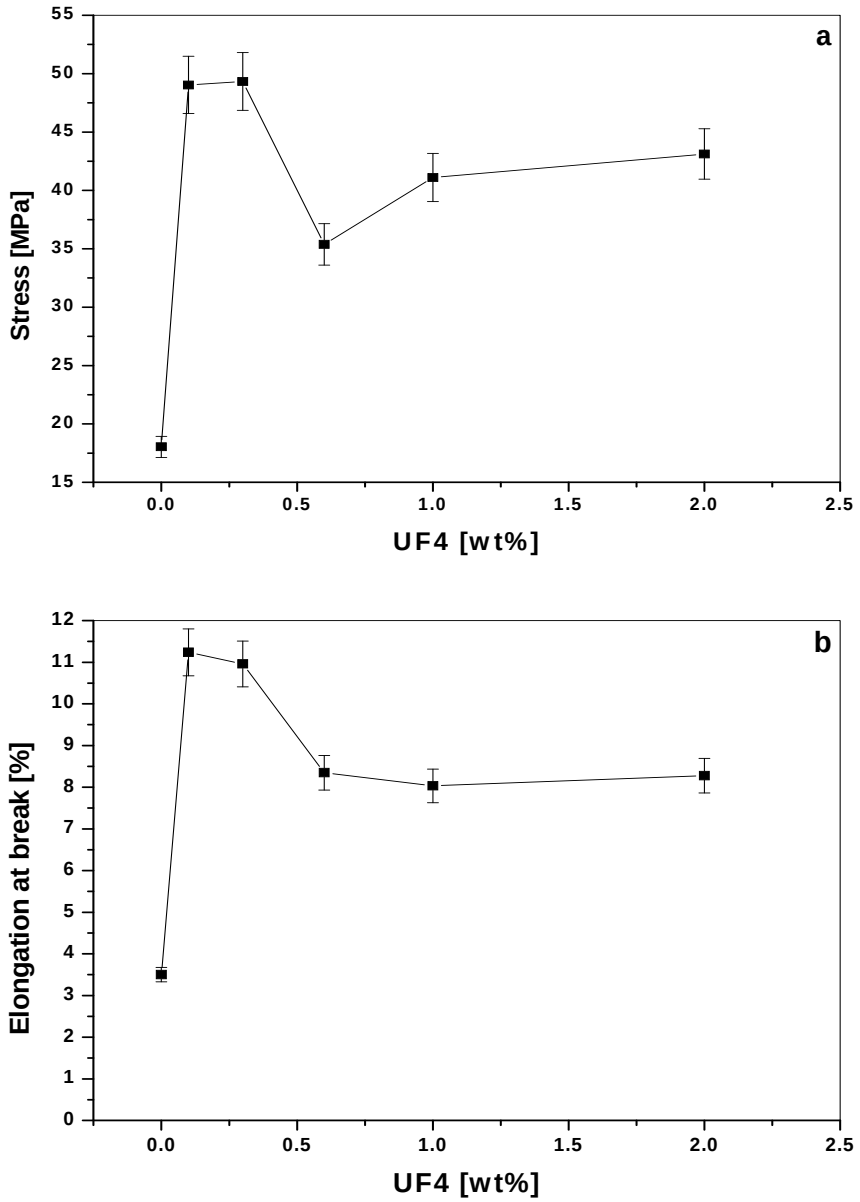

Fig. 5.23 (a) The average values of ultimate tensile strength, (b) The average values of percentage elongation at break for nylon 12/ UF4 nanocomposites.

In above figure 5.23, average values of UTS and elongation at break are calculated over five samples each and error bars are added to represent the standard deviation. As clearly presented in above figure, with 0.3wt% UF4, the ultimate tensile strength and elongation at break of the nylon 12 was improved by ～ 62% and ～73%, respectively. For nanocomposites with higher fractions of UF4, the mechanical response turns to somewhat brittle as percentage elongation starts to decrease continuously upon their inclusions. The reason could be poorer dispersion resulting from higher loadings of the nanofiller. This improvement in UTS was again attributed to improved interfacial adhesion between UF4 and nylon 12. An increase of 12% in Young's modulus, calculated from the slopes of stress-strain curves, was observed upon incorporation of 0.3 wt% UF4 and it started to decrease for higher concentrations of UF4, as shown in figure 5.24.

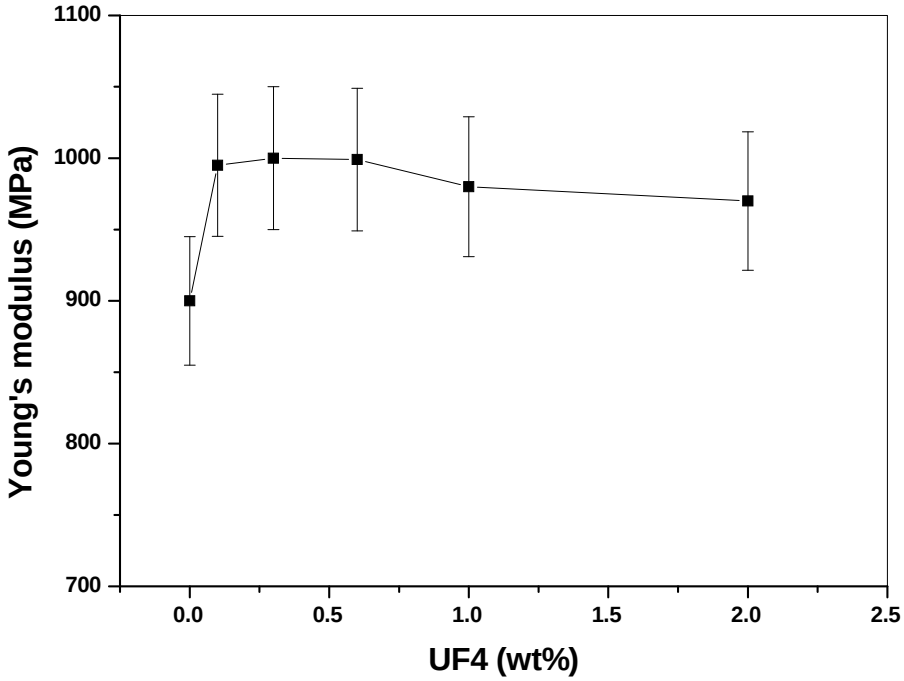

Fig.5.24 Young's modulus of nylon 12 and its nanocomposites as a function of UF4 loadings.

Furthermore, an increase of ~4°C in glass transition temperature upon incorporation of 0.3wt% UF4 strengthened our hypothesis of stronger interface, since an increase in glass transition temperature is usually believed to be a resultant of interfacial attractions. Since increase in T_g can also be explained on the basis of decrease in free volume of the mixture, therefore it was considered that these volume contractions might had been caused because of the strong interaction between the amide group of nylon 12 and the functional groups present on the surface of graphene. The fracture surface topology of nylon 12 and UF4/nylon 12 nanocomposites was observed using FEGSEM. The size scale (nanosheets thickness) and morphology of the UF4 as well their surface chemistry lead towards its interfacial adhesion with the nylon 12 matrix, as illustrated by figure below (figure 5.25).

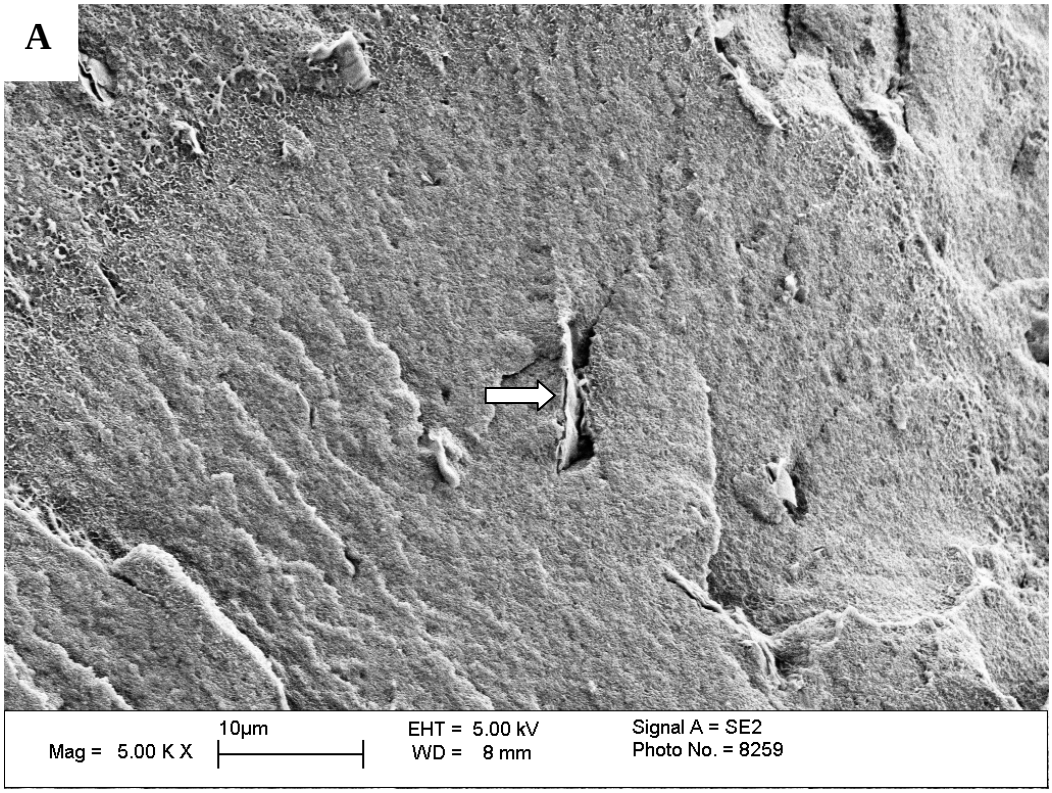

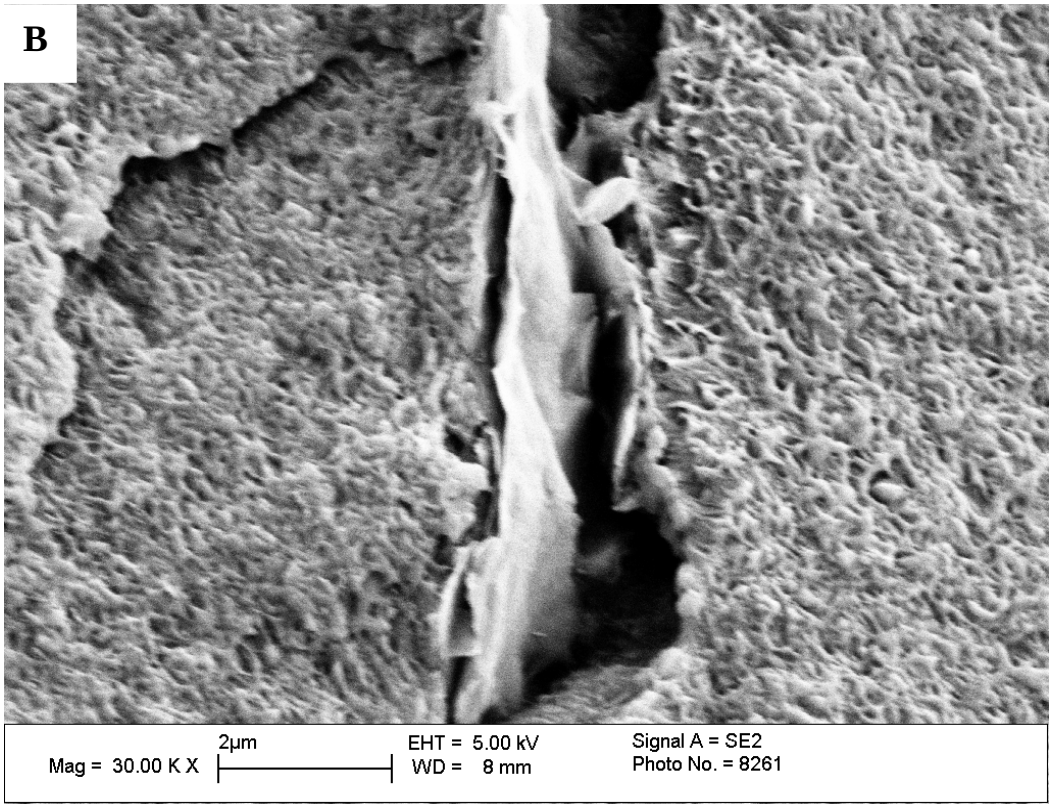

Fig.5.25 SEM images (A and B) of the facture surface of 0.3 wt% UF4/ nylon 12 nanocomposites, indicating the thin planar graphene sheets embedded in the nylon 12 matrix. Image B reflects the highlighted area in image A with higher magnification.

5.6 Toughness of UF4/ Nylon 12 nanocomposites

A significant increase in percentage elongation at break of nylon 12, upon addition of UF4, persuaded to explore the toughening ability of UF4. In order to compare the toughening ability of the two different sized nanofillers with same geometry (UF4 and FG), same techniques were used to evaluate the toughness of UF4 / nylon 12 composites as were used for the FG based nylon 12 composites.

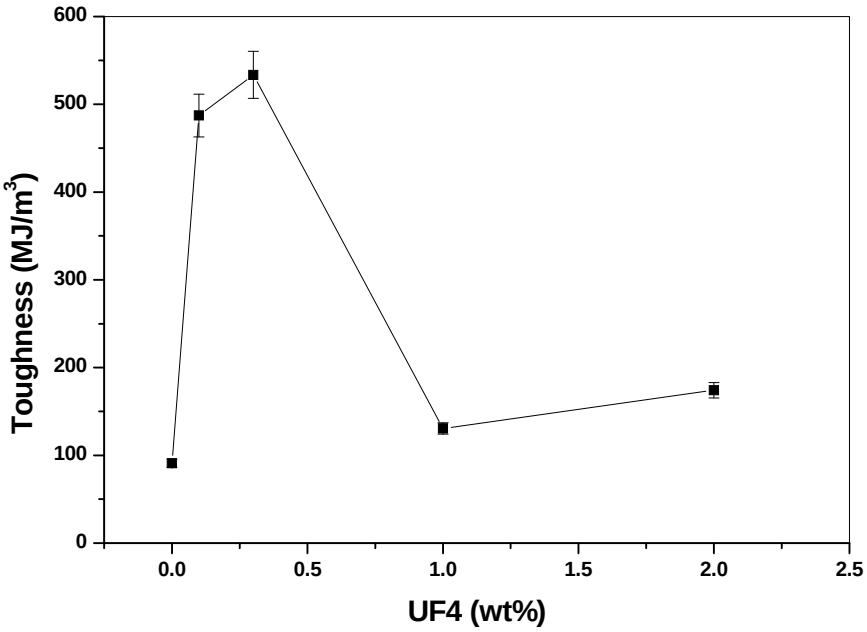

Fig.5.26 Toughness of neat nylon 12 and UF4/nylon 12 nanocomposites; evaluated by calculating area under the stress strain curves.

Firstly area under the stress curve was calculated to evaluate the toughness of UF4/ nylon 12 nanocomposites, as area under the stress-strain curve is proportional to the toughness. This increase in toughness is shown in above figure 5.26.

Plane strain fracture toughness testing is another test that indicates the fracture toughness of the material which was performed to measure the Mode I fracture

toughness (K_{1c}) of pure nylon 12 and its nanocomposites at various loadings of UF4. Equation 5.1 was used to quantify the value of K_{1c}. The compliance calibration factor was calculated as described earlier in this chapter for the case of UF4/nylon 12 nanocomposites. An initial pre-crack was created in the notched samples by gently tapping a fresh razor blade to a depth of 0.1mm. Five samples were tested to check for the reproducibility of the results and error bars for standard deviation are shown, as shown in figure 5.27.

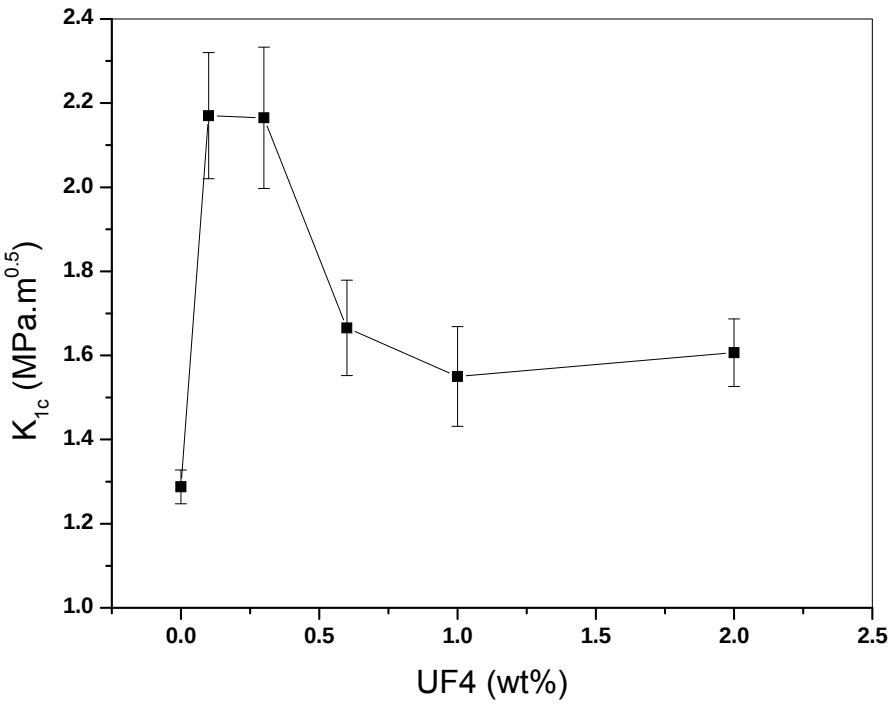

Fig. 5.27 Mode I fracture toughness (K_{1c}) of nylon 12 plotted as a function of the weight fraction of UF4.

Referring to the figure 5.27, incorporation of only 0.3wt% UF4 in nylon 12 increased its K_{1c} value from 1.28 to ~ 2.20 MPa.m$^{0.5}$ which corresponds to more than 90% increase in toughness. For higher loadings fractions, the enhancement in K_{1c} diminishes which might be because of poor dispersion of UF4 above a weight

fraction of 0.3wt%. This is quite understandable as dispersion of these two dimensional sheets becomes more challenging for higher percentages unlike to other nanofillers like CNT's [24]. IFWIT results also confirmed that there is an increment in impact failure energy upon incorporation of UF4 as shown in figure 5.28.

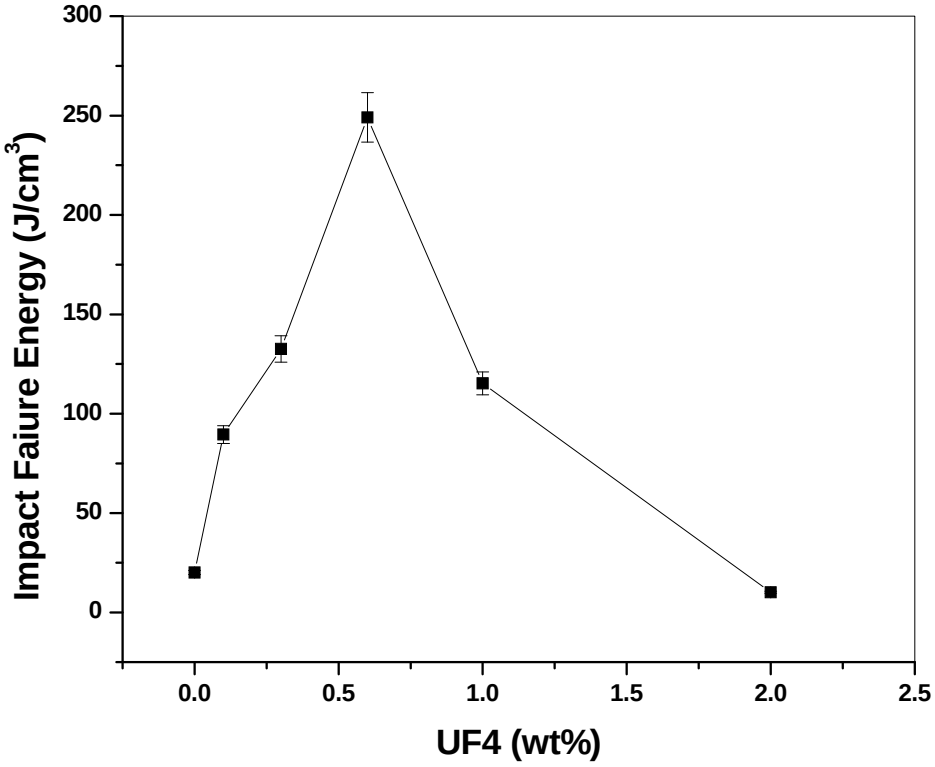

Fig.5.28 Impact failure energy of nylon 12 and its various nanocomposites obtained from falling weight impact tester.

As was the case with FG based nylon 12 nanocomposites, it was thought that it might be the strengthening of hydrogen bonding, increase in the γ-phase and decrease in crystal size upon inclusion of UF4, which might had lead to an improvement in toughness of these systems. In order to figure out the any molecular interaction arising from the polar nature of nylon 12 and active functionalities on UF4,

FTIR analysis of nanocomposites was performed. Similar to FG, addition of UF4 caused a slight shift in the characteristic peaks of the –NH group and did not affect the peaks belonging to –OH and –C=O did not present any change. This is an indication that oxygen functionalities of UF4 could form hydrogen bonding with amide groups (–NH) of nylon 12. These FTIR results are shown in figure 5.29.

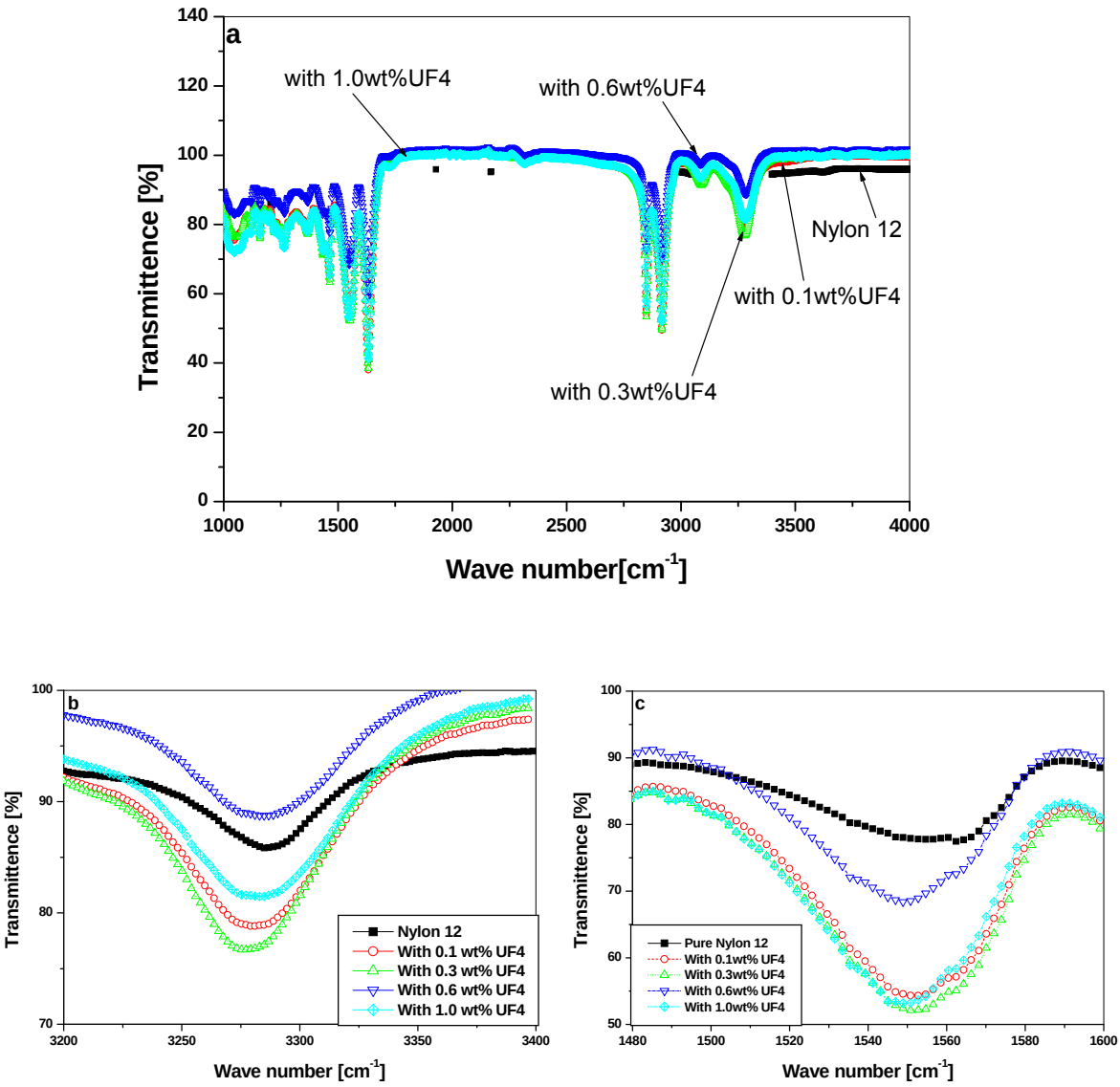

Fig.5.29 (a) FTIR spectra of the nylon 12 and UF4 (0.1, 0.3, 0.6 and 1 wt %) /nylon 12 nanocomposites. (b) and (c) are magnified images for the peak belonging to stretching and bending vibration of –NH group, respectively.

It was considered that this hydrogen bonding could play a crucial role in stress transfer from the matrix to UF4, leading to enhanced mechanical properties.

Optical microscopy images ,exposed in figure 4.10, reveal the fact that average crystal size of nylon 12 decreases upon incorporation of UF4 (up to 0.3 wt%) and then it starts to increase for the higher fractions of UF4. This decrease in crystal size could be a possible reason for toughening of these systems.

The crystalline morphology of UF4 based nylon 12 composites was also studied by X-ray diffraction (XRD). The results are shown in figure 5.30.

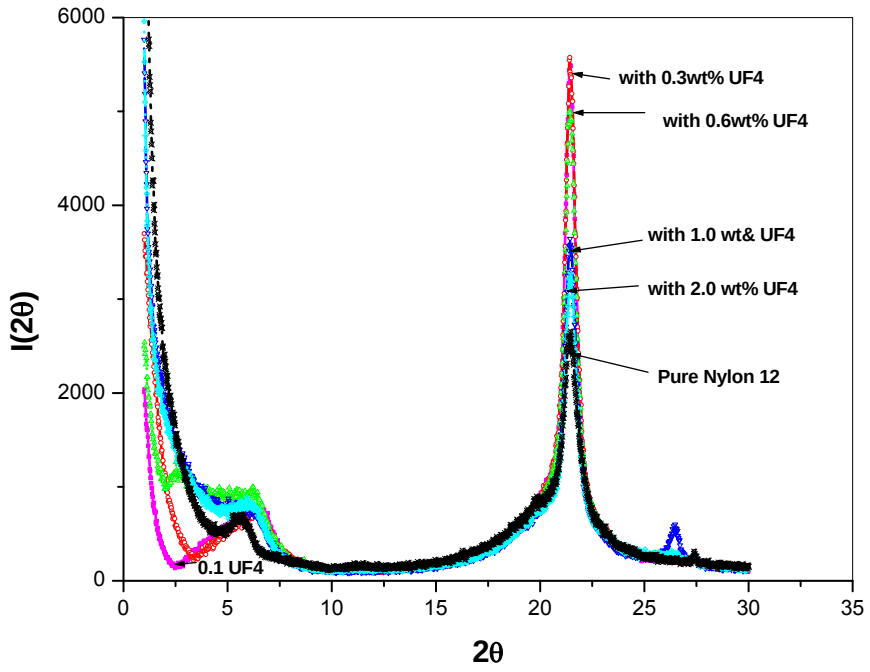

Fig.5.30 XRD patterns of nylon 12 and its nanocomposites with various percentages of UF4.

With reference to the above figure, two reflections at 2θ = 5.5^{o} and 21.5^{o} can be, attributed to the (200) and (001) planes of γ-phase in semi-crystalline nylon 12 [9, 10]. The increasing reflections of the γ-phase, as a result of 0.3% UF4 inclusion,

indicate the increase in amount of the γ-phase in the nylon 12 nanocomposites. Moreover the γ-phase decreased with 0.6 and 1% UF4 which indicates their brittle behaviour as the γ-phase is ductile crystals in nylon materials [25]. Hence it was concluded that the toughness of nylon 12 could be enhanced by increasing its γ-phase and by decreasing its crystal size.

From the above results of mechanical characterization, it can be concluded that a different size of graphene sheets does not alter their mechanical performance. Upon incorporation of both nanoreinforcements (FG and UF4), nylon 12 gained a significant improvement in its tensile strength, impact strength and fracture toughness.

5.7 Mechanical performance of masterbatches

A certain limitations of nylon 12 powder to be used at industrial scale motivated us to check whether this toughening behaviour of functionalized graphene (FG) can be injected to nylon 12 pellets or not! Masterbatches of various concentrations of FG/nylon 12 powder were blended with nylon 12 pellets in order to prepare their composites. For the comparison purposes, three individual systems of masterbatches were prepared i.e.

(i) 0.1wt% nylon 12 powder with nylon 12 pellets (named as 0.1 M.B.) and 0.1wt% nylon 12 powder with FG blended in nylon 12 pellets (named as 0.1 M.B. with FG)

(ii) 0.3wt% nylon 12 powder with nylon 12 pellets (named as 0.3 M.B.) and 0.3wt% nylon 12 powder with FG blended in nylon 12 pellets (named as 0.3 M.B. with FG)

(iii) 0.6wt% nylon 12 powder with nylon 12 pellets (named as 0.6 M.B.) and 0.6wt% nylon 12 powder with FG blended in nylon 12 pellets (named as 0.6 M.B. with FG)

Figure 5.31 shows the stress strain curves of masterbatches. For 0.1wt% masterbatch, there was no significant improvement in the mechanical performance upon addition of FG. At the moment it is not fully clear that why there is decrease in these properties for masterbatches containing 0.1wt% FG. It was suggested that a critical amount of nanofiller was required to favour the mechanical behaviour of masterbatches.

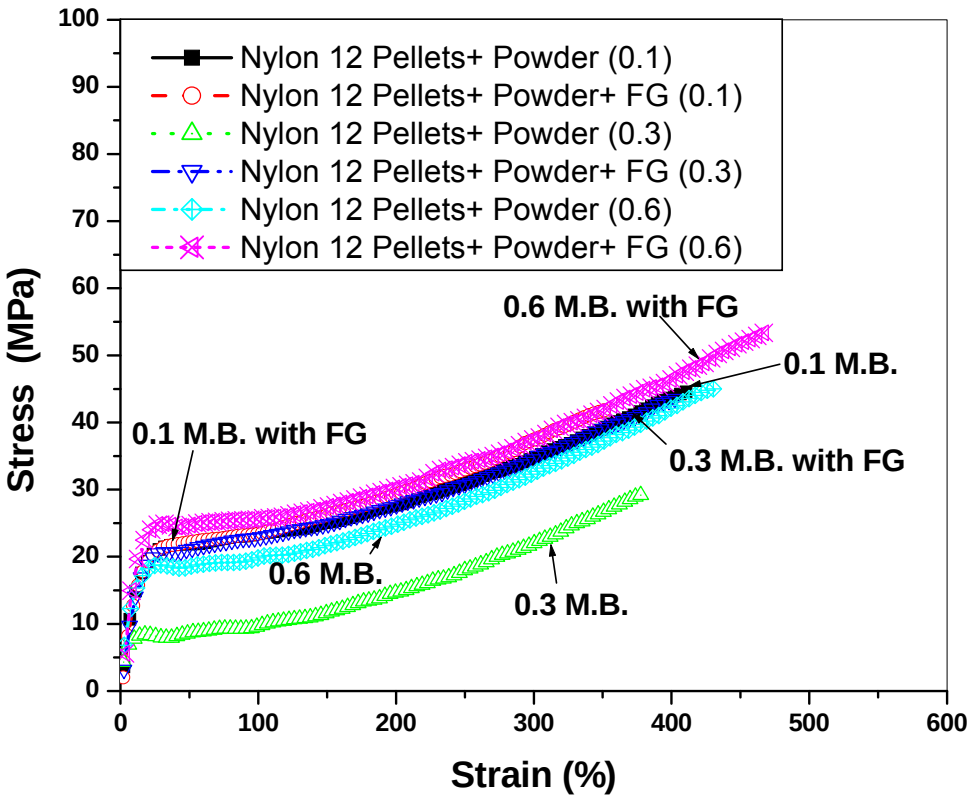

Fig. 5.31 Stress strain curves for masterbatch systems.

Figure 5.32 (a and b) represents an increasing trend in stress at break and percentage elongation at break of masterbatches upon addition of FG.

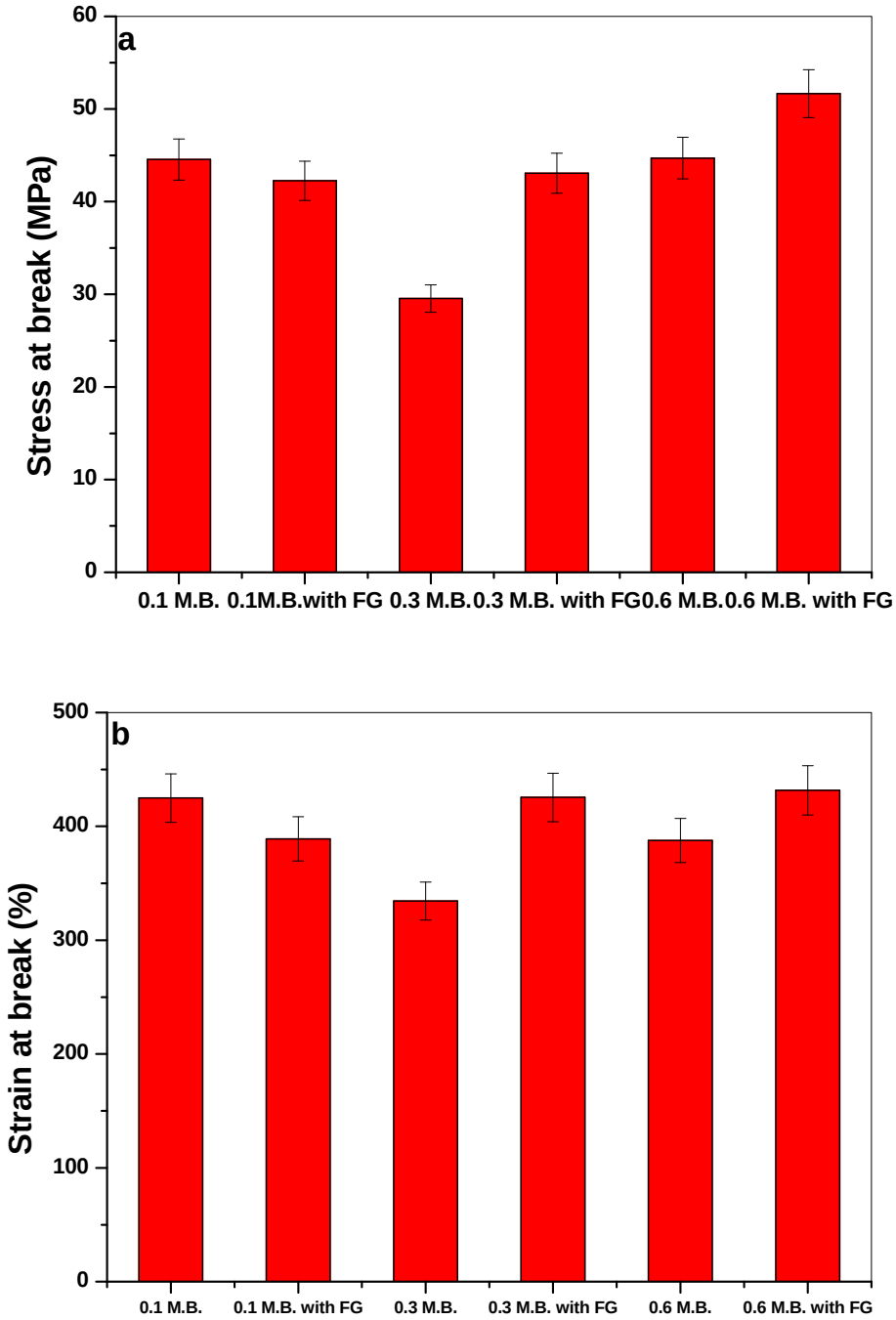

Fig.5.32 Stress at break (a) and strain at break (b) for masterbatches with and without FG.

The uniform dispersion of 0.3 wt% FG in the masterbatch was observed using SEM and it has been shown in figure 5.33.

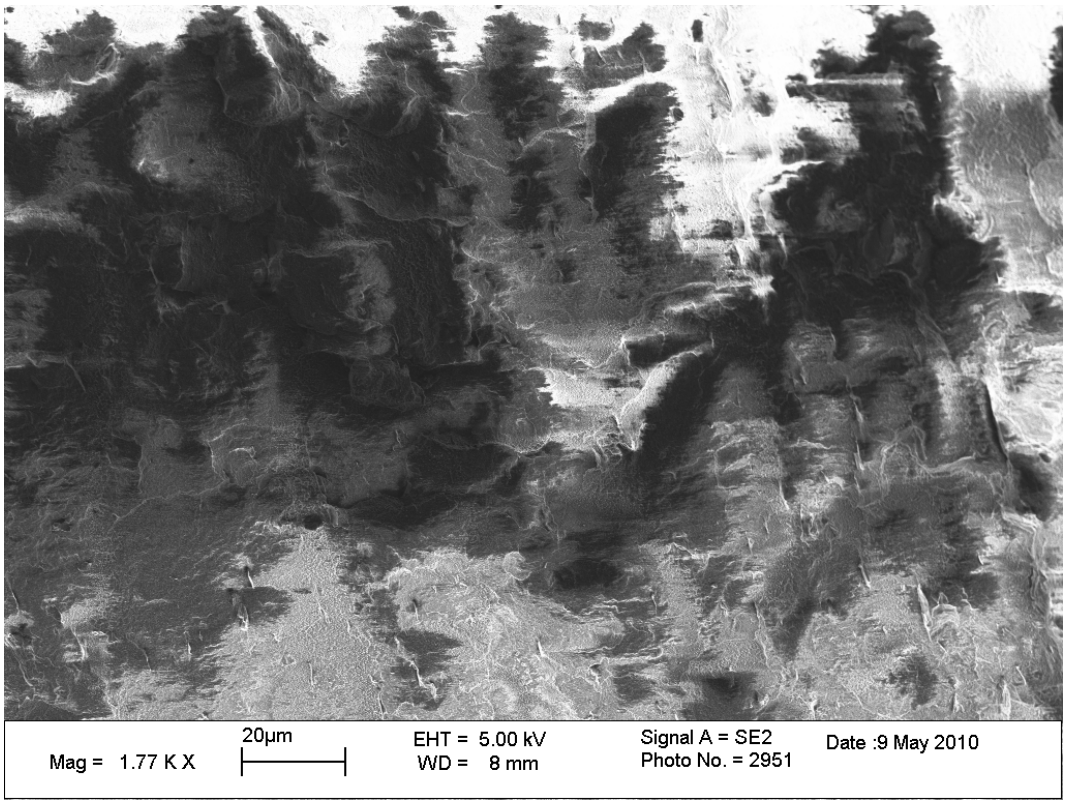

Fig.5.33 Dispersion of FG in the masterbatch (0.3 M.B. with FG) of nylon 12.

As depicted in figure 5.33, a uniform dispersion of 0.3wt% FG in the masterbatch was achieved which is beneficial for the enhanced interfacial adhesion between FG and nylon 12 pellets. This interaction between nanofiller and nylon 12 was thought to be a candidate for improving the mechanical properties of the nylon 12 masterbatches. With the addition of FG, an increase in Young's modulus was observed for all the masterbatches which is an evident of successful interfacial adhesion between FG and the masterbatches (as shown in figure 5.34). Upon addition of FG a slight increase in T_g of nylon 12 masterbatches was observed. This increase in T_g was extracted from the DSC analysis.

The typical values of T_g for the three systems has been shown in table 5.1.

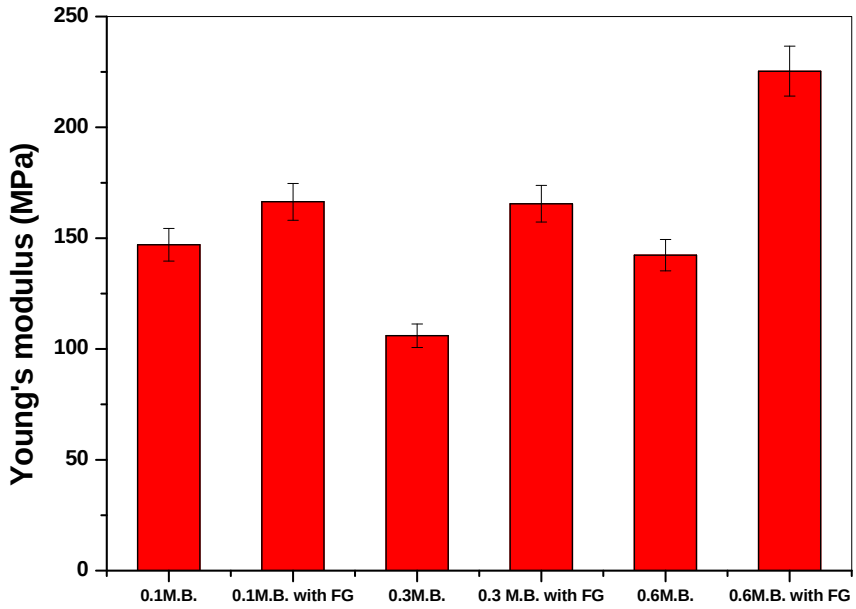

Fig.5.34 Young's modulus of masterbatches with and without various percentages of FG.

System	T_g (^oC)
0.1 M.B	58.50
0.1 M.B. with F.G.	58.56
0.3 M.B	56.71
0.3 M.B. with F.G.	60.36
0.6 M.B	55.07
0.6 M.B. with F.G.	57.97

Table 5.1 Glass transition temperatures of masterbatches with and without functionalized graphene.

T_g and Young's modulus of masterbatches with 0.1wt% FG were only slightly increased as compared to other two systems, which gives strength to our claim that there must be a critical amount of FG required for imparting the stronger interfacial adhesion. The interactions between FG and masterbatches were revealed by using FTIR spectrometer. Figure 5.35 shows the FTIR patterns for 0.3 M.B and 0.3M.B. with F.G. As seen clearly in 5.35 (b and c), upon incorporation of FG, peaks belonging to amide groups at 3284 cm^{-1} and 1546 cm^{-1} presented a significant shift to 3292 cm^{-1} and 1554 cm^{-1}, respectively. The similar trend of amide shift was observed for the 0.6wt% FG based masterbatches. There was no significant shift in peaks belonging to –OH and –C=O groups. These FTIR results indicated that hydrogen bonding was formed between FG and the masterbatches. This also implies that this hydrogen bonding could play a key role for the better mechanical performance of masterbatches.

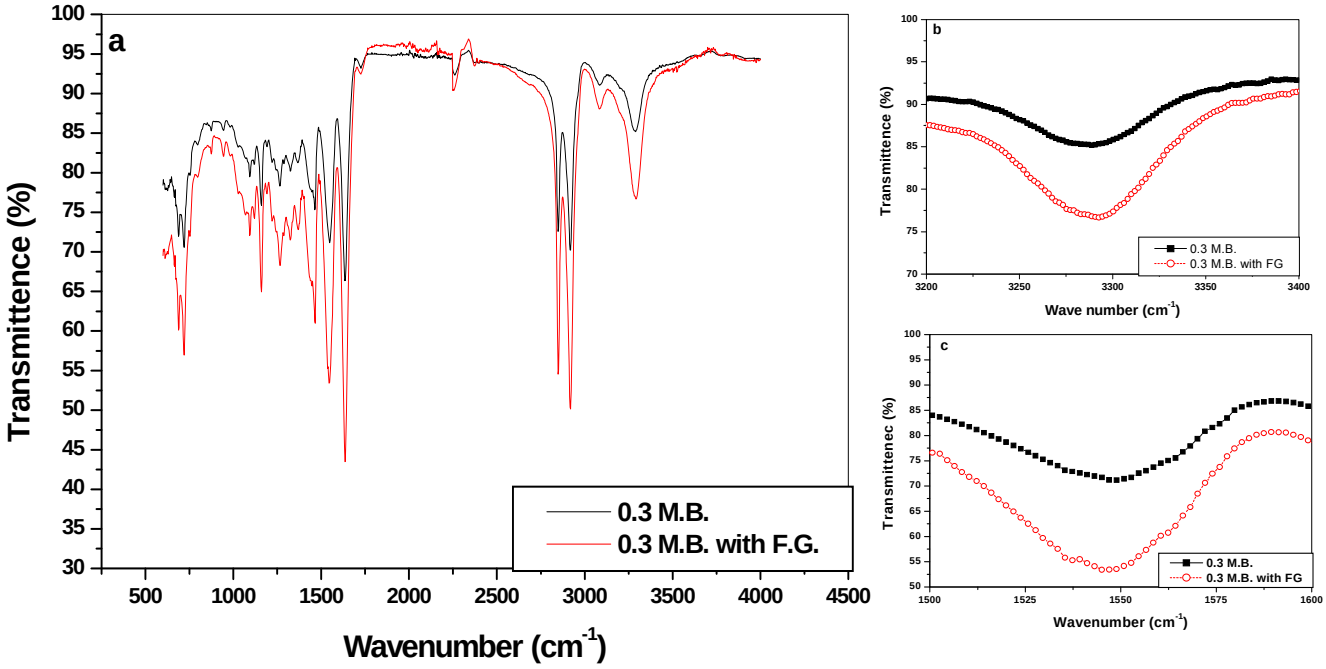

Fig.5.35 (a) FTIR curves for masterbatches as a function of FG, (b) and (c) represent magnified portion of FTIR curve to represent the shift of amide groups.

Interestingly, with 0.1wt% FG there was no shift of amide groups for either stretching or vibration motion. Under the lights of this result we can say that there was no major interaction between 0.1 wt% FG and the substrate masterbatch which could possibly lead towards the relatively poorer mechanical performance of this particular nanocomposite. In order to answer the question of whether FG inclusion can improve the toughness of masterbatches or not; various toughening testing methods were applied. For an initial check, area under the stress strain curves was calculated and results are shown in figure 5.36. As can be seen clearly that initially for 0.1wt%FG there was no increase in toughness was observed, but there was a significant increase in the toughness values for the higher percentages of FG. These results also conclude that there is a limiting percentage of FG to interact with masterbatch to improve the toughness.

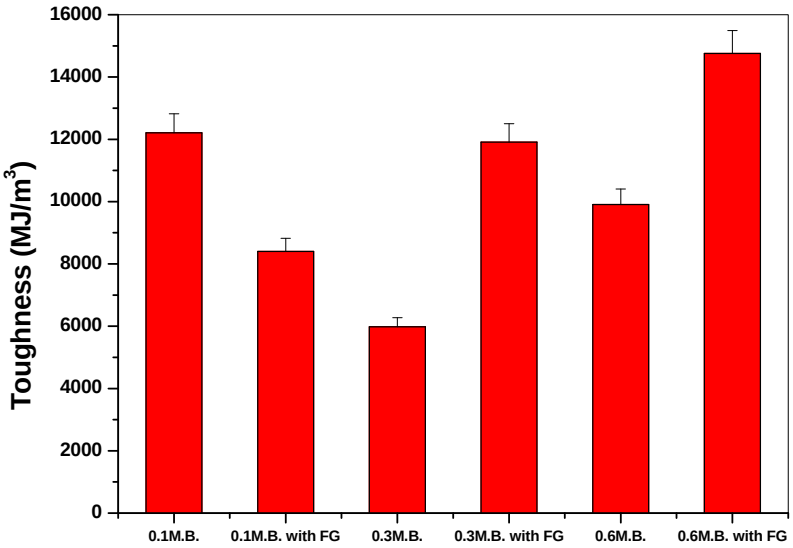

Fig.5.36 Toughness of masterbatches taken from area under the stress strain curves.

IFWIT was used to evaluate the impact failure energy of masterbatches. The results shown in figure 5.31 recognise the fact that impact failure energy did not increase by

the incorporation of 0.1wt% FG but was increased up to 31% and 38% respectively for the other two systems having 0.3 and 0.6 wt% FG. This might again be due to the fact that there is a critical fraction of FG required to increase the toughness of the masterbatches.

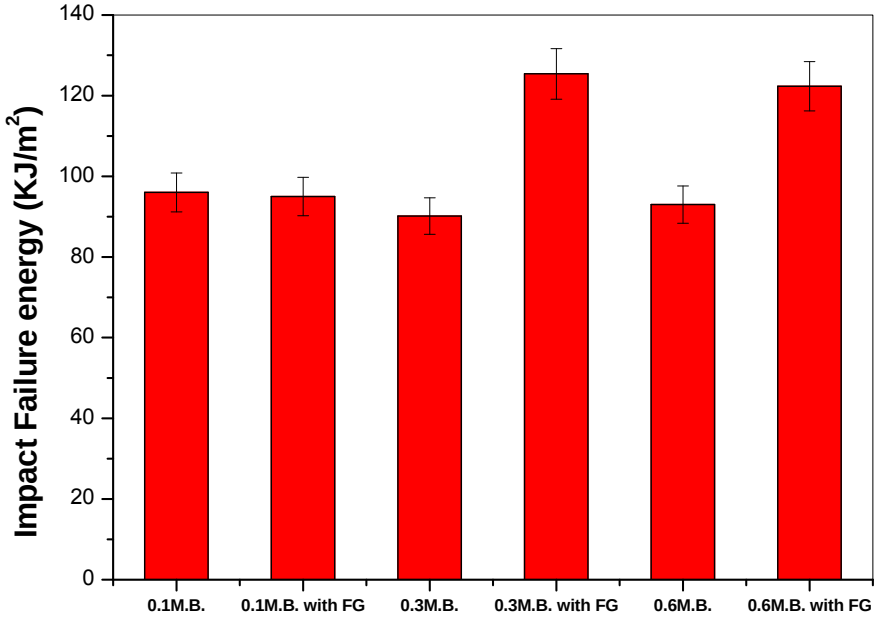

Fig.5.37 Impact failure energy of nylon 12 masterbatches obtained from IFWIT representing 0.3wt% FG as the one with the highest toughness.

To further compliment our toughness results, Mode I fracture toughness (K_{1c}) testing was performed. K_{1c} value test results were not different from the other two toughness evaluation techniques. As presented clearly in figure 5.38, K_{1c} of 0.1 wt% masterbatch was not increased at all, while for the higher percentage of FG there was noticeable increment in K_{1c} of nylon 12. In order to elucidate the toughening mechanism of the masterbatches, upon dispersion of functionalised graphene sheets, XRD was used. Since it was considered for UF4 and FG based nylon 12 (powder) nanocomposites that an increase in the γ-phase and decrease in crystal size were the possible toughening mechanisms, therefore x-ray diffraction and

polarized optical microscopy was used to observe any phase change and variation in the crystal size, respectively. The characteristic OM results for 0.6 masterbatches are displayed in figure 5.39 which presents that crystal size of 0.6 Masterbatch was reduced upon incorporation of 0.6wt% FG. A similar decrease in crystal size of 0.3 M.B. was also observed for 0.3wt% FG. As was noticed for the other properties of masterbatches, crystal size of 0.1 M.B. was not changed upon incorporation of FG.

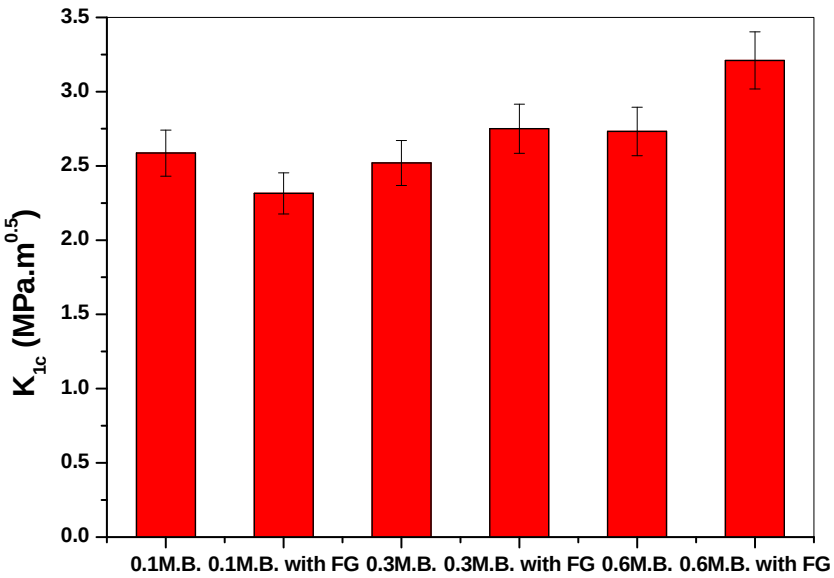

Fig.5.38 K_{1c} values of masterbatches as a function of graphene loadings.

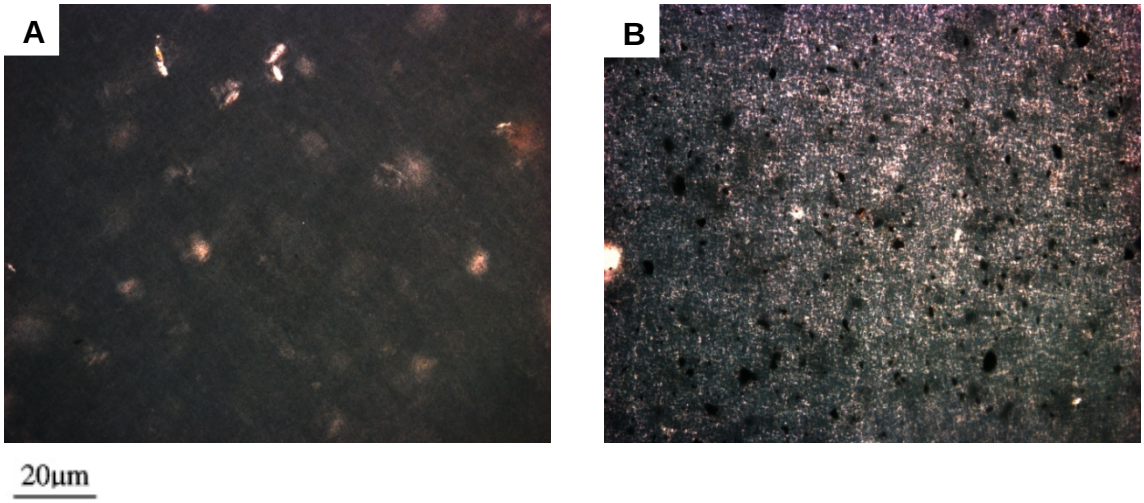

Fig.5.39 POM images of (A) 0.6 M.B. and, (B) 0.6 M.B. with FG.

This unchanged crystal size of '0.1M.B. with FG' might had lead towards its unchanged (rather decreased) toughness. To further enhance our understanding of toughening mechanism XRD was applied and results indicated that the γ-phase was improved upon inclusion of 0.3 and 0.6wt% FG. But, as expected, there was no increase in the γ-phase. Figure 5.40 (a and b) shows the effect of 0.1 and 0.3wt% FG on γ-phase of the masterbatches.

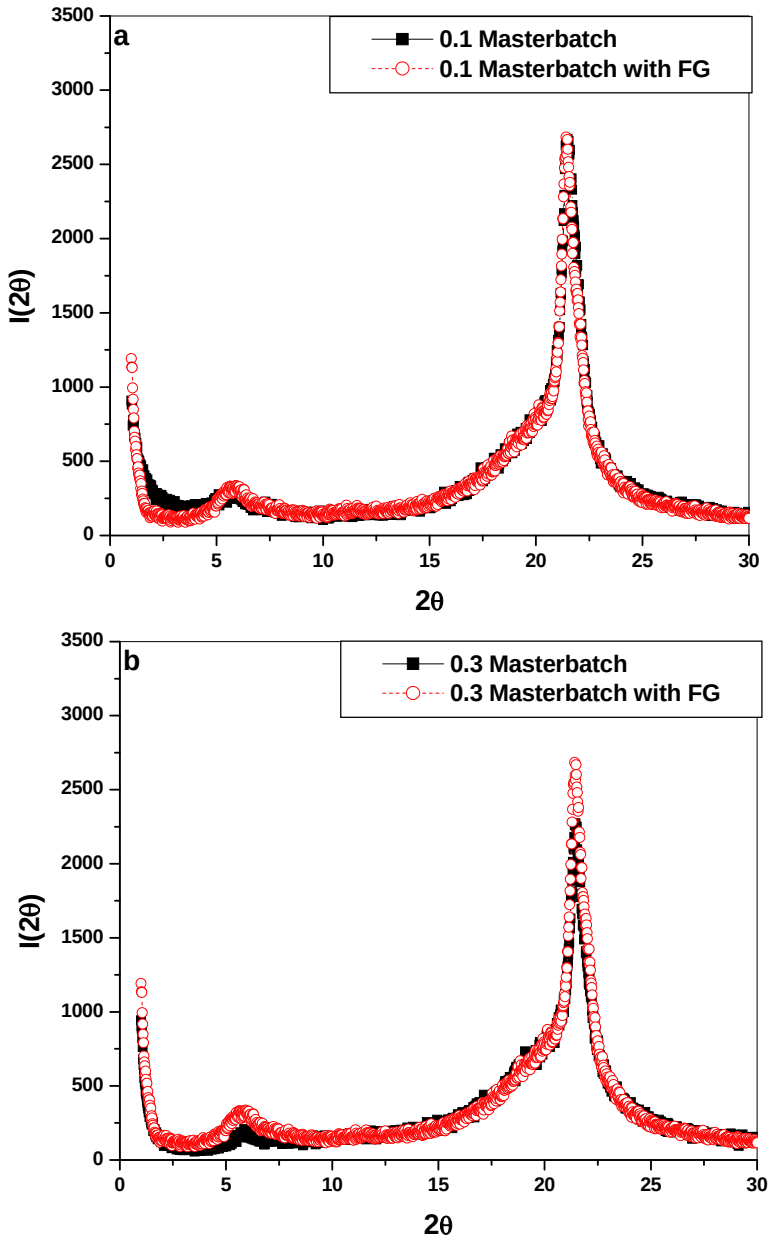

Fig.5.40 Effect of (a) 0.1wt%FG (b) 0.3wt%FG on XRD patterns of nylon 12 masterbatches.

XRD results confirmed that for 0.1M.B. system, there was no change in the γ-phase upon addition of FG; while a significant improvement was noticed for the case of other two masterbatches. As a result of the γ-phase consistency and unchanged crystal size of 0.1M.B. upon inclusion of FG, its toughness was unchanged (rather was decreased). While for the other two masterbatch systems, toughness was improved to a noticeable extent upon addition of FG.

5.8 Conclusions

In conclusion, an ultra-toughened FG/nylon 12 nanocomposite with low amount of functionalised graphene (FG) was developed. It was found that the incorporation of very small amount of the FG (0.6 wt%) caused a significant improvement in ultimate tensile strength, percentage elongation at break, impact energy and toughness of the nylon 12, although no significant improvement in Young's modulus occurred. With 0.6wt% FG ultimate tensile strength and elongation at break of the nylon 12 is improved by ～ 35% and ～200%, respectively. The K_{1c} of the nylon 12 is ～1.28 $MPa.m^{0.5}$ and the incorporation of 0.6wt% FG causes a significant increase of 72 % (～2.2 $MPa.m^{0.5}$). 0.6wt% FG causes also a significant improvement of 175 % in impact failure energy of the nylon 12. The incorporation of FG caused the increase in the amount of γ phase of nylon12 which could be the direct reason for the enhancement of toughness of nylon12.

Addition of UF4 in nylon 12 caused an obvious improvement in strength, elongation at break and toughness. The optimum percentage of UF4 to impart these considerable increments in various mechanical properties was found to be 0.3wt% (lesser than that of FG for which it was 0.6wt %).

To extend the role of functionalized graphene as strengthening and toughening nanofiller, various masterbatches of nylon 12 pellets, nylon 12 powder and graphene were prepared and tested. Lower percentage of FG did not cause any increment in strength, elongation at break, impact failure energy or in the toughness of masterbatches. This was because the addition of lower percentage of FG did not change the amount of γ phase, decrease the crystal size and they were not uniformly dispersed. On the other hand, graphene loadings of 0.3 and 0.6wt% imposed a substantial increment in the mechanical performance of the masterbatches.

5.9 References

[1] Weng et al. Fabrication and characterization of Nylon 6/Foliated graphite: Electrically conducting nanocomposite. Journal of Polymer Science: Part B: Polymer Physics.2004; 42:v2844–2856

[2] Gacitua et al. Polymer nanocomposites: Synthetic and natural fillers: a review. Maderas. Ciencia y tecnología 2005; 7(3): 159-178

[3] K. Kalaitzidou, H. Fukushime, L.T. Drzal. Mechanical properties and morphological characterization of exfoliated graphite-polypropylene nanocomposite. Composites 2007;38: 1675-1682

[4] D. Cai, M. Song. A simple route to enhance the interface between graphite oxide nanoplatelets and a semi-crystalline polymer for stress transfer Nanotechnology 2009; 20: 315708.

[5] H. Song, I. Srivastava, J. Rafiee, M.A. Rafiee, N. Koratkar, Z. Wang and Z. Yu. Fracture and fatigue in graphene nanocomposites, Small 2009; 6: 179–183.

[6] J. Robbins, B.S. Majumdar. Deformation mechanisms and toughening in carbon nanotube-reinforced polycarbonate matrix composites. Materials Science and Technology (MS&T) 2006; Materials and systems - Volume 2: 303-311

[7] A. J. Lovinger and M. L. Williams. Tensile properties and morphology of blends of polyethylene and polypropylene. J. Appl. Polym. Sci. 1980; 25(8): 1703-13

[8] J. L. Way, J. R. Atkinson, J. Weitting. The effect of spherulite size on the fracture morphology of polypropylene. J. Mater. Sci. 1974; 9: 293-99

[9] J. L. White, S. Rhee. Crystal structure and morphology of biaxially oriented polyamide 12 films J. Polym. Sci. Part B 2002; 40: 1189-1200

[10] A. Saiter, B. Alexandre, D. Langevin, H. Couderc, Q.T. Nguyen, P. Médéric, S. Marais, T. Aubry. Water barrier properties of polyamide 12/ montmorillonite nanocomposite membranes: Structure and volume fraction effects J. Membrane Sci. 2009; 328: 186–204

[11] B. Chen, J. R. G. Evans. Impact strength of polymer-clay nanocomposites. Soft Mater 2009; 5: 3572-84

[12] A.R. Jeefferie, M.Y. Yuhazri et al. Thermomechanical and morphological interrelationship of PP/MWCNTs nanocomposites. Inernational Journal of basic and applied sciences 4: 29-35

[13] Effect of frequency on the modulus and glass transition temperature of PET www.tainstruments.com/library_download.aspx?file=TS62.pdf

[14] Introduction to Dynamic Mechanical Analysis (DMA), A Beginner's Guide

[15] B. Lecouvet, J.G. Gutierrez, M. Sclavons, C. Bailly. Structure- property relationships in polyamide 12/halloysite nanotube nanocomposites. Polymer Degradation and Stability 2011; 96: 226-235

[16] Loan T. Vo, Spiros H. Anastasiadis, Emmanuel P. Giannelis. Dielectric study of poly(styrene-co-butadiene) composites with carbon black, silica, and nanoclay. Macromolecules 2011

[17] Kevin P. Menard. Dynamic mechanical analysis; a practical introduction. CRC Press. Chapter 7

[18] H.P. Menard. Dynamic mechanical analysis; a practical introduction 2nd edition. CRC Press. Chapter 6

[19] M.S.P. Shaffer, A.H. Windle. Fabrication and characterization of carbon nanotube/ poly (vinyl alcohol) composites. Advanced Materials 1999; 11: 937-941

[20] F.T. Fisher, A. Eitan et al. Spectral response and effective viscoelastic properties of MWNT- reinforced polycarbonate. Adv. Comp. Lett. 2004; 13: 105-111

[21] Z. Jin, K.P. Pramoda et al. Dynamic mechanical behaviour of melt-processed multi-walled carbon nanotube/ poly(methyl methacrylate) composites. Chem. Phys. Lett. 2001; 37: 43-47

[22] A. Arsad, A.R. Rahmat et al. Mechanical and rheological characterization of PA6 and ABS blends-with and without short glass fibre. Journal of Applied Sciences 2011; 11: 2313-2319

[23] Dynamic mechanical analysis basics: Part 2 Thermoplastic transitions and properties, www.perkinelmer.com

[24] H. Song, I. Srivastava, J. Rafiee, M. A. Rafiee, N. Koratkar, Z. Wang, Z. Z. Yu. Fracture and fatigue in graphene nanocomposites Small 2009; 6:179-83

[25] X. Gao, C. Qu, Q. Zhang, Y. Peng, Q. Fu. brittle-ductile transition and toughening mechanism in POM/TPU/CaCO3 ternary composites. Macromol. Mater. Eng. 2004; 289: 41–48

Chapter 6

A comparative study of various nanofillers toughening nylon 12

6.1 Introduction

Particles, tubes and platelets are three kind of typical reinforcements which have been used in preparation of polymer nanocomposites and refluxing various nanoreinforcements with several acids, in order to create some active sites, has been a key factor to form a interactional bridge between these nanofillers and the polymeric matrices [1,2]. It has been reported that treating organic nanofillers (like CNTs, planar graphene sheets etc) with concentrated acid creates acidic sites such as carboxylic, carbonyl, and hydroxyl groups on these nano-inclusions [1, 2]. Carbon black, with an entire different geometry compared with carbon nanotubes and graphene, has also been used as nanofiller to improve the mechanical performance of various polymers like nylon 12 and polypropylene [3, 4].

In chapter 5, a detailed discussion on the toughness of nylon 12 upon incorporation of graphene sheets was given. It was found that upon adding different sized graphene sheets, there was no significant difference in their toughening efficiency. Although the toughening mechanism of graphene/ nylon 12 nanocomposites was found to be an increase in γ-phase and decrease in crystal size of nylon 12, but it is still not clear that whether an organic nanofiller with varied geometry can toughen nylon 12 or not!

To answer this query, multiwalled carbon nanotubes (with diameter 8-15nm) and carbon black (with particle size of about 26nm) were chosen as candidates along

with nano-graphite or UF4 graphite (having a planar geometry), to be incorporated in nylon 12 and tested for toughness. Prior to the blending of nanofillers with nylon 12; all three nanofillers were equally treated with a mixture of H_2SO_4 and HNO_3. In this chapter, the detailed functionalization treatment and toughness comparison of three different shaped nanofillers was disclosed.

6.2 Characterization of acid treated nanofillers and their nanocomposites

Since strong interactions between filler surface and polymeric matrices has a significant influence on the mechanical properties, therefore an attempt was made to increase the quantity of functional groups on the surfaces of graphite, multiwalled carbon nanotubes and carbon black . A mixture (40ml) of nitric and sulphuric acid in the ratio of 1:3 was used for the treatment of these nanofillers. Detailed experimental procedure has already been described in chapter 3. Type of functional groups to be added to nanofillers, which are beneficial for stronger interaction, will depend upon functional groups available on the nylon 12 matrix. It was thought from the FTIR results (discussed in chapter 5) that it could be –CONH- groups of nylon 12 who might form hydrogen bonding with –OH groups present on the surface of nanofiller. So it was of interest to functionalise –OH groups on the surface of the each nanofiller to enhance their chemical linkage with nylon 12. It has been well acknowledged that the mixture of nitric and sulphuric acids can introduce oxygen-containing groups, especially hydroxyl, carbonyl and carboxylic functionalities [5,6]. These considerations lead to an application of a mixture of nitric and sulphuric acids for the surface treatment of expanded nano-graphite (UF4), MWCNTs and carbon black. FTIR was applied to qualitatively establish the nature of the surface groups of the fillers before and after the acid treatment. FTIR spectra of untreated UF4 and acid treated UF4 is shown in figure 6.1. After treatment, a shift in stretching vibrations of –

OH from 3456 to 3461cm^{-1} and an appearance of an additional peak at 1740 cm^{-1} which belongs to stretching vibration of C=O groups [7] confirmed the introduction of additional free groups on the surface of expanded graphite (UF4).

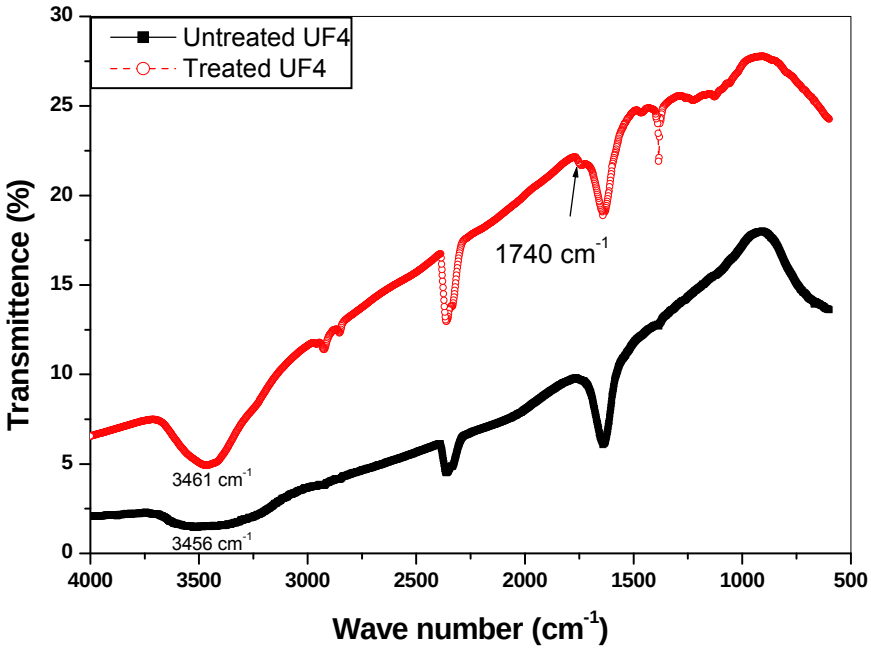

Fig.6.1 FTIR spectra of UF4, before and after acidic treatment.

Esumi et al. [8] reported that the mixture of concentrated nitric and sulphuric acid in volume ratio of 1:3 and a treatment time of 20 minutes could effectively introduce a large concentration of acidic sites on carbon nanotube. Upon acidic treatment of MWCNTs, an increase in the intensity (as was observed for UF4) of wave number of hydroxyl group (3455 cm^{-1} to 3466 cm^{-1}) was noticed and an additional peak for -C=O was located at 1746cm^{-1} as well. This introduction of additional free groups on the surface of MWCNTs has been shown in figure 6.2. Upon acidic mixture treatment, similar to other two nanofillers, carbon black also showed a significant increase in additional free groups which can strongly link with the free sites of nylon 12 [4].

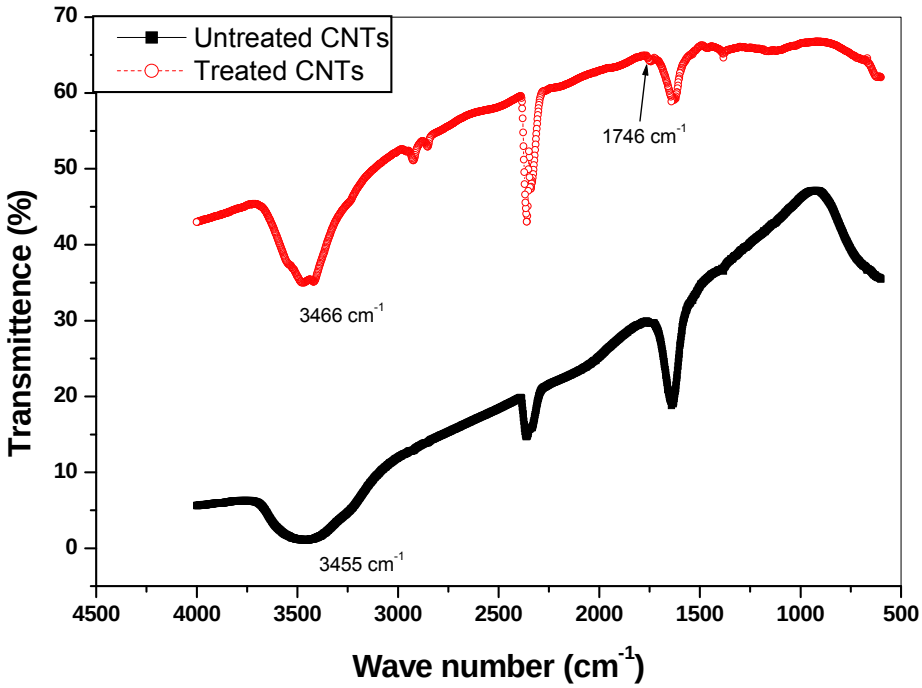

Fig.6.2 FTIR spectra of CNTs, before and after acidic treatment

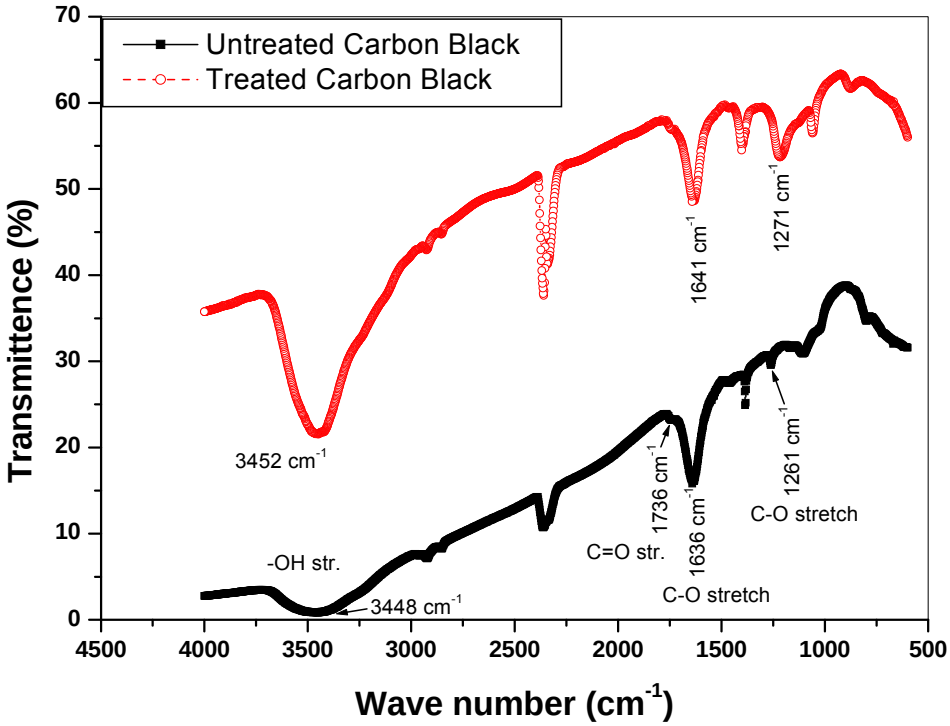

Fig.6.3 FTIR spectra of carbon black, before and after acidic treatment

Figure 6.3 displays that upon acid treatment of carbon black, peaks belonging to hydroxyl, -OH, C-O and C=O groups presented a shift to higher wave numbers which implies that there is an increase of functional groups on the surface of carbon black. All three similar treated nanofillers of different geometry were blended with nylon 12 to prepare their nanocomposites. Figure 6.4 shows a comparison of FTIR spectra of nylon 12 and its nanocomposites with 0.6wt% of UF4, MWCNTS and carbon black.

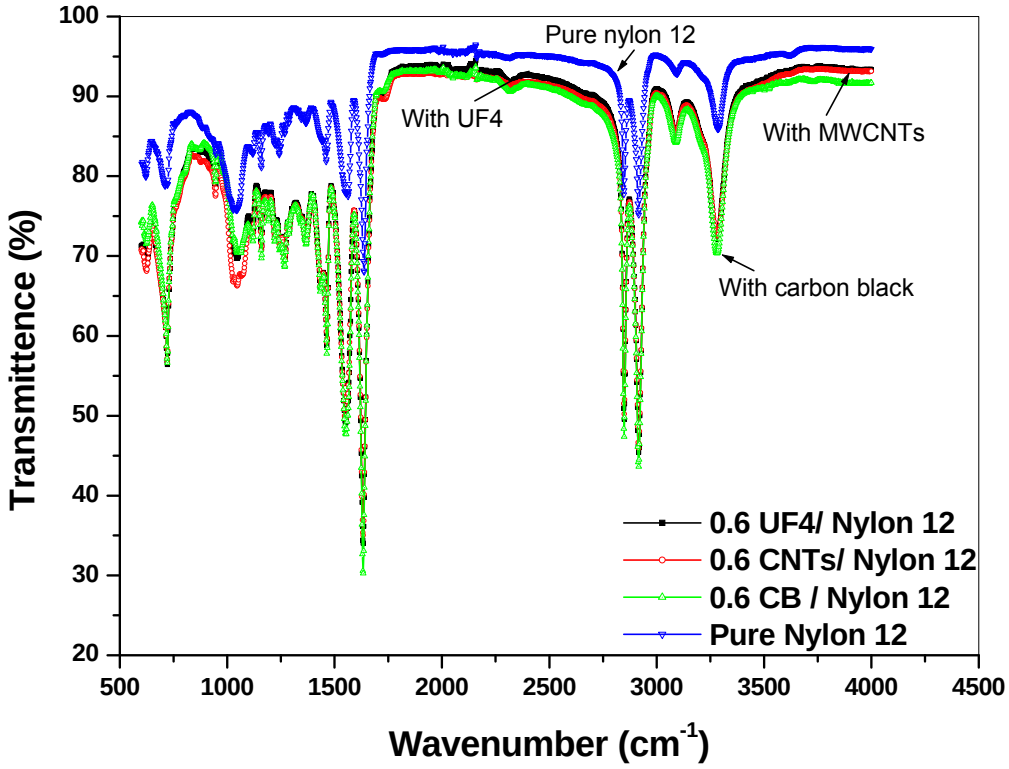

Fig.6.4 FTIR spectra of nylon 12 and its nanocomposites with 0.6wt% UF4, MWCNTs and carbon black.

Pristine nylon 12 shows an amide stretch at 3284 cm^{-1} and 1554 cm^{-1}. In the nanocomposites with nitric and sulphuric acid treated nanofillers, these peaks were shifted down with all three reinforcements, indicating the interaction between the nylon 12 matrix and functional groups on the surface of nanofillers. These FTIR results suggested that the each nanofiller with its unique geometry was successfully

interacting with the nylon 12. In other words, all three nanofillers were treated the same and their nanocomposites with nylon 12 were also prepared in exactly the same way. This was necessary for the fair testing of effect of different geometry nanofillers on the toughness of nylon 12.

6.3 Effect of various nanofillers on the toughness of nylon 12

In order to elucidate how different shaped nanofillers with the same pre-treatment effect the toughness of nylon 12, area under the stress-strain curve and Mode I fracture toughness (K_{Ic}) testing were used. Figure 6.5 represents the stress strain curves of nylon 12 and its nanocomposites. As can be seen clearly that the ultimate tensile strength and percentage elongation was increased straight away, upon incorporation of any nano-reinforcement.

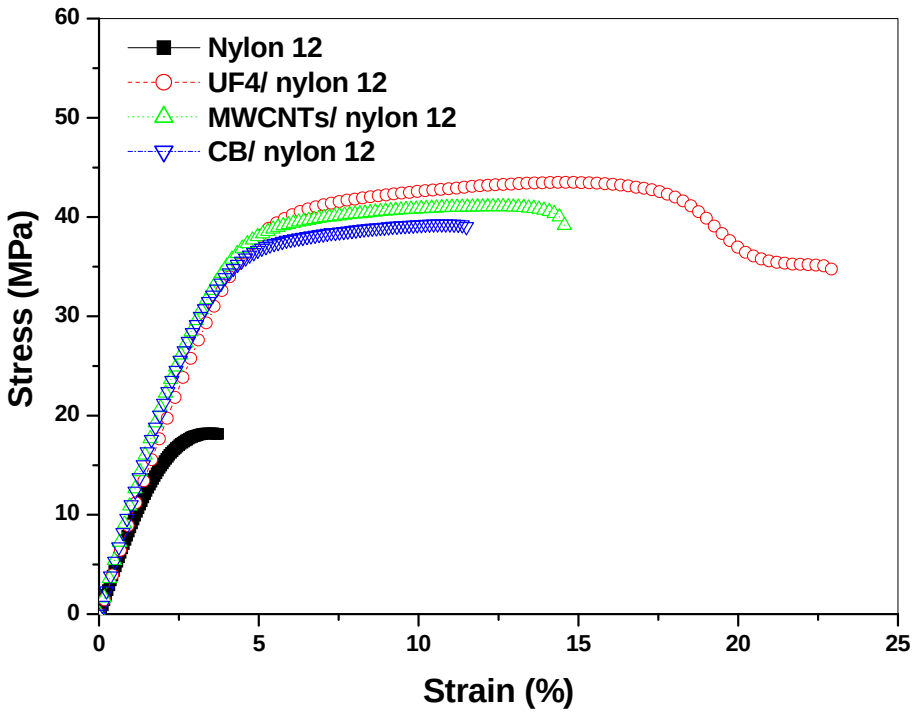

Fig.6.5 Stress strain curves of nylon 12 composites with various nanofillers

This increase in UTS of nylon 12 was more prominent upon incorporation of UF4 (139%) while it was 125% & 116% for MWCNTs and carbon black respectively. These figures represent that UF4 made a relatively better contribution towards the strengthening of nylon 12 as compared to other two nanofillers. This also implies that although treated with the same method, planar UF4 sheets had better interfacial adhesion compared to CB particles and multiwalled carbon nanotubes.

Area under the stress strain curve, which is proportional to the toughness, was calculated to find out the effect of geometry of nanofiller on the toughness of nylon 12. Five samples for pure nylon 12 and each nanocomposite were tested and their average results with error bars are shown in figure 6.6.

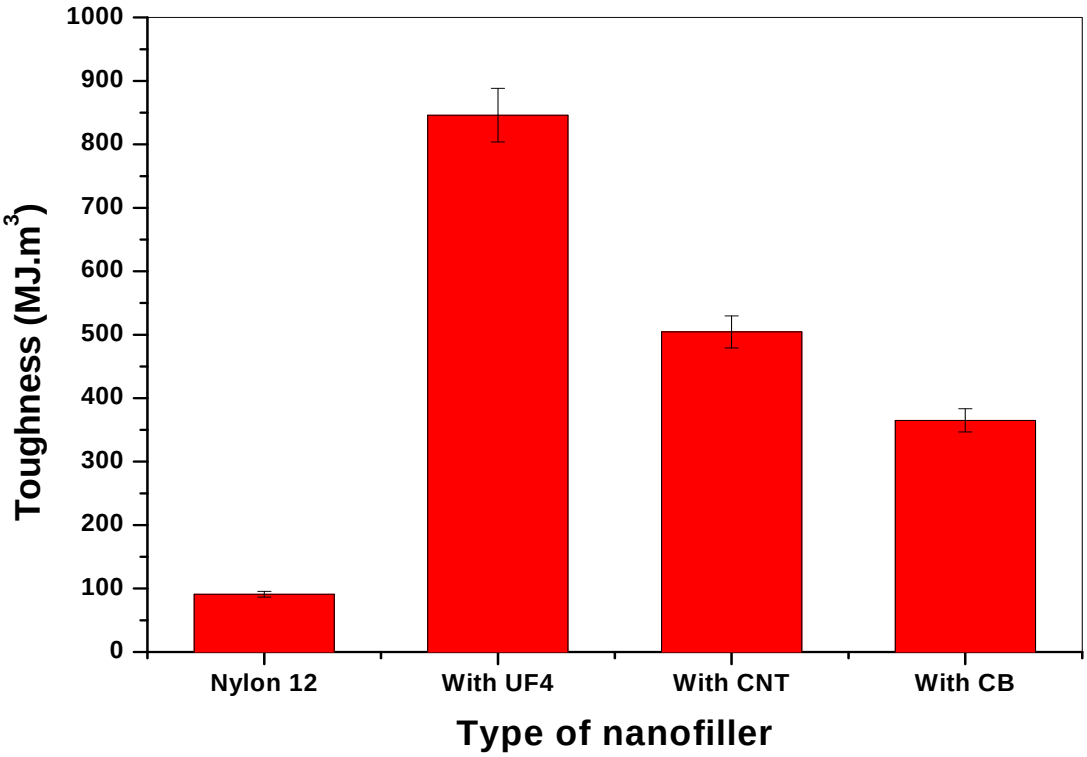

Fig.6.6 Toughness, calculated by using area under the curve, of nylon 12 and its nanocomposites with 0.6 wt% UF4, CB and MWCNTs.

As clearly shown in above figure 6.6, toughness was enhanced very significantly upon incorporation of UF4. Although there is a crucial improvement in the area under the curve of nylon 12 upon incorporation of MWCNTs and carbon black, but it is not as significant as it is for UF4 addition. A great deal of increase in the improvement of toughness of nylon 12 upon inclusion of UF4 suggested that this planar filler had more tendency to impart the toughening effect in nylon 12 as compared to particle or tube shaped fillers (CB and MWCNTs). The consistent strong interaction between nylon 12 and UF4 might had reduced the polymer chain mobility and had facilitated a uniform dispersion. Consequently, the amount of interfacial area between polymer and UF4 was increased which hence resulted in toughening of nylon 12. K. Kalaitzidou et al [9] compared the effect of carbon black, carbon nano-fibres, clay and exfoliated graphene nanoparticles on the toughness of polypropylene (PP). In general, with the addition of carbon nano-fibres and graphene; the toughness of PP was enhanced. An increment of about 100% was observed in the case of graphene nanoparticles inclusion; while it was only 10% for the case of CNTs. Interestingly carbon black based PP nanocomposites did not show any improvement in toughness. On the other hand, an improvement in toughness of PP upon incorporation of treated carbon black has also been reported by Zhu et al [4].

In order to further investigate the toughening ability of three different shaped nanofillers, Mode I fracture toughness testing was carried out. The results of K_{1c} testing are shown in the figure 6.8. Referring to figure 6.7, planar UF4 had tremendously increased the toughness as compared to CNTs and carbon black. Upon incorporation of carbon black, toughness was even reduced to an appreciable extent. From the fracture toughness testing results it could be established that the extraordinary effectiveness of treated UF4, to resist the fracture of nylon 12, is

related to deflection processes associated with its planar / two dimensional geometry. This unique geometry of UF4 enabled it to deflect the cracks more effectively than one dimensional MWCNTs and lower aspect ratio nanoparticles of carbon black. It has been suggested that the deformability or flexibility of the graphene sheet has the tendency to contribute towards nanocomposite strengthening and toughening by reducing the relative value of the Poisson ratio of the composite [10]. Wang et al [11] also reported that graphene nanoparticles (a graphite derivated nanofiller) has a much better toughening effect than CB for HDPE. They reported an increase of 100% in the toughness of HDPE upon incorporation of graphene while toughness of HDPE was decreased substantially upon incorporation of carbon black.

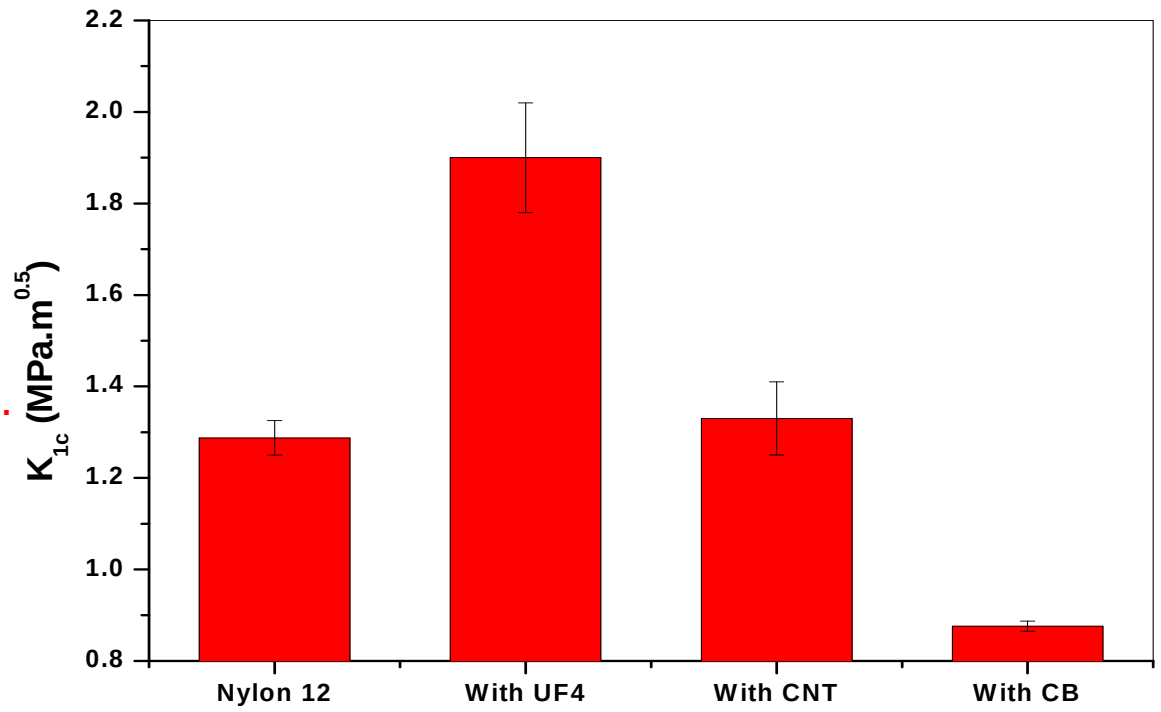

Fig.6.7 K_{Ic} values of nylon 12 and its nanocomposites with 0.6 wt% UF4, CB and MWCNTs calculated by three point bending tests.

6.4 Effect of untreated UF4 on toughness of nylon 12

To find out whether it is the only geometry of nano-graphite (UF4) which increases toughness or it is the synergetic effect of additional free groups and the two dimensional geometry of the nanofillers which is crucial for toughness enhancement and overall better mechanical performance. Untreated UF4 (as received from the company) was melt blended with nylon 12 in order to prepare 0.1, 0.3, 0.6, 1 and 3wt% nanocomposites. A uniform dispersion of UF4 in nylon 12 was confirmed by FEGSEM, as shown in figure 6.8. Tensile testing results for nylon 12 and its composites with untreated UF4 are presented in table 6.1. A decreased Young's modulus and ultimate tensile strength upon adding UF4 gives us an indication of very weak interfacial adhesion between the filler and the matrix.

Graphite Content /%	Young's Modulus /GPa	Strength /MPa	Elongation /%
0.0	1.0462±0.0090	45.86±0.26	12.05±0.07
0.1	1.0775±0.0101	41.54±0.95	9.65±0.29
0.3	1.1139±0.0108	32.04±0.94	7.87±0.32
0.6	1.0736±0.0411	40.04±2.36	7.50±0.99
1.0	1.1282±0.0547	38.87±1.27	6.90±0.30
3.0	1.1369±0.0532	33.83±3.12	6.97±0.51

Table 6.1 Mechanical properties of nylon 12 and its nanocomposites.

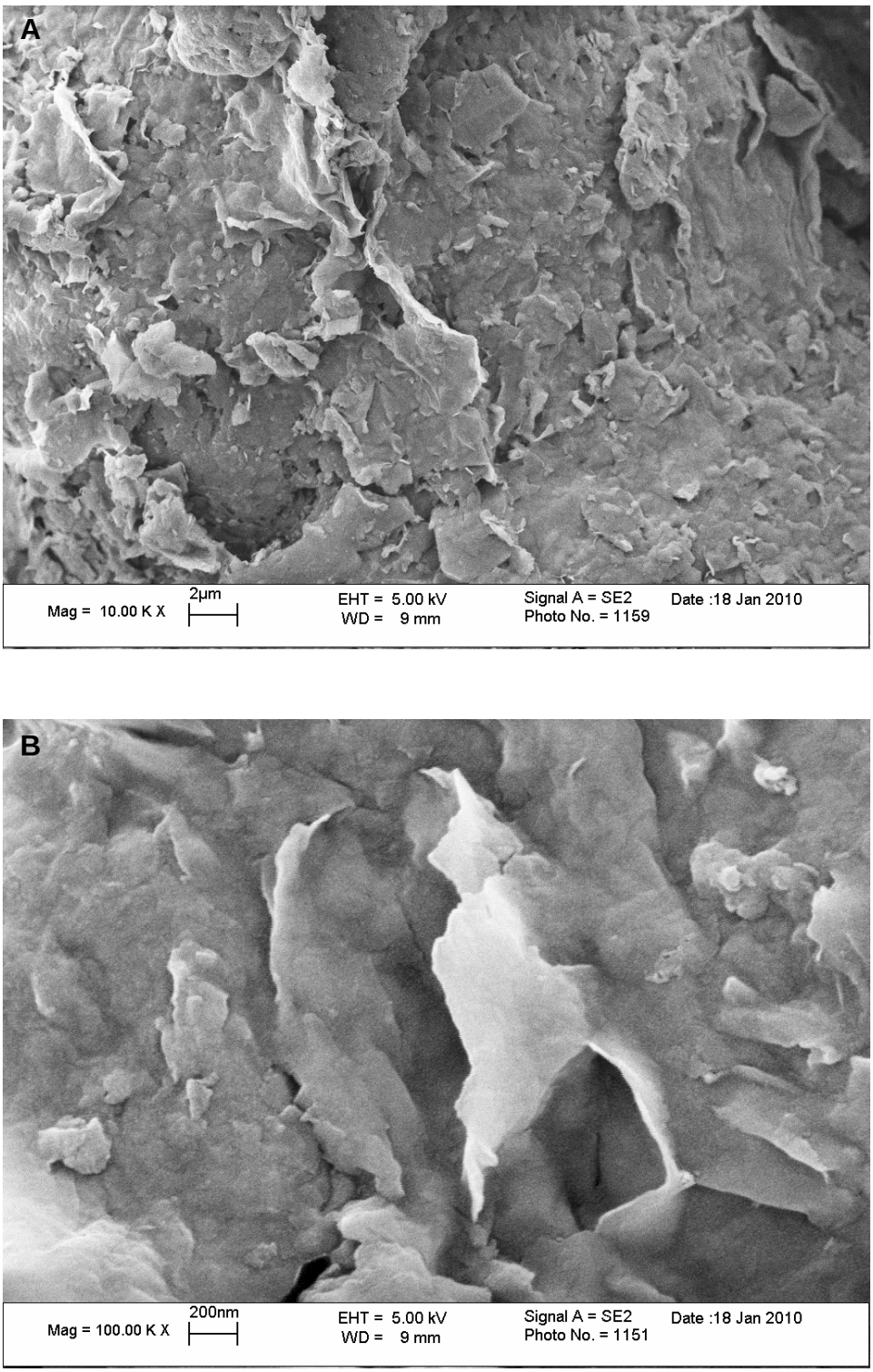

Fig.6.8 (A and B) SEM images nylon 12/ UF4 (0.3 wt %) nanocomposite

The toughness of untreated nylon 12 nanocomposites, as evidenced by increase in elongation at break given in table 6.1, was decreased drastically with the incorporation of untreated UF4 nano-graphite.

Although a homogenous dispersion of nano-graphite in the polymer was achieved but the tensile stress, Young's modulus and elongation at break of nylon 12 were greatly decreased when the untreated UF4 nano-graphite was incorporated. Keeping the tensile testing results in mind it can be established that to improve the mechanical performance and toughness of the nanocomposites, in addition to a good dispersion of nano-graphite in polymer, the existence of the interfacial interaction between filler and polymer is also a key issue.

6.5 Conclusions

By using an "acid treatment" method, UF4, carbon nanotubes and carbon black were successfully functionalized and blended with nylon 12. This functionalization of the nanofillers was confirmed with FTIR results which proved the existence of additional oxygen containing groups existing on the surface of each filler after acid treatment, which might prove to be beneficial for their interaction with nylon 12. Effect of these three functionalized nanofillers with unique geometry on the toughness of nylon 12 was evaluated by using area under the curve and fracture toughness testing. Both testing techniques concluded that although three nanofillers were equally pre-treated and their same weight percentage was distributed in the matrix but it was the planar structure of UF4 which proved to be the best nanofiller to impart toughening of nylon 12 and the overall mechanical performance. In contrast, a different geometry of CB and CNTs lead to the existence of weaker interface, limiting their ability to enhance the toughness and other mechanical properties of nylon 12. Also, it was noticed that the effect of carbon nanotubes on the overall mechanical performance of nylon 12

was better than that of carbon black. Furthermore, it was found that only planar geometry of UF4 is not enough to increase toughness and other mechanical properties of nylon 12, but the presence of active functional groups is also necessary.

6.6 References

[1] W.D. Zhang, L. Shen, I. Y. Phang, T. Liu. Carbon nanotubes reinforced nylon 6 composite prepared by simple melt-compounding. Macromolecules 2004; 37: 256-259

[2] H. Kim, A.A. Abdala, C. W. Macosko. Graphene/ polymer nanocomposites. Macromolecules 2010; 43: 6515–6530

[3] S.R. Athreya, K. Kalaitzidou, S. Das. Processing and characterization of a carbon black-filled electrically conductive nylon-12 nanocomposite produced by selective laser sintering. Materials Science and Engineering A 2010; 527 : 2637–2642

[4] P. Zhu, J. Chen, C. Wu. Crystallization behaviour and mechanical properties of polypropylene/modified carbon black composites. Polymer composites 2009: 391-398

[5] R. Verdejo, S.Lamoriniere, B. Cottam, A. Bismarck, M. Shaffer. Removal of oxidation debris from multi-walled carbon nanotubes. Chem. Commun. 2007: 513–515

[6] M. S. P. Shaffer, X. Fan , A. H. Windle. Dispersion and packing of carbon nanotubes. Carbon 1998; 36: 1603–1612.

[7] D. A. Skoog, F. J. Holler, T. A. Nieman. Principles of instrumental analysis 5th edition; 1998: chapter 17

[8] K.Esumi, M. Ishigami, A.Nakajima, K. Swawda, H.Honda..carbon 1996;34:279-281

[9] K. Kalaitziduo, H. Fukushima, L.T. Drzal. Mechanical properties and morphological characterization of exfoliated graphite-polypropylene nanocomposites. Composites (Part A) 2007; 38: 1675-1682

[10] B. Li, W.H. Zhong. Review on polymer/graphite nanoplatelet nanocomposites. J Mater. Sci. 2011; 46:5595–5614

[11] L. Wang, J. Hong, G. Chen. Comparison study of graphite nanosheets and carbon Black as fillers for high density polyethylene. Polym. Engg. & Sci. 2010; 50: 2176-2181

Chapter 7

Effect of functionalized graphene on the barrier properties of nylon 12

7.1 Introduction

Impermeable nanofillers exhibiting high aspect ratios have been intensively used to improve the barrier properties of various polymers [1, 2]. The incorporation of very small amount of graphene and graphene oxide derived nanofillers can significantly reduce gas and water permeation through a given polymeric matrix [3]. It is usually suggested that the platelet geometry of graphene can provide a tortuous path, which retards the molecular diffusion through the matrix which hence results in decrease in permeability. Permeability of any nanocomposite can be explained on the basis of volume fraction of the nanofiller, orientation of the nanofiller with respect to the diffusion molecules and the aspect ratio of added nanofillers [2]. Both graphene nanoplatelets and other graphene oxide derived nanofillers have been investigated in permeation studies of various polymers like polypropylene, polycarbonate, polystyrene [4] and it has been proven that these nanofillers have a potential to enhance the barrier properties the above said polymers. Traditionally permeability can be given as product of diffusivity and solubility; this is why diffusion coefficient (D) and solubility parameters (S) are predominantly considered to be the permeability mechanism controllers. Since the nanofillers are added in very small percentages, therefore they impart a very little change in the matrix volume, therefore solubility parameter is considered to be less dominant than diffusion

coefficient [2, 5]. This diffusion coefficient is directly linked with the tortuosity which is affected by the shape and dispersion of nanofillers.

An increasing use of nylon 12 in the food packaging industry [6] persuaded us for an attempt to increase its barrier properties by incorporation of the functionalized graphene sheets (FG). Both oxygen barrier property and water barrier property were tested to assess the effect of graphene sheets on the barrier properties of nylon 12.

7.2 Equipment used for the water permeability testing

Before the discussion of the experimental results and models, an overview of the equipment for measuring the water barrier properties of nylon 12 and its nanocomposites has been given. The MOCON PERMATRAN-W Model 398, used to analyze and measure the water vapour transmission rate, has been given in figure 7.1.

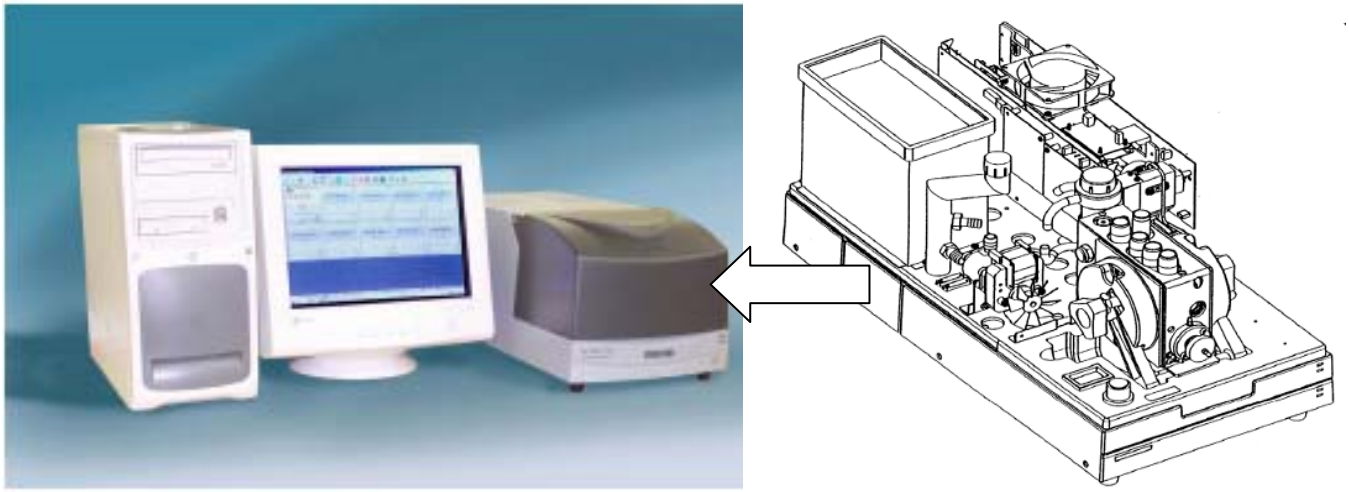

(a) (b)

Fig.7.1 (a) PERMATRAN-W Model 398 System (b) inside view of the testing chamber shown in (a) correlated with an arrow

Testing principle: The PERMATRAN-W Model 398 measures the water vapour transmission rate of barrier materials. A sample of the material is placed in the test cell and is clamped in place. A cavity of HPLC-Grade water is located in the head of the test cell parallel to the sample, providing a source of water vapour. The cavity in the block acts as an accumulation chamber for water vapour passing through the sample. When a test is initiated, valves open automatically to allow dry N_2 to flow through the accumulation chamber. This process is referred to as the “Purge Cycle”. The valves remain open until the relative humidity (%RH) in the chamber drops to the minimum value of the Target RH range.

After the minimum value is reached, the valves close and the humidity inside the chamber begins to climb as water vapour permeates through the sample. This process is referred to as the “Test Cycle”. The RH in the chamber is permitted to rise until it reaches the maximum value of the Target RH range. The purge cycle and the test cycle will repeat until the user has decided the water vapour transmission rate has come to equilibrium. At this time, the user would end the test and may print the results of the experiment. The water vapour transmission rate is calculated based on the amount of time it takes the relative humidity to accumulate from the minimum to the maximum values of the test range. This amount of time is directly proportional to the water vapour transmission rate.

Compression moulding was used in order to prepare samples with the dimensions of about 0.05×10.16×10.16 cm. All the samples were dried for 48 hours in a vacuum oven to get rid of any existing moisture in them prior to mounting them in the testing chamber. The test temperature was set to ambient temperature (23°C) and a pressure of 760mmHg was used during the testing. Relative humidity of the permeant was set to be 100% and the testing area of the each sample was 50cm^2.

7.3 Effect of functionalized graphene on the water permeability of nylon 12

Before the discussion of the experimental permeation results and models, it was necessary to calculate the volume fraction of the nanofillers added. These volume fractions of FG loadings were calculated according to the conventional rule of mixtures, and the values are given in table 7.1. It was necessary to calculate volume fraction as it had to be used in the various models for the prediction of minimum reduction in permeability upon inclusion of a nanofiller.

Mass fraction	Volume fraction
0.001	0.0005
0.003	0.0014
0.006	0.0029
0.01	0.0048

Table 7.1 Mass and volume fractions of FG added into nylon 12.

The water vapour permeability results of nylon 12 and its nanocomposites are given in table 7.2. As can be seen clearly that with the increase in percentage of FG, the water permeability decreases (up to 0.6 wt% FG). These results are in agreement with the tortuous path models. It is well known [7] that the functionalized graphene sheets, which are a few nanometres thick and about 2 micron long, can impart a greater reduction on the permeability of the matrix to which it has been added. However, with 1.0wt% FG, a less decrease in water vapour permeability of the nylon 12 was observed.

	Water Permeability gm - mil / [m² - day]	%age reduction in permeability
Nylon 12	25.10	0
Nylon 12/FG (0.1 wt%) nanocomposites	16.75	33
Nylon 12/FG (0.3 wt%) nanocomposites	16.60	34
Nylon 12/FG (0.6 wt%) nanocomposites	15.65	38
Nylon 12/FG (1.0 wt%) nanocomposites	18.22	27

Table 7.2 Water permeability results for nylon 12 and its FG based nanocomposites.

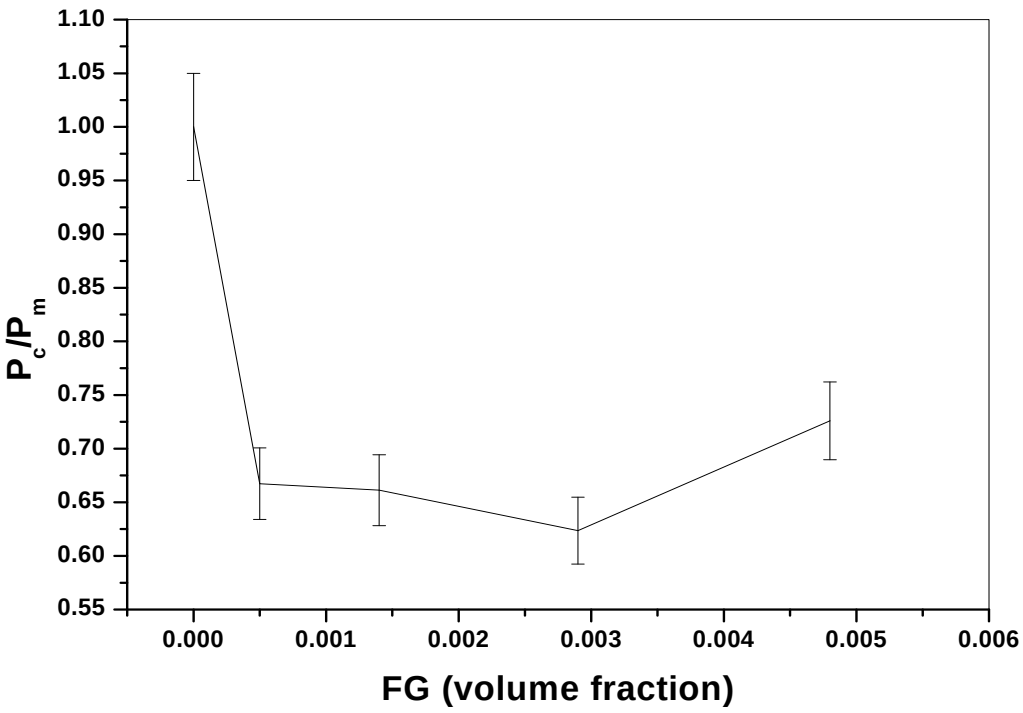

Fig.7.2 Relative water permeability of nylon 12 and its nanocomposites

The relative water permeability coefficient of nylon 12 nanocomposites as a function of FG (P_c/P_m, where P_c is the permeability of composite and P_m is the water permeability of pristine nylon 12 matrix) was calculated for the conventional representation of permeability data against volume fraction of nanofiller and the results are given in figure 7.1. It was suggested that this decrease in water permeability of nylon 12 was due to increase in tortuous path which was provided by functionalized graphene sheets. Nielson's model (given in equation 7.1) was applied in order to predict the relative permeability coefficient as it has been shown to be accurate for predicting permeability of nanocomposites with randomly distributed nanofillers of high aspect ratio, as is the case for our FG/nylon 12 nanocomposites.

$$\frac{Pc}{Pm} = \frac{1-\emptyset}{1+0.5\alpha \times \emptyset} \qquad (7.1)$$

Where α is the aspect ratio (length/width of the nanofiller) and ϕ is the volume fraction of the nanofiller added.

The permeability coefficient for our FG/ nylon 12 nanocomposites at low concentrations of FG was much lower than anticipated from Nielson's model. However, this high barrier effectiveness was not completely unexpected, as excellent increase in mechanical properties have been reported at similar loadings of graphene based nanocomposites [7,8,9]. As Nielson's model was developed for rigid two dimensional nanofillers with limited interaction between the nanofillers and the matrix, therefore it might not suitably explain our nanocomposites at lower loadings of nanofillers where FG (due to additional functional groups) have improved interaction with the matrix. For example at 0.0005 vol. fraction of FG, the Nielson model would require the two dimensional graphene sheets to have an aspect ratio of

approximately 2000, while from TEM measurements we can only assign an average aspect ratio of 1000 [7]. TEM results are given in figure 3.1 and 3.2 (chapter 3). Indeed Nielson's model has been unsuccessful in describing barrier performance of high aspect ratio nanofillers [4, 7, 10 and 11].

Given the aforementioned large discrepancy in Nielson's predicted behaviour and our experimental results, we also compared our data with Cussler's model [11]. Cussler's model assumes a well ordered stacked array of nanoplatelets that extends through the entire polymer matrix and estimates the effect of low concentration of nanofiller on the permeability of polymers. This Cussler's model is given in equation 7.2.

$$P_c/P_m = 1 + (\alpha^2 + \phi^2 / 1-\phi)^{-1} \qquad (7.2)$$

Where P_c and P_m are the permeability of composite and the matrix respectively, α aspect ratio of the nanofiller and ϕ is the volume fraction of nanofiller.

Our permeability coefficient (P_c/P_m) at 0.05 vol% loading was described correctly by Cussler's model which assumed an aspect ratio of ~ 1100. This aspect ratio is similar to what we predicted from TEM results. It has also been studied [12] that sheet-like morphology of a nanofiller, such as graphene sheets, is particularly efficient at maximizing the path length due to the large length to width ratio compared to other shapes of nanofillers. Above prediction from Cussler's model suggested that the presence of FG might had introduced a tortuous path for the diffusing penetrant (water). The reduction of water permeability was the result of the longer diffusive path that the penetrant must travel in the presence of regularly arranged filler (FG in the present case) and this increase in tortuous path is illustrated in figure 7.2.

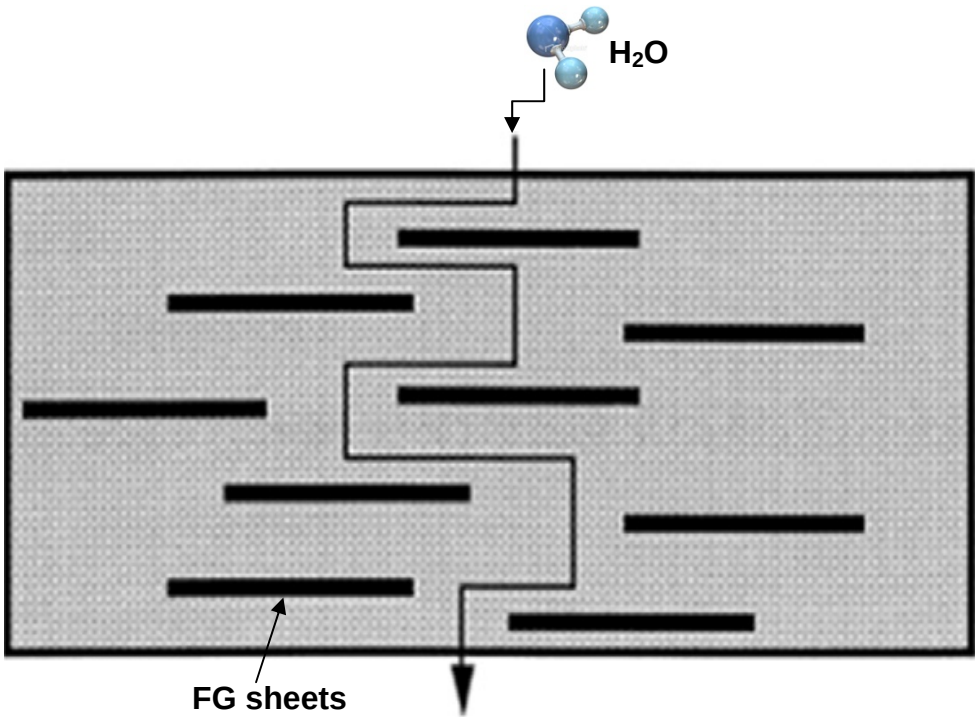

Fig.7.3 Schematic representation of water molecules following a tortuous path through FG/nylon 12 nanocomposites with sheets arranged according to Cussler's model.

At 1.0wt% of FG, the water permeability started to increase, although it was still less than pristine nylon 12. This result was not predicted from the Cussler's model. Of course in this model, the possibility of changes in the crystallinity because of the presence of nanofiller (FG in this case), nature of interface between nanofiller and the matrix were not taken into account. Alexander et al. [10] have also found a similar threshold percentage of clay in an attempt to decrease the water permeability of nylon 12. This difference in permeability trend can be explained on the basis of difference in percentage crystallinity. Picard et al [1] claimed that increase in crystallinity of polymer, upon incorporation of nanofiller, can be impermeable to water molecules, hence resulting in an increased tortuosity. Referring to table 4.1 (Chapter 4), it is obvious that crystallinity of nylon 12 starts to decrease upon addition of 1wt%

FG, which indicates that the interaction between the 1.0 wt% FG and nylon 12 is weaker as compared to the interaction between the lower percentages of FG and nylon 12. This decrease in crystallinity was also confirmed by XRD results (Chapter 5). Also Weak interfacial interactions between filler and the matrix are thought to result in poor barrier properties due to the creation of preferential paths in between the filler and the matrix [12]. Hence, an increase in water permeability upon higher loading of FG can be explained by (i) a decrease in crystallinity, which is an influencing factor for increase in the tortuous path (ii) a poor dispersion of FG as relatively higher percentages of FG might had resulted in an agglomeration!

Various percentages of a smaller sized graphene sheets derived from UF4 using *'Hummer's method'* were also incorporated in nylon 12 using melt blending. The effect of these UF4 based graphene sheets (named as UF4) on the water permeability of nylon 12 has been given in table 7.3.

	Water Permeability gm - mil / [m² - day]	**%age reduction in permeability**
Nylon 12	25.10	0
Nylon 12/UF4 (0.1 wt%) nanocomposites	16.72	33
Nylon 12/UF4(0.3 wt%) nanocomposites	15.64	38
Nylon 12/UF4 (0.6 wt%) nanocomposites	15.38	39

Table 7.3 Water permeability results for nylon 12 and its UF4 based nanocomposites

As seen in table 7.3, the water permeability decreases up to a maximum of 39% upon incorporation of 0.6wt% UF4. This decrease in the water barrier properties of

UF4/nylon 12 nanocomposites was also associated with the better dispersion of the nanofiller, increase in crystallinity and increase in the tortuous path provided by the UF4.

Is it only the planar geometry of graphene which causes an improvement in the barrier properties of nylon 12 or it is the synergetic effect of treatments along with the 2D geometry? To find the answer of this question, untreated and treated UF4 (with various techniques) was melt blended with the nylon 12. The water vapour permeability of nylon 12 upon incorporation of untreated and UF4 treated via ultrasonication, with Hummer's method and the 'new method' is given in table 7.4. As seen clearly from table 7.4, upon incorporation of untreated UF4 (as supplied by the company) there is a decrease of 28% in the water permeability of nylon 12, which implies that graphite, with several graphene layers stacked together, can increase the tortuous path. Upon ultrasonication of UF4, some of the graphene layers were separated from each other. The reduction in water permeability of nylon 12 was similar (~ 29%) to what we found in the case of untreated UF4. This implied that ultrasonication (US) was not enough for the stable exfoliation of UF4, as already discussed in Chapter 3. Since US treated UF4 was failed to maintain its exfoliated structure for longer time, therefore it was considered that the agglomeration of UF4 flakes had occurred which resulted in its poorer dispersion, hence not effectively reducing the water permeability. A noticeable decrease in the water permeability of nylon 12 was observed (referring to table 7.4) when treated UF4, to produce functionalized graphene sheets, via Hummer's (39%) and our *'new method'* (41%) was incorporated in it. This significant decrease in the water permeability of nylon 12 upon inclusion of treated UF4 reveals that although a 2D UF4 graphite (untreated and ultrasonicated) lowered the water permeability of nylon 12, but it was much less

than what we found in the case of treated UF4. Also, UF4 exfoliated via our new method was proven to be more efficient in terms of improving the barrier properties of nylon 12 than UF4 exfoliated using Hummer's method. This also testifies the significance of our *'new method'* for the successful preparation of functionalized graphene sheets.

Summarizing all of the above discussion, we are in a state to answer our earlier raised question. Although 2D geometry of the graphene sheets, whether untreated or treated via ultrasonication, can improve the barrier properties of nylon 12 by enhancing the tortuous path but the functionalized graphene sheets (along with their planar geometry) with active functional groups are the better contestants to cause a significant improvement in the barrier properties of nylon 12. The improved barrier properties upon inclusion of UF4 based functionalized graphene sheets also attracts our attention towards the effect of interaction between nanofiller and matrix, and the better dispersion of nanofiller in the matrix.

It is well known that layered clays can also significantly reduce the water permeability of polymers [1, 2, 5 and 14]. Three kinds of clays; Barrisurf^{TM} HX (BHX), Barrisurf ^{TM}LX (BLX), and sodium montmorillonite were used in preparation of nylon 12/clay nanocomposites by following exactly the same procedure and operating conditions as were used for graphene based nylon 12 nanocomposites. Samples for 'water permeability testing' were prepared using compression moulding and the operation conditions of MOCON Permatran-W, for the water permeability measurements, were also kept the same as were used for the FG based systems. Upon comparison of the effect of two nanofillers with similar geometry, it was noticed that the decrease in water permeability of nylon 12 upon incorporation of even 1.5wt% clay (of each type) was not comparable to the effect of only 0.6wt% FG. For

the case of 0.6wt% FG, the reduction in water permeability of nylon 12 was 41% while upon incorporation of Na^+, BHX and BLX clays the reduction in water permeability was 35, 36 and 30% respectively. These results are summarized as ratio of permeability of composite (P_c) to that of the matrix (P_m) and given in figure 7.3.

	Water Permeability gm - mil / [m² - day]	**%age reduction in permeability**
Nylon 12	25.10	0
Nylon 12 with untreated UF4	18.08	28
Nylon 12 with ultra-sonicated UF4	17.73	29
Nylon 12 with UF4 treated via Hummer's method	15.38	39
Nylon 12 with UF4 treated via our 'new method'	14.73	41

Table 7.4 Effect of UF4, treated by various techniques, on the water permeability of nylon 12.

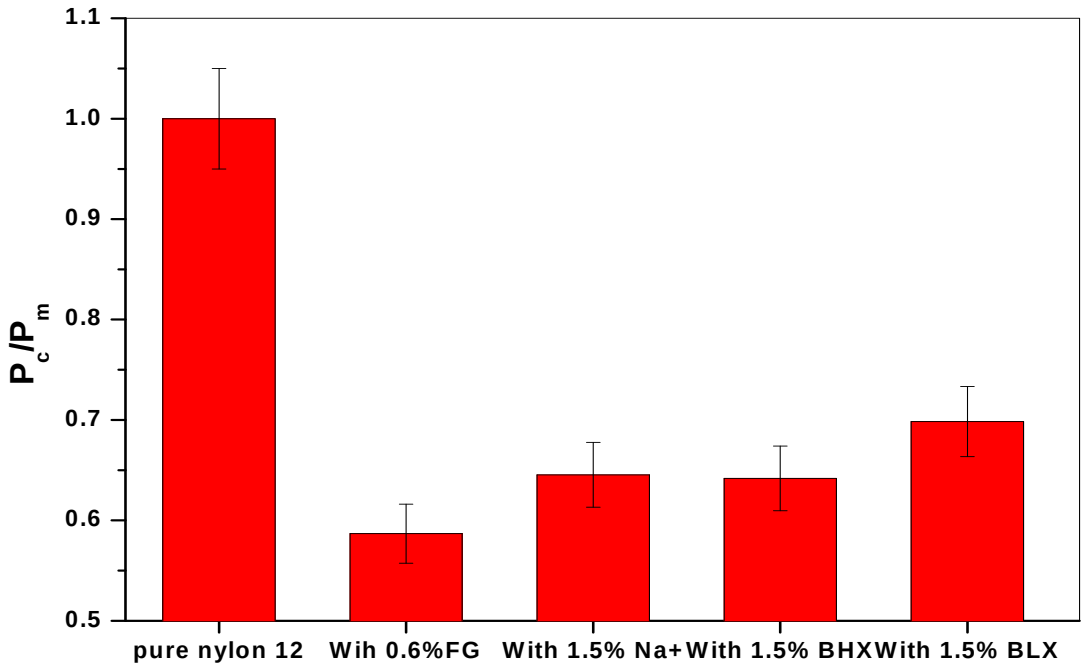

Fig.7.4 Permeability coefficient for nylon 12 and its nanocomposites with different nanofillers.

From the comparative study of the effect of various clays and graphene on the water barrier properties of nylon 12, we can conclude that even with the similar geometry to the clay, FG has proven to be the better among the 2D nanofillers. This also means that the water permeability through nylon 12 is also affected by the interaction of nanofiller with the matrix, which was better for FG as compared to the clays. This comparatively better interaction between FG and nylon 12 could be a reason for the better improvement in the water barrier properties.

This concept of enhancement of barrier properties of nylon 12 powder, by incorporation FG, was extended to nylon 12 pellets for an industrial outlook. Masterbatches of 0.1, 0.3 and 0.6wt% nylon 12 powder with nylon 12 pellets without FG (named as 0.1,0.3 and 0.6 M.B. respectively) and with FG (named as 0.1 M.B. with FG, 0.3 M.B. with FG, and as 0.6 M.B. with FG) were prepared and their water

permeability was tested. The results are summarized in table 7.5. Water permeability of 0.1 M.B. was not decreased a lot which might be due to poorer interaction between FG and 0.1 wt% masterbatch. For 0.3 and 0.6 masterbatches, an appreciable improvement in water barrier properties was observed. This threshold amount of required FG has also been observed for improvement in mechanical performance of the masterbatches, as discussed in chapter 5.

	Water Permeability gm - mil / [m² - day]	**%age reduction in permeability**
0.1 M.B.	53	
0.1 M.B. with FG	51	4
0.3 M.B.	76	
0.3 M.B. with FG	48	37
0.6 M.B.	57	
0.6 M.B. with FG	46	19

Table 7.5 Water permeability of masterbatches with and without functionalized graphene sheets (FG).

7.4 Effect of functionalized graphene on the oxygen permeability of nylon 12

Oxygen transport properties were targeted in the composites because ingress of this gas in food packages is very detrimental from a food quality and preservation point of view. The gas permeability was determined by OX-TRAN@ Model 1/50, as shown in figure 7.4. ASTM F1927- standard test method for oxygen transmission was adopted. For each test run, the samples were cut into fixed shapes and put into the mould (as shown in figure 7.5). The area of 25mm thick samples was set to be 50 cm^2 and the examination time was set to be 20 minutes. The entire tests were conducted in mode which is convergence by cycles at a temperature of 23°C. In Convergence-by-Cycles mode, the system will compare the latest transmission rate results with those measured a specified number of exam cycles previous and make the equilibrium determination. The tests were finished when the transmission rate was stabilized after 20 test cycles.

Fig.7.5 OX-TRAN Model 1/50 System [15]

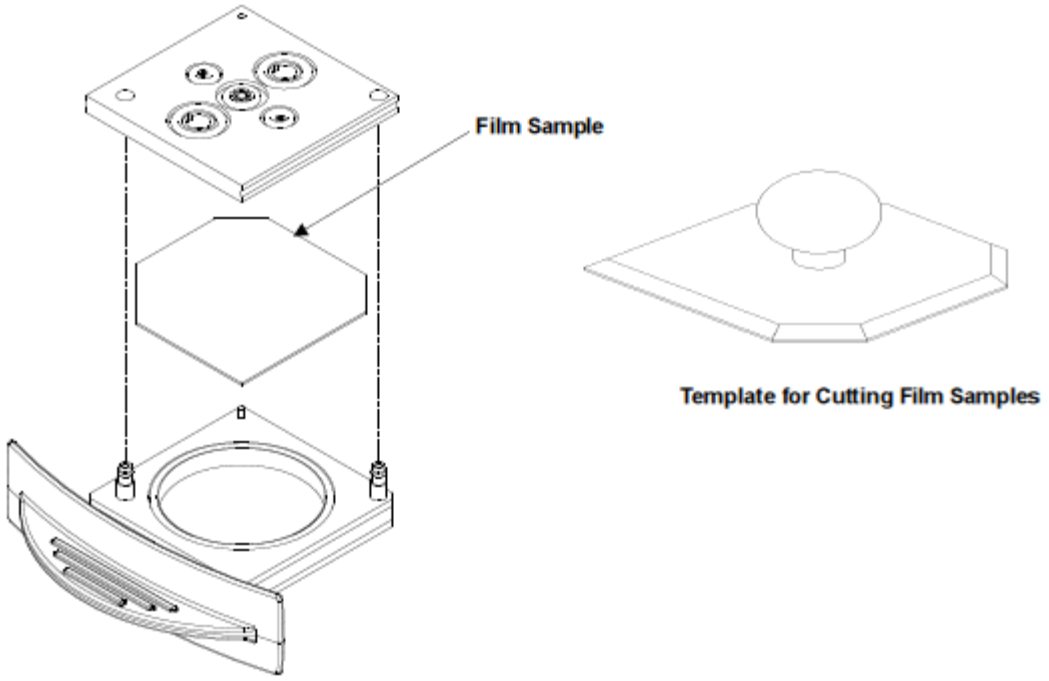

Fig.7.6 Mounting the sample for oxygen barrier testing [15]

The OX-TRAN Model 1/50 measures the oxygen transmission rate of the barrier materials. The flat film sample material is placed in a test cell. Test cells are divided into two chambers separated by the sample material. The upper chamber is filled with dry or humidified Nitrogen and the lower chamber with the dry or humidified test gas (Oxygen).To the extent that there is a oxygen sensor reading, permeation through the barrier material must have occurred. The rate of permeation is calculated using the oxygen sensor reading and the area of the sample. This rate of permeation is referred to as the oxygen transmission rate [15].

When a sample of the material is placed in the test cell and is pneumatically clamped in place, test gas is applied to the bottom side of the cell and a 5 minute nitrogen purge cycle is initiated on the top side of the cell. The test gas (permeant) used is 100% oxygen. The purge cycle removes any ambient oxygen in the “test”

side of the cell. After five minutes, the purge valves are closed and the test side of the cell is directly coupled to the oxygen sensor. Measurements are made as oxygen permeations from the film to the test side of the cell and the values are given in terms of oxygen transmission rate (OTR) [15]. OTR is the volume of oxygen penetrating the film per unit area, time and oxygen partial pressure difference was registered over time from time zero to the steady state. Effect of functionalized graphene sheets (0.3, 0.6, 1.0 and 3.0 wt %) on the oxygen permeability of nylon 12, measured by OXTRAN, is given in table 7.6. A continuous decrease in oxygen transmission rate (OTR) was observed upon increasing the percentage of functionalized graphene. These gas permeability results were in agreement with the Cussler's model (Equation 7.2).

	OTR cc / [m² - day]	**%age reduction in OTR**
Nylon 12	27.55	0
Nylon 12/FG (0.3 wt%) nanocomposites	19.24	30
Nylon 12/FG (0.6 wt%) nanocomposites	18.71	32
Nylon 12/FG (1.0 wt%) nanocomposites	16.70	39
Nylon 12/FG (3.0 wt%) nanocomposites	15.30	44

Table 7.6 Oxygen permeability of nylon 12 and its nanocomposites.

These improved oxygen barrier properties were considered as a resultant of an increase in tortuous path provided by planar sheets of functionalized graphene. Also at higher contents of FG, more tortuous path was created to prevent small gas molecule from diffusing through nylon 12 nanocomposites. A similar significant decrease in the oxygen permeability of polystyrene, upon incorporation of graphene nanoplatelets, has been reported and an increased tortuous path was suggested as a possible cause for this decrease in oxygen permeability [7].

Our understanding of how graphene, derived from different sized graphite (UF4), would affect the oxygen permeability of nylon 12 was expanded by preparing various UF4/nylon 12 nanocomposites and by evaluating the effect of UF4 derived graphene sheets on the oxygen permeability of nylon 12 using OXTRAN. The effect of UF4 on the OTR of nylon 12 is summarized in table 7.7.

	OTR cc / [m² - day]	**%age reduction in OTR**
Nylon 12	27.55	0
Nylon 12/UF4 (0.1 wt%) nanocomposites	23.36	15
Nylon 12/UF4 (0.3 wt%) nanocomposites	20.45	26
Nylon 12/UF4 (0.6 wt%) nanocomposites	18.23	34

Table 7.7 Effect of UF4 on the oxygen permeability of nylon 12.

It was noticed that a smaller sized graphene sheets (UF4) and FG decreased the OTR of nylon 12 in a similar way. This similarity between UF4 and FG has also been observed for the improvement of the thermal and mechanical properties of nylon 12 (as described in the earlier chapters).

Effect of untreated UF4 and UF4 treated by various methods on the oxygen barrier properties of nylon12 was also established. 0.6 wt% of Untreated UF4, ultrasonicatedUF4, treated via Hummer's method and by our *'new method'* was incorporated in nylon 12 to prepare nanocomposites for each category of UF4.

	OTR cc / [m² - day]	**%age reduction in OTR**
Nylon 12	27.55	0
Nylon 12 with untreated UF4	24.15	12
Nylon 12 with ultra-sonicated UF4	21.50	22
Nylon 12 with UF4 treated via Hummer's method	18.23	34
Nylon 12 with UF4 treated via our 'new method'	19.15	31

Table 7.8 Effect of untreated UF4, ultrasonicated UF4, and UF4 treated by Hummer's and new method, on the oxygen barrier properties of nylon 12.

Referring to table 7.8, a distinguished improvement in oxygen barrier properties of nylon 12 was observed, as compared to untreated and ultrasonicated UF4, when treated UF4 was incorporated in it. This implies that although geometry of nanofiller is crucial issue for gas property enhancement, but the interaction between a nano-reinforcement and polymer cannot be neglected too. Considering the above comparative study we can comment that better is the interaction between nanofiller (with planar geometry) and the matrix, improved are the oxygen barrier properties of the matrix to which they are included.

Comparative study of the barrier efficiency of graphene sheets with that of BLX and BHX clays acknowledged the better performance of the functionalized graphene. At 3wt% FG, decrease in OTR was about 44% while at the similar loadings of BLX and BHX clays it was only 5% and 17% (table 7.9). This significant different quantifies the better barrier ability of graphene as compared to the other nanofillers which belong to its planar family.

	OTR cc / [m² - day]	**%age reduction in OTR**
Nylon 12	27.55	0
Nylon 12/FG nanocomposites	15.30	44
Nylon 12/BHX 3% nanocomposites	22.93	17
Nylon 12/BLX 3% nanocomposites	25.58	5

Table 7.9 OTR comparison of clay and graphene based nylon 12 composites.

	OTR cc / [m² - day]	%age reduction in OTR
0.1 M.B.	59	
0.1 M.B. with FG	57	3
0.3 M.B.	48	
0.3 M.B. with FG	43	10
0.6 M.B.	36	
0.6 M.B. with FG	32	10

Table 7.10 OTR (Oxygen Transmission Rate) of the masterbatches, with and without functionalized graphene sheets (FG).

The incorporation of FG in 0.1, 0.3 and 0.6 wt% masterbatches also resulted in decrease in their oxygen permeability. The OTR results for masterbatches, with and without FG, are given in table 7.10. Due to a critical percentage of FG required for the property enhancement of the masterbatches, the addition of FG in 0.1M.B. did not decrease its OTR to an appreciable extent. For the rest of two masterbatches, incorporation of FG enforced an improvement of about 10% in their oxygen barrier properties by guiding the permeant through a longer path.

7.5 Conclusions

Water and the oxygen barrier properties of nylon 12 and its various nanocomposites were investigated and a significant improvement in barrier properties of nylon 12 was achieved when graphene sheets were introduced in it. The water permeation results revealed that the permeability of nylon 12 decreases up to 0.6 wt% of FG and UF4, which was in accordance with tortuous path model. A comparative study of untreated, ultrasonicated and treated UF4 (From Hummer's and our *'new method'*) conveyed that for the better barrier properties of a composite, a nanofiller should not only have planar geometry but a fair interaction with the matrix as well. Various known treatments provide active functional sites which can improve this interaction and the distribution of nanofiller in the matrix. Water permeability comparison of graphene and clay based nylon 12 nanocomposites proved graphene to be the better nanofiller for the barrier property enhancement of nylon 12. Water permeability of the masterbatches was also decreased to an appreciable extent upon addition of graphene sheets.

The oxygen permeability of all the systems under investigation was quantified in terms of oxygen transmission rate (OTR). A decrease of 44% in the OTR of nylon 12 was achieved upon incorporation of 3% FG which was substantially greater than that with various clays. Addition of UF4 (graphene sheets derived from smaller sized graphite) impressively decreased the OTR of nylon 12. Decrease in OTR of the masterbatches was not that promising upon addition of FG.

7.6 References

[1] E. Picard, A. Vermogen, J.-F.G´erard, E. Espuch. .Barrier properties of nylon 6-montmorillonite nanocomposite membranes prepared by melt blending: Influence of the clay content and dispersion state Consequences on modelling. Journal of Membrane Science 2007; 292:133–144

[2] G. Choudalakis , A.D. Gotsis. Permeability of polymer/clay nanocomposites: A review. European Polymer Journal 2009;45:967–984.

[3] H. Kim, Y. Miura, C.W. Macosko. Graphene/polyurethane nanocomposites for improved gas barrier and electrical conductivity. Chem. Mater.2010; 22: 3441–3450

[4] J.R. Potts, R.S. Rouff, D.R. Dreyer, C.W. Bielawski. Graphene-based polymer nanocomposites. Polymer 2011; 52: 5-25.

[5] B. Xu, Q. Zheng , Y. Song, Y. Shangguan. Calculating barrier properties of polymer/clay nanocomposites: Effects of clay layers. Polymer 2006; 47 : 2904–2910

[6] Niels H. Stoffers. Certified reference materials for food packaging specific migration tests: development, validation and modelling. Chapter 4

[7] S.T. Nguyen, O.C. Compton, S. Kim, C.Pierre, J.M. Torkelson. Crumpled graphene nanosheets as highly effective barrier property enhancers. Adv. Mater. 2010:1-5.

[8] B. Z. Jang , A. Zhamu. Processing of nanographene platelets (NGPs) and NGP nanocomposites: a review. J. Mater. Sci. 2008; 43:5092–5101

[9] H. Kim, A.A. Abdala, C.W. Macosko. Graphene/Polymer Nanocomposites. Macromolecules 2010; 43: 6515–6530

[10] A. Saiter, B. Alexandre, D. Langevin, H. Couderc, Q.T. Nguyen, P. Médéric, S. Marais, T. Aubry, Water barrier properties of polyamide 12/ montmorillonite nanocomposite membranes: Structure and volume fraction effects. J. Membrane Sci.2009; 328:186–204.

[11] E.L. Cussler. Diffusion Fundamentals 2007;6:72.1 - 72.12

[12] A..Fendler, M. P. Villanueva, E. Gimenez, J. M. Lagaron. Characterization of the barrier properties of composites of HDPE and purified cellulose fibers. Cellulose 2007 ; 14: 427–438

[13] R. K. Bharadwaj. Modeling the barrier properties of polymer-layered silicate nanocomposites. Macromolecules 2001; 34: 9189-9192

[14] B. Alexandre, S. Marais, D. Langevin, P. Médéric , T. Aubry. Nanocomposite-based polyamide 12/montmorillonite: relationships between structures and transport properties. Desalination 2006; 199 : 164–166

[15] OX-TRAN Model 1/50 Operator's Manual, U.S. Patent Numbers 5,107,696 and 5,159,829

Chapter 8

Conclusions and future works

8.1 Introduction

This research involves the development of functionalized graphene sheets (FG) and its nylon 12 based nanocomposites with improved thermal, mechanical and barrier properties. Expandable graphite was used to yield FG by a well known 'Hummer's method' and also by using a lately invented *'new method'* by our research group. Graphene sheets were also prepared by using smaller sized graphite (nano-graphite) and were named as UF4 in this research. UF4 based nylon 12 nanocomposites with improved thermal, mechanical and barrier performance were also prepared and characterized. To understand the effect of varied geometry nanofillers on the mechanical performance of nylon 12, a smaller sized graphite; named as nano-graphite, multiwalled carbon nanotubes (MWCNTs) and carbon black were treated with a mixture of concentrated sulphuric and nitric acids, prior to melt blending with nylon 12. This treatment was considered for improving the hydroxyl group functionalities on the surface of each nanofiller with its own unique geometry. Masterbatches of nylon 12 powder and FG were prepared and introduced in the nylon 12 pellets; in an attempt to extend the laboratory scale results to an industrial scale. A promising increase in overall performance of the masterbatches upon incorporation of FG was achieved, as attested by various characterization techniques. Many techniques were employed to characterize the all composite

systems; thus morphological, thermal, mechanical and barrier properties of all the samples were obtained. Conclusions can be drawn as follows based on the obtained experimental results.

8.2 Conclusions

Functionalized graphene sheets, with an aspect ratio of 500-1000, were successfully prepared by using Hummer's method. Their preparation was confirmed by using TEM. Because of certain issues related to Hummer's method, an updated *'new method'* was developed for the preparation of graphene oxide and then exfoliating it to functionalized graphene sheets. Successful exfoliation of graphene sheets prepared by *'new method'* was also confirmed by TEM. Untreated nano-graphite was ultrasonicated to exfoliate the layers of graphite. Although the exfoliation of graphite layers was achieved (observed by TEM), but these graphite layers (graphene) could not keep their individuality for long and started to aggregate. This result proves the upper hand of chemical methods (Hummer's method and the *'new method'*) upon physical methods of production of graphene sheets. Oxidation of expanded graphite into graphene oxide from chemical methods was confirmed by X-ray photoelectron spectroscopy (XPS). A decreased carbon to oxygen atomic ratio of treated graphite, as confirmed by XPS, was an evident of oxidation reaction. This oxidation effect was observed in the case of Hummer's method and also for the *'new method'*. FTIR results showed that acidic treatment of nano-graphite, MWCNTs, and carbon black was very effective in introducing the additional carboxyl and hydroxyl groups, which could be beneficial for the interaction between each of the nanofillers and the nylon 12 matrix.

FG was melt blended with nylon 12 powder using Haake Rheomix, in order to prepare 0.1, 0.3, 0.6, 1 and 3wt% nanocomposites. Various percentages of UF4 were also melt blended with nylon 12 to prepare 0.1, 0.3, 0.6 and 1wt% UF4/nylon 12 nanocomposites. SEM investigations confirmed that melt blending was enough for embedding the FG and UF4 in the nylon 12 matrix. Furthermore, masterbatches of nylon 12 powder and FG were prepared in order to add into nylon 12 pellets, for the concept of industrial scaling up. The presence of graphene sheets in the masterbatches was assured by SEM. The interaction between nanofiller and the matrix in each case was also confirmed by FTIR, which proven the hydrogen bonding between amide linkage of nylon 12 and the active functional groups present on the surface of functionalized graphene sheets.

Isothermal frequency response (at 28, 32 and 36°C) of nylon 12 and its 0.6wt%FG/nylon 12 nanocomposites was investigated using Dynamic mechanical analysis (DMA) to confirm any interaction between functionalized graphene sheets and the nylon 12. Increase in storage modulus and a decrease in tan δ acclaimed the interaction between FG and nylon 12.

Thermal analysis of nylon 12 and its various nanocomposites was studied using DSC. An increase in T_g of nylon 12 upon incorporation of UF4 and FG, as was evidenced by DSC, was an indication of interaction between nanofiller and the matrix. The incorporation of UF4 or FG did not strongly affect the crystallization mechanism. But on the other hand, both nanofillers did act as nucleating agent by increasing crystallinity of nylon 12. A threshold percentage of each nanofiller (FG and UF4) was an indication of an optimum concentration after which nanofiller started to agglomerate inside nylon 12, hence causing a decrease in crystallinity. Crystal size of nylon 12 was decreased until the addition of the optimum weight

percentage of each nanofiller and then started to increase for the higher percentages. This decreased crystal size was also an indication of strong nucleating effect caused by graphene sheets which gave rise to a lot of nucleating sites in a limited space; hence crystals were restricted to grow to a larger size. Furthermore, the crystal geometry of nylon 12 was not influenced upon incorporation of graphene.

Mechanical analysis of nylon 12 and its nanocomposites proved that the incorporation of either UF4 or FG caused an increase in ultimate tensile strength, elongation at break and more importantly the toughness of nylon 12. However, no significant increase in the Young's modulus of nylon 12 was observed upon incorporation of graphene. Toughness of each system was characterized by using three techniques; (i) area under the stress-strain curve which is proportional to the toughness, (ii) impact failure energy taken from the falling weight impact tester, and (iii) Mode I fracture toughness testing (K_{Ic}). Each characterization method attested that the toughness of nylon 12 was enhanced upon inclusion of graphene sheets. An increase in γ-phase of semicrystalline nylon 12 was observed upon addition of the optimum weight percentage of FG/UF4, as was studied using XRD. Decrease in crystal size, as observed by polarized optical microscope, and increase in the γ-phase of nylon 12 on addition of graphene sheets was thought to be the possible toughening mechanism. Comparison of equally acid treated nano-graphite, MWCNTs, and carbon black on the toughness of nylon 12 showed that it was synergetic effect of treatment and the two dimensional geometry of graphene which proved it to be the best toughening nanofiller among the three.

A promising decrease in water and oxygen permeability of nylon 12 was achieved upon incorporation of only 0.6wt%FG. These results were in accordance with that of the Cussler's model. Improved gas and water barrier properties were resultant of an

increase in the tortuous path provided by the functionalised graphene sheets, good dispersion of FG in the nylon 12 matrix and increased crystallinity of the FG/nylon 12 nanocomposites. A comparative study of clay and FG based nylon 12 nanocomposites proved FG as better nanofiller for the enhancement of barrier properties.

An attempt was made to understand whether a nanofiller with planar geometry is enough to improve the barrier properties or a fair interaction of the nanofiller with the matrix is also necessary. Nanocomposites of untreated nano-graphite, ultrasonicated nano-graphite and graphene sheets produced by treating nano-graphite with Hummer's method and our *'new method'* with nylon 12 were prepared and tested for the barrier properties. The results conveyed to enhance the barrier properties of a composite, planar geometry of nanofiller along with a fair interaction with the matrix is obligatory.

8.3 Recommendations for the future work

In this research, thermal, mechanical and barrier properties of nylon 12 were enhanced using functionalized graphene sheets. Although, we had some remarkable achievements during this research, however, for the material to be used in industrial applications it needs further development in which the following aspects could be included;

1) Attempting to prepare graphene sheets at a larger scale using our *'new method'.*
2) Investigation of the effect of graphene sheets on the surface and sub-surface mechanical properties such as hardness, modulus and creep behaviour of the nylon-12 by means of Nanoindentation analysis.

3) An investigation of electrical and thermal conductivity of graphene based nylon 12 nanocomposites.
4) To study the effect of higher percentages of MWCNTs and carbon black on the toughness of nylon 12.
5) Incorporating graphene sheets in other famous polymer matrices like PE, PP and characterizing mechanical, thermal and barrier properties of these systems.
6) Investigation of effect of graphene sheets produced by new method on mechanical and thermal properties of nylon 12.

Appendix

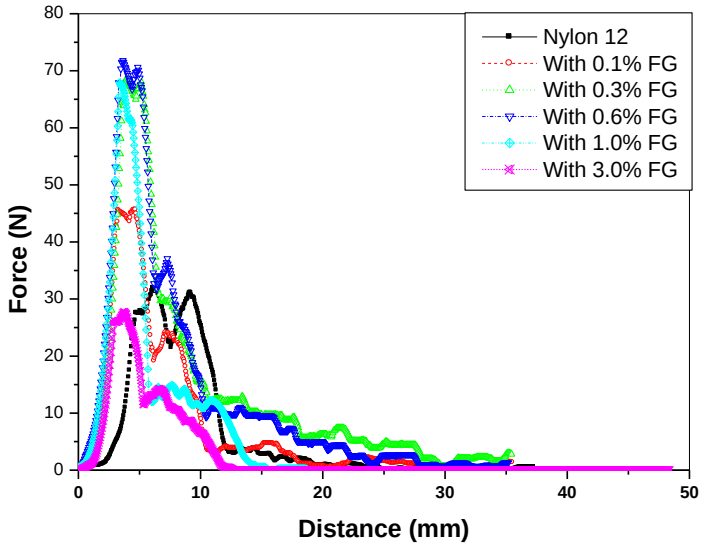

Figure S.1 Force versus distance curves for nylon 12 and its nanocomposites with functionalized graphene obtained from a falling weight impact test.

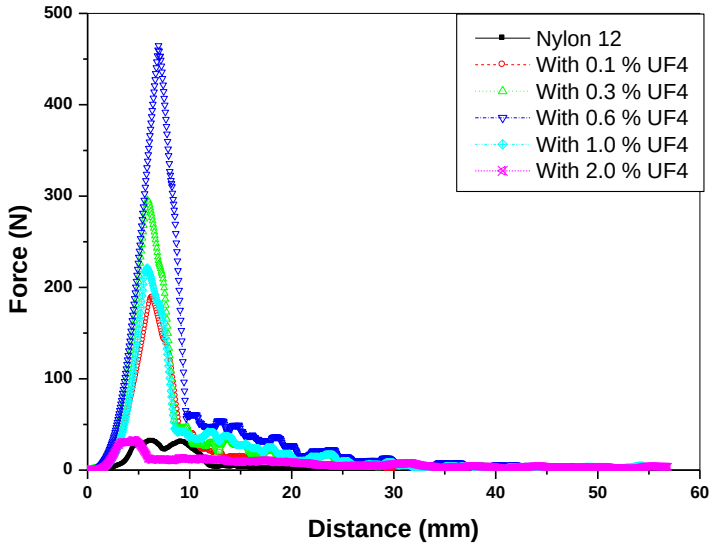

Figure S.2 Force versus distance curves for nylon 12 and its nanocomposites with UF4 obtained from a falling weight impact test.

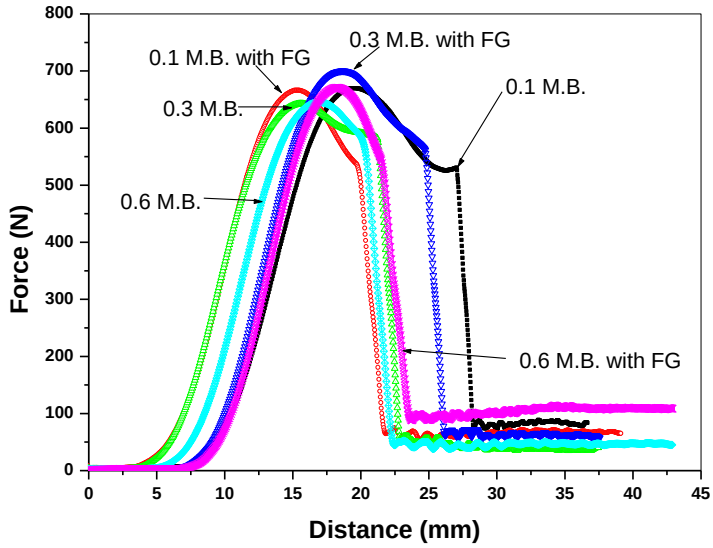

Figure S.3 Force versus distance curves for nylon 12 masterbatches with and without FG obtained from a falling weight impact test.